AD-A115 559 AIR FORCE INST OF TECH WRIGHT-PATTERSON AFB OH SCHOO--ETC F/G 17/7
ANALYSIS AND DESIGN OF A DIGITAL CONTROLLER FOR A SEISMICALLY S--ETC(U)
DEC 81 S W FRANCIS
UNCLASSIFIED AFIT/GE/EE/81D-22 NL

1 OF 4
AD
A 115559

DEPARTMENT OF THE AIR FORCE
AIR UNIVERSITY (ATC)

AIR FORCE INSTITUTE OF TECHNOLOGY

Wright-Patterson Air Force Base, Ohio

AFIT/GE/EE/81*D-22

ANALYSIS AND DESIGN OF A DIGITAL CONTROLLER FOR A SEISMICALLY STABLE PLATFORM

THESIS

AFIT/GE/EE/81*D-22 Stanley W. Francis
Capt USAF

Approved for public release; distribution unlimited

AFIT/GE/EE/81*D-22

ANALYSIS AND DESIGN OF A DIGITAL CONTROLLER FOR A SEISMICALLY STABLE PLATFORM

THESIS

Presented to the Faculty of the School of Engineering

of the Air Force Institute of Technology

Air University

In Partial Fulfillment of the

Requirements for the Degree of

Master of Science

by

Stanley W. Francis

Capt USAF

Graduate Electrical Engineering

December 1981

Preface

The purpose of this study is to construct a dynamics model and to investigate the feasibility of a digital controller for the Seismically Stable Platform at the Central Inertial Guidance Facility at Holloman AFB.

I would like to thank my advisor, Dr. Gary Lamont, of the Air Force Institute of Technology for his guidance and assurance in completing this study. I would like to extend my appreciation to my thesis committee members - Dr. Constantine Houpis, Dr. Peter Maybeck and Captain James Silverthorn, for their valuable suggestions and enriching comments. I would like to thank the Model Shop for building an excellent scale seismic demonstration model.

I would like to thank Mr. Dick Alexander for proposing this thesis topic and Lieutenant Lee Schelonka and Master Sergeant Cleon Barker for their technical support from the Central Inertial Guidance Test Facility.

Finally, I would like to express my gratitude to my wife, Vicki, for her dedication to my career and perseverance and excellent typing of my thesis.

Stanley W. Francis

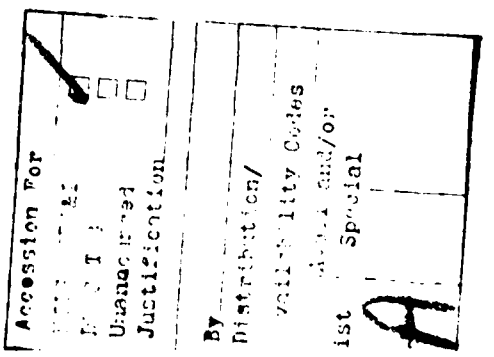

Table of Contents

List of Figures

List of Tables

List of Symbols

A	System state matrix
AS	Attenuation slope approximated at 100 Hz
B	Input state matrix
B_D	Discrete input matrix
c	Scalar damping coefficient
c_S	Scalar second stage damper
c_{SX}, c_{SY}, c_{SZ}	Second stage damper components
c_{FX}, c_{FY}, c_{FZ}	First stage isolation components in X, Y and Z directions
C	Damper matrix, output state matrix
C_D	Discrete output matrix
C_S, C_F, C_G	Second, first, and ground isolation damper matrices
CGTPIF	Command Generator Tracker - Proportional Plus Integral Filter
CIGTF	Central Inertial Guidance Test Facility
CSDL	Charles Stark Draper Laboratory
D	Feedthrough state matrix
D_D	Discrete feedthrough state matrix
$\underline{e}$	Earth frame
$\hat{e}_1, \hat{e}_2, \hat{e}_3$	Translational degrees of freedom
f	Frequency in hertz
f_{VN}	Vertical natural frequency
f_{HN}	Horizontal natural frequency
$f_{VN}, f_{VS}, f_{VE}, f_{VW}$	Lower level actuators

F	First stage pneumatic isolation, applied force
F_C	Damper forces
FJSRL	Frank J. Sieler Research Laboratory
$-\bar{F}_{PE}$, $-\bar{F}_{PN}$ $-\bar{F}_{PW}$, $-\bar{F}_{PS}$	Active controller actuators connected between upper level and pier foundations
F_S	Spring forces
$\bar{F}_{UE}$, $\bar{F}_{UN}$, $\bar{F}_{UW}$, $\bar{F}_{US}$	Active controller upper level actuators between upper level and pier for indicated corner
FV	Final value
F_{VN}, F_{VS}, F_{VE}, F_{VW}	Upper level actuator force orientation as indicated
F_X, F_Y, F_Z	Resultant forces X,Y,Z direction
G	Ground level isolation
G_C^*	Optimum gain matrix
$G_{C_1}^*$, $G_{C_2}^*$	Partitions of G_C^*
GM	Gain margin
$\bar{H}$	Vector angular momentum
$\mathring{\bar{H}}$	Angular momentum time derivative in an inertial frame
I	Identity matrix
I_U	Moment of inertia matrix
I_{UX}, I_{UY}, I_{UZ}	Upper level body moments of inertia about $\hat{e}_1$, $\hat{e}_2$, $\hat{e}_3$ axes
J	Quadratic cost function
k	Scalar spring constant
k_F	Scalar first stage spring constant
k_G	Scalar ground spring constant

k_S	Scalar second stage spring constant
k_{SX}, k_{SY}, k_{SZ}	Second stage damper component
K	Spring constant matrix; transfer function constant
K_F	First stage spring matrix
K_G	Ground spring matrix
K_S	Second stage spring matrix
K_X	State feedback matrix
K_Z	Output feedback matrix
l_{UN}, l_{US}, l_{UW}, l	Isolation lengths for indicated corner
L	Lower level
$\overset{oo}{L}$	Lower level acceleration
$\overline{LE}, \overline{LN}, \overline{LW}, \overline{LS}$	Lower level corner vector, orientation as indicated
$\overset{o}{\overline{LE}}, \overset{o}{\overline{LN}}, \overset{o}{\overline{LW}}, \overset{o}{\overline{LS}}$	Lower level corner velocity vector, orientation as indicated
LmT(jω)	Log magnitude, base 10, function of frequency
LQ	Linear quadratic
meru's	Mili earth rate units
m_U, m_L, m_P	Upper, lower, pier mass
M	Moment
$\overline{M}$	Body moments
MAC	Measurement Analysis Corporation
M_{UX}, M_{UY}, M_{UZ}	Upper level moments about $\hat{e}_1$, $\hat{e}_2$, $\hat{e}_3$ axes
P	Pier level
$\overset{oo}{P}$	Pier level acceleration
PI	Proportional plus integral

p_1, p_2, p_3 p_4, p_5, p_6	Transfer function poles
$\overline{PE}, \overline{PN}, \overline{PW}, \overline{PS}$	Pier corner vectors, orientation as indicated
$\dot{\overline{PE}}, \dot{\overline{PN}}, \dot{\overline{PW}}, \dot{\overline{PS}}$	Pier corner velocity vectors, orientation as indicated
PM	Phase margin
PSD	Power spectral density
r	Radial action arm
$\overline{r}$	Radial action arm vector
Re	Real part, rectangular components
RMS	Root mean square
S	Second stage pneumatic isolators
SSP	Seismically Stable Platform
t_ψ, t_ϕ, t_Θ	Resultant torques, lower level ψ, ϕ, and Θ direction
T_ψ, T_ϕ, T_Θ	Resultant torques, upper level ψ, ϕ, and Θ direction
T	One sample delay
TD	Duplication time
TGG	Third Generation Gyro
$T(j\omega)$	Transmissibility transfer function
TP	Peak time
TR	Rise time
TS	Setting time
U_c, U_r	control cost weight, control rate cost weight
$\overline{U}$	Control input vector
U	Upper level
$\ddot{\overline{U}}$	Upper level acceleration
$\overline{U}^*$	Optimum input control

$\overline{UE}, \overline{UN}, \overline{US}, \overline{UW}$	Upper level corner vector, orientation as indicated
$\dot{\overline{UE}}, \dot{\overline{UN}}, \dot{\overline{US}}, \dot{\overline{UW}}$	Upper level corner velocity vector, orientation as indicated
x	Displacement
$\dot{x}$	Velocity
$\overline{x}$	Displacement vector
$\dot{\overline{x}}$	Velocity vector
$\overline{X}$	State vector
$\dot{\overline{X}}$	State vector derivative
$\overline{X}(t)$	State vector, column vector
$\dot{\overline{X}}(t)$	State vector derivative with respect to time, column vector
$X_0(j\omega)$	Output displacement
$X_1(j\omega)$	Input displacement
$\overline{Y}$	Output vector
Y_C	Output cost weighting matrix
z_1, z_2	Transfer function zero
z_G	Ground displacement
Φ	State transistion matrix
ψ, ϕ, Θ	SSP rotational angles or tilts
$\dot{\psi}$, $\dot{\phi}$, $\dot{\Theta}$	SSP rotational angular rates
ψ_U, ϕ_U, Θ_U	Rotational angles for upper level
ζ	Damping ratio
ω_N	Generalized function of natural frequency
$\overline{\omega}_u$	Angular velocity vector
Π	Feedback state matrix

Abstract

The Seismically Stable Platform (SSP) at the Central Inertial Guidance Facility, Holloman AFB, is a dual reactionary mass isolation platform designed to remove 10^{-8} g RMS/Hz accelerations and ± 0.02 arcseconds angular position or tilt disturbances in all axes from a test environment intended for evaluating "Third Generation Gyro" inertial instruments. Disturbances are removed by two stages of pneumatic isolators comprising a passive isolation system and augmented by an active control system to cover the operational bandwidth from 10^{-8} Hz to 100 Hz.

A dynamic model of the SSP confirmed the passive vibration transmissibilities and identified severe limitations on gain and phase margin to the active controller design. The proposed digital controllers identified the SSP to be weakly controllable. The discrete state representation of the SSP and control law exhibited numerical difficulties detrimental to system stability.

This study recommends single stage pneumatic isolation or fluid isolators monitored by disturbance parameter estimation schemes.

ANALYSIS AND DESIGN OF A DIGITAL CONTROLLER FOR A SEISMICALLY STABLE PLATFORM

I. Introduction

The purpose of this investigation is to analyze and design an active control system for the Seismically Stable Platform (SSP) at the Central Inertial Guidance Test Facility, (CIGTF) at Holloman Air Force Base, New Mexico.

An inertial test platform such as the Seismically Stable Platform must have translation and rotational ground vibrations attenuated or isolated below the candidate test instrument's measurement sensitivity thresholds. An active controller should augment the existing passive isolation system to limit SSP translations to less than 10^{-8}g RMS/Hz and angular tilts to less than 0.02 arcseconds over the required bandwidth of 10^{-8} Hz to 100 Hz. (Ref 1, 14).

To understand the implication of these specifications, a historical overview of seismic platforms is discussed before the problem and approach are revealed.

Historical Perspective

Seismic isolation platforms serve as a controlled environment to test and evaluate inertial grade instruments

needed in aerospace navigation and guidance applications. New missions have demanded greater accuracy and sensitivity. To meet these instrument requirements, the Third Generation of Gyros (TGG) has emerged from instrument technology making past test procedures and environments ineffective. (Ref 15). To judge properly instrument attributes, the bias, drifts, and accuracy profiles must be distinguishable and predictable from test platform background disturbances. Angular tilts and specific force or acceleration disturbances are critical in gyroscope and accelerometer sensor evaluations. Disturbances may be either measured, modeled and compensated in test profiles or completely (or nearly) removed or isolated from testing parameters. The SSP will isolate disturbances.

Early Air Force efforts in gyro testing and tilt stabilization were at the Frank J. Sieler Research Laboratory, United States Air Force Academy using the Iso-Pad isolation test platform (Ref 21). Numerous efforts (Ref 4, 5, 23) were made to control tilt or position as well as angular acceleration (translational acceleration, in accelerometer testing). Tilt control was possible but translational accelerations were limited to 10^{-8}g RMS/Hz above 10 Hz only (Ref 3:18).

On the basis of the Iso-Pad control design efforts, a seismic platform was needed with a lower structure resonance.

Engineers at FJSRL and CIGTF reviewed the dual reactionary mass concept and had an isolation system constructed at Holloman A.F.B. (Ref 24).

Background

The dual reactionary mass system was added to an existing seismic concrete block by the contractor, Measurement Analysis Corporation (MAC). Concrete pillars were added to the seismic block and a steel box-beam ring was placed on pneumatic isolators atop the pillars. On the ring were placed yet another set of pneumatic isolators with a steel platform which would contain the gyro table work station. The pneumatic isolators and steel structures comprise a passive isolation system, as shown in Figure 1.1. This system is designed to respond as a double low pass filter above 20 Hz, limiting tilt less than ±0.02 arcseconds, and accelerations to less than 10^{-8}g RMS/Hz. Recent measurements by CIGTF engineers (Ref 18) do not support the desired passive response. These discrepancies are expanded in Chapter IV, SSP Passive Response.

Problem

The objective of this thesis investigation is to analyze and design an active control system that stabilizes the CIGTF Seismically Stable Platform (SSP) to within ±0.02 arcseconds rotation and 10^{-8}g RMS/Hz translation in all axes over the

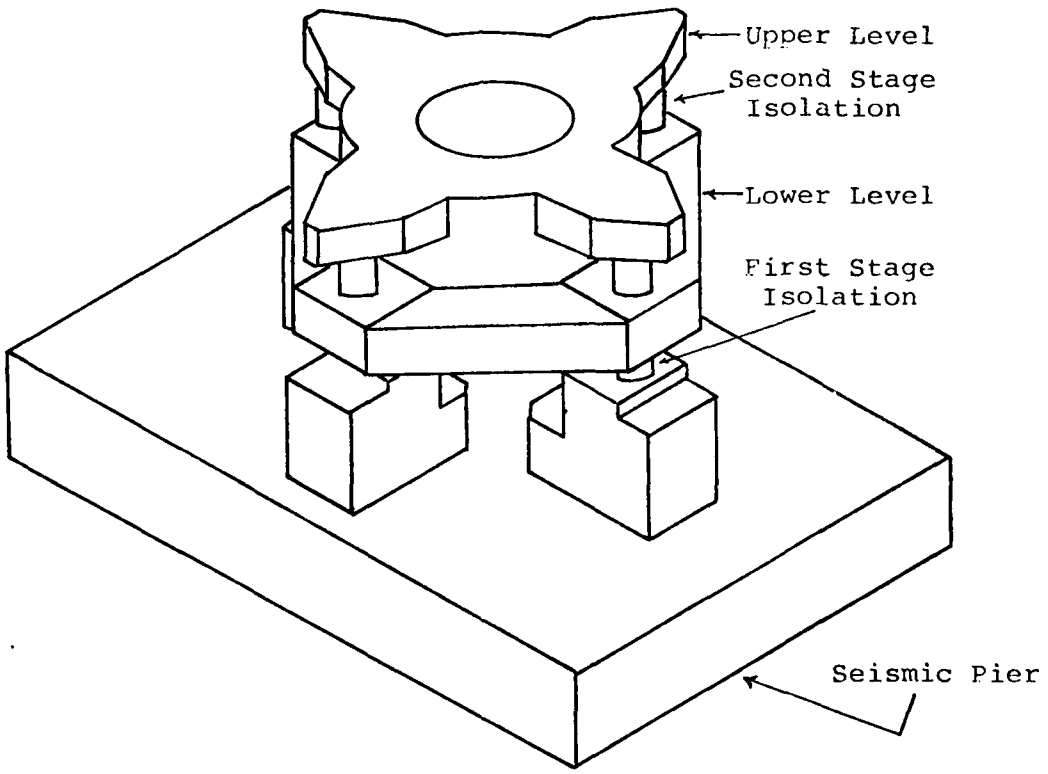

Figure 1.1. SSP Passive Isolation System

bandwidth of 10^{-8} Hz to 20 Hz. These constraints result from accuracy and sensitivities generic to the TGG evaluation and are expanded in Chapter II, SSP Functional Requirements.

Scope and Assumptions

The analysis fully investigates the SSP dynamics model to predict and to verify passive response characteristics. A control law is built on the SSP dynamics to meet the specifications using Linear Quadratic (LQ) theory. (Ref 6:415).

The Separation Theorem or Principle (Ref 12) is imposed to consider the state estimation and controller design issues separately. Basically, the control law considerations are investigated assuming the SSP sensors provide perfect state information. The state representation looks at the three body dynamics of the seismic concrete block and two structural members of the SSP perturbed about a nominal system orientation. Only first order effects and linearized equations are included in the SSP perturbation models. The dynamics development clearly identifies when these approximations are made, completely portraying rotation and translation coupling modes. Finally, the study assumes that the passive isolation system is effective in removing rotational and translation disturbances from 20 Hz to 100 Hz. The individual body structural resonances of the SSP are assumed to be above 100 Hz (Ref 14:E-3). The control law assumes influence over bandwidth of 10^{-8} Hz to 20 Hz.

The FPS - foot, pound, second - units system is used throughout the study to be consistent with other SSP reports (Ref 14:D-19, Ref 20). Mass units are expressed in lb-sec^2/ft with the acceleration due to gravity, a constant, equal to 32.2 ft/sec^2 (Ref 10).

Approach

The plan of attack is divided in two areas - dynamics model and control law development.

The control law specifies a Linear Quadratic (LQ) - Proportional Plus Integral (PI) controller as the optimum solution (Ref 6). LQ cost weighting emphasizes system states critical to meeting a given performance specification. Proportional Plus Integral control structures are recommended typically (Ref 6:340) for disturbance rejection and were proposed by MAC for the SSP (Ref 14:D-22). Discrete time and actuator energy cost criteria validate the feasibility of the control problem solution.

Overview

The remainder of the thesis is divided into a set of controller requirements, dynamics modeling, passive response and LQ design.

Chapter II, SSP Functional Requirements, covers the important dynamic model constraints and expected control responses needed to outline the active controller design.

Chapter III, SSP Dynamics, develops the full six degree of freedom equations for each of the three body complete systems.

Chapter IV, SSP Passive Response, examines various stages of isolation for transmissibility and stability analysis.

Chapter V, Active Controller Design, develops the truth model and the reduced order state equations into a control law resulting in a steady error within the problem requirements. Reduced order alternative models are compared with the system truth model.

Chapter VI, Conclusions and Recommendations, summarizes the dynamics modeling and controller problem which leads to recommendations for future work.

II. SSP Functional Requirements

Introduction

To understand better the Seismically Stable Platform (SSP) specifications, a discussion of the generating inertial instrument's requirements and the SSP is necessary. In 1975, the Charles Stark Draper Laboratory commented on gyro testing environments needed to support the Third Generation of Gyros (TGG) (Ref 15). These considerations are the driving force behind SSP development. With these constraints in mind, the SSP system analysis considers tilt disturbance constraints which are important in gyro evaluation, and translation acceleration disturbance constraints as the prime error in accelerometer testing.

SSP Description

The SSP is a dual reactionary mass isolation platform designed to have a passive transmissibility to seismic disturbances of -40 dB/decade above 20 Hz to 100 Hz (Ref 15:5). The active controller is concerned with the transmissibility from 10^{-8} Hz to 20 Hz.

The dual reactionary mass concept is explained best by describing the SSP subsystems in Figure 2.1. The top isolation level or subsystem is a welded steel cylinder with reinforced walls, suspended by its top at four symmetrical horizontal points by steel boxed beam tabs. This upper level housing

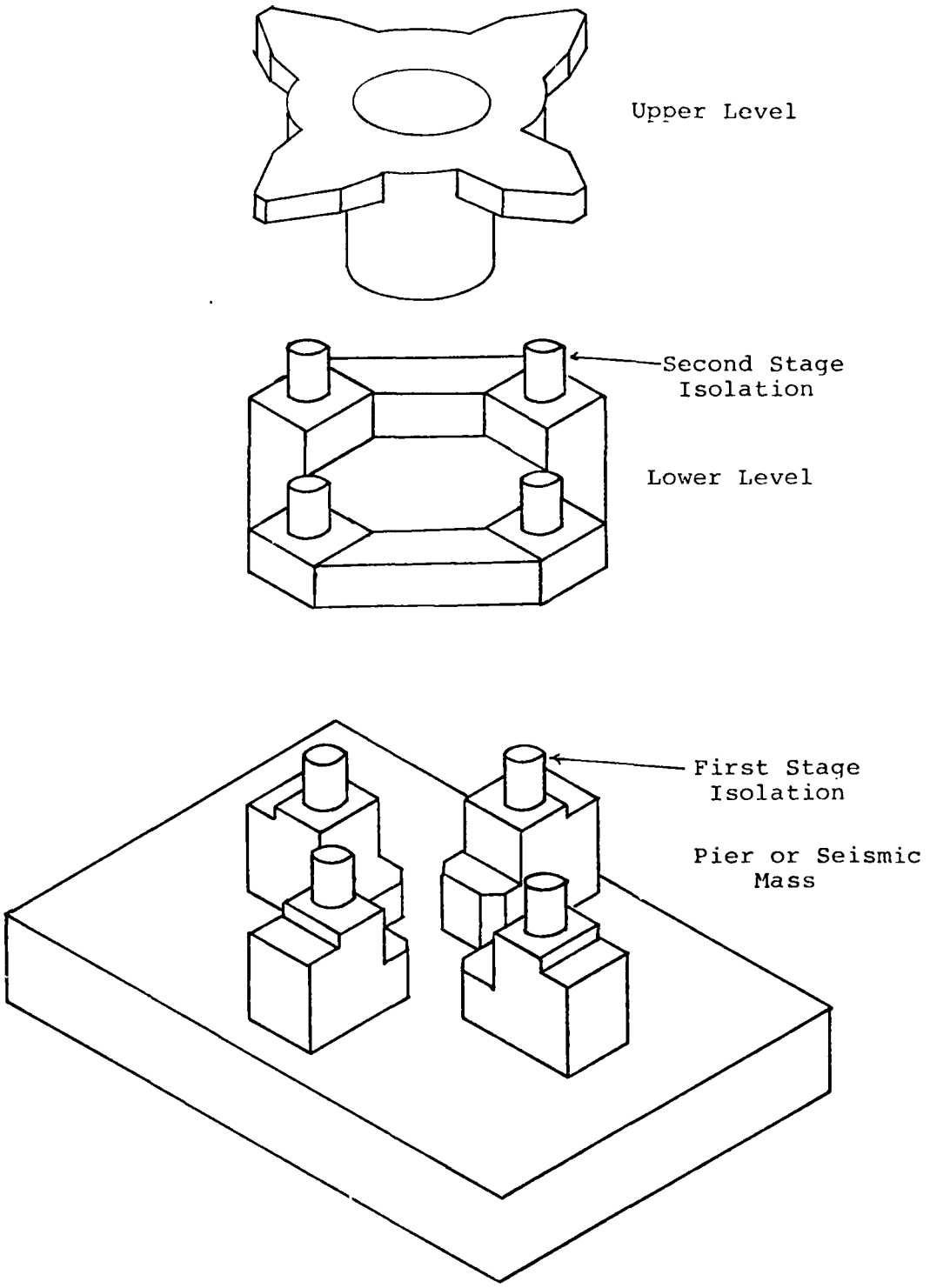

Figure 2.1 SSP Subsystems

is recessed for a gyro test table. Below the suspension points are four Barry AL-133-12 pneumatic isolators, referred to as the "Second Stage Isolation" in the study analysis. The top steel structure and gyro table are the "Upper Level", known as primary mass or reactionary mass in other literature (Ref 14).

Directly below the second stage isolation is a second subsystem, the "Lower Level" which is also identified in other reports as the secondary mass or intermediate mass. The lower level is an octagonal box beam recessed on the top and bottom to receive the second stage and first stage pneumatic isolators as shown.

Appendix A discusses the subsystem dimensions and physical attributes. The upper level mass is twice the weight of the lower level to give a two stage transmissibility attenuation to disturbances, with the lower stage giving the first low pass second order response, and the second stage following a lower frequency cutoff second order response. Chapter IV, Passive Response, fully explains the theoretical responses and transmissibility concept.

The SSP is centered on a concrete seismic mass atop concrete pillars or piers. Future analysis will include the concrete piers and seismic block as simply the "pier". The pier subsystem is physically isolated below ground level from the laboratory vibration environment by a rubber grouted air gap. Figure 2.2 shows the general orientation of the SSP, the seismic pier and laboratory. The seismic

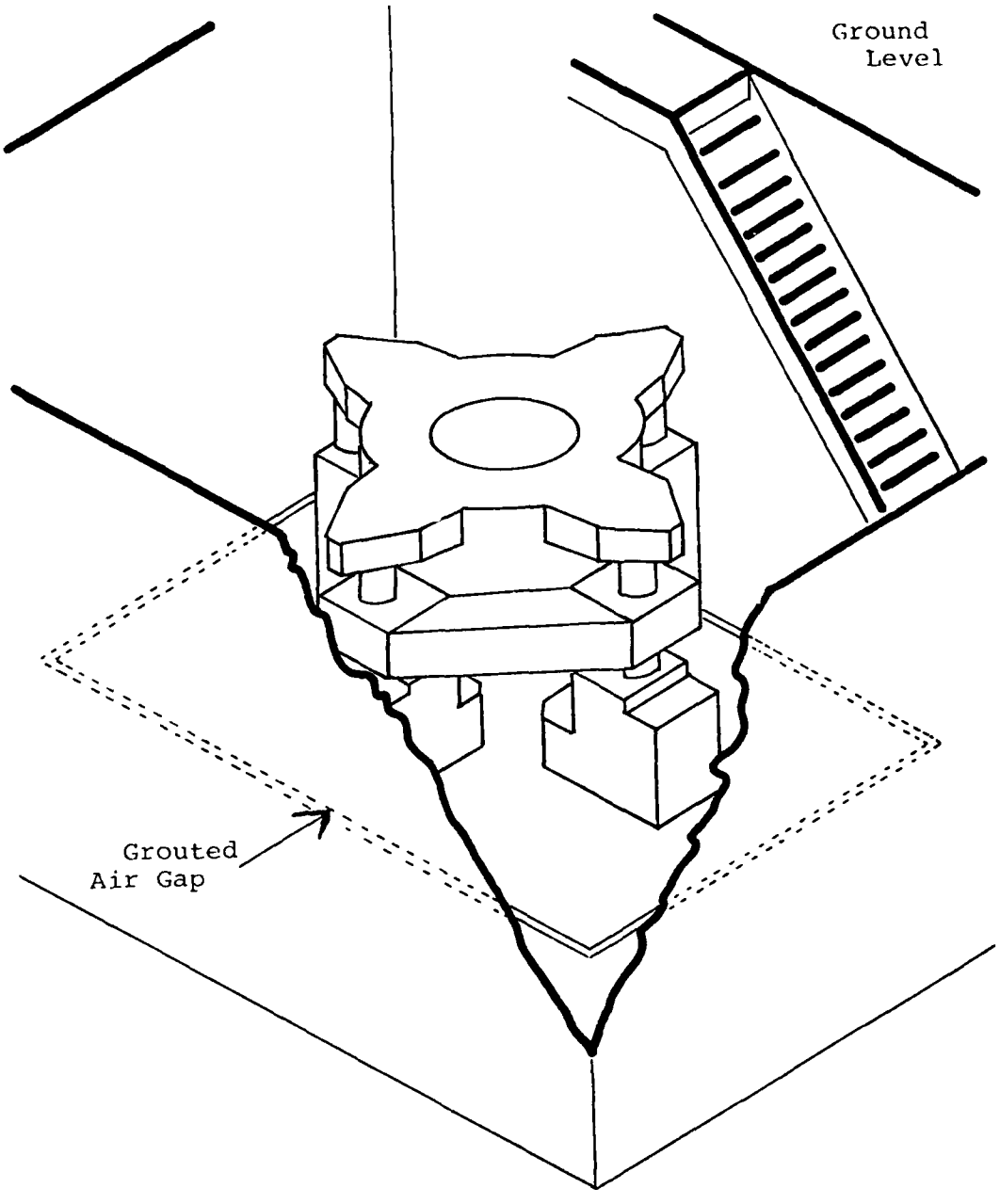

Figure 2.2. SSP Laboratory Environment

block subsystem and supporting soil should offer yet another second order low pass response concerned with frequencies higher than the SSP isolation. Again, Chapter IV develops the expected dynamics further.

The supporting piers, lower and upper structures and the pneumatic isolators comprise the passive isolation system. How the SSP problem specifications and the TGG specifications apply to the passive system are examined next.

Third Generation Gyro (TGG) Specifications

Quoting from Charles Stark Draper Laboratory (CSDL) Report, (Ref 15:1).

> "The resolution of these new inertial instruments is expected to be so fine that instrumentation errors and uncertainties must be modeled and verified in order to establish the sources of instrument noise... the following assumptions will be made for performance goals of the next generation of instruments:
>
> (1) Angular motion uncertainty 10^{-5}meru.
>
> (2) Linear motion uncertainty 10^{-9}g.
>
> (3) Measurement bandwidth 10^{-7}Hz to 10^{-2}Hz."

Each CSDL - TGG specification is examined to determine the implied constraints on the SSP dynamics and performance specifications.

Item (1) concerns the angular motion uncertainty of 10^{-5} meru's - milli earth rate units, or 1.5 X 10^{-7} arcseconds/second. This conversion is shown in Appendix B. The SSP specifications do not include an angular acceleration requirement. For a pure ±0.02 arcsecond tilt and using time averaging (see Appendix B), the angular acceleration over the 10^{-8} Hz to 100 Hz bandwidth results in angular rates from ± 2 X 10^{-10} arcseconds/second to 2 arcseconds/second. This study was not given a pure angular acceleration specification. Translation accelerations are limited in all axes to 10^{-8} g RMS/Hz.

Item (2) arises from a navigational error of one hundred feet on the Earth's surface averaged over an hour flight. Appendix B shows how the 10^{-9} g measure is achieved and demonstrates the use of average linear velocity and acceleration approximations. The SSP translation acceleration constraint is now 10^{-8} g's, but future plans (Ref 20) include a nano-g (10^{-9} g) performance specification.

Item (3) concerns the measurement bandwidth which is implied by the need to observe the test environment for disturbances lasting 100 second periods to the full test cycle of 120 days. Appendix B shows this basic derivation. CIGTF presently has a goal of 90 days. The SSP bandwidth requirement matches the lower limit but exceeds the CSDL item (3) specification in order to remove existing ground

motions above 10^{-3} Hz to 20 Hz; 20 Hz and above is augmented with the passive isolation system.

The sources and characteristics of seismic disturbances are next discussed to understand the source of acceleration and tilt vibrations.

Environmental Disturbances

The SSP passive isolation system and an active control system together must remove translational and rotational disturbances detrimental to inertial instrument evaluation. Until the possible disturbance mechanisms and physical strengths (magnitude excursions) are understood, the control issues in relation to design specification are not clear.

Seismic disturbances arise from distant earthquakes, micro-seismic waves, cultural noise, low frequency tilt, acoustical noise, test environment temperature changes, and stray electro-magnetic fields (Ref 15:5).

Earthquakes can induce accelerations typically on the order of 1.6×10^{-6} g at 0.2 Hz and surface waves of 0.4 inches displacement at 0.05 Hz and 100×10^{-6} g (Ref 15:5). Micro-seismic waves, or microseisms are minute waves that continually move through the surface of the Earth and are caused by weather fronts and ocean waves. The most prominent and important microseisms are at frequencies 0.14 Hz to 0.25 Hz with accelerations of 0.8×10^{-6} g to 6×10^{-6} g with amplitudes from 400 to 1000 micro inches (Ref 15:4).

Cultural noise is a manmade disturbance caused from vehicle traffic, aircraft, rocket sled tracks and mechanical machinery such as air compressors and air conditioners. Cultural noise typically peaks at 29 Hz and 59 Hz with acceleration of 10^{-3} g (Ref 11:10).

Low-frequency tilts may be caused from building temperature distortions in a predominately northerly direction (northern hemisphere) of about 20 arcseconds with seasonal variations of 90 arcseconds. This temperature distortion can occur at rates of 34 X 10^{-3} meru (Ref 15:2).

Acoustic wavefronts within the test area can cause low-frequency motions much like barometric variations caused by weather effects and sonic noises caused by jet aircraft. In a test environment, pressure and temperature are usually monitored and controlled; but their effects are very critical in the operation of seismometers as well as any gradients across structures like the SSP.

Electromagnetic fields can cause small torque disturbances. These field intensities also may induce very low frequency signal noise effects into sensor measurements through voltages induced in cabling directly or indirectly through ground loops in instrument amplifiers or A/D converters.

Seismometer theory is not addressed in this study since perfect system knowledge is assumed, but the disturbance characterizations just mentioned for various phenomena have one significant dilemma. All the disturbances typified are

using measurement technology that cannot approach periods of longer than 1000 seconds (10^{-3} Hz) and the required 10^{-8} g's sensitivity (Ref 8). Projected future test platform bandwidths for inertial testing require 90 day (10^{-8} Hz) test cycles or periods. Measurement considerations have been detailed in several reports (Ref 14:10-11; 20:15-19; 22), but inertial testing needs to rely on parameter estimation techniques (Ref 12) and the hope of future seismic instrumentation technology.

Another problem unique to the SSP is vertical leveling of the four support points for the upper and lower masses or levels. A problem arises in getting all four isolators adjusted to level each corner of the SSP structure (Ref 2). Each isolator has a mechanical limit switch preadjusted to keep isolator height constant under load variations. In a four point suspension, Management Analysis Corporation (MAC) feared that one isolator would be above or below the nominal plane for a given level, and the affected level would warble or tip; similar to the problem of cutting a chair's four legs to the same length. A three point suspension avoids this tipping phenomena, so the South and East isolator for each stage have their air supply regulated by only one stage limit switch. The dynamics and controller analysis account for this characteristic. With problem requirements outlined, the SSP dynamics model is now developed.

III. Dynamics Analysis

Introduction

The SSP dynamics are described by linearized differential equations using force and angular momentum relationships. A full six degree of freedom development - three translational and three rotational modes, considers perturbed states of the upper and lower level, and pier subsystems.

The perturbed states are described about a nominal coordinate frame for each of the three bodies for the six degrees of freedom. Each coordinate frame uses a unique subscript notation to identify clearly the SSP dynamics derived from a lumped spring/damper network model. Once the representative equations of motion are obtained, translational and rotational cross coupling terms are identified. Before the analysis begins, a coordinate frame is defined for each SSP structure along with variables describing each structure's motion.

SSP Coordinate Frames

Before even a simple mass spring system can be analyzed, all coordinate frames, variables and references must be defined. With the SSP dynamics, naming conventions are particularly important because the resulting complex differential equations exhibit forms common to much simpler mechanical

models. Also, validity checks on the equations are much easier to relate physically to the SSP.

A body coordinate frame is fixed to the upper level (U), lower level (L) and the pier (P). Figure 3.1 shows the body frames and their orientation. A right-handed unit vector is defined by $\hat{u}_3 = \hat{u}_1 \times \hat{u}_2$ for the upper level and similarly for the lower and pier frames. Notice at $\hat{u}_2$, $\hat{l}_2$, and $\hat{p}_2$ are oriented in the navigational North sense, in the nominal position. Additionally, a nominal state is assigned with $\hat{u}_3$, $\hat{l}_3$ and $\hat{p}_3$ oriented along the local vertical $\hat{e}_3$. The $\underline{e}$ frame, the Earth frame, is taken as inertial.

Rotation angles in each frame are as shown, with ψ_u, ϕ_u and Θ_u for rotations about the Earth frame $\hat{e}_1$, $\hat{e}_2$ and $\hat{e}_3$ respectively for the upper level body. The lower level and pier rotations are defined similarly. Appendix C details the direction cosine transformation matrices necessary to express position and velocity vectors in the respective body frames to the Earth frame. The transformation matrices are derived using small angle, first order approximations as verified by Likins (Ref 10:102). Such approximations assume the SSP oriented in a nominal state and perturbed in small angular motions about the respective centers of mass.

To understand the importance of the direction cosine transformation and to gain the insight necessary to write the

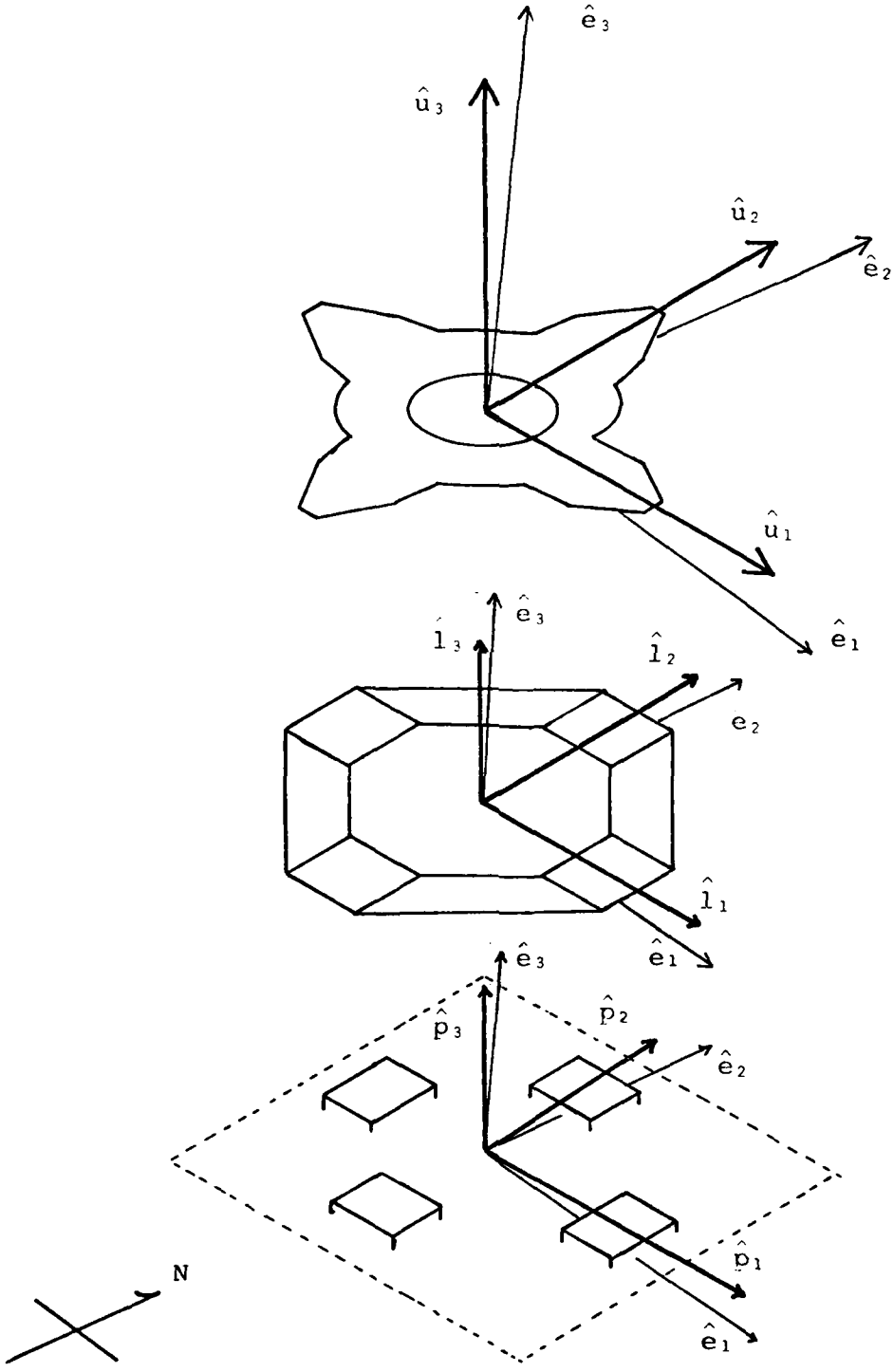

Figure 3.1 SSP Body Frames

full six degree equations of motion, the motion of a single typical corner of the SSP is analyzed for a small perturbation about a nominal orientation.

Corner Perturbation Derivative

The perturbed state of a body corner or isolator suspension point is derived in Appendix D. Details of derivation relate translational and rotational modes can be more clearly understood from Figure D.1. The vector notation $\overline{UE}$, which is a position vector in Earth frame relating to the upper level (U), easterly (E) corner, is used extensively to write the equations of motion. Similarly $\overset{\circ}{\overline{UE}}$ means the time derivative, Earth frame.

Now the isolator suspension points are defined in matrix notation; the pneumatic isolator characteristics are related in vector components.

Isolator Lumped Parameters

Before the SSP equations of motion can be written, the pneumatic isolator is represented by a directional lumped spring/damper network or conceptually as spring/damper matrices.

According to studies by MAC (Ref 14:C-10), the pneumatic isolator has nearly the same resiliency in the vertical and two horizontal axes for small load deflections. Essentially,

the isolator is depicted as in Figure 3.2, Isolator Model. Notice the symbology used as well as the matrix notation. For example,

$$C_F = \begin{bmatrix} c_{FX} & 0 & 0 \\ 0 & c_{FY} & 0 \\ 0 & 0 & c_{FZ} \end{bmatrix} \left[\underline{e} \right] \qquad (3\text{-}1)$$

implies a matrix damper (C) for the first state isolation (F). The matrix then is expressed in Earth ($\underline{e}$) unit vectors, with c_{FX} meaning first stage isolation, X or $\hat{e}_1$ direction. Likewise K would be a matrix spring. The isolator characteristics are expressed in Earth frame components without direction cosine transformation. This assumption is made because vertical characteristics are due mainly to the pneumatic isolator itself, with horizontal characteristics due mainly to the isolator seal (elastomer diaphragm) stiffness (Ref 14:C-10). Since the perturbation of the isolator would not reorientate these characteristics appreciably, no matrix transformation is done. Vector spring and damper effects of the relative subsystems' displacement and velocity accounts for any compensation in isolator dynamics orientation.

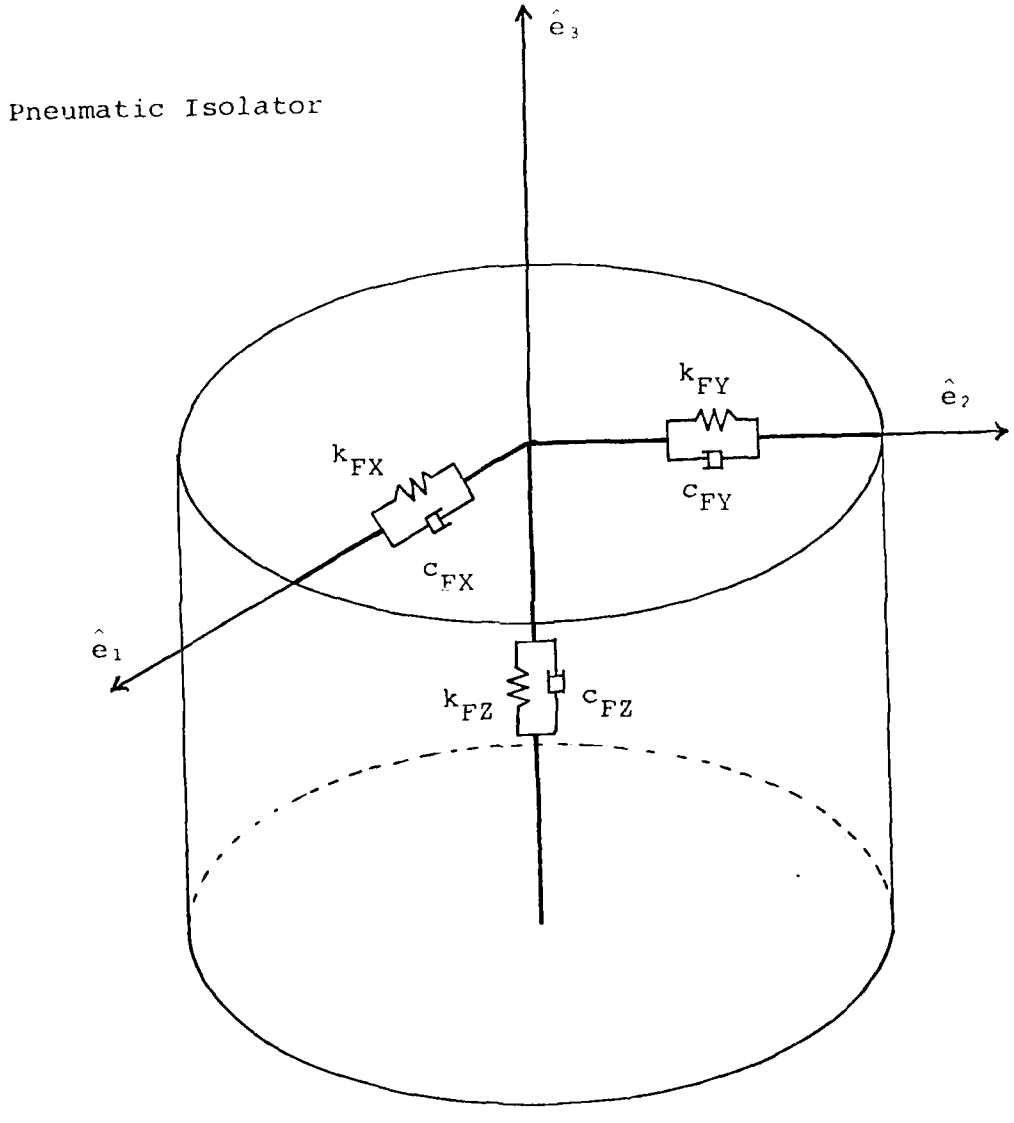

$$K_F = \begin{bmatrix} k_{FX} & 0 & 0 \\ 0 & k_{FY} & 0 \\ 0 & 0 & k_{FZ} \end{bmatrix} \qquad C_F = \begin{bmatrix} c_{FX} & 0 & 0 \\ 0 & c_{FY} & 0 \\ 0 & 0 & c_{FZ} \end{bmatrix}$$

F, first stage isolation

Figure 3.2 Isolator Model

The Barry Controls AL-133-12 Serva-Levl pneumatic isolator characteristics have been studied by MAC (Ref 14:C-53). Essentially the vertical characteristics are a function of the individual isolator's load and air supply, MAC determined the vertical natural frequency (f_{VN}) to be 1.8 Hz. From the same report, the horizontal natural frequency (f_{HN}) is 4.0 Hz and 3.8 Hz for the upper and lower level isolators, respectively. Each isolator axis represents a second order system, comprised of a single mass, spring and damper shown in Figure 3.3. The differential equation, using Laplace operator, zero initial conditions, is

$$ms^2 X(s) = -csX(s) - kX(s) + F(s) \qquad (3\text{-}2)$$

$$\frac{X(s)}{F(s)} = + \frac{1/m}{s^2 + \frac{c}{m} s + \frac{k}{m}} \qquad (3\text{-}3)$$

The denominator of Eq 3-3 is in a classical second order form or in generalized function of natural frequency (ω_N) and damping ratio (ζ).

$$s^2 + 2\zeta\omega_N s + \omega^2_N \qquad (3\text{-}4)$$

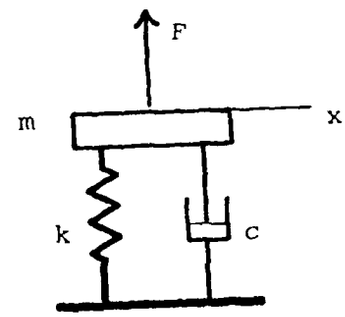

m, mass

k, spring stiffness

c, damping coefficient

x, displacement

F, applied force, positive x direction

Figure 3.3 Single Mass, Spring and Damper

Equalling like order coefficients of Eq 3-3 to Eq 3-4, the following relations are implied:

$$2\zeta\omega_N = \frac{c}{m} \tag{3-5}$$

$$c = 2\zeta\omega_N m \qquad \omega_N = 2\pi f \tag{3-6}$$

f, frequency in hertz

$$c = 4\pi\zeta f m \tag{3-7}$$

also

$$\omega_N^2 = \frac{k}{m} \tag{3-8}$$

$$k = \omega_N^2 m \tag{3-9}$$

$$k = (2\pi f)^2 m \tag{3-10}$$

Using these relationships and the MAC derived natural frequencies, the second stage isolator spring and damper coefficients are calculated using one fourth (four isolators) the upper level mass (Ref 14:C-53):

$$f_{VN} = 1.8 \text{ Hz} \quad \text{Load} = m_U/4 = 132.56 \ \frac{\text{lb-sec}^2}{\text{ft}} \tag{3-11}$$

where

$$m_U = 530.22 \ \frac{\text{lb-sec}^2}{\text{ft}}$$

$$k_{SZ} = 16955.12 \text{ lb/ft}$$

$$c_{SZ} = 89.95 \ \frac{\text{lb-sec}}{\text{ft}}$$

$$f_{VH} = 4.0 \text{ Hz} \qquad (3\text{-}12)$$

$$K_{SX} = 83728.99 \text{ lb/ft}$$

$$C_{SX} = 199.89 \ \frac{\text{lb-sec}}{\text{ft}}$$

Appendix E summarizes all the lumped spring and damper parameters used in this study. References are given to appropriate pages in MAC study (Ref 14) which give further details and derivations.

Now the subsystem coordinate frames and dynamical characteristics are described using matrix notation generic to the SSP.

SSP Equations of Motion - Six Degrees of Freedom

The SSP has six degrees of freedom - three translational ($\hat{e}_1$, $\hat{e}_2$, $\hat{e}_3$) and three rotational (ψ, 0, ϕ) for three bodies or structures - the upper level (U), lower level (L) and pier (P). An equation is written for each corner (such as $\overline{UE}$, $\overline{UN}$, $\overline{UW}$, $\overline{US}$) of each body. Then each equation is

resolved into Earth components and the translational and rotation effects segregated.

A lumper parameter model for the SSP is shown in Figure 3.4. Various levels of isolation are indicated for the soil or ground (G) isolation, first stage pneumatic isolators (F) and second stage pneumatic isolators (S) using the matrix spring and damper concepts. The spring and damper characteristics are expressed in $\underline{e}$ unit vectors, but the spring and damper end points are vector points. For example, $\overline{LE}$ and $\overline{UE}$ have K_s and C_s connecting them. $\overline{LE}$, $\overline{LN}$, $\overline{LW}$, $\overline{LS}$ all are points in the plane representing the lower level steel-boxed ring. Similarly the upper level platform and pier seismic block are described.

From basic spring and damper dynamics for one dimension, the following equations result for the spring (F_S) and damper (F_C) forces.

$$F_S = kx \tag{3-13}$$

where

x, spring displacement

k, spring constant

in vector case, using column vectors

$$F_S = [K_S]\ \bar{x} \tag{3-14}$$

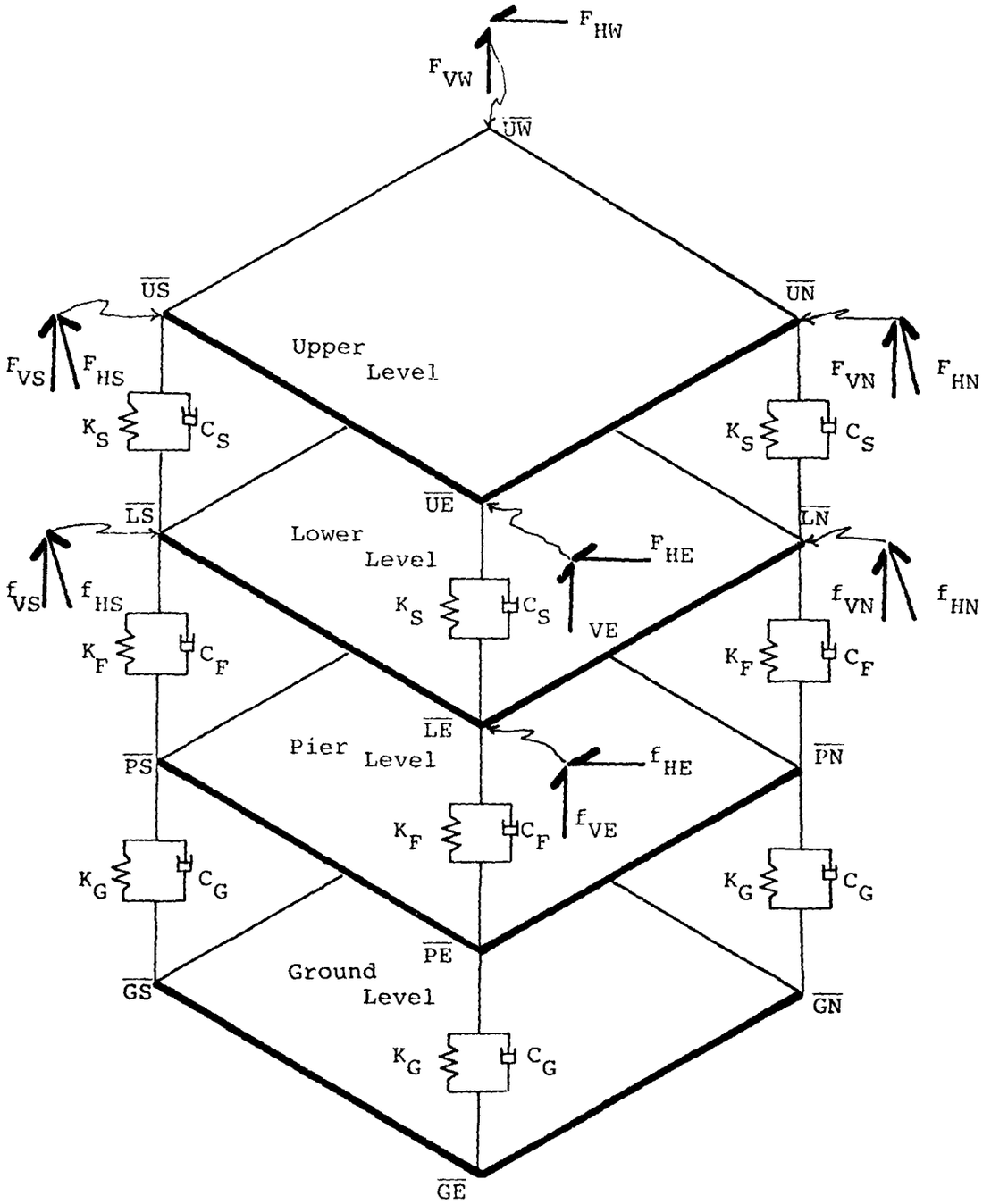

Figure 3.4 SSP Lumped Parameter Model

where $\bar{F}$, $\bar{x}$, K_S

$$\bar{F}_S = \begin{bmatrix} F_x \\ F_y \\ F_z \end{bmatrix} , \quad \bar{X} = \begin{bmatrix} x \\ y \\ z \end{bmatrix} \tag{3-15}$$

$$K_S = \begin{bmatrix} k_{SX} & 0 & 0 \\ 0 & k_{SY} & 0 \\ 0 & 0 & k_{SZ} \end{bmatrix} \tag{3-16}$$

$$\begin{bmatrix} F_x \\ F_y \\ F_z \end{bmatrix} = \begin{bmatrix} k_{SX} & 0 & 0 \\ 0 & k_{SY} & 0 \\ 0 & 0 & k_{SZ} \end{bmatrix} \bar{x} = \begin{bmatrix} k_{SX}x \\ k_{SY}y \\ k_{SZ}z \end{bmatrix} \tag{3-17}$$

The form of Eq 3-14 is chosen to make algebraic manipulation easier.

The equations for the damper in scalar and vector case are

$$F_c = c\dot{x} \tag{3-18}$$

where,

$\dot{x}$, damper velocity

c, damping coefficient

$$F_{cs} = [C_S] \overset{\circ}{\bar{x}} \tag{3-19}$$

where $\bar{F}$, $\bar{x}$, C_S

$$\bar{F}_c = \begin{bmatrix} F_x \\ F_y \\ F_z \end{bmatrix}, \quad \overset{\circ}{\bar{x}} = \begin{bmatrix} \overset{\circ}{x} \\ \overset{\circ}{y} \\ \overset{\circ}{z} \end{bmatrix} \quad C_S = \begin{bmatrix} c_{SX} & 0 & 0 \\ 0 & c_{SY} & 0 \\ 0 & 0 & c_{SZ} \end{bmatrix}$$

$$\begin{bmatrix} F_X \\ F_Y \\ F_Z \end{bmatrix} = \begin{bmatrix} c_{SX} & 0 & 0 \\ 0 & c_{SY} & 0 \\ 0 & 0 & c_{SZ} \end{bmatrix} \overset{\circ}{\bar{x}} = \begin{bmatrix} c_{SX}\overset{\circ}{x} \\ c_{SY}\overset{\circ}{y} \\ c_{SZ}\overset{\circ}{z} \end{bmatrix} \tag{3-20}$$

Again Eq 3-19 is written in a form to simplify equations later in development. The displacement vector $\bar{x}$ and velocity vector $\overset{\circ}{\bar{x}}$ concept can easily be written using $\overline{UE}$ and $\overset{\circ}{\overline{UE}}$ notation by writing components as column vectors in the $\underline{e}$ frame. Eqs D-6, D-10, in Appendix D, show $\overline{UE}$ and $\overset{\circ}{\overline{UE}}$ in vector notation.

Extending the above dynamic force vectors, $\bar{F} = m\bar{a}$ can be written for the SSP from Figure 3.4. The SSP is a constant mass system. Newton's Second Law concerns the inertial center of mass acceleration of each body as $\overset{\circ\circ}{\bar{U}}$, $\overset{\circ\circ}{\bar{L}}$ and $\overset{\circ\circ}{\bar{P}}$ for the upper level, lower level and pier, respectively.

Summing the forces on each body due to isolator spring/damper equivalents and active controller actuators, results in the following equations. For the upper level, the summing forces yields,

$$\begin{aligned} m_U\ddot{\overline{U}} = \; & C_S(\dot{\overline{LE}} - \dot{\overline{UE}}) + K_S(\overline{LE} - \overline{UE}) \\ & + C_S(\dot{\overline{LN}} - \dot{\overline{UN}}) + K_S(\overline{LN} - \overline{UN}) \\ & + C_S(\dot{\overline{LW}} - \dot{\overline{UW}}) + K_S(\overline{LW} - \overline{UW}) \\ & + C_S(\dot{\overline{LS}} - \dot{\overline{US}}) + K_S(\overline{LS} - \overline{US}) \\ & + \overline{F}_{UE} + \overline{F}_{UN} + \overline{F}_{UW} + \overline{F}_{US} \end{aligned} \qquad (3\text{-}21)$$

Where $\overline{F}_{UE}$, $\overline{F}_{UN}$, $\overline{F}_{UW}$ and $\overline{F}_{US}$ are the four active controller actuators between the upper level and pier.

Similarly, the lower level equations are as follows,

$$\begin{aligned} m_L\ddot{\overline{L}} = \; & -C_S(\dot{\overline{LE}} - \dot{\overline{UE}}) - K_S(\overline{LE} - \overline{UE}) \\ & - C_S(\dot{\overline{LN}} - \dot{\overline{UN}}) - K_S(\overline{LN} - \overline{UN}) \\ & - C_S(\dot{\overline{LW}} - \dot{\overline{UW}}) - K_S(\overline{LW} - \overline{UW}) \\ & - C_S(\dot{\overline{LS}} - \dot{\overline{US}}) - K_S(\overline{LS} - \overline{US}) \end{aligned}$$

$$+C_F(\dot{\overline{PE}} - \dot{\overline{LE}}) \quad - K_F(\overline{PE} - \overline{LE})$$

$$+C_F(\dot{\overline{PN}} - \dot{\overline{LN}}) \quad - K_F(\overline{PN} - \overline{LN})$$

$$+C_F(\dot{\overline{PW}} - \dot{\overline{LW}}) \quad - K_F(\overline{PW} - \overline{LW})$$

$$+C_F(\dot{\overline{PS}} - \dot{\overline{LS}}) \quad - K_F(\overline{PS} - \overline{LS}) \qquad (3\text{-}22)$$

Likewise, the pier force equations are as follows:

$$\begin{aligned} m_P\ddot{P} = \; & -C_F(\dot{\overline{PE}} - \dot{\overline{LE}}) - K_F(\overline{PE} - \overline{LE}) \\ & -C_F(\dot{\overline{PN}} - \dot{\overline{LN}}) - K_F(\overline{PN} - \overline{LN}) \\ & -C_F(\dot{\overline{PW}} - \dot{\overline{LW}}) - K_F(\overline{PW} - \overline{LW}) \\ & -C_F(\dot{\overline{PS}} - \dot{\overline{LS}}) - K_F(\overline{PS} - \overline{LS}) \\ & +C_G(\dot{\overline{GE}} - \dot{\overline{PE}}) - K_G(\overline{GE} - \overline{PE}) \\ & +C_G(\dot{\overline{GN}} - \dot{\overline{PN}}) - K_G(\overline{GN} - \overline{PN}) \\ & +C_G(\dot{\overline{GW}} - \dot{\overline{PW}}) - K_G(\overline{GW} - \overline{PW}) \\ & +C_G(\dot{\overline{GS}} - \dot{\overline{PS}}) - K_G(\overline{GS} - \overline{PS}) \\ & - \overline{F}_{PE} - \overline{F}_{PN} - \overline{F}_{PW} - \overline{F}_{PS} \end{aligned} \qquad (3\text{-}23)$$

Notice that the $-\overline{F}_{PE}$, $-\overline{F}_{PN}$, $-\overline{F}_{PW}$ and $-\overline{F}_{PS}$ forces result from the four active controller actuators being connected between the upper level corners and the pier foundations.

Appendix F manipulates Eqs 3-21, 3-22 and 3-23 into differential equations for the $\underline{e}$ components of each body acceleration and applied dynamic forces. Appendix F yields the differential equations describing the three degrees of translational for the SSP. Although rotational terms are present, two important points are made. First, for small angular movements the rotational terms certainly aid translational positions and velocities, as a quick units check verifies. Secondly, if the SSP isolator placement is theoretically symmetrical, all rotation contributions vanish, which is physically reassuring showing that the equations are correct. Now the three degrees of rotational freedom are investigated to complete the dynamics description of the SSP.

Rotational equations of motions of the three bodies - upper level, lower level and pier, result from summing moments about each body center of mass and examining the resultant angular accelerations. Expressed more formally, the rotational equivalent of Newton's Second Law is $\overline{M} = \overset{\circ}{\overline{H}}$ (Ref 10:438), where $\overline{M}$ is the moment vector about the body center mass and $\overset{\circ}{\overline{H}}$ is the time derivative in an inertial frame of the vector angular momentum, $\overline{H}$.

The angular momentum and its derivative are expanded to show the mathematical relationship to the body moments of the SSP. Angular momentum is written as

$$\bar{M} = \mathring{\bar{H}} \tag{3-24}$$

where,

$\bar{H}$, angular momentum

$\mathring{\bar{H}}$, time derivative, inertial frame

$\bar{M}$, body moments

The relationship is derived for the upper body as,

$$\bar{H}_U = I_U \bar{\omega}_U \tag{3-25}$$

where,

I_U , moment of inertia matrix

$\bar{\omega}_U$, angular velocity vector

$$I_U = \begin{bmatrix} I_{UX} & 0 & 0 \\ 0 & I_{UY} & 0 \\ 0 & 0 & I_{UZ} \end{bmatrix} \tag{3-26}$$

I_{UX} , I_{UY} , I_{UZ} are body moments of inertia about $\hat{u}_1$, $\hat{u}_2$, $\hat{u}_3$ axes.

$$\bar{\omega}_U = \mathring{\psi}\hat{u}_1 + \mathring{\phi}\hat{u}_2 + \mathring{\Theta}\hat{u}_3 \tag{3-27}$$

$\mathring{\psi}$, $\mathring{\phi}$, $\mathring{\Theta}$ are tilt rates defined in Appendix C.

$$\bar{H}_U = \begin{bmatrix} I_{UX} & 0 & 0 \\ 0 & I_{UY} & 0 \\ 0 & 0 & I_{UZ} \end{bmatrix} \begin{bmatrix} \overset{\circ}{\psi}\hat{u}_1 \\ \overset{\circ}{\phi}\hat{u}_2 \\ \overset{\circ}{\theta}\hat{u}_3 \end{bmatrix} \tag{3-28}$$

$$\bar{H}_U = I_{UX}\overset{\circ}{\psi}\hat{u}_1 + I_{UY}\overset{\circ}{\phi}\hat{u}_2 + I_{UZ}\overset{\circ}{\theta}\hat{u}_3 \tag{3-29}$$

The components of the upper level moment matrix are written as,

$$M_U = M_{UX}\hat{u}_1 + M_{UY}\hat{u}_2 + M_{UZ}\hat{u}_3 \tag{3-30}$$

where,

M_{UX} , M_{UY} , M_{UZ} are moments about $\hat{u}_1$, $\hat{u}_2$ and $\hat{u}_3$ axes.

Equating components in $\underline{u}$ frame, and transforming to $\underline{e}$ frame using small angle, first order approximations derived in Appendix C, the upper level moments relate to angular accelerations as,

$$M_{UX}\hat{u}_1 = I_{UX}\overset{\circ\circ}{\psi}_U\hat{u}_1 = [I_{UX}\overset{\circ\circ}{\psi}_U - \overset{\circ}{\phi}_U\overset{\circ}{\theta}_U (I_{UY} - I_{UZ})]\hat{e}_1 \tag{3-31}$$

$$M_{UY}\hat{u}_2 = I_{UY}\overset{\circ\circ}{\phi}_U\hat{u}_2 = [I_{UY}\overset{\circ\circ}{\phi}_U - \overset{\circ}{\theta}_U\overset{\circ}{\psi}_U (I_{UZ} - I_{UX})]\hat{e}_2 \tag{3-32}$$

$$M_{UZ}\hat{u}_3 = I_{UZ}\overset{\circ\circ}{\theta}_U\hat{u}_3 = [I_{UZ}\overset{\circ\circ}{\theta}_U - \overset{\circ}{\psi}_U\overset{\circ}{\phi}_U (I_{UX} - I_{UY})]\hat{e}_3 \tag{3-33}$$

Eqs 3-31, 3-32, and 3-33 are known as Euler's equations (Ref 10:439) and may be reduced further using small angle, first order approximations to

$$M_{UX}\hat{u}_1 = I_{UX}\ddot{\psi}_U\hat{e}_1 \tag{3-34}$$

$$M_{UY}\hat{u}_2 = I_{UY}\ddot{\phi}_U\hat{e}_2 \tag{3-35}$$

$$M_{UZ}\hat{u}_3 = I_{UZ}\ddot{\theta}_U\hat{e}_3 \tag{3-36}$$

Using similar transformations and approximations, the lower level is described as

$$M_{LX}\hat{l}_1 = I_{LX}\ddot{\psi}_L\hat{e}_1 \tag{3-37}$$

$$M_{LY}\hat{l}_2 = I_{LY}\ddot{\phi}_L\hat{e}_2 \tag{3-38}$$

$$M_{LZ}\hat{l}_3 = I_{LZ}\ddot{\theta}_L\hat{e}_3 \tag{3-39}$$

and for the pier subsystem,

$$M_{PX}\hat{p}_1 = I_{PX}\ddot{\psi}_P\hat{e}_1 \tag{3-40}$$

$$M_{PY}\hat{p}_2 = I_{PY}\ddot{\phi}_P\hat{e}_2 \tag{3-41}$$

$$M_{PZ}\hat{p}_3 = I_{PZ}\ddot{\theta}_P\hat{e}_3 \tag{3-42}$$

Now the body moments are related to the angular acceleration and moment inertia. The rotation equations are written as vectors for each body and respective isolator and actuator dynamics. A moment is easily described in the scalar case as

$$M = rF \tag{3-43}$$

where,

M, moment

r, radial action arm

F, the applied force

For the vector case, consider a x, y, z cartesian coordinate frame, with r_X in the X direction, F_Z applied in positive Z and M_Y a clockwise moment about the Y axis. In cross product notation this reduces to

$$\bar{M} = \bar{r} \times \bar{F} = -r_X F_Z \hat{y} \tag{3-44}$$

The minus sign indicates a clockwise moment for the example. Now consider the east corner of the upper level

$\overline{(UE)}$ and the lumped parameter vector damper force $[\overline{LE} - \overline{UE}]^T c_S$. Using the concept of Eq 3-19, the damper force in the $\underline{e}$ frame.

$$C_S[\dot{\overline{LE}} - \dot{\overline{UE}}] = c_{SX}(\dot{X}_L - \dot{X}_U)\hat{e}_1 \rightarrow A\hat{e}_1$$
$$+c_{SY}(\dot{Y}_L - \dot{Y}_U + l_{LE}\dot{\Theta}_L - l_{UE}\dot{\Theta}_U)\hat{e}_2 \rightarrow B\hat{e}_2$$
$$+c_{SZ}(\dot{Z}_L - \dot{Z}_U - l_{LE}\dot{\phi}_L + l_{UE}\dot{\Theta}_L)\hat{e}_3 \rightarrow C\hat{e}_3 \quad (3\text{-}45)$$

The moment arm of the isolator on corner $\overline{UE}$ is

$$\overline{UE} = (X_U + l_{UE})\hat{e}_1 + (Y_U + l_{UE}\Theta_U)\hat{e}_2$$
$$+ (Z_U - l_{UE}\phi_U)\hat{e}_3 \quad (3\text{-}46)$$

Since the dynamics analysis is to be a linear model, the moment arm in Eq 3-46 reduces to $l_{UE}\hat{e}_1$. Use of the other terms would include variable products and their derivatives due to the cross product operation. From a physical standpoint, under small angle approximations and perturbations about a nominal body position, such non-linear product terms would be neglectable.

To find the moment offered by the $\overline{UE}$ damper, the cross product is done as

$$\bar{M}_{CS} = [l_{UE}\hat{e}_1] \times C_S[\overline{LE} - \overline{UE}] \qquad (3\text{-}47)$$

Using Eq 3-47, $\bar{M}_{CS}$ is

$$\bar{M}_{CS} = \begin{bmatrix} \hat{e}_1 & \hat{e}_2 & \hat{e}_3 \\ l_{UE} & 0 & 0 \\ A & B & C \end{bmatrix}$$

$$= -l_{UE}C\hat{e}_2 + l_{UE}B\hat{e}_3 \qquad (3\text{-}48)$$

The indicated operations in Eq 3-48 result in the components of $\bar{M}_{CS}$ as

$$\bar{M}_{CS} = (-c_{SZ}l_{UE}\overset{\circ}{Z}_L + c_{SZ}l_{UE}\overset{\circ}{Z}_U + c_{SZ}l_{UE}l_{LE}\overset{\circ}{\phi}_L - c_{SZ}l_{UE}l_{UE}\overset{\circ}{\phi}_U)\hat{e}_2$$

$$+(c_{SY}l_{UE}\overset{\circ}{Y}_L - c_{SY}l_{UE}\overset{\circ}{Y}_U - c_{SY}l_{UE}l_{LE}\overset{\circ}{\theta}_L - c_{SY}l_{UE}l_{UE}\overset{\circ}{\theta}_U)\hat{e}_3$$

The first two terms in the $\hat{e}_2$ and $\hat{e}_3$ components represent the translation cross coupling terms and the last two in each component are the pure rotation contributions. Appendix G carries out the cross product process similar to Eq 3-48 for all SSP subsystem corners and gives the rotational differential equations. As is done in Appendix F, the equations are separated into the $\hat{e}_1$, $\hat{e}_2$ and $\hat{e}_3$ degrees of freedom with the cross coupling term indicated.

Summary

The differential equations developed in Chapter III and tabulated in Appendix F - Translation and Appendix G - Rotation are the linearized differential equations describing the upper, lower and pier level perturbed motions. These motions are for a constant mass system about a nominal position in each body's center of mass. No acceleration terms due to gravity are present, because the variance of gravity is small and the nominal orientation is an equilibrium state where all gravity forces, isolator forces, and actuator forces result in the nominal position.

Close examination of the translational differential equations in Appendix F clearly show the X and Y directions to have θ cross coupling terms. The Z direction has cross coupling terms from ϕ and ψ. These observations hold for all three levels and is a physical check of the described motions.

Similarly, Appendix G shows the rotation differential equations for each level to have cross coupling present. The ψ and ϕ have Z cross coupling influences and θ has X and Y cross coupling components.

Chapter IV evaluates the passive response using Laplace operator solutions of the SSP differential equations in the frequency domain. Chapter V converts the SSP differential equations into state space notation for time response analysis

using LQ synthesis. The next chapter highlights the SSP passive response to gain insight into the actual controller problem analysis in Chapter V.

The dynamics equations written for the SSP give insight to the "leveling problem" for adjusting isolator height. A nominal position would imply that height of the isolators would already place a level in equilibrium. For the study, a nominal position is assumed and the isolators adjusted or leveled. The differential equations in Appendix F and G could be analyzed in terms of each corner relative to the level center of mass to describe any "leveling" induced motion.

IV. SSP Passive Response

Introduction

Before designing an active controller, the SSP passive response is analyzed to identify resonant frequencies and their effects on magnitude and phase responses. On the basis of the passive response characteristics, the systems poles and zeros then give possible insight for reduced order approximations in Chapter V, SSP Active Controller Design.

Simple mass, spring and damper networks are investigated and their characteristic Laplace solutions are related to the differential dynamic equations resulting from Chapter III.

Once the vibration transmissibility concept is developed, the lumped spring and damper parameters are entered into the transmissibility expressions for each of the six degrees of freedom to obtain the system passive response with the controller actuators deactivated. Various isolation levels are modeled to identify dominant SSP dynamics and possibly explain passive responses actually measured by CTGIF.

Before the simple mechanical models are studied, analysis assumptions and methods are presented.

Analysis Method and Assumptions

The passive analysis implies no controller actuator forces and represents the SSP system open loop transfer function. For the passive response, the SSP symmetry cancels any translation or rotation coupling, since all isolators are equidistant from the body centers of mass.

In Chapter III, Dynamics Analysis, the pier center of mass is assumed in the plane of the lower level isolators. The pier is modeled as a plane having a lumped parameter for inertia about the Z direction ($\hat{e}_3$) with equivalent spring and damper matrices representing soil dynamics in the vertical direction on each corner. Another simplification is also made for the moment of inertia in the ($\hat{e}_2$) direction by using the same lumped parameter given for the X($\hat{e}_1$) direction. Spring and damper matrices in the two horizontal directions - North and South, East and West - are equated to the values calculated for the X($\hat{e}_1$) direction. These pier simplifications basically consider the X and Y translation dynamics as well as the ψ and ϕ rotation dynamics the same. In contrast, the pier simplifications are made by assumption for analysis convenience, while the upper and lower level dynamics are the same for X, Y and ψ, ϕ directions by symmetry. The pier simplifications are detailed in Appendix E and do not impact on active controller design because measured pier effects are above controller bandwidth at 200 Hz (Ref 19). To standardize the dynamics qualitatively, the transmissibility concept is defined next.

Transmissibility is in general a transfer function or ratio between input and output vibrations or displacements (Ref 17:16). Expressed in the frequency domain, transmissibility is written as a transfer function

$$T(j\omega) = \frac{x_0(j\omega)}{x_1(j\omega)} \tag{4-1}$$

where, as functions of frequency

$x_0(j\omega)$, output

$x_1(j\omega)$, input

$T(j\omega)$, transmissibility transfer function

Transmissibility logarithmic magnitude and phase angle for Bode plot representation are written as

$$LmT(j\omega) = 20 \log \left| \frac{x_0(j\omega)}{x_1(j\omega)} \right| \text{ dB} \tag{4-2a}$$

$$T(j\omega) = \tan^{-1} \frac{Im[T(j\omega)]}{Re[T(j\omega)]} \tag{4-2b}$$

where,

$LmT(j\omega)$, log magnitude, base 10, decibels

$T(j\omega)$, phase angle, degrees

Im, Re, imaginary, real part rectangular components.

Vibration transmissibilities (Ref 17:16) can represent displacement responses, but also velocity and acceleration. By assuming $T(j\omega)$ to be a linear transfer function and sinusoid velocity or acceleration inputs, the displacement derivative responses are easily obtained. This assumption is commonly made in seismology studies for low frequency Earth movements which are naturally free of high frequency components (Ref 17:16). For the SSP, the acceleration transmissibility responses are needed for the translation passive responses and are easily implied from displacement transfer functions. The SSP rotational passive response is obtained directly from the angular position of tilt transmissibilities. Once transmissibility transfer functions are computed for the six SSP degrees of freedom, probable acceleration (by approximation) and tilt responses are available.

Transmissibility magnitude Bode plots are also a convenient representation of power spectral density (PSD). Mathematically the two are related as

$$PSD(j\omega) = 10 \log\left[\frac{x_0(j\omega)}{x_1(j\omega)}\right]^2 = 20 \log\left[\frac{x_0(j\omega)}{x_1(j\omega)}\right] \qquad (4\text{-}3)$$

The acceleration SSP specification for all axes is a PSD requirement in terms of root mean square (RMS). Acceleration RMS calculations are not made because of available computer software, so only peak transmissibility values are considered.

Simple Three Mass, Spring and Damper Networks

A simple three mass network shown in Figure 4.1 offers considerable insight into the transmissibility differential equation solution of more complex networks such as the SSP.

From Figure 4.1, the one degree of freedom, Z translational differential equations can be written for the three masses using F = ma. All accelerations are inertial-Earth frame with all masses constant. A displacement input z_G is assumed as shown. The equations of motion for the three masses are

$$m_U \ddot{z}_U = c_S(\dot{z}_L - \dot{z}_U) + k_S(z_L - z_U) \qquad (4\text{-}4)$$

$$m_L \ddot{z}_L = -c_S(\dot{z}_L - \dot{z}_U) - k_S(z_L - z_U) + c_F(\dot{z}_P - \dot{z}_L) + k_F(z_P - z_L) \qquad (4\text{-}5)$$

$$m_P \ddot{z}_P = -c_F(\dot{z}_P - \dot{z}_L) - k_F(z_P - z_L) + c_G(\dot{z}_G - \dot{z}_P) + k_G(z_G - z_P) \qquad (4\text{-}6)$$

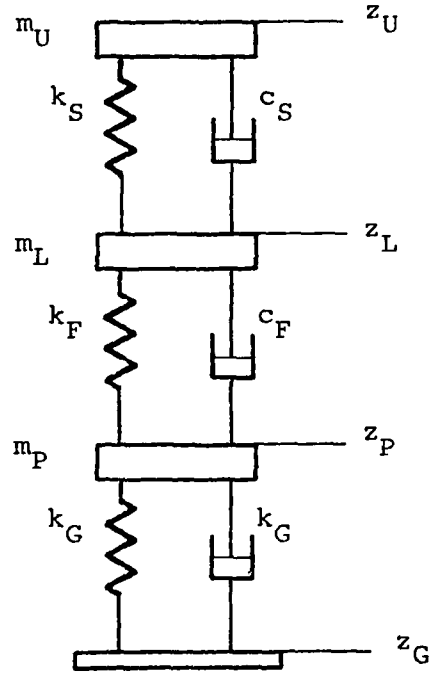

m_U , upper mass

m_L , lower mass

m_P , pier or seismic mass

k_S, c_S , second stage isolation

k_F, c_F , first stage isolation

k_G, c_G , ground isolation

Figure 4.1 Simple Three Mass Network

Eqs (4-4), (4-5) and (4-6) are rearranged and written in Laplace notation, assuming zero initial conditions.

$$Z_U(s)[m_U s^2 + c_S s + k_S s] = Z_L(s)[c_S s + k_S] \qquad (4\text{-}7)$$

$$Z_L(s)[m_L s^2 + (c_F + c_S)s + (k_F + k_S)] = Z_P s[c_F s + k_F] + Z_U(s)[c_S s + k_S] \qquad (4\text{-}8)$$

$$Z_P(s)[m_P s^2 + (c_G + c_F)s + (k_G + k_F)] = Z_G(s)[c_G s + k_G] + Z_L(s)[c_F s + k_F)] \qquad (4\text{-}9)$$

Eqs (4-7), (4-8) and (4-9) are rewritten with variables representing the bracketed terms in preparation for algebraic manipulations; these equations follow term for term below:

$$Z_U(s)[a] = Z_L(s)[b] \qquad (4\text{-}10)$$

$$Z_L(s)[e] = Z_P(s)[c] + Z_U(s)[d] \qquad (4\text{-}11)$$

$$Z_P(s)[f] = Z_G(s)[g] + Z_L(s)[h] \qquad (4\text{-}12)$$

Solving these expressions for the transmissability $Z_U(s)/Z_G(s)$, the transfer function is

$$\frac{Z_U(s)}{Z_G(s)} = \frac{bcg}{aef - b^2f - c^2a} \tag{4-13}$$

which is the basic form

$$\frac{Z_U(s)}{Z_G(s)} = \frac{(c_S + k_S)(c_F s + k_F)(c_G s + k_G)}{(m_U \ldots)(m_L \ldots)(m_P \ldots) - (c_G s + k_S)^2 (m_P \ldots) - (c_F s + k_F)^2 (m_U \ldots)} \tag{4-14}$$

Eq 4-13 with the indicated operations carried out to obtain a ratio of polynomials, becomes a transfer function of the following form,

$$\frac{Z_U(s)}{Z_G(s)} = \frac{As^3 + Bs^2 + Cs + D}{Es^6 + Fs^5 + Gs^4 + Hs^3 + Is^2 + Js + K} \tag{4-15}$$

The polynomial coefficients of Eq 4-15, A thru F are tabulated in Appendix H in terms of the variables for this simple system once the spring, damper and mass variables are specified.

Now that a scalar Z transmissibility transfer function solution is available in Eq 4-15, the translation equations of Chapter III and Appendix F are reexamined. Eq 4-4 is

repeated again in differential equation form (terms collected).

$$m_U \ddot{z}_U = -c_S \dot{z}_U - k_S z_U + c_S \dot{z}_L + k_S z_L \qquad (4\text{-}16)$$

Now consider the m_U component of $\hat{e}_3$ in Eq F-11, no rotation coupling terms, and actuator forces zero.

$$m_U \ddot{z}_U = -4c_{SZ} \dot{z}_U - 4k_S z_U + 4c_{SZ} \dot{z}_L + 4k_{SZ} z_L \qquad (4\text{-}17)$$

The scalar development of three mass networks represented in Eq 4-16 characterizes the forms given in Appendix F. Namely, the simple c_S second stage damper parallels the SSP second stage by a factor of four, which is physically reassuring, since the SSP second stage has four isolators. Extended further, Appendix H gives the solution for three stages of isolation, no rotational coupling, no active control actuator forces by the simple substitution:

$$4c_{SZ} \rightarrow c_S \qquad (4\text{-}18a)$$

$$4k_{SZ} \rightarrow k_S \qquad (4\text{-}18b)$$

$$4c_{FZ} \rightarrow c_F \qquad (4\text{-}18c)$$

$$4k_{FZ} \rightarrow k_F \qquad (4\text{-}18d)$$

$$4c_{GZ} \rightarrow c_G \tag{4-18e}$$

$$4k_{GZ} \rightarrow k_G \tag{4-18f}$$

The same parallel differential equation structures exist for the $\hat{e}_1$ direction in Eqs F-5, F-6, and F-7. Similarly, the $\hat{e}_2$ direction has the same solution form by using Eqs F-8, F-9 and F-10.

For the rotational differential equations developed in Appendix G, the parallel solution can be extended again. Eq 4-16 is repeated.

$$m_U \ddot{z}_U = -c_S \dot{z}_U - k_S z_U + c_S \dot{z}_L + k_S z_L \tag{4-16}$$

If Eq G-9, the I_{UZ} component of Θ is rewritten with $c_{SX} = c_{SY}$ and all isolator lengths $l_{UN} = l_{US} = l_{UW} = l$, because of symmetry, the following rotational equation results.

$$\begin{aligned} I_{UZ}\ddot{\Theta}_U = & -4c_{SX}l^2\dot{\Theta}_U - 4k_{SX}l^2\Theta_U \\ & +4c_{SX}l^2\dot{\Theta}_L + 4k_{SX}l^2\Theta_U \end{aligned} \tag{4-19}$$

Now a solution for the Θ direction is readily available by simple substitution.

$$I_{UZ} \rightarrow m_U \tag{4-20a}$$

$$4c_{SX}l^2 \rightarrow c_S \tag{4-20b}$$

$$4k_{SX}l^2 \rightarrow k_S \tag{4-20c}$$

$$4c_{FX}l^2 \rightarrow c_F \tag{4-20d}$$

$$4k_{FX}l^2 \rightarrow k_F \tag{4-20e}$$

$$4c_{GX}l^2 \rightarrow c_G \tag{4-20f}$$

$$4k_{GX}l^2 \rightarrow k_G \tag{4-20g}$$

Physically this follows from the SSP dynamics because the c_{SX} , k_{SX} , c_{SY} and k_{SY} vector springs and dampers act as four individual components about the $\hat{e}_3$ axis for θ in the upper level rotational dynamics. Similar analogies can be made for the lower level and first stage isolation effects.

These substitutions do not hold for ψ and ϕ . The I_{UX} component of ψ , Eq G-7 is rewritten using the same assumptions used in I_{UZ} .

$$\begin{aligned} I_{UX}\ddot{\psi}_U = & -2c_{SZ}l^2\dot{\psi}_U - 2k_{SZ}l^2\psi_U \\ & +2c_{SZ}l^2\dot{\psi}_L + 2k_{SZ}l^2\psi_L \end{aligned} \tag{4-21}$$

The ψ substitution becomes:

$$I_{UX} \rightarrow m_U \tag{4-22a}$$

$$2c_{SZ}l^2 \rightarrow c_S \tag{4-22b}$$

$$2k_{SZ}l^2 \rightarrow k_S \tag{4-22c}$$

$$2c_{FZ}l^2 \rightarrow c_F \tag{4-22d}$$

$$2k_{FZ}l^2 \rightarrow k_F \tag{4-22e}$$

$$2c_{GZ}l^2 \rightarrow c_G \tag{4-22f}$$

$$2k_{GZ}l^2 \rightarrow k_G \tag{4-22g}$$

The rotational spring and damper equivalents are halved because the c_{SZ} and k_{SZ} dynamics act in pairs on opposite corners in a see-saw fashion about $\hat{e}_1$ for ψ and $\hat{e}_2$ for ϕ in the upper level. Similar comparisons can be made for the lower level and pier rotational equations.

Deriving the Eqs 4-7 through 4-16 is only a vehicle for solving the three mass isolation networks. The parallel made between Eqs 4-16 and 4-17 gives very realistic insight into solving the $\hat{e}_3$ equations found in Appendix F. When the θ, ψ and ϕ differential equation coefficient substitutions are made, these scalar variables become rotational springs and dampers and the Z notation of Eq 4-16 represents just a scalar variable, with no translation implications.

SSP Full Isolation

With the insight and substitutions gained from three simple mass, spring and damper networks, the SSP full isolation offered in the $X(\hat{e}_1)$, $Y(\hat{e}_2)$ and $Z(\hat{e}_3)$ translation directions as well as the $\psi(\hat{e}_1)$, $\phi(\hat{e}_2)$ and $\theta(\hat{e}_3)$ are evaluated. The transmissibility concept will provide transfer functions in the required directions using the physical spring and damper values in Appendix E, the polynomial solution in Appendix H and the substitutions just derived by the simple mechanical network analysis.

Each transmissibility is defined in the frequency domain from the solution polynomial and expressed in a factored form and a Bode plot from TOTAL (Ref 9). Actual polynomial coefficients are listed in Appendix I. Table 4.1 summarizes break frequencies, phase margins, gain margins and general low pass attenuation offered. An expression for each SSP directional transmissibility is now listed along with an accompanying plot reference.

Z-Response (Full Isolation)

$$TZ_{U/G}(j\omega) = Z_U(j\omega)/Z_G(j\omega)$$

$$= \frac{223.3(j\omega + 128.5)(j\omega + 188.5)^2}{(j\omega + 0.1882 \pm j8.421) \times (j\omega + 1.715 \pm j25.37) \times (j\omega + 86.47 \pm j121.4)} \qquad (4\text{-}23)$$

Bode plot is shown in Figure 4.2.

Table 4.1 Full Isolation Frequency Characteristics Summary

T(jω)	GM(f)	PM(f)	f(MP)	AS
$TZ_{U/G}(j\omega)$	5.12db(3.0 Hz)	5.66°(2.0 Hz)	1.3 Hz(23.63dB) 4.0 Hz(-0.19dB)	-40dB/decade -60dB/decade
$TX_{U/G}(j\omega)$	4.52db(6.3 Hz)	5.06°(4.5 Hz)	2.9 Hz(28.12dB) 8.6 Hz(0.78dB)	-40dB/decade -60dB/decade
$T\Theta_{U/G}(j\omega)$	0.13db(7.4 Hz)	0.26°(7.4 Hz)	4.1 Hz(25.20dB) 12.0 Hz(3.83dB)	-40dB/decade -60dB/decade
$T\psi_{U/G}(j\omega)$	5.60db(4.6 Hz)	7.96°(3.1 Hz)	2.0 Hz(24.58dB) 6.1 Hz(-3.43dB)	-50dB/decade -60dB/decade

where,

GM, gain margin

PM, phase margin

MP, magnitude peak

AS, attenuation slope approximated at 100 Hz.

T(jω), transmissability frequency function

(Ref 6:82)

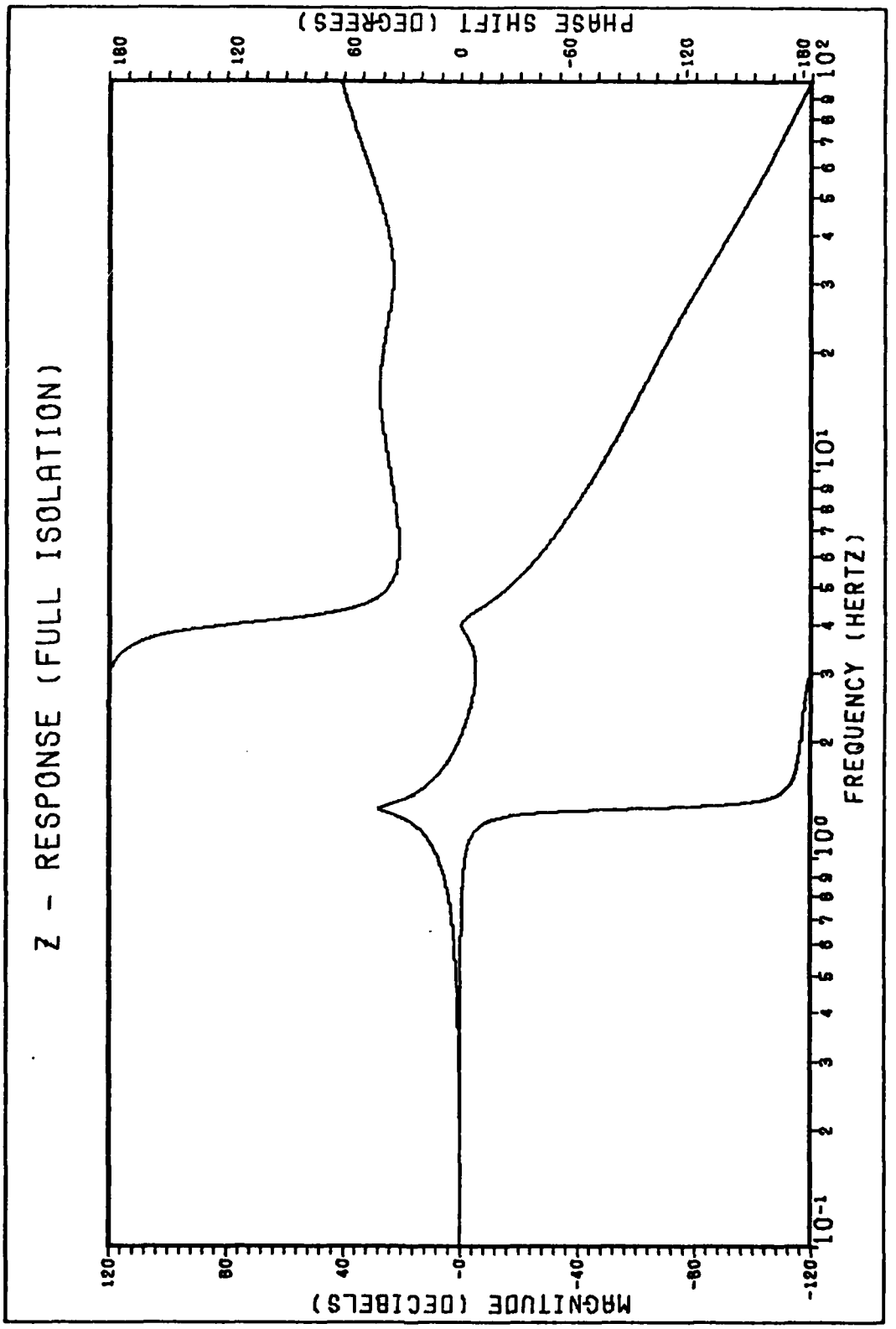

Figure 4.2 Z-Response (Full Isolation)

X-Response (Full Isolation) (also Y-Response)

$$TX_{U/G}(j\omega) = X_U(j\omega)/X_G(j\omega) = Y_U(j\omega)/Y_G(j\omega)$$

$$= \frac{606.8(j\omega + 199.6)(j\omega + 397.9)(j\omega + 418.9)}{(j\omega + 0.4080 \pm j18.21)} \times (j\omega + 3.718 \pm j54.94) \times (j\omega + 50.17 \pm j132.5) \quad (4\text{-}24)$$

Bode plot is shown in Figure 4.3.

Theta-Response (Full Isolation)

$$T\Theta_{U/G}(j\omega) = \Theta_U(j\omega)/\Theta_G(j\omega)$$

$$= \frac{(886.4(j\omega + 199.6)(j\omega + 397.9)(j\omega + 418.9)}{(j\omega + 0.8367 \pm j126.07)} \times (j\omega + 15.65 \pm j78.52) \times (j\omega + 8.684 \pm j81.78) \quad (4\text{-}25)$$

Bode plot is shown in Figure 4.4.

PSI-Response (Full Isolation) (also PHI Response)

$$T\psi_{U/G}(j\omega) = \psi_U(j\omega)/\psi_G(j\omega) = \phi_U(j\omega)/\phi_G(j\omega)$$

$$= \frac{590.1(j\omega + 128.5)(j\omega + 188.5)^2}{(j\omega + 0.42 \pm j12.57)} \times (j\omega + 4.159 \pm j39.37) \times (j\omega + 42.23 \pm j95.24) \quad (4\text{-}26)$$

Bode plot is shown in Figure 4.5.

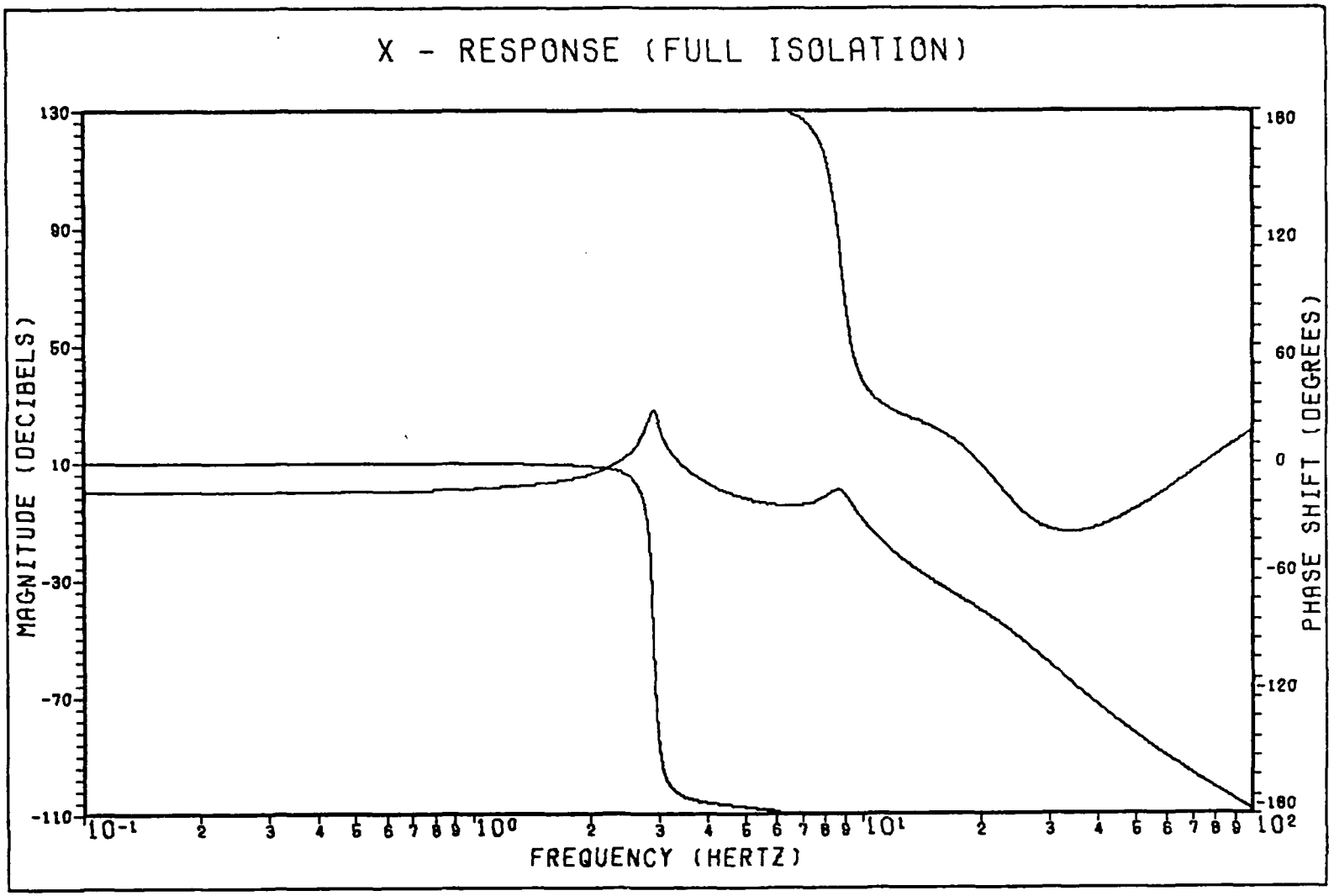

Figure 4.3 X-Response(Full Isolation)

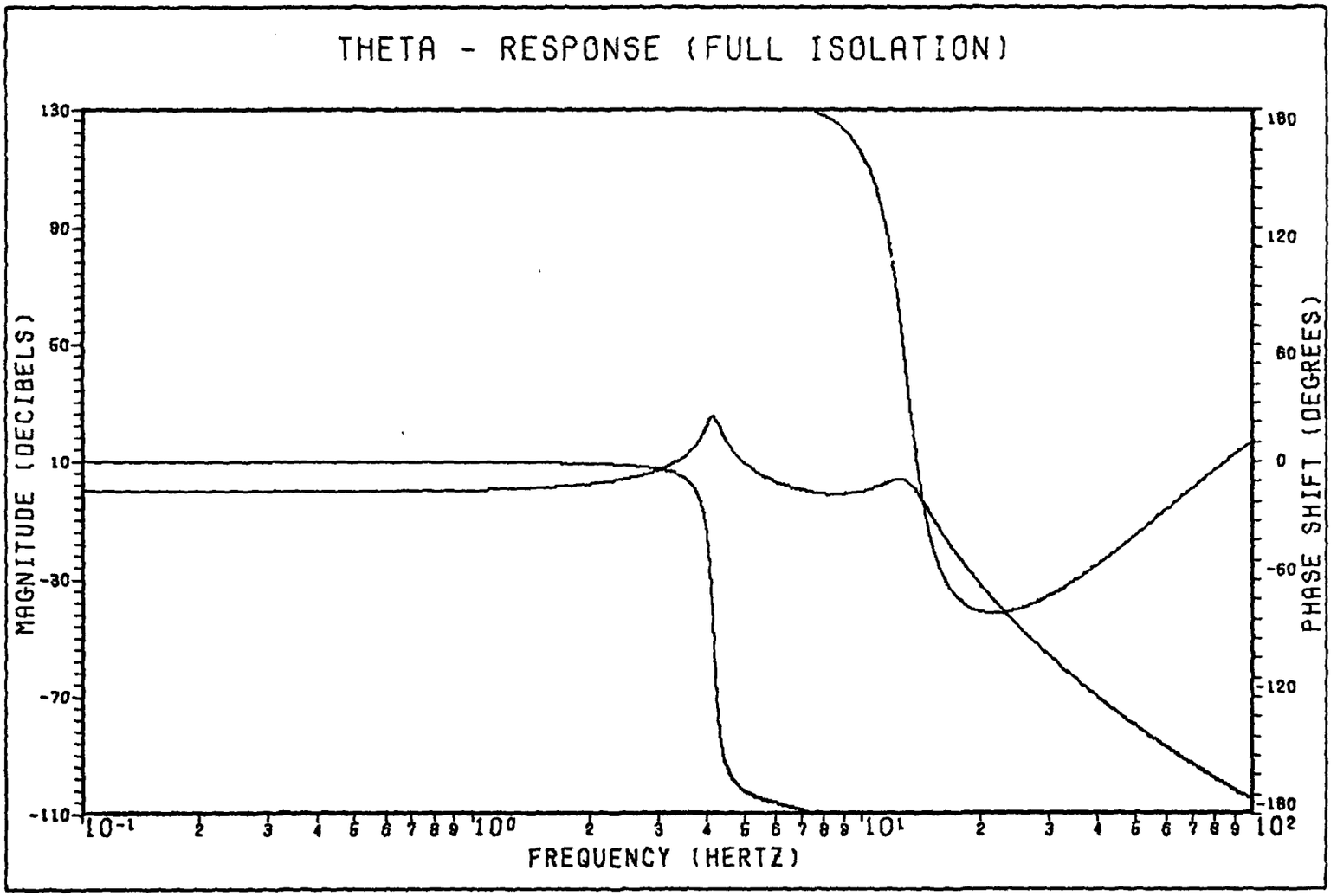

Figure 4.4 Theta-Response (Full Isolation)

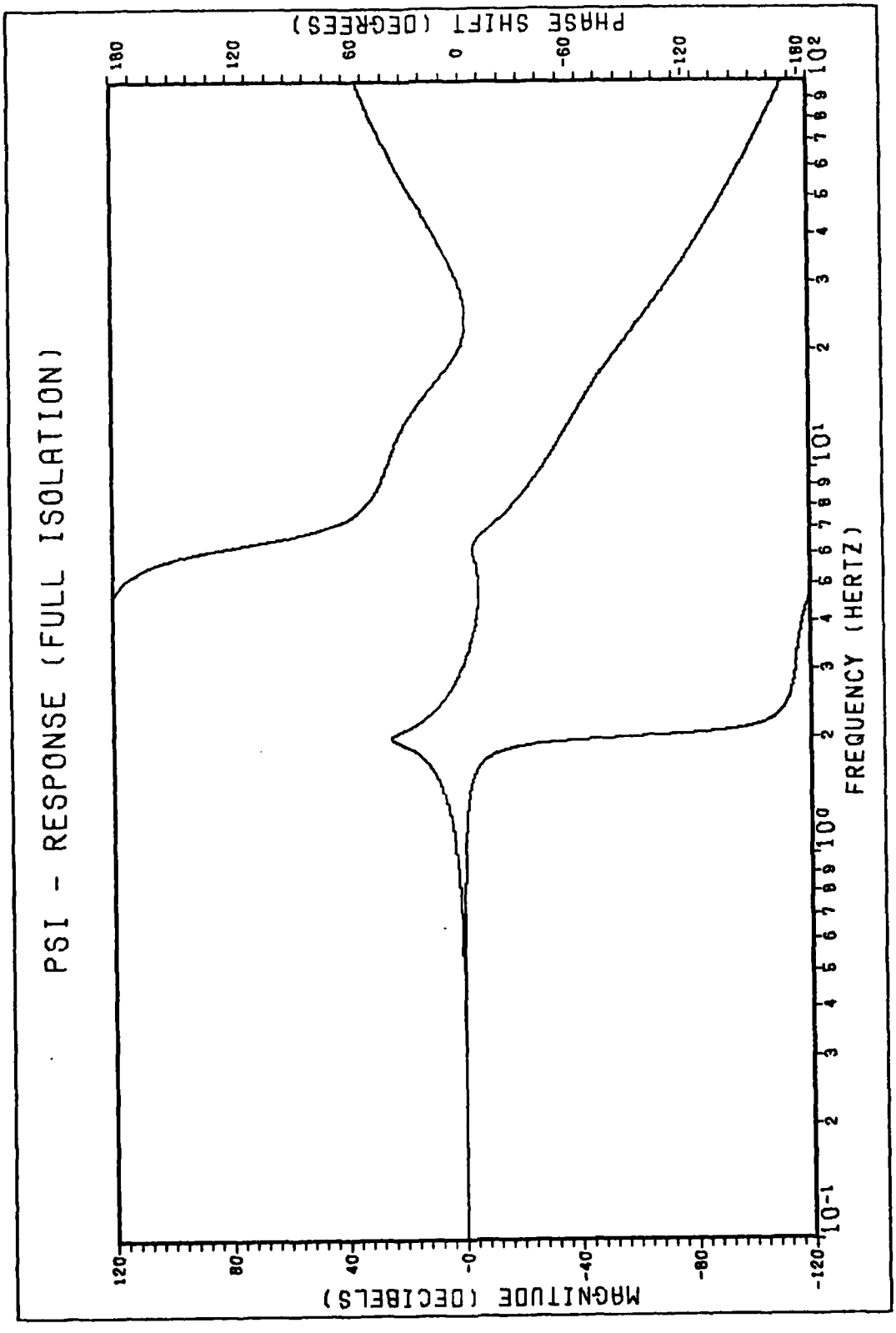

Figure 4.5 PSI-Response (Full Isolation)

Full Isolation Analysis

The theoretical magnitude and phase plots are plotted using Eqs 4-2a and 4-2b respectively. Tabulated values for Table 4.1 are obtained from TOTAL to the indicated magnitude, and frequency resolutions. Analysis conclusions are stated now for each direction.

The full Z isolation position resonances are theoretically at 1.3 Hz and 4.0 Hz which compares closely with the vertical acceleration resonances at 1.2 Hz and 3.5 Hz measured by FSJRL engineers (Ref 19). A phase shift is at 2.0 Hz with a measured 180° phase shift at about 1.0 Hz measured at CIGTF (Ref 19). These good correlations give validity to the SSP dynamics modeling approach for acceleration transmissibilities.

No measurements are available from CIGTF for X and Y acceleration transmissibilities. Figure 4.3 predicts the X transmissibility as well as the Y transmissibility due to the symmetry of lumped spring and damper dynamic matrices. Theoretical horizontal position resonances are at 2.9 Hz and 8.6 Hz.

The θ direction has azimuth resonances predicted at 4.1 Hz and 12.0 Hz but no measurements are available. Transmissibilities for ψ and ϕ are the same due to symmetry with resonances predicted at 2.0 Hz and 12.0 Hz. No tilt transmissibility measurements are available for the SSP. The θ direction has a small gain margin and phase margin while the ψ direction has gain and phase margins comparable to the Z and X directions. Table 4.1 summarizes these points. No input

signal magnitudes are specified because the transfer function is calculated for a normalized response.

Time response characteristics from TOTAL resulting from a unit step input are given in Table 4.2 for all full isolation transmissiblity functions. These time responses only emphasize the lightly damped dynamics of the SSP. Unit step responses specify no input magnitude since they also can be scaled or normalized for a linear system

Simple Two Mass, Spring and Damper Network

Similar to the three mass solutions just derived for the full isolation transmissibility transfer function, a two mass system is analyzed. Two mass, spring and damper models characterize transmissibilities result from the three SSP levels of isolation in active isolation combination two at a time. In actual operation, the SSP could have one level of pneumatic inoperative or the SSP dynamics could be evaluated neglecting the pier isolation. The possible scalar combinations for the Z direction are shown in Figure 4.6. Again, the whole driving force behind the scalar development is to characterize the differential equations, use the substitutions recognized in Eqs 4-18, 4-20, and 4-22, and offer solutions for the needed transmissibility transfer function. The scalar Z is used because it is easier to visualize without complex free body diagrams and it parallels easily into the SSP Z direction solution.

Table 4.2 Full Isolation Unit Step Time Response Summary

f(t)	TR(sec)	TD(sec)	TP(sec)	TS(sec)	MP	FV
$TZ_{U/G}(t)$	0.0931	0.1837	0.3699	21.2895	1.9838	1.0000
$TX_{U/G}(t)$	0.0412	0.0850	0.1713	9.8472	1.9885	1.0000
$T\Theta_{U/G}(t)$	0.0270	0.0619	0.1018	4.8352	2.1051	1.0000
$T\psi_{U/G}(t)$	0.0615	0.1213	0.2517	9.5132	1.9757	1.0000

where,

TR, rise time TD, duplication time TP, peak time

TS, setting time MP, peak value FV, final value

(Ref 6:82)

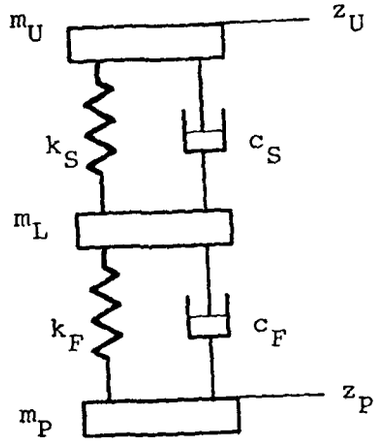

Figure 4.6A SSP Isolation

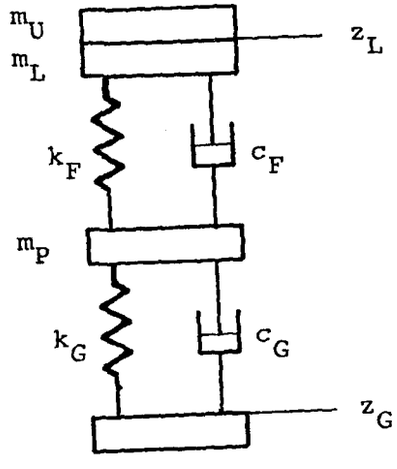

Figure 4.6B First Stage/Pier Isolation

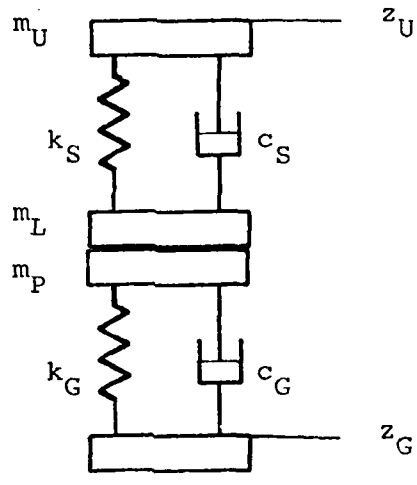

m_U , upper mass

m_L , lower mass

m_P , pier or seismic mass

k_S, c_S , second stage isolation

k_F, c_F , first stage isolation

k_G, c_G , ground isolation

Figure 4.6C Second Stage/Pier Isolation

SSP Isolation

Figure 4.6A shows no pier dynamics or just the SSP structure upper and lower levels. The F = ma differential equations for the two masses are

$$m_U \ddot{z}_U = c_S(\dot{z}_L - \dot{z}_U) + k_S(z_L - z_U) \tag{4-27}$$

$$m_L \ddot{z}_L = c_F(\dot{z}_P - \dot{z}_L) + k_F(z_P - z_L) - c_S(\dot{z}_L - \dot{z}_U) - k_S(z_L - z_U) \tag{4-28}$$

Rearranging Eqs 4-27 and 4-28 and using the Laplace operator, zero initial conditions, and some algebraic manipulation, the transmissability function becomes

$$\frac{Z_U(s)}{Z_P(s)} = \frac{as^2 + bs + c}{ds^4 + es^3 + fs^2 + gs + h} \tag{4-29}$$

where the numerator and denominator polynomial coefficients are

$$a = c_F c_S \tag{4-30a}$$

$$b = c_F k_S + c_S k_F \tag{4-30b}$$

$$c = k_F k_S \tag{4-30c}$$

$$d = m_U m_L \tag{4-30d}$$

$$e = m_U(c_F + c_S) + m_L c_S \tag{4-30e}$$

$$f = m_U(k_F + k_S) + c_F c_S + m_L k_F \tag{4-30f}$$

$$g = b \tag{4-30g}$$

$$h = c \tag{4-30h}$$

A solution similar to Appendix H, the full isolation solution is now available. To solve all four transmissibility functions - Z, X(or Y), θ , and ψ(orϕ) substitutions from Eqs 4-18, 4-20 and 4-22 are used.

First Stage/Pier Isolation

Figure 4.6B shows the second stage isolation inactive. The configurations have a solution of the form given in Eq 4-29 with the polynomials described by Eq 4-30. If the following scalar variable solutions are made, the transmissibility transfer function is easily obtained.

$$m_U + m_L \rightarrow m_U \tag{4-31a}$$

$$m_P \rightarrow m_L \tag{4-31b}$$

$$k_F \rightarrow k_S \tag{4-31c}$$

$$c_F \rightarrow c_S \tag{4-31d}$$

$$k_G \rightarrow k_F \tag{4-31e}$$

$$c_G \rightarrow c_F \tag{4-31f}$$

Now the scalar change of variables are transformed, the same substitutions made in Eqs 4-18, 4-20 and 4-22 are used.

Second Stage/Pier Isolation

Figure 4.6C shows the first stage isolation inactive. The following scalar variable substitutions are made in the polynomials described in Eq 4-29.

$$m_L + m_P \rightarrow m_L \qquad (4\text{-}32a)$$

$$k_G \rightarrow k_F \qquad (4\text{-}32b)$$

$$c_G \rightarrow c_F \qquad (4\text{-}32c)$$

As is done in the other configurations, the same substitutions made in Eqs 4-18, 4-20 and 4-22 are used. Transmissability transfer functions in factored form are obtained from TOTAL. Polynomial coefficients are listed in Appendix I. Bode plot references are indicated, frequency performance data and unit step time response information are listed in Tables 4.3 and 4.4, respectively.

Table 4.3

Dual Isolation Frequency Characteristics Summary

T(jω)	GM(f)	PM(f)	f(MP)
$TZ_{U/P}(j\omega)$	5.25db(3.0 Hz)	5.71°(2.0 Hz)	1.3 Hz(23.57dB) 4.0 Hz(-0 .43dB)
$TZ_{L/P}(j\omega)$	39.68db(23.0 Hz)	9.42°(2.6 Hz)	1.8 Hz(24.50dB) 22.0 Hz(-38.93dB)
$TZ_{U/P}(j\omega)$	38.11db(21.0 Hz)	9.42°(2.6 Hz)	1.8 Hz(24.50dB) 22.0 Hz(-38.11dB)
$TX_{U/P}(j\omega)$	5.29db(6.5 Hz)	5.39°(4.5 Hz)	2.9 Hz(27.99dB) 8.6 Hz(- 0.46dB)
$TX_{L/P}(j\omega)$	18.62db(14.0 Hz)	8.90°(5.5 Hz)	3.8 Hz(24.63dB) 16.0 Hz(-20.24dB)
$TX_{U/G}(j\omega)$	17.46db(14.0 Hz)	8.70°(5.8 Hz)	4.0 Hz(24.69dB) 20.0 Hz(-22.08dB)
$T\Theta_{U/P}(j\omega)$	6.32db(9.8 Hz)	7.10°(7.0 Hz)	4.2 Hz(24.30dB) 13.0 Hz(- 4.56dB)
$T\Theta_{L/P}(j\omega)$	0.83db(8.9 Hz)	4.20°(9.5 Hz)	5.0 Hz(15.78dB) 10.0 Hz(- 0.71dB)
$T\Theta_{U/G}(j\omega)$	2.07db(8.8 Hz)	22.12°(11.0 Hz)	5.7 Hz(23.21dB) 12.0 Hz(- 1.92dB)
$T\psi_{U/P}(j\omega)$	6.33db(4.7 Hz)	8.30°(3.1 Hz)	2.0 Hz(24.45dB) 6.1 Hz(- 4.57dB)
$T\psi_{L/P}(j\omega)$	20.97db(13.0 Hz)	13.50°(4.0 Hz)	2.7 Hz(21.04dB) 14.0 Hz(-22.99dB)
$T\psi_{U/G}(j\omega)$	21.22db(12.0 Hz)	13.40°(3.9 Hz)	2.7 Hz(20.99dB) 13.0 Hz(-22.25dB)

where,

GM, gain margin PM, phase margin MP, magnitude peak

AS, attenuation slope approximate leaving MP, towards positive increasing frequency

T(jω), transmissability frequency function

(Ref 6:82)

Table 4.4 Dual Isolation Unit Step Time Response Summary

f(t)	TR(sec)	TD(sec)	TP(sec)	TS(sec)	MP	FV
$TZ_{U/P}(t)$	0.0940	0.1836	0.3698	21.2832	1.9825	1.0000
$TZ_{L/P}(t)$	0.0910	0.1363	0.2727	11.4226	1.9169	1.0000
$TZ_{U/G}(t)$	0.0909	0.1363	0.2727	11.4209	1.9172	1.0000
$TX_{U/P}(t)$	0.0434	0.0848	0.1712	9.8330	1.9823	1.0000
$TX_{L/P}(t)$	0.0407	0.0648	0.1294	5.4220	1.9378	1.0000
$TX_{U/G}(t)$	0.0382	0.0615	0.1229	5.1483	1.9424	1.0000
$T\Theta_{U/P}(t)$	0.0309	0.0585	0.1210	4.7081	1.9697	1.0000
$T\Theta_{L/P}(t)$	0.0254	0.0471	0.0868	2.6538	2.1163	1.0000
$T\Theta_{U/G}(t)$	0.0134	0.0176	0.0353	0.2457	1.5745	1.0000
$T\psi_{U/P}(t)$	0.0645	0.1214	0.2505	9.5070	1.9668	1.0000
$T\psi_{L/P}(t)$	0.0575	0.0894	0.1786	4.9833	1.8945	1.0000
$T\psi_{U/G}(t)$	0.0585	0.0908	0.1818	5.2438	1.9697	1.0000

where,

TR, rise time TD, duplication time TP, peak time

TS, setting time MP, peak value FV, final value

f(t), transmissability time function

(Ref 6:82)

Z-Response (SSP Isolation)

$$TZ_{U/P}(j\omega) = Z_U(j\omega)/Z_P(j\omega)$$

$$= \frac{1.292(j\omega + 188.5)^2}{(j\omega + 0.1883 \pm j8.422)(j\omega + 1.716 \pm j25.37)} \quad (4\text{-}33)$$

Bode plot is shown in Figure 4.7.

Z-Response (First Stage/Pier Isolation)

$$TZ_{L/P}(j\omega) = Z_L(j\omega)/Z_G(j\omega)$$

$$= \frac{117.3(j\omega + 128.5)(j\omega + 188.5)}{(j\omega + 0.3391 \pm j11.30)(j\omega + 86.47 \pm j121.4)} \quad (4\text{-}34)$$

Bode plot is shown in Figure 4.8.

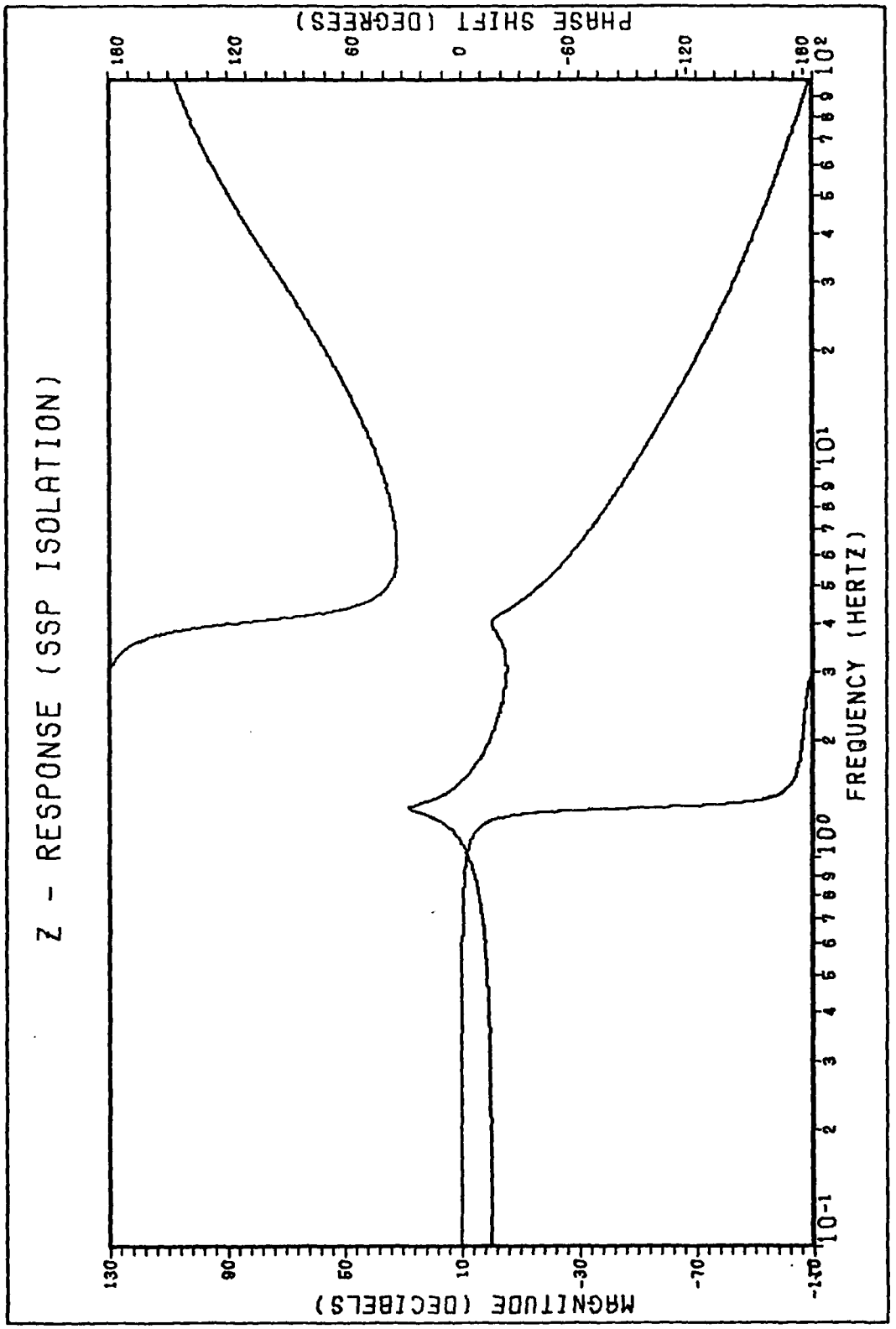

Figure 4.7 Z-Response (SSP Isolation)

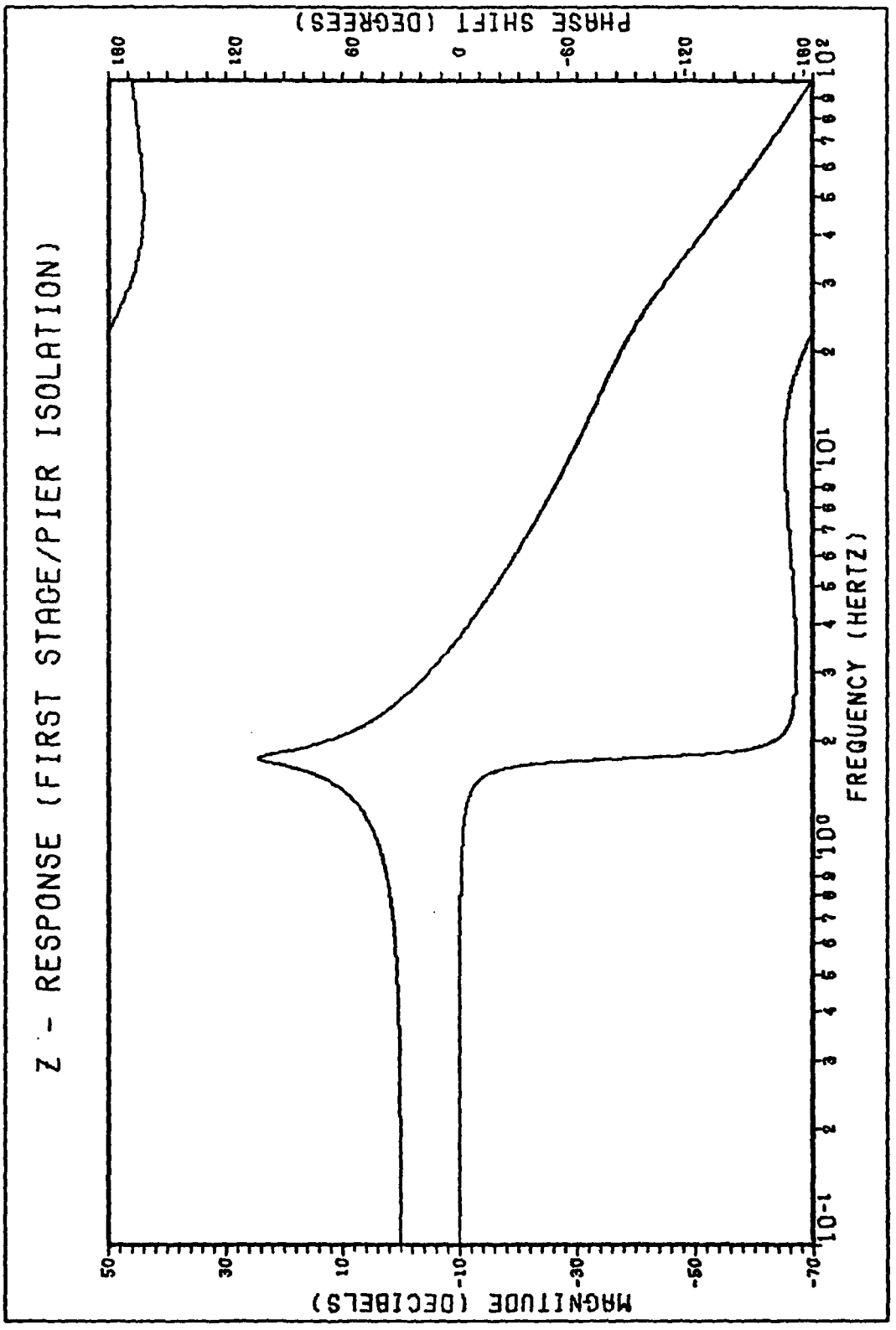

Figure 4.8 Z-Response (First Stage/Pier Isolation)

Z-Response (Second Stage/Pier Isolation)

$$TZ_{U/G}(j\omega) = Z_U(j\omega)/Z_G(j\omega)$$

$$= \frac{111.2(j\omega + 128.5)(j\omega + 188.5)}{(j\omega + 0.3392 \pm j11.30)(j\omega + 82 \pm j119.8)} \quad (4\text{-}35)$$

Bode plot is shown in Figure 4.9.

X-Response (SSP Isolation)

$$TX_{U/P}(j\omega) = X_U(j\omega)/X_P(j\omega) = Y_U(j\omega)/Y_P(j\omega)$$

$$= \frac{6.061(j\omega + 397.9)(j\omega + 418.9)}{(j\omega + 0.4079 \pm j18.23)(j\omega + 3.717 \pm j55.00)} \quad (4\text{-}36)$$

Bode plot shown in Figure 4.10

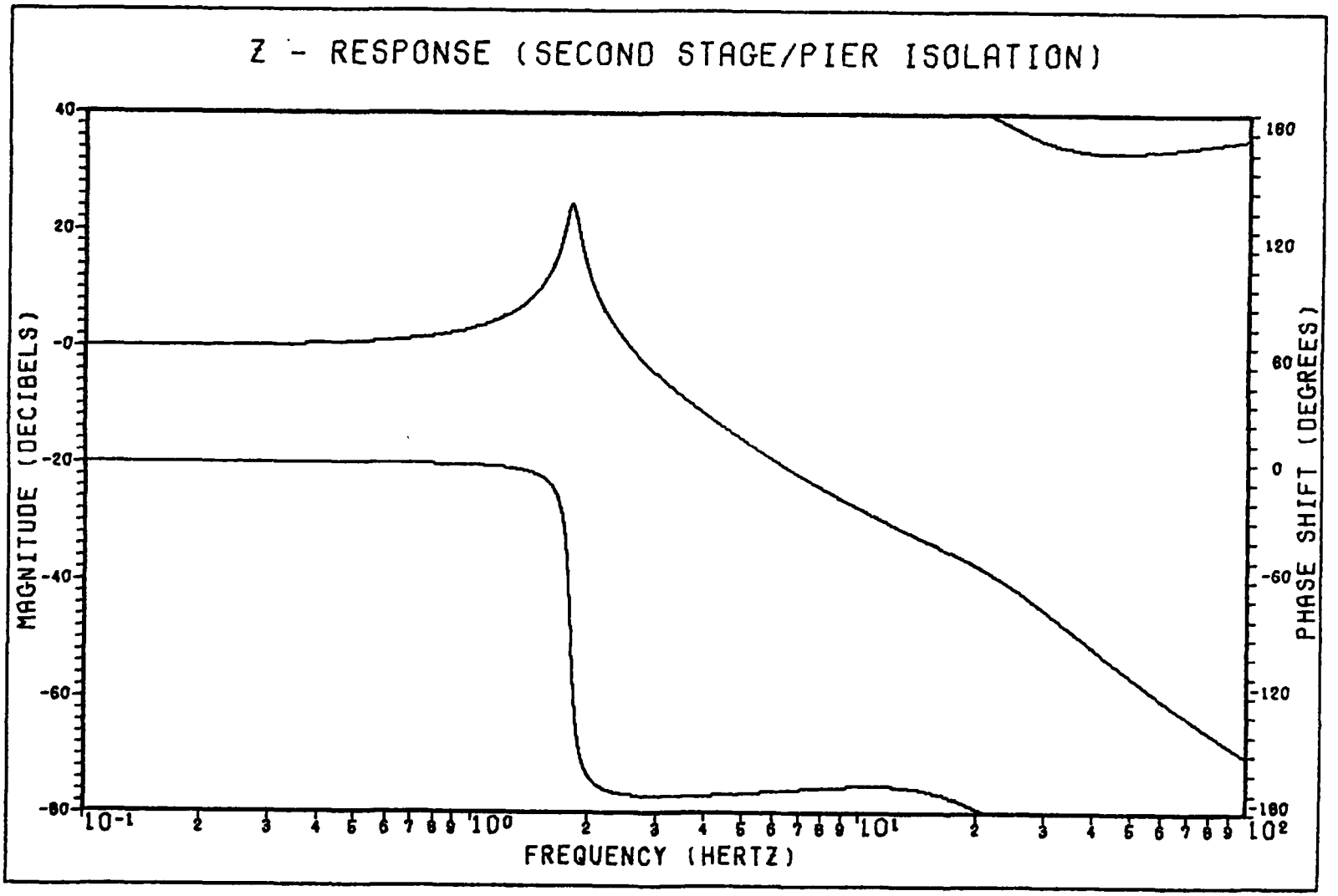

Figure 4.9 Z-Response (Second Stage/Pier Isolation)

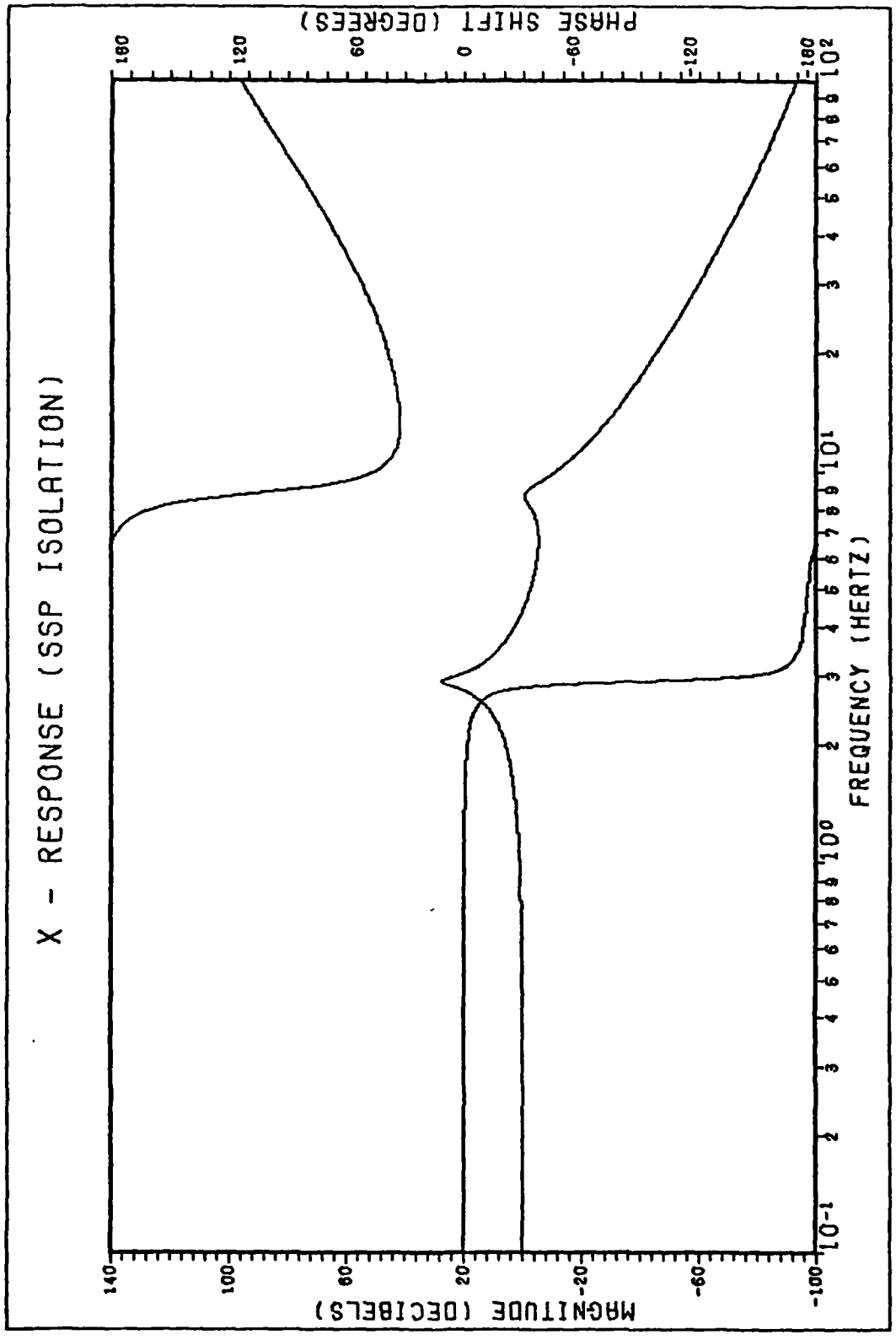

Figure 4.10 X-Response (SSP Isolation)

X-Response (First Stage/Pier Isolation)

$$TX_L(j\omega) = X_L(j\omega)/X_P(j\omega) = Y_L(j\omega)/Y_P(j\omega)$$

$$= \frac{143.4(j\omega + 199.6)(j\omega + 397.9)}{(j\omega + 0.1763 \pm j23.81)(j\omega + 50.17 \pm j132.5)} \quad (4\text{-}37)$$

Bode plot shown in Figure 4.11.

X-Response (Second Stage/Pier Isolation)

$$TX_{U/G}(j\omega) = X_U(j\omega)/X_G(j\omega) = Y_U(j\omega)/Y_G(j\omega)$$

$$= \frac{143.2(j\omega + 199.6)(j\omega + 418.9)}{(j\omega + 0.7543 \pm j25.08)(j\omega + 47.55 \pm j129.4)} \quad (4\text{-}38)$$

Bode plot is shown in Figure 4.12.

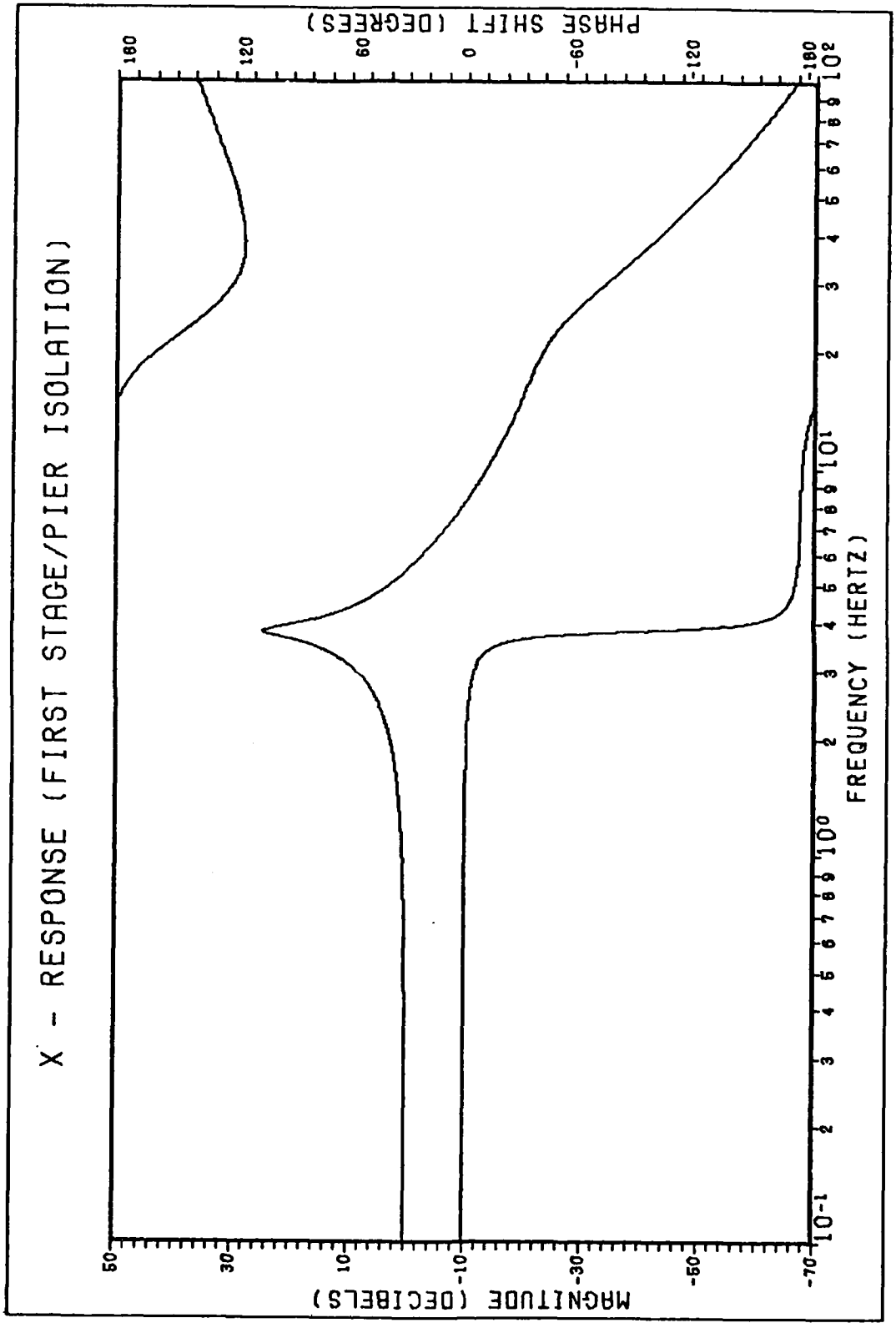

Figure 4.11 X-Response (First Stage/Pier Isolation)

AD-A115 559 AIR FORCE INST OF TECH WRIGHT-PATTERSON AFB OH SCHOO--ETC F/G 17/7
ANALYSIS AND DESIGN OF A DIGITAL CONTROLLER FOR A SEISMICALLY S--ETC(U)
DEC 81 S W FRANCIS
UNCLASSIFIED AFIT/GE/EE/81D-22 NL

2 OF 4
AD
A115559

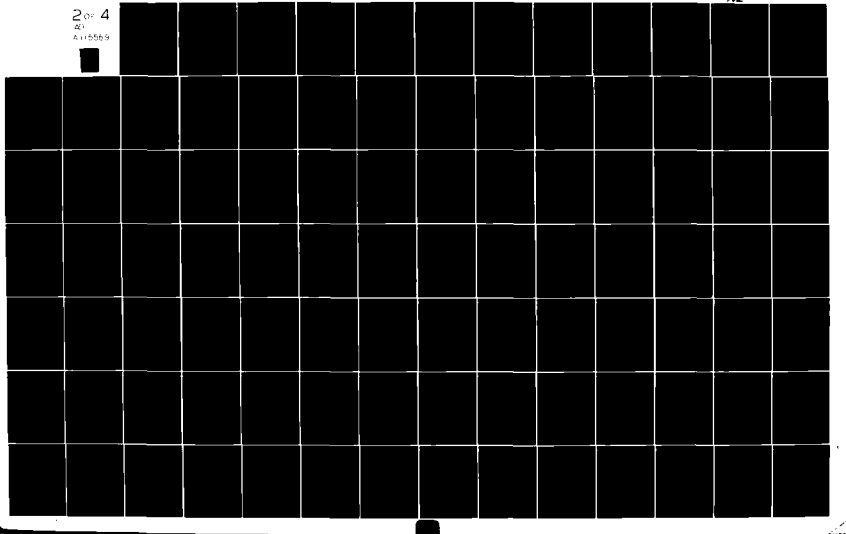

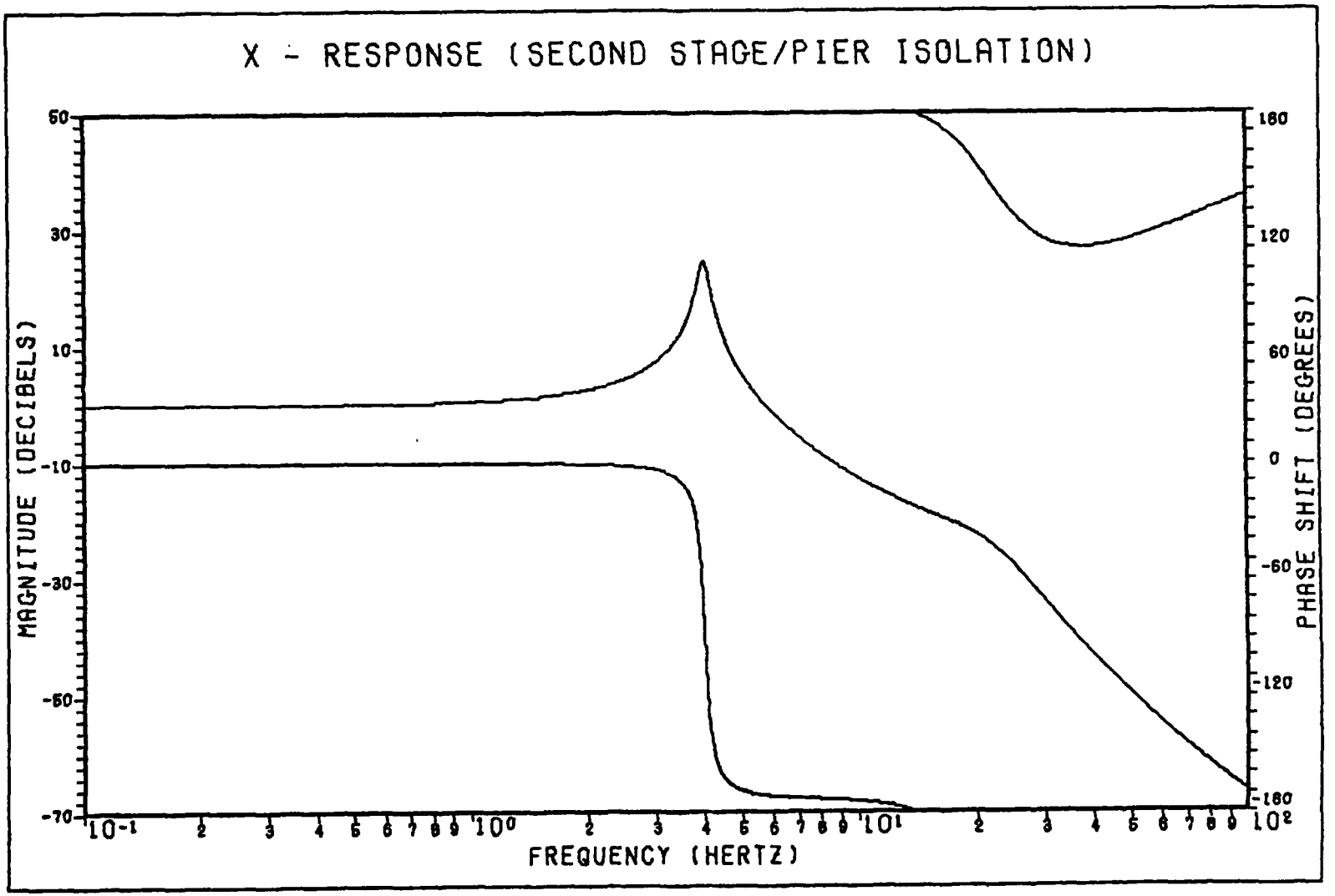

Figure 4.12 X-Response (Second Stage/Pier Isolation)

Theta-Response (SSP Isolation)

$$T\Theta_{U/P}(j\omega) = \Theta_U(j\omega)/\Theta_P(j\omega)$$

$$= \frac{27.66(j\omega + 397.9)(j\omega + 418.9)}{(j\omega + 0.8363 \pm j26.10)(j\omega + 8.273 \pm j81.81)}$$

(4-39)

Bode plot is shown in Figure 4.13.

Theta-Response (First Stage/Pier Isolation)

$$T\Theta_{L/P}(j\omega) = \Theta_L(j\omega)/\Theta_P(j\omega)$$

$$= \frac{96.53(j\omega + 199.6)(j\omega + 397.9)}{(j\omega + 1.508 \pm j34.50)(j\omega + 16.06 \pm j78.57)}$$

(4-40)

Bode plot is shown in Figure 4.14.

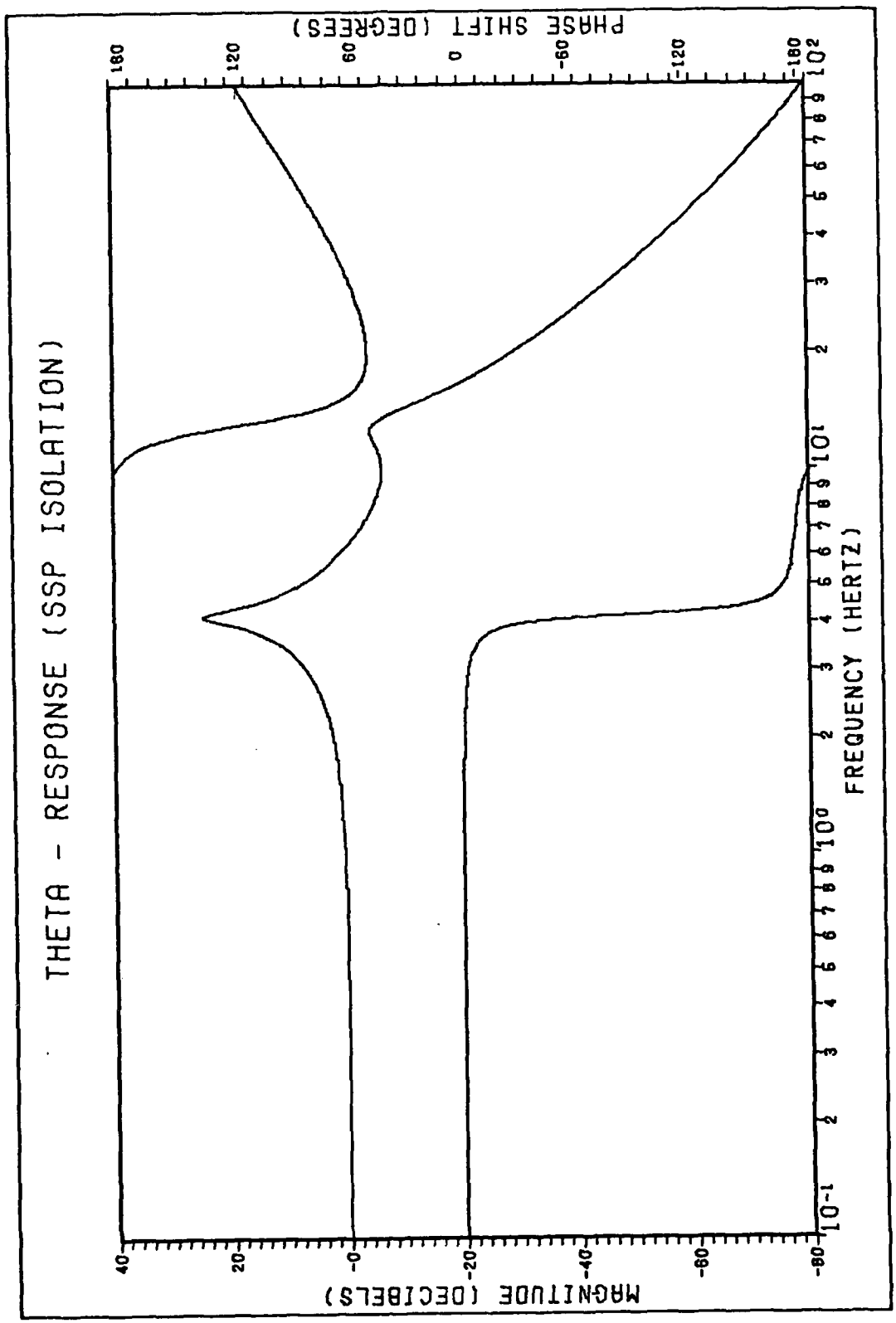

Figure 4.13 Theta-Response (SSP Isolation)

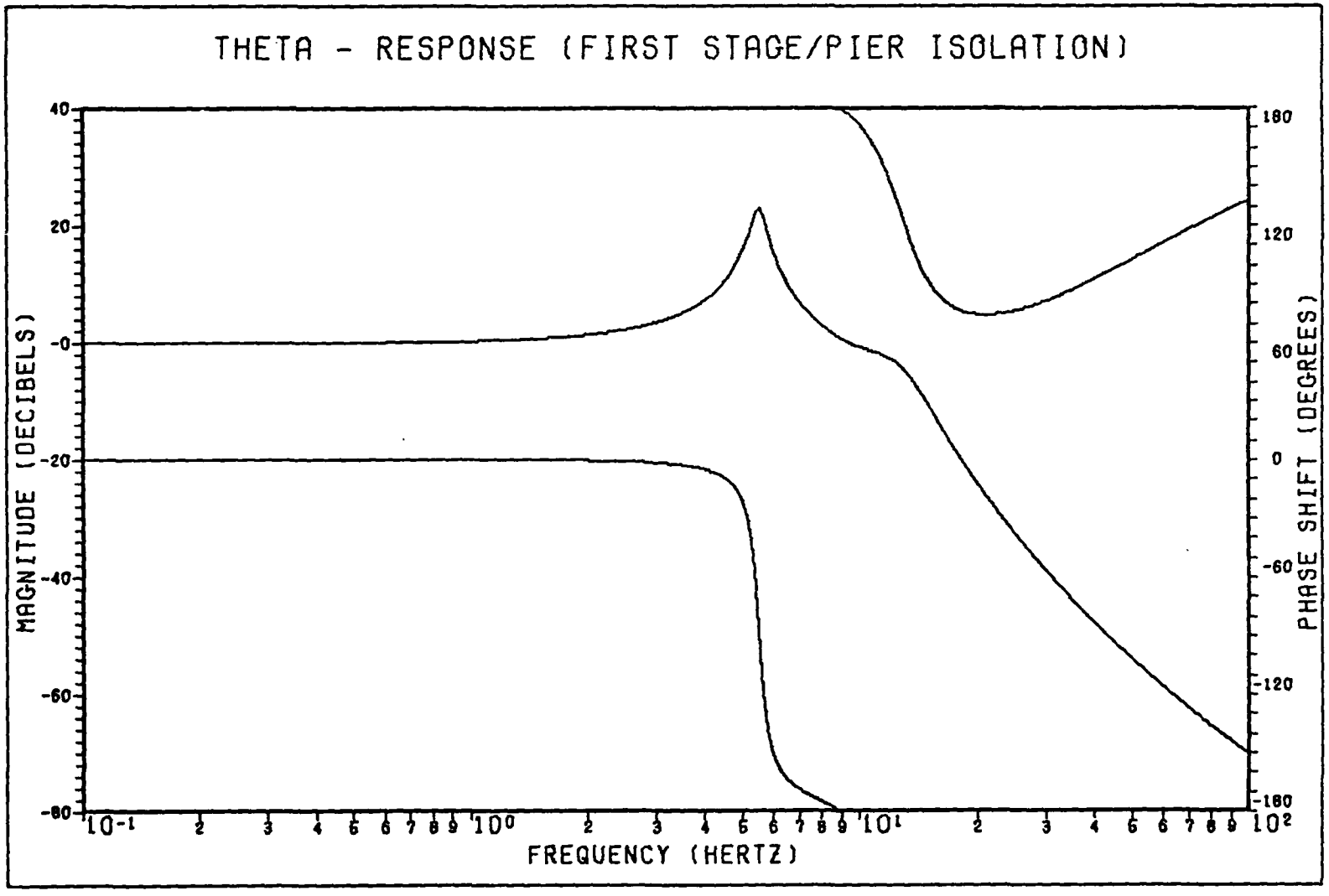

Figure 4.14 Theta-Response (First Stage/Pier Isolation)

Theta-Response (Second Stage/Pier Isolation)

$$T\Theta_{U/G}(j\omega) = \Theta_U(j\omega)/\Theta_G(j\omega)$$

$$= \frac{97.34(j\omega + 199.6)(j\omega + 418.9)}{(j\omega + 1.532 \pm j35.71)(j\omega + 15.92 \pm j78.23)} \quad (4\text{-}41)$$

Bode plot is shown in Figure 4.15.

PSI-Response (SSP Isolation)

$$T\psi_{U/P}(j\omega) = \psi_U(j\omega)/\psi_P(j\omega) = \phi_U(j\omega)/\phi_P(j\omega)$$

$$= \frac{6.99(j\omega + 188.5)^2}{(j\omega + 0.4201 \pm j12.58)(j\omega + 4.160 \pm j39.38)} \quad (4\text{-}42)$$

Bode plot is shown in Figure 4.16.

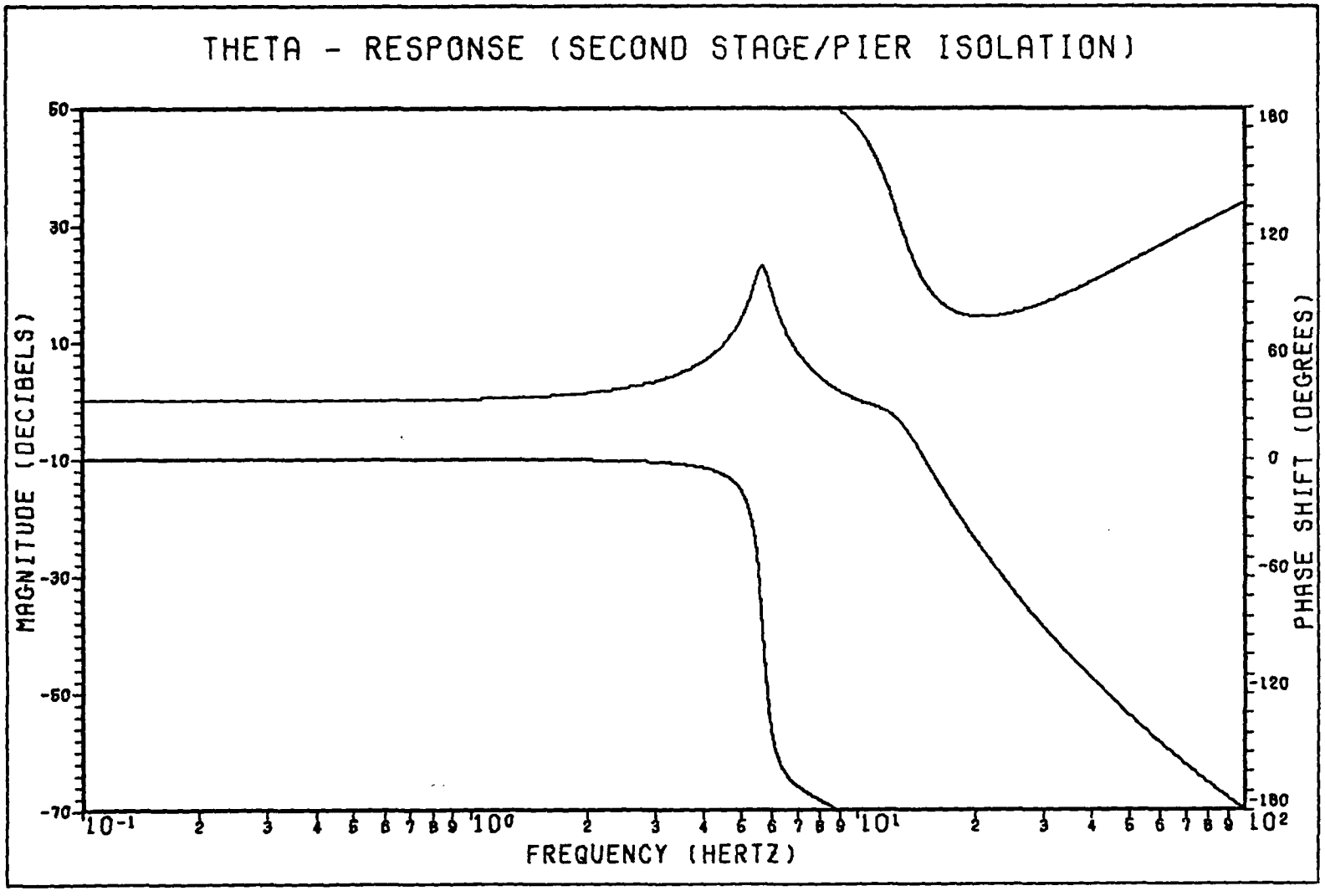

Figure 4.15 Theta-Response (Second Stage/Pier Isolation)

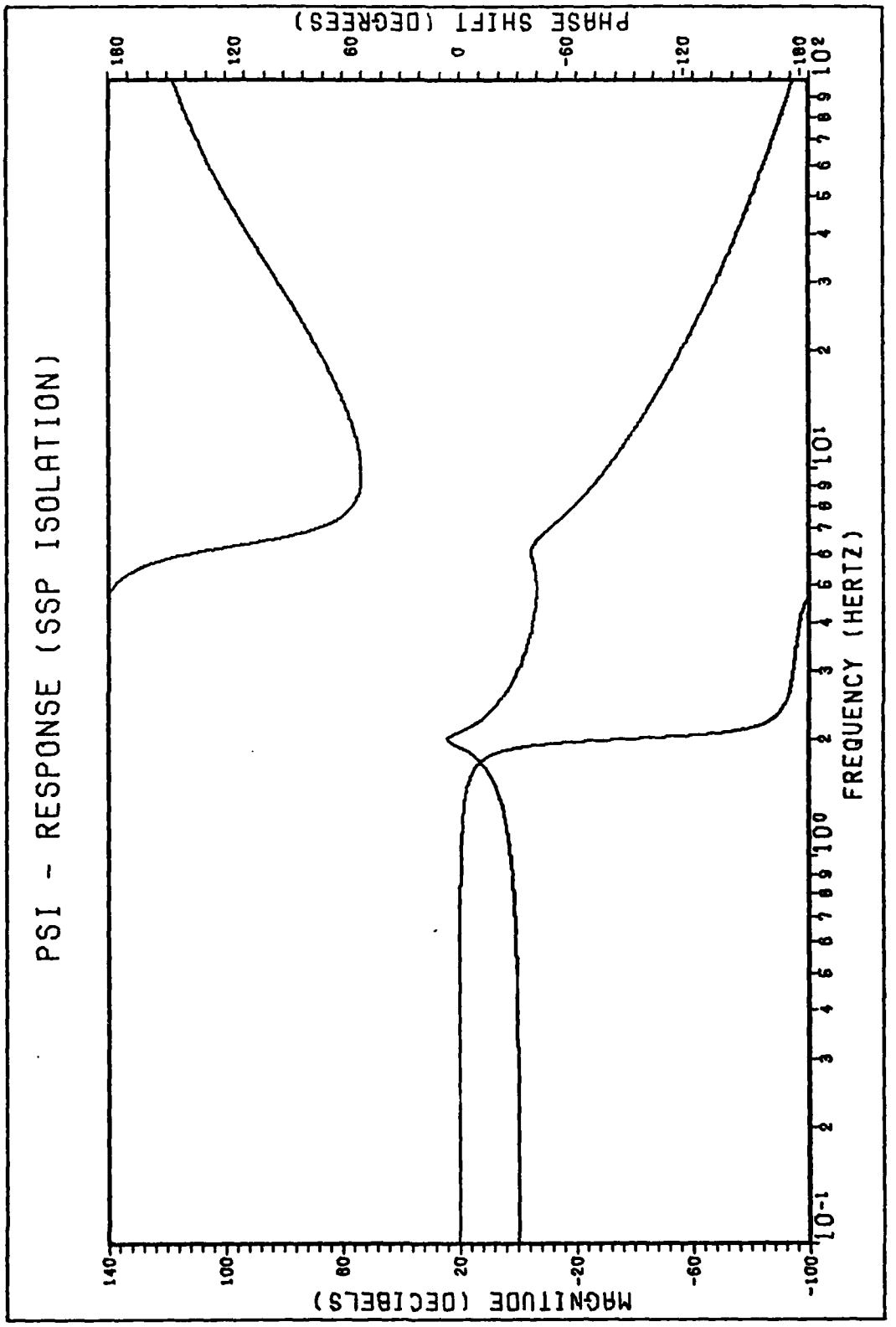

Figure 4.16 PSI-Response (SSP Isolation)

PSI-Response (First Stage/Pier Isolation)

$$T\psi_{L/P}(j\omega) = \psi_L(j\omega)/\psi_P(j\omega) = \phi_L(j\omega)/\phi_P(j\omega)$$

$$= \frac{131.1(j\omega + 128.5)(j\ \ + 188.5)}{(j\omega + 0.7764 \pm j17.09)(j\omega + 42.23 \pm j95.24)}$$

(4-43)

Bode plot is shown in Figure 4.17.

PSI-Response (Second Stage/Pier Isolation

$$T\psi_{U/G}(j\omega) = \psi_U(j\omega)/\psi_G(j\omega) = \phi_U(j\omega)/\phi_G(j\omega)$$

$$= \frac{125.2(j\omega + 128.5)(j\omega + 188.5)}{(j\omega + 0.7496 \pm j16.79)(j\omega + 41.77 \pm j94.82)}$$

(4-44)

Bode plot is shown in Figure 4.18.

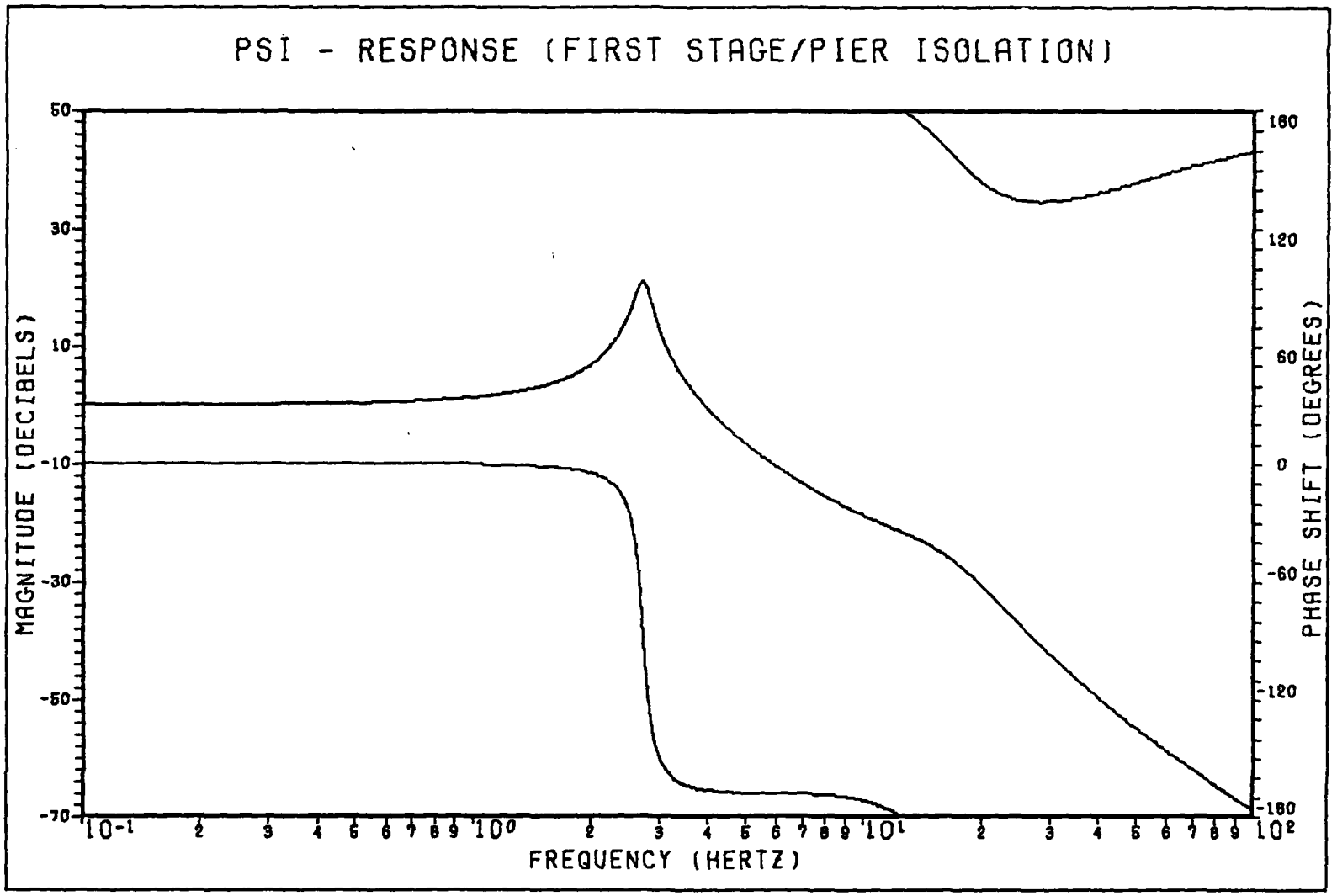

Figure 4.17 PSI-Response (First Stage/Pier Isolation)

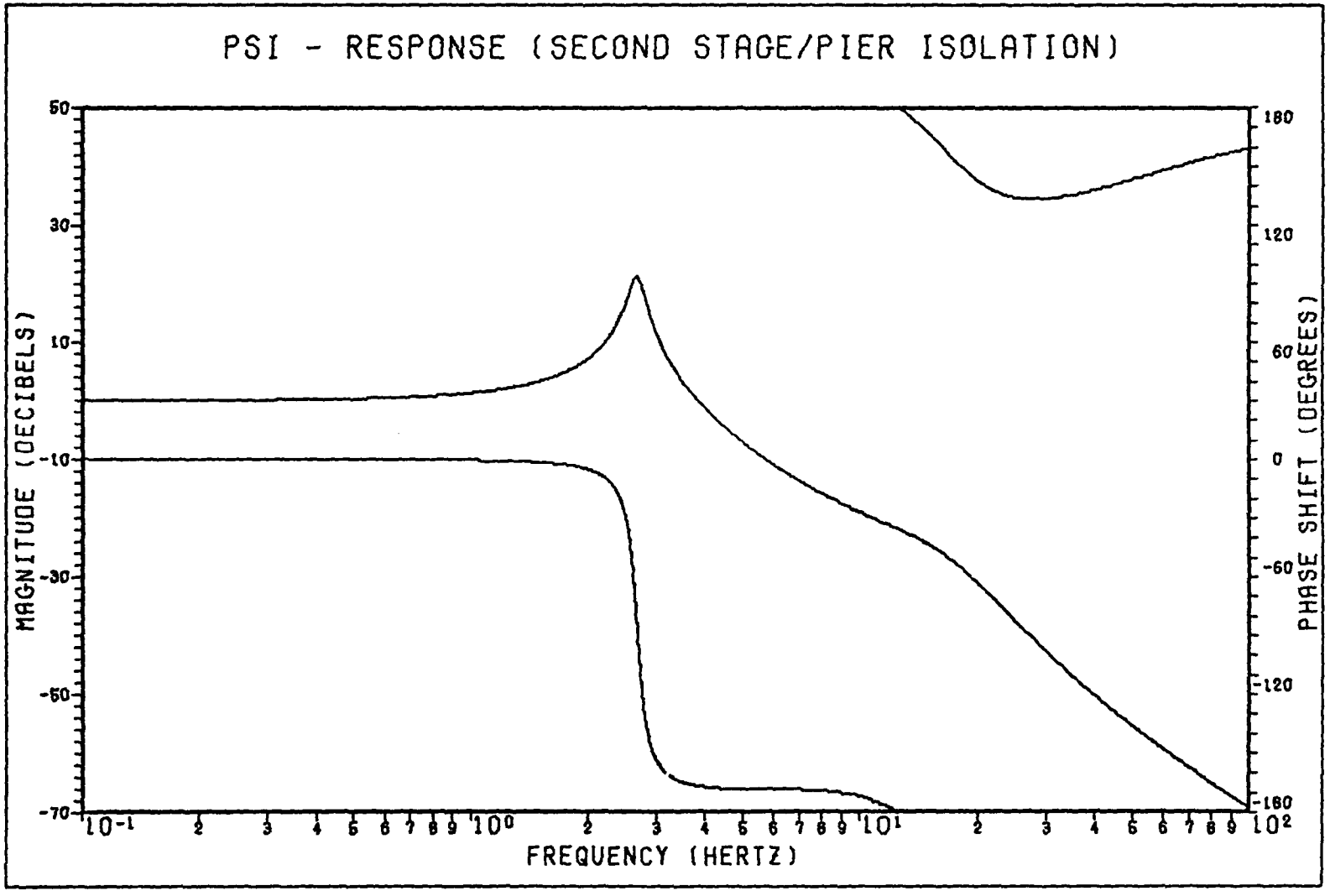

Figure 4.18 PSI-Response (Second Stage/Pier Isolation)

Dual Isolation Analysis

Two important results are gained from the analysis of the dual isolation configurations. First, the SSP isolation dynamics do dominate the passive transmissibility responses. Secondly, the small gain and phase margins are directly attributable to the SSP isolator dynamics.

Table 4.3 summarizes the frequency characteristics for the dual isolation response. The Z direction is a good example of the SSP isolation dynamics role. The SSP isolation dynamics in the Z direction compare directly to the theoretical first and second resonant peaks discussed for the Z full isolation, clearly showing the dominance of the SSP isolation over the pier dynamics. When the first stage or the second stage isolation are considered with the pier, the pneumatic isolator dynamics dominate and compare exactly to the isolator vertical design frequency in Appendix E. The second resonance of either isolation stage and the pier dynamics is at 22 Hz.

The SSP isolation configuration in the Z direction has the same small gain and phase margin as did the full Z isolation case. Only when one level of pneumatic isolation is considered does the gain and phase margin increase as shown in Table 4.3.

The same SSP isolation dynamics analysis and results can be extended for the X (or Y), θ and ψ(orϕ) directions.

A summary of unit step responses from TOTAL for the dual isolation configurations are presented in Table 4.4. Clearly, the long settling times and peak overshoots are identified with the SSP isolation dynamics.

Simple Single Mass, Spring and Damper Networks

A single mass, spring and damper single level isolation system is shown in Figure 4.19A. Figures 4.19B through 4.19D show the various SSP single level isolation configurations possible using the Z scalar derivations used in the other simple three and two mass mechanical networks. The position transmissibility for Figure 4.19A is written in Laplace operator notation, zero initial conditions:

$$\frac{Z_2(s)}{Z_1(s)} = \frac{cs + k}{ms^2 + cs + k} \tag{4-45}$$

Or in the frequency domain, the transmissibility is written as

$$\frac{Z_2(j\omega)}{Z_1(j\omega)} = \frac{cj\omega + k}{mj\omega^2 + cj + k} \tag{4-46}$$

The transmissibilities for the various single levels are solved by substituting the active SSP isolation level spring and damper for k and c respectively. The mass, m, simply becomes the total mass supported by the isolation level. These substitutions are summarized for the indicated figures as follows:

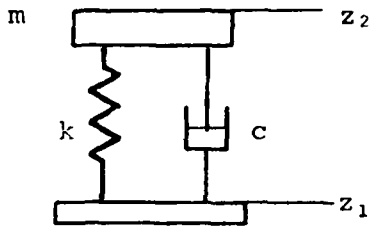

Figure 4.19A Simple Mass, Spring and Damper Network

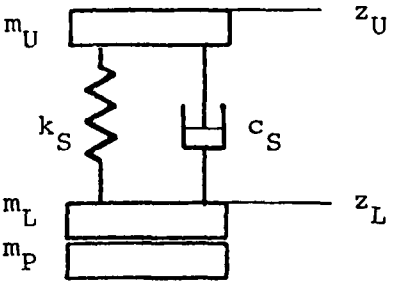

Figure 4.19B Second Stage Isolation

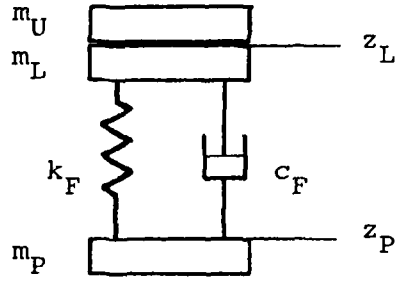

Figure 4.19C First Stage Isolation

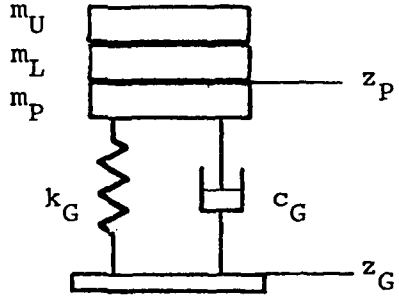

Figure 4.19D Pier Isolation

Figure 4.19B	m_U	→	m	(4-47a)
	c_S	→	c	(4-47b)
	k_S	→	k	(4-47c)
Figure 4.19C	$m_U + m_L$	→	m	(4-48a)
	c_F	→	c	(4-48b)
	k_F	→	k	(4-48c)
Figure 4.19D	$m_U + m_L + m_P$	→	m	(4-49a)
	c_G	→	c	(4-49b)
	k_G	→	k	(4-49c)

Once the scalar substitutions have been made, appropriate parallel forms are identified as s done for the other networks using Eqs 4-18, 4-20 and 4-22.

The three transmissibilities just solved are now expressed in factored form for the six degrees of freedom with Bode plot references given. Tables 4.5 and 4.6 summarize key frequency and unit time response performance values, respectively.

Table 4.5

Single Isolation Frequency Characteristics Summary

$T(j\omega)$	Resonant Frequency	Peak Magnitude
$TZ_{U/L}(j\omega)$	1.8 Hz	24.45dB
$TZ_{L/P}(j\omega)$	1.8 Hz	24.45dB
$TZ_{P/G}(j\omega)$	19.0 Hz	3.01dB
$TX_{U/L}(j\omega)$	4.0 Hz	24.45dB
$TX_{L/P}(j\omega)$	3.8 Hz	24.45dB
$TX_{P/G}(j\omega)$	19.0 Hz	5.42dB
$T\Theta_{U/L}(j\omega)$	5.7 Hz	21.39dB
$T\Theta_{L/P}(j\omega)$	5.5 Hz	21.25dB
$T\Theta_{P/G}(j\omega)$	20.0 Hz	8.79dB
$T\psi_{U/L}(j\omega)$	2.7 Hz	20.78dB
$T\psi_{L/P}(j\omega)$	2.7 Hz	20.79dB
$T\psi_{P/G}(j\omega)$	15.0 Hz	4.37dB

where,

$T(j\omega)$, transmissibility frequency function

(Ref 6:82)

Table 4.6 Single Isolation Unit Step Time Response Summary

f(t)	TR(sec)	TD(sec)	TP(sec)	TS(sec)	MP	FV
$TZ_{U/L}(t)$	0.0919	0.1362	0.2725	11.4159	1.9116	1.0000
$TZ_{L/P}(t)$	0.0919	0.1362	0.2725	11.4160	1.9116	1.0000
$TZ_{P/G}(t)$	0.0066	0.0085	0.0171	0.0529	1.2769	1.0000
$TX_{U/L}(t)$	0.0413	0.0613	0.1226	5.1371	1.9116	1.0000
$TX_{L/P}(t)$	0.0435	0.0645	0.1291	5.4075	1.9116	1.0000
$TX_{P/G}(t)$	0.0077	0.0099	0.0198	0.0803	1.4220	1.0000
$T\Theta_{U/L}(t)$	0.0292	0.0427	0.0854	2.5496	1.8774	1.0000
$T\Theta_{L/P}(t)$	0.0302	0.0441	0.0883	2.5525	1.8754	1.0000
$T\Theta_{P/G}(t)$	0.0178	0.0233	0.0466	0.2794	1.5319	1.0000
$T\psi_{U/L}(t)$	0.0623	0.0908	0.1817	5.0744	1.8726	1.0000
$T\psi_{L/P}(t)$	0.0612	0.0892	0.1784	4.9769	1.8705	1.0000
$T\psi_{P/G}(t)$	0.0096	0.0123	0.0246	0.0975	1.3644	1.0000

where,

TR, rise time TD, duplication time TP, peak time

TS, setting time MP, peak value FV, final value

f(t), transmissibility time function

(Ref 6:82)

Z-Response (Second Stage Isolation)

$$TZ_{U/L}(j\omega) = Z_U(j\omega)/Z_L(j\omega)$$

$$= \frac{0.6786(j\omega + 188.5)}{(j\omega + 0.3393 \pm j11.30)} \qquad (4\text{-}50)$$

Bode plot is shown in Figure 4.20.

Z-Response (First Stage Isolation)

$$TZ_{L/P}(j\omega) = Z_L(j\omega)/Z_P(j\omega)$$

$$= \frac{0.6786(j\omega + 188.5)}{(j\omega + 0.3393 \pm j11.30)} \qquad (4\text{-}51)$$

Bode plot is shown in Figure 4.21.

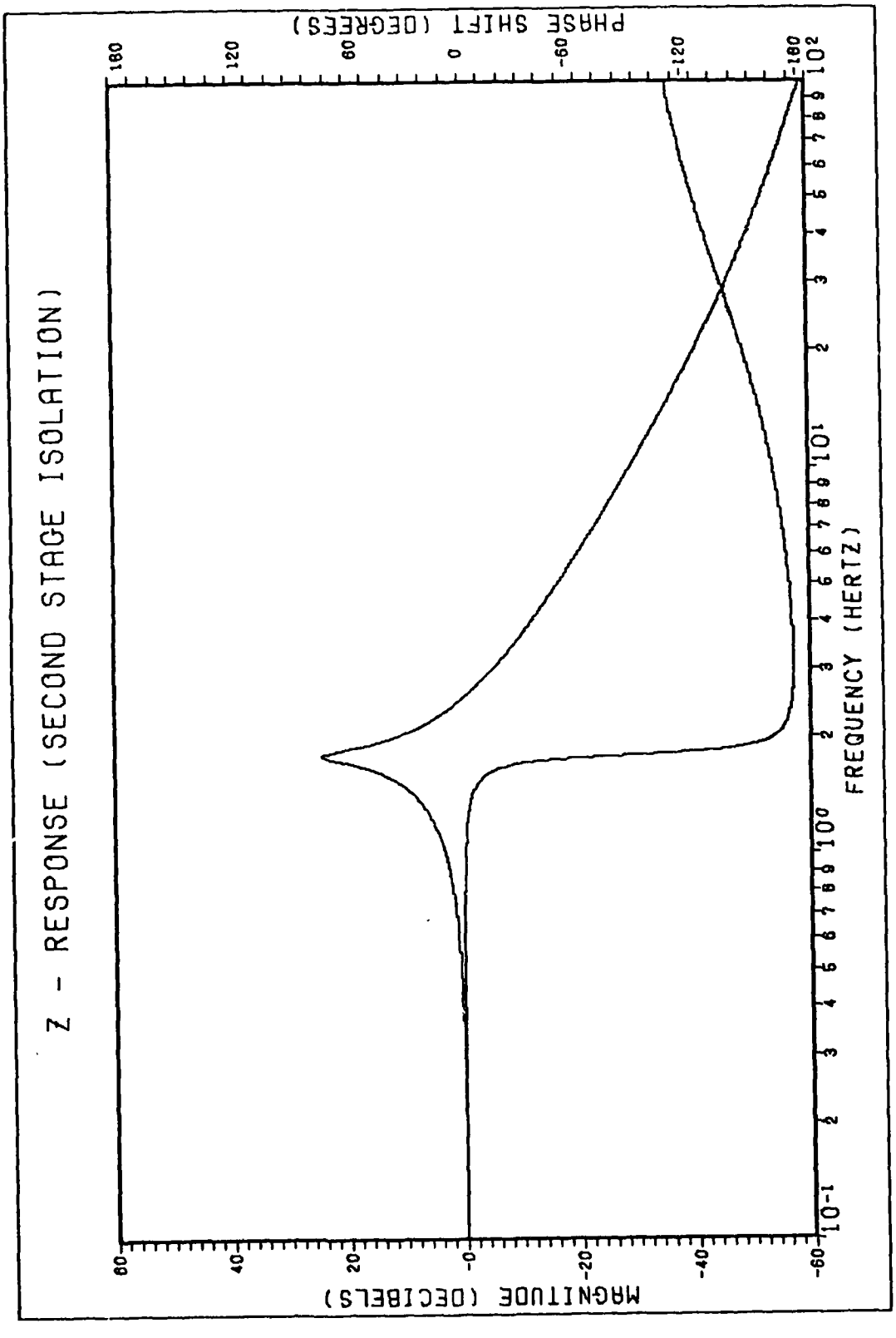

Figure 4.20 Z-Response (Second Stage Isolation)

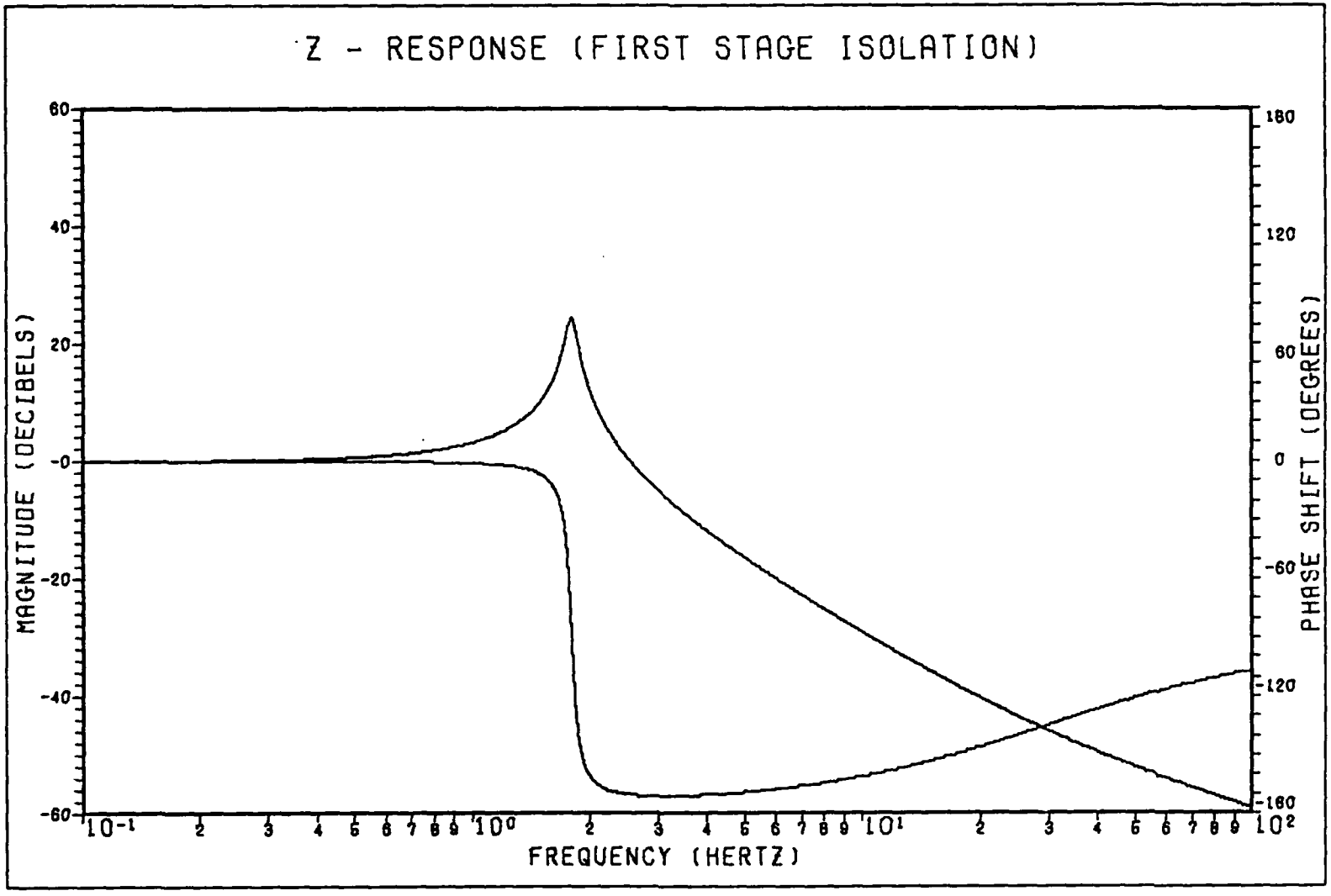

Figure 4.21 Z-Response (First Stage Isolation)

Z-Response (Pier Isolation)

$$TZ_{P/G}(j\omega) \approx Z_P(j\omega)/Z_G(j\omega)$$

$$= \frac{150.0(j\omega + 128.5)}{(j\omega + 74.99 \pm j116.8)} \qquad (4\text{-}52)$$

Bode plot is shown in Figure 4.22.

X-Response (Second Stage Isolation)

$$TX_{U/L}(j\omega) \approx X_U(j\omega)/X_L(j\omega) = Y_U(j\omega)/Y_L(j\omega)$$

$$= \frac{1.508(j\omega + 418.9)}{(j\omega + 0.7540 \pm j25.12)} \qquad (4\text{-}53)$$

Bode plot is shown in Figure 4.23.

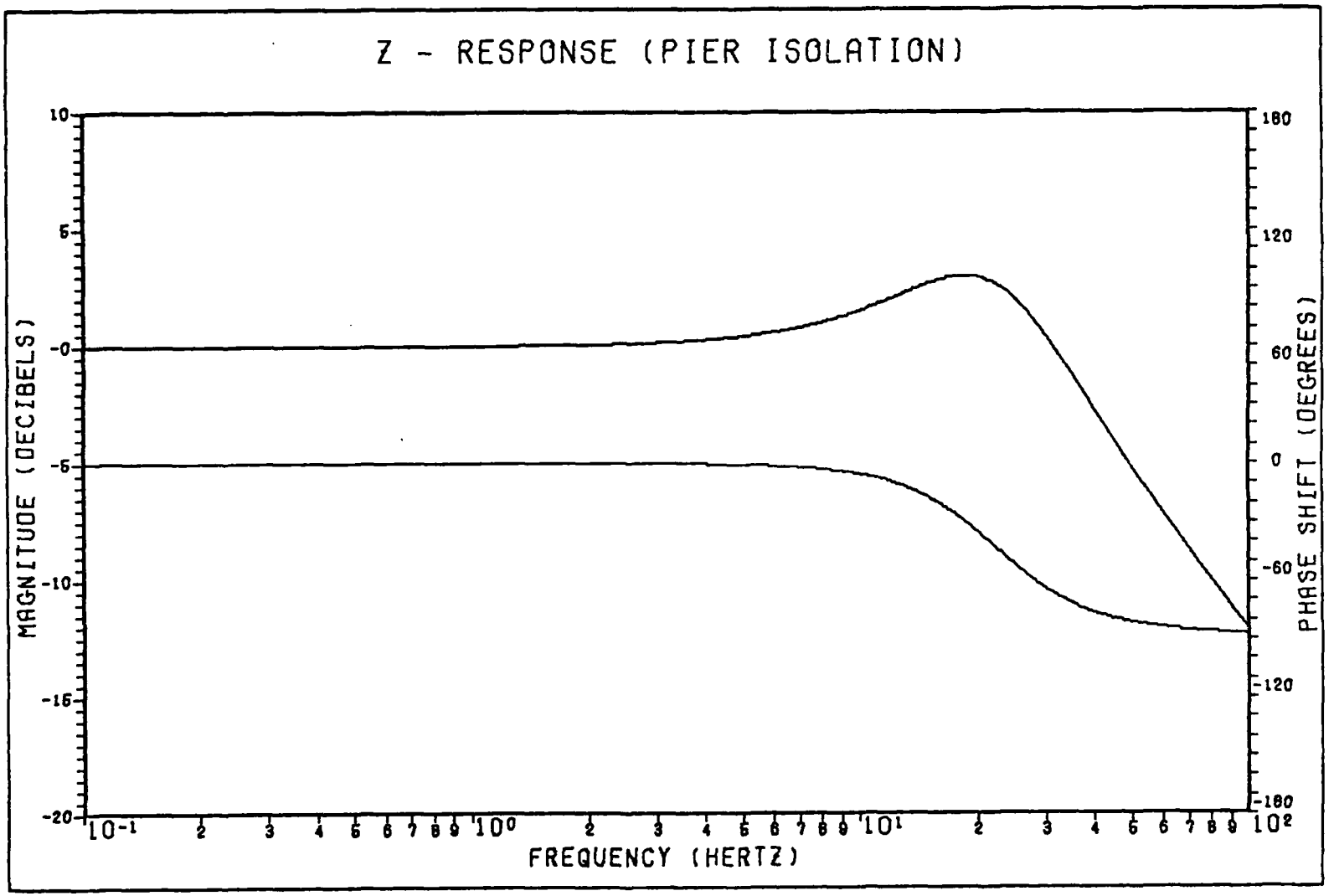

Figure 4.22 Z-Response (Pier Isolation)

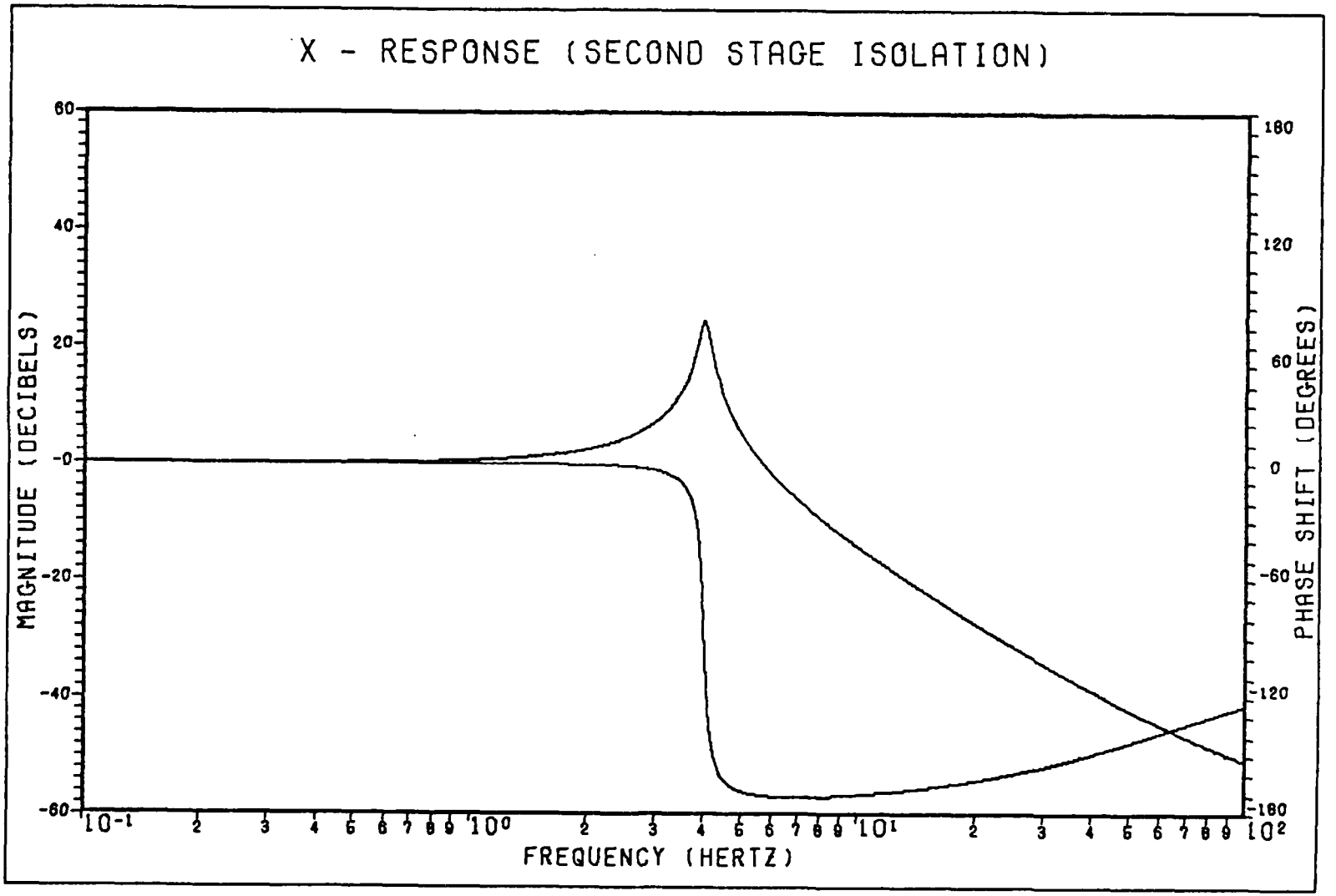

Figure 4.23 X-Response (Second Stage Isolation)

X-Response (First Stage Isolation)

$$TX_{L/P}(j\omega) = X_L(j\omega)/X_P(j\omega) = Y_L(j\omega)/Y_P(j\omega)$$

$$= \frac{1.433(j\omega + 397.9)}{(j\omega + 0.7163 \pm j23.87)} \qquad (4\text{-}54)$$

Bode plot is shown in Figure 4.24.

X-Response (Pier Isolation)

$$TX_{P/G}(j\omega) = X_P(j\omega)/X_G(j\omega) = Y_P(j\omega)/Y_G(j\omega)$$

$$= \frac{86.87(j\omega + 199.6)}{(j\omega + 43.44 \pm j124.3)} \qquad (4\text{-}55)$$

Bode plot is shown in Figure 4.25.

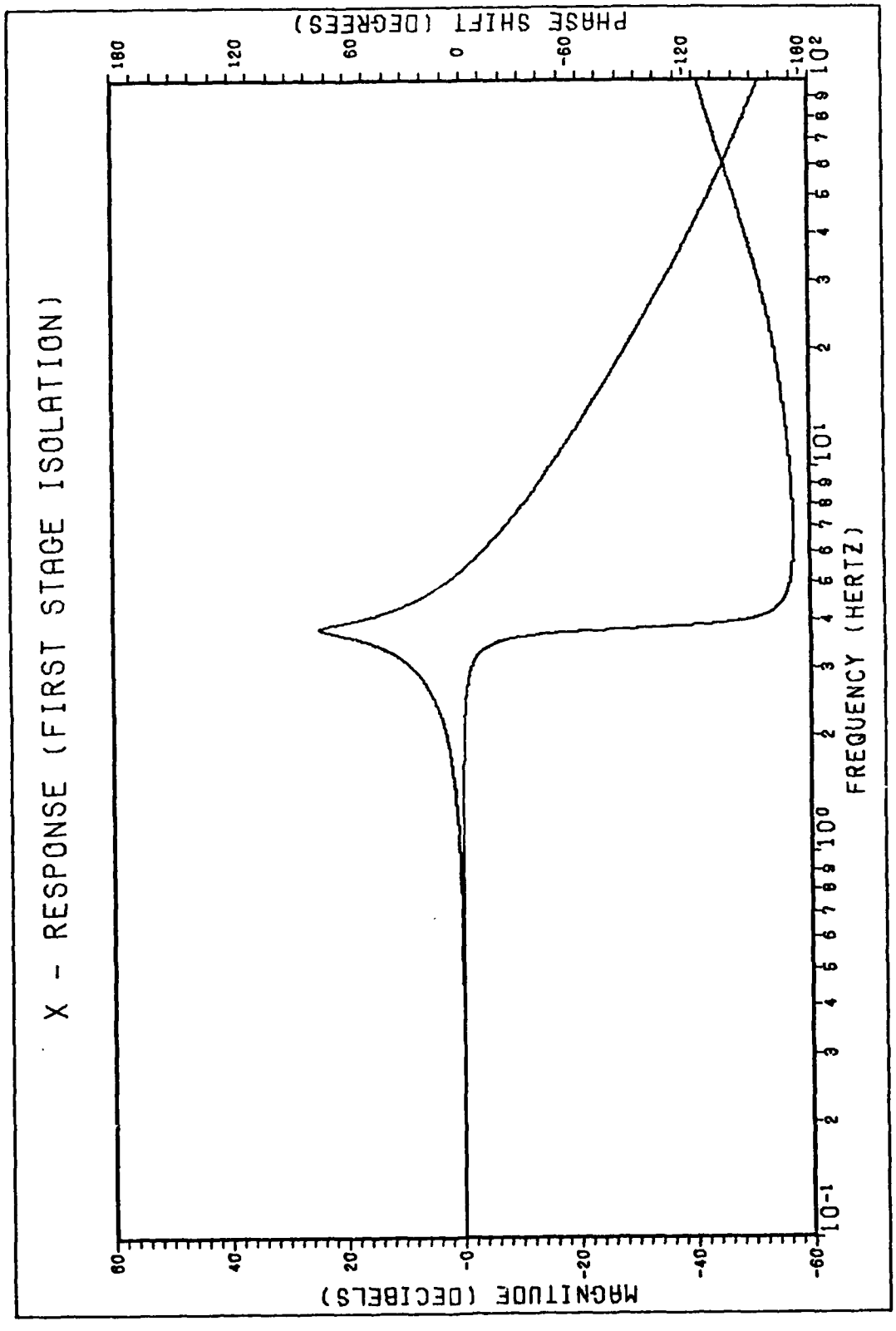

Figure 4.24 X-Response (First Stage Isolation)

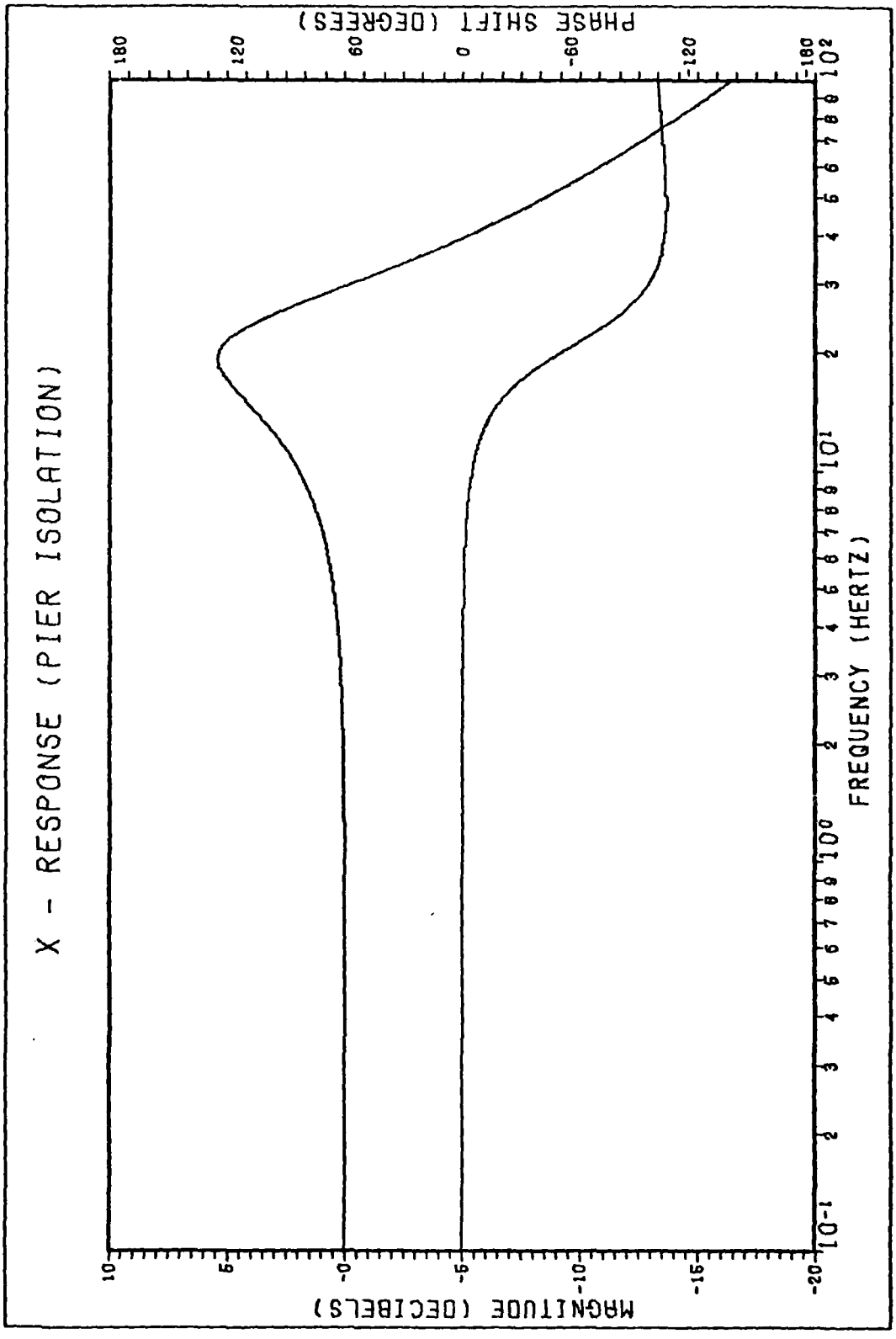

Figure 4.25 X-Response (Pier Isolation)

PSI-Response (Second Stage Isolation)

$$T\psi_{U/L}(j\omega) = \psi_U(j\omega)/\psi_L(j\omega) = \phi_U(j\omega)/\phi_L(j\omega)$$

$$= \frac{1.50(j\omega + 188.5)}{(j\omega + 0.7499 \pm j16.80)} \qquad (4\text{-}56)$$

Bode plot is shown in Figure 4.26.

PSI-Response (First Stage Isolation)

$$T\psi_{L/P}(j\omega) = \psi_L(j\omega)/\psi_P(j\omega) = \phi_L(j\omega)/\phi_P(j\omega)$$

$$= \frac{1.554(j\omega + 188.5)}{(j\omega + 0.7768 \pm j17.10)} \qquad (4\text{-}57)$$

Bode plot is shown in Figure 4.27.

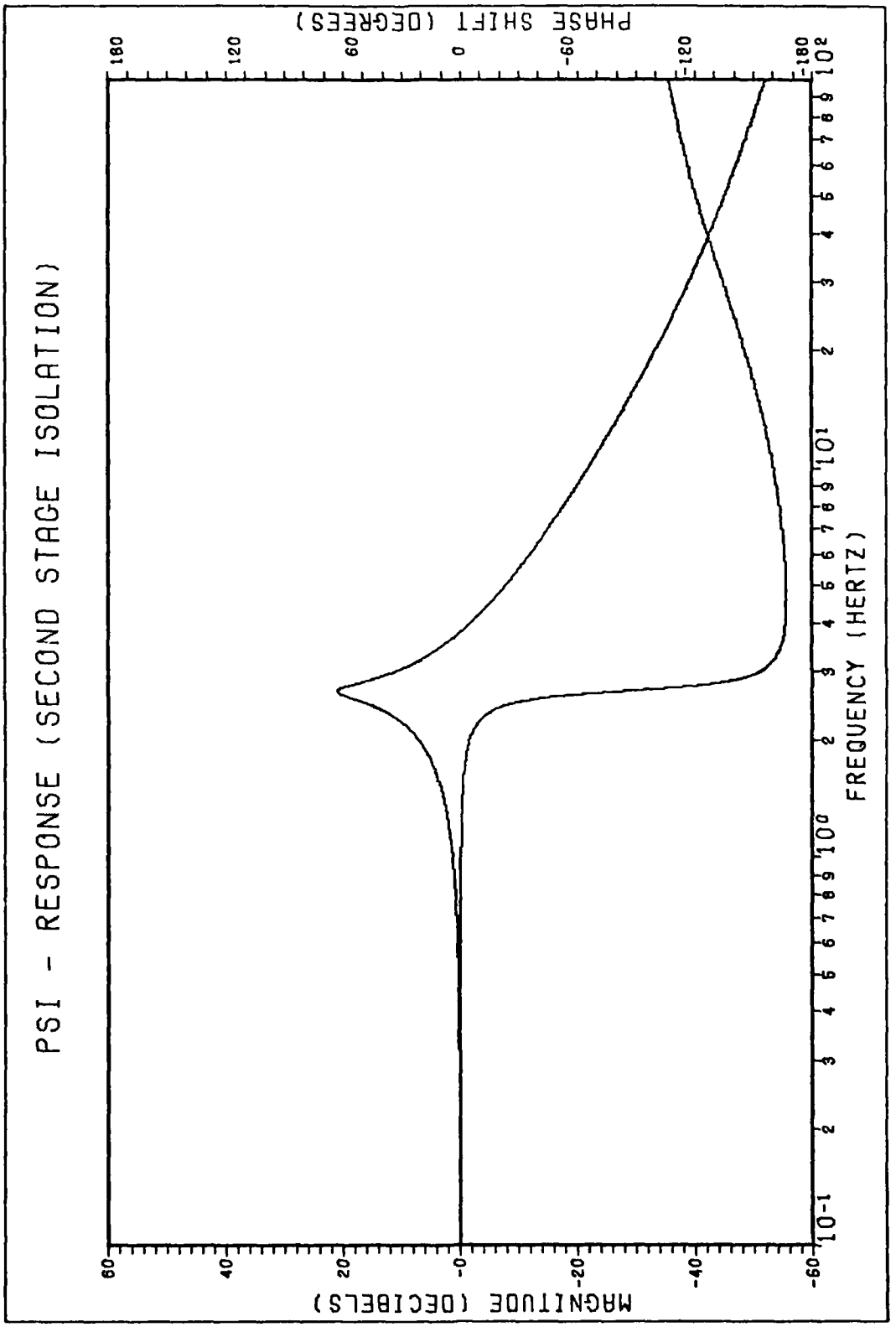

Figure 4.26 PSI-Response (Second Stage Isolation)

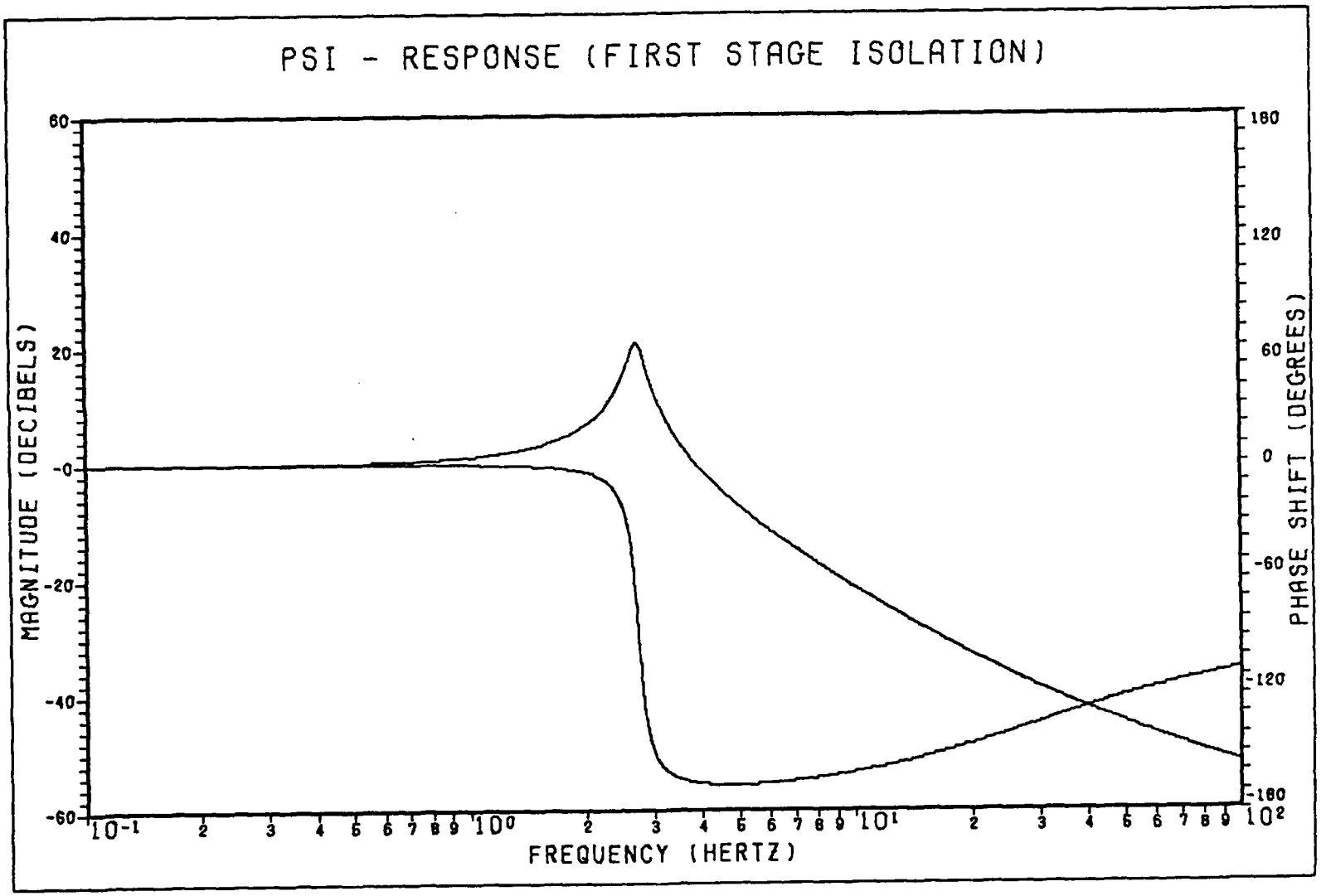

Figure 4.27 PSI-Response (First Stage Isolation)

PSI-Response (Pier Isolation)

$$T\psi_{P/G}(j\omega) = \psi_P(j\omega)/\psi_G(j\omega) \approx \phi_P(j\omega)/\phi_G(j\omega)$$

$$= \frac{81.75(j\omega + 128.5)}{(j\omega + 40.88 \pm j93.98)} \qquad (4\text{-}58)$$

Bode plot is shown in Figure 4.28.

Theta-Response (Second Stage Isolation)

$$T\Theta_{U/L}(j\omega) \approx \Theta_U(j\omega)/\Theta_L(j\omega)$$

$$= \frac{3.061(j\omega + 418.9)}{(j\omega + 1.530 \pm j35.77)} \qquad (4\text{-}59)$$

Bode plot is shown in Figure 4.29.

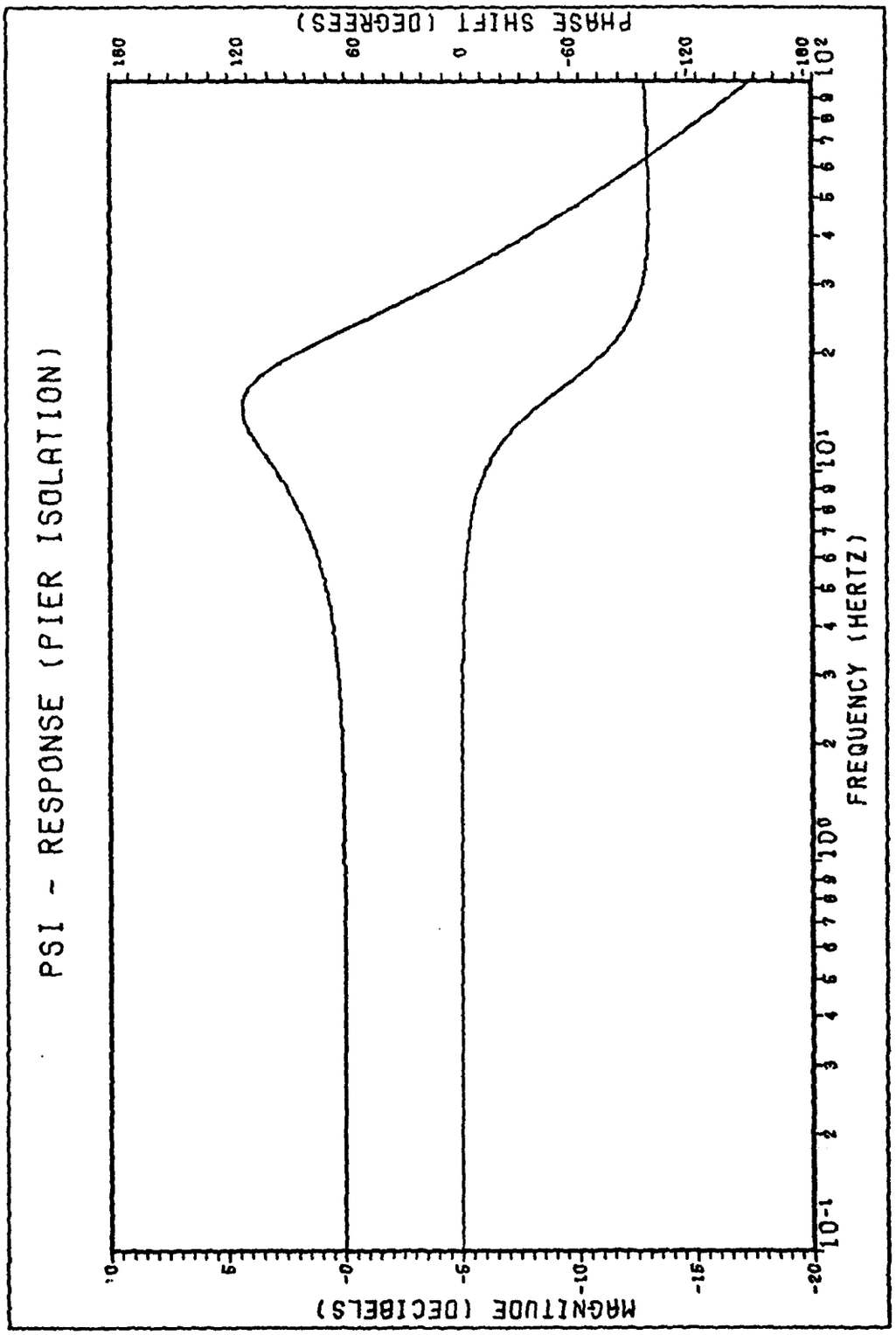

Figure 4.28 PSI-Response (Pier Isolation)

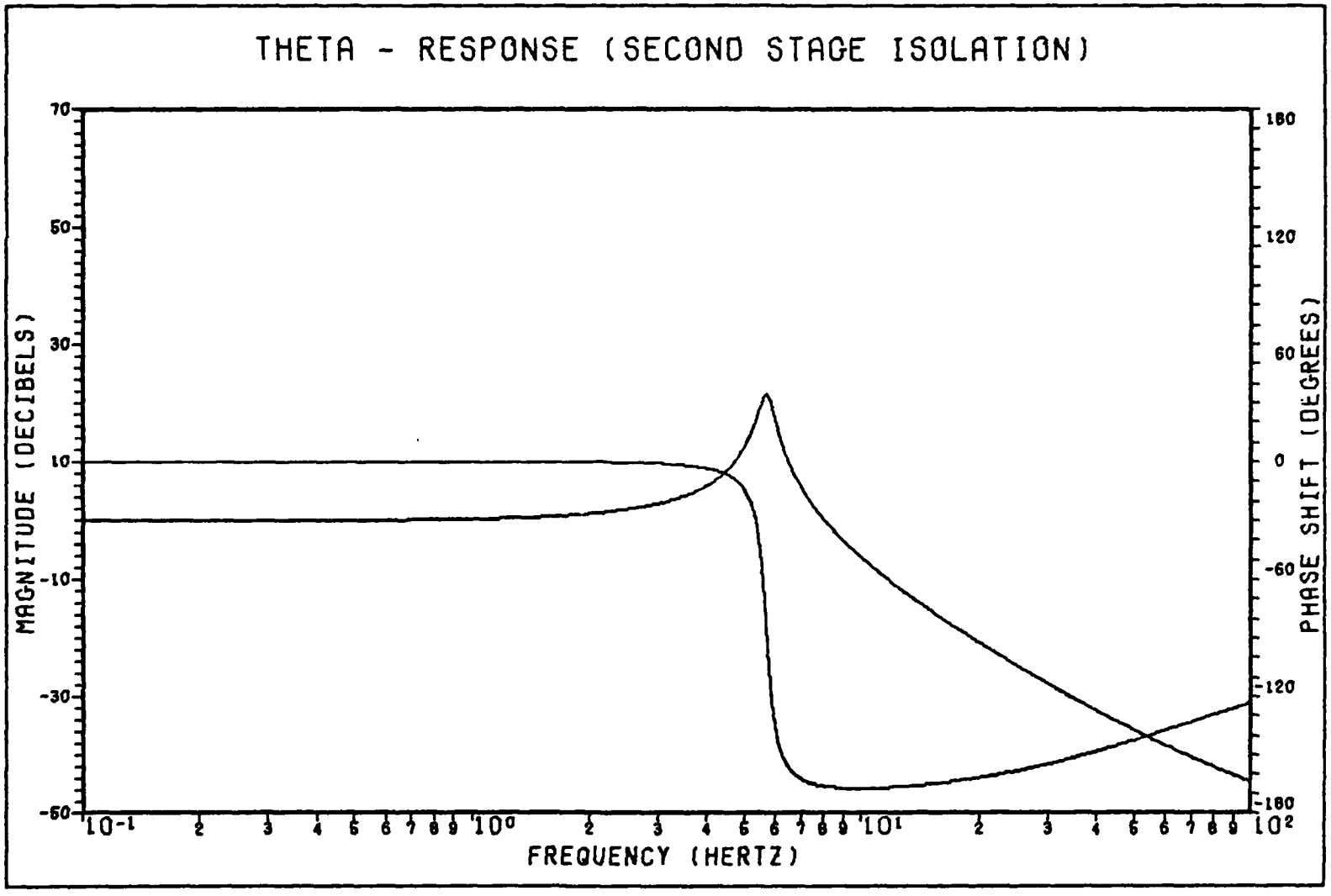

Figure 4.29 Theta-Response (Second Stage Isolation)

Theta-Response (First Stage Isolation)

$$T\Theta_{L/P}(j\omega) = \Theta_L(j\omega)/\Theta_P(j\omega)$$

$$= \frac{3.012(j\omega + 379.9)}{(j\omega + 1.506 \pm j34.59)} \qquad (4\text{-}60)$$

Bode plot is shown in Figure 4.30.

Theta-Response (Pier Isolation)

$$T\Theta_{P/G}(j\omega) = \Theta_P(j\omega)/\Theta_G(j\omega)$$

$$= \frac{31.32(j\omega + 199.6)}{(j\omega + 15.66 \pm j77.51)} \qquad (4\text{-}61)$$

Bode plot is shown in Figure 4.31.

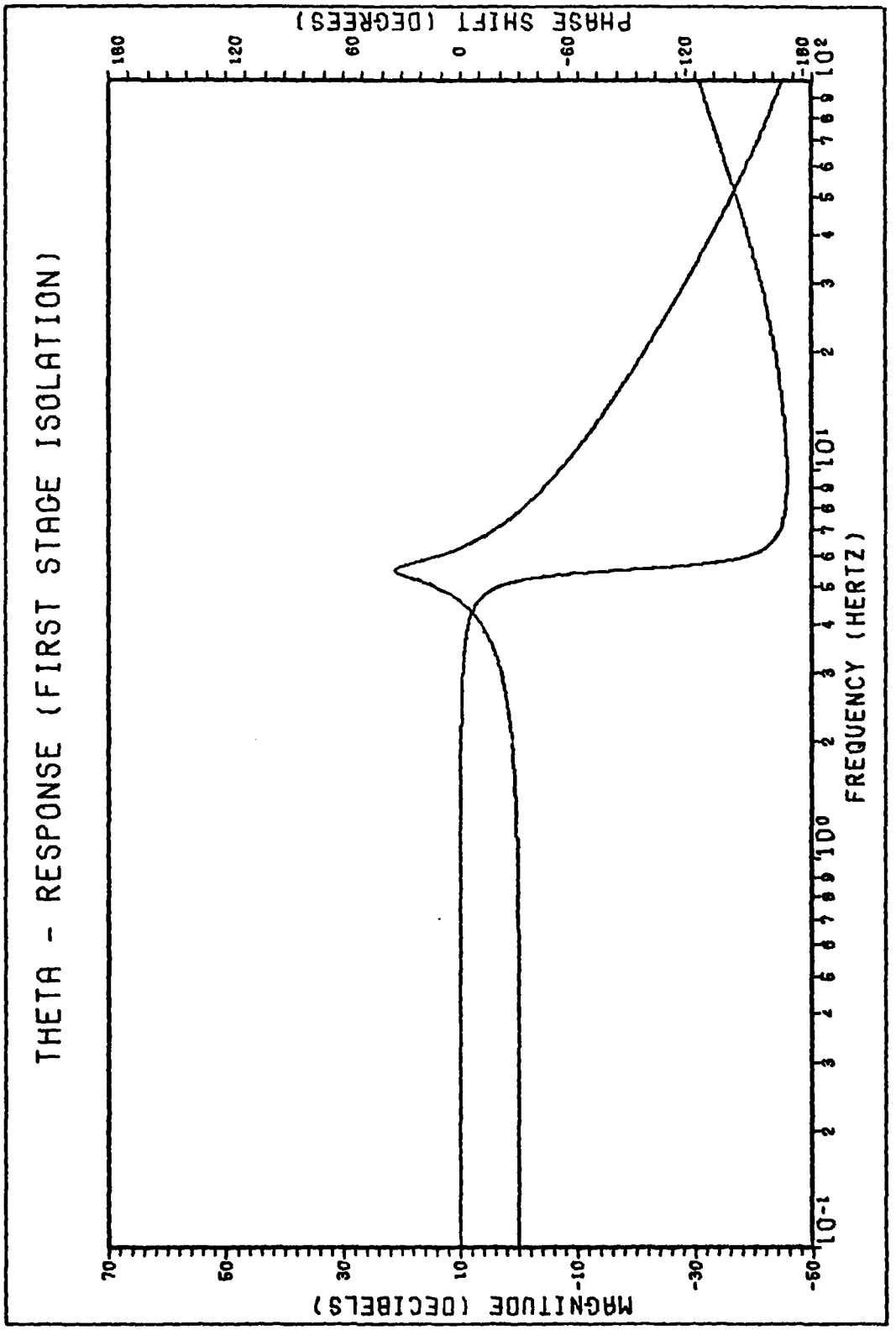

Figure 4.30 Theta-Response (First Stage Isolation)

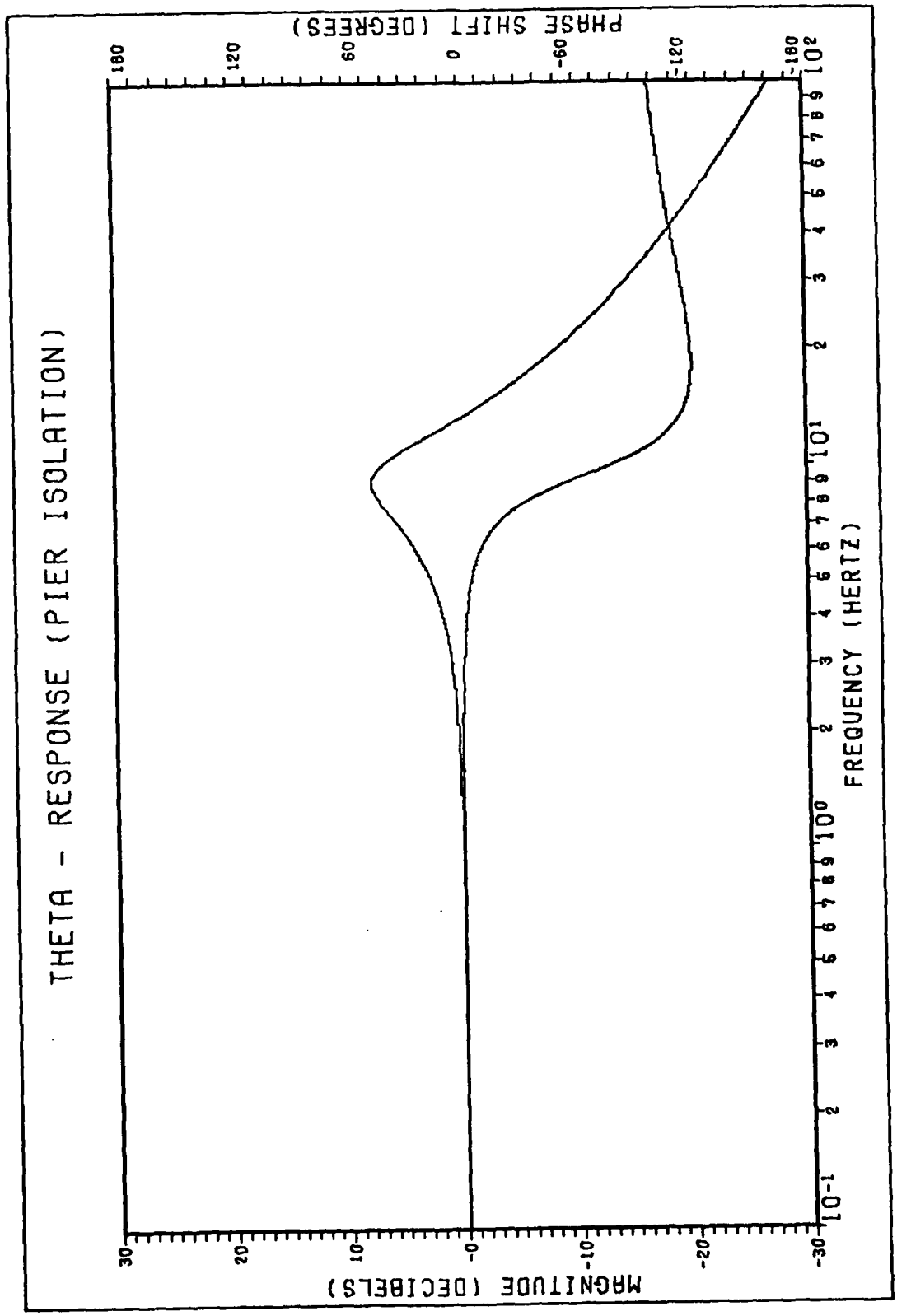

Figure 4.31 Theta-Response (Pier Isolation)

Single Isolation Analysis

Analysis of the full and dual isolation schemes clearly demonstrates the dominance of SSP isolation dynamics. The single level isolation configurations verify isolator design considerations for translation resonances and yield some new insight into rotational isolator effects.

Reviewing the contents of Table 4.5, the Z direction resonant frequencies for the second and first stage isolation are at 1.8 Hz; the intended vertical resonance for each isolator calculated in Appendix E. Similarly, the X (or Y) direction has resonant frequencies of 4.0 Hz and 3.8 Hz for second and first stage horizontal single isolator resonances as planned in Appendix E.

An interesting result of the rotational transmissibilities is the rotational isolator dynamics. The Θ resonance is at 5.7 Hz and 5.5 Hz for the second and first stage resonances. A difference in resonance frequency for the two levels is due to loading effects on isolator stiffness as is presented in the X direction between the second and first stage isolator horizontal resonances. The $\psi(\text{or}\phi)$ direction has the same resonant frequency of 2.7 Hz for both stages of isolation which follows the same vertical frequency resonance for both levels since the intended isolator vertical frequencies are designed the same. In all, the translational and rotational transmissibilities, the resonant magnitudes are nearly five times greater for the second or first stage isolation dynamics compared to the pier effects.

In general, the pier dynamics are prominent at 20 Hz, the upper limit of the active controller bandwidth. The unit step time responses in Table 4.6 show the characteristic slow time responses introduced by either the second or first stage isolation dynamics.

Transmissibility Pole and Zero Analysis

The transmissibility transfer functions for the various levels of isolation are analyzed for each of the six degrees of freedom. For any direction, the full isolation case represents the complete set of poles and zeros. By eliminating an isolation level, the effects on the overall transmissiblity can be verified.

The upper level dynamics in all directions predominate the system performance. The lower level poles are possible sources of instability as is discussed in Chapter V, with the effects on the root locus. The pier dynamics do come theoretically at the edge of the active controller bandwidth at 20 Hz, but in actual measurements, the pier effects are well above 200 Hz (Ref 18). Since the poles and zeros of the various isolation levels do parallel those of the full system, the solutions are verifiable. The slight differences in pole and zero location are due to scaling caused by different configurations having different applied loads.

The rotational transfer functions have an interesting result. The Θ transmissibility zeros are the same as those of the X or Y transmissibility zeros. Similarly, the ψ

and ϕ transmissibility zeros are identical to the Z transmissibility zeros because the same spring and damper dynamic matrices are used in the Θ and X(or Y) or ψ(orϕ) and X(or Y) transmissibilities.

The Z transmissibility and X(or Y) transmissibility pole/zero analysis summaries are in Table 4.7 and 4.8, respectively. For the Θ and ψ(orϕ) rotational transmissibility pole/zero summaries see Table 4.9 and 4.10, respectively. Several analytical checks are possible using the results of these tables. First, the full isolation in any given direction is equal to the combination of all three single isolation levels. Secondly, the full isolation in any given direction is equal to two levels of isolation plus a single level of isolation in that direction. Care must be taken in these calculations because the resonant frequencies (see Eq 3-8) are a function of the isolator applied load. If single levels are to be added for the full isolation verification, each single level must consider the load applied to it. Analyzing Figure 4.1 to emphasize the loading effect, the second stage isolation load is m_U while the first stage load is m_L (not $m_U + m_L$) and the pier stage load is m_P (not $m_P + m_U + m_L$). Each pole and zero for the single stage correspond exactly to the full isolation poles and zeros when properly loaded. This verification is reassuring for the transmissiblities methods used and the physical intuition of the SSP. This verification was used successfully

Table 4.7 Z-Transmissibility Transfer Function Zeros and Poles

$T(j\omega)$	K	z_1	z_2	z_3	$p_{1,2}$	$p_{3,4}$	$p_{5,6}$
$TZ_{U/G}(j\omega)$	223.3	-128.5	-188.5	-188.5	-0.182±j8.421	-1.715±j25.37	-86.47±j121.4
$TZ_{U/P}(j\omega)$	1.3		-188.5	-188.5	-0.188±j8.422	-1.716±j25.37	
$TZ_{L/P}(j\omega)$	117.3	-128.5	-188.5			-0.339±j11.30	-86.47±j121.4
$TZ_{U/G}(j\omega)$	111.2		-188.5		-0.339±j11.30		-82.00±j119.8
$TZ_{U/L}(j\omega)$	0.7			-188.5	-0.339±j11.30		
$TZ_{L/P}(j\omega)$	0.7		-188.5			-0.339±j11.30	
$TZ_{P/G}(j\omega)$	150.0	-128.5					-74.99±j116.8

where,

K - constant for transfer function

z_1 , z_2 - transfer function zero

$p_{1,2}$, $p_{3,4}$, $p_{5,6}$ - transfer function complex poles

$T(j\omega)$ - transmissibility transfer frequency function

(Ref 6:82)

Table 4.8 X or Y Transmissibility Transfer Function Zeros and Poles

$T(j\omega)$	K	z_1	z_2	z_3	$p_{1,2}$	$p_{3,4}$	$p_{5,6}$
$TX_{U/G}(j\omega)$	606.8	-199.6	-397.9	-418.9	-0.4080±j18.21	-3.718±j54.94	-50.17±j132.5
$TX_{U/P}(j\omega)$	6.1		-397.9	-418.9	-0.4079±j18.23	-3.717±j55.00	
$TX_{L/P}(j\omega)$	143.4	-199.6	-397.9			-0.716±j23.81	-50.17±j132.5
$TX_{U/G}(j\omega)$	143.2	-199.6		-418.9	-0.7543±j25.00		-47.55±j129.4
$TX_{U/L}(j\omega)$	1.5			-418.9	-0.7540±j25.12		
$TX_{L/P}(j\omega)$	1.4		-397.9			-0.7163±j23.87	
$TX_{P/G}(j\omega)$	86.8	-199.6					-43.44±j124.3

where,

K - constant for transfer function

z_1 , z_2 - transfer function zero

$p_{1,2}$, $p_{3,4}$, $p_{5,6}$ - transfer function complex poles

$T(j\omega)$ - transmissibility transfer frequency function

(Ref 6:82)

Table 4.9 Theta-Transmissibility Transfer Function Zeros and Poles

$T(j\omega)$	K	z_1	z_2	z_3	$p_{1,2}$	$p_{3,4}$	$p_{5,6}$
$T\Theta_{U/G}(j\omega)$	886.4	-199.6	-379.9	-418.9	-0.8367±j2607	-8.684±j81.78	-15.65±j78.52
$T\Theta_{U/P}(j\omega)$	27.7		-397.9	-418.9	-0.8363±j26.10	-8.273±j81.81	
$T\Theta_{L/P}(j\omega)$	96.5	-199.6	-397.9			-1.508±j34.50	-16.06±j78.57
$T\Theta_{U/G}(j\omega)$	97.3	-199.6		-418.9	-1.532±j35.71		-15.92±j78.23
$T\Theta_{U/L}(j\omega)$	3.1			-418.9	-1.530±j35.77		
$T\Theta_{L/P}(j\omega)$	3.0		-397.9			-1.506±j34.59	
$T\Theta_{P/G}(j\omega)$	31.3	-199.6					-15.66±j77.51

where,

K - constant for transfer function

z_1 , z_2 - transfer function zero

$p_{1,2}$, $p_{3,4}$, $p_{5,6}$ - transfer function complex poles

$T(j\omega)$ - transmissibility transfer frequency function

(Ref 6:82)

Table 4.10 PSI or PHI Transmissibility Transfer Function Zeros and Poles

$T(j\omega)$	K	z_1	z_2	z_3	$p_{1,2}$	$p_{3,4}$	$p_{5,6}$
$T\psi_{U/G}(j\omega)$	590.1	-128.5	-188.5	-188.5	-0.4200±j12.57	-4.159±j39.37	-42.23±j95.24
$T\psi_{U/P}(j\omega)$	7.0		-188.5	-188.5	-0.4201±j12.58	-4.160±j39.38	
$T\psi_{L/P}(j\omega)$	131.1	-128.5	-188.5			-0.7764±j17.09	-42.23±j95.24
$T\psi_{U/G}(j\omega)$	125.2	-128.5		-188.5	-0.7496±j16.79		-41.77±j94.82
$T\psi_{U/L}(j\omega)$	1.5			-188.5	-0.7499±j16.80		
$T\psi_{L/P}(j\omega)$	1.6		-188.5			-0.7768±j17.10	
$T\psi_{P/G}(j\omega)$	81.8	-128.5					-40.88±j93.98

where,

K - constant for transfer function

z_1 , z_2 - transfer function zero

$p_{1,2}$, $p_{3,4}$, $p_{5,6}$ - transfer function complex poles

$T(j\omega)$ - transmissibility transfer frequency function

(Ref 6:82)

during the early phases of the study to check the various transmissibility solutions.

Besides an interesting analytic check, the poles and zeros typify the resonant frequencies and responses for a given isolation configuration. These level traits are used extensively in Chapter V to build active controller designs.

Summary

A thorough passive response study for each level is not done for two reasons. First, the pneumatic isolator and seismic pier soil characteristics are not known precisely; so approximating the SSP performance on the basis of equivalent lumped parameter springs and dampers would only be a qualitative treatment. Secondly, the theoretical SSP frequency responses can give only general insight into problems faced by the active digital controller. Chapter V does expand on the directional transmissibility poles and zeros using root-locus concepts (Ref 4:203). Other important points gained from the passive frequency responses are now summarized.

The pneumatic isolators do have individual resonant frequencies for the upper and lower levels taken separately (single stage isolation) of 1.8 Hz for the vertical direction and 3.8 Hz and 4.0 Hz for the horizontal motion (single stage isolation) for the first and second stages, respectively. The full isolation theoretically results in the first cutoff at 1.3 Hz and second at 4.0 Hz. Actual SSP measurement at

Holloman by FJSRL engineers calculated (Ref 19) vertical frequency breakpoints at 1.2 Hz and 3.5 Hz.

Rotational isolator dynamics have not been specified by MAC, but theoretical θ resonant frequencies of 5.7 Hz and 5.5 Hz for second and first stage isolation and 2.7 Hz for ψ transmissibilities (both stages) are predicted.

In general, the poles and zeros do analytically follow from one (direction) isolation configuration to another in the complex frequency plane characteristics, when the appropriate load scaling effects are considered. The transmissibility solutions are mathematically and dynamically correct.

Eq 4-35 is repeated for convenience as

$$TZ_{U/G}(j\omega) = Z_U(j\omega)/Z_G(j\omega)$$

$$= \frac{111.2(j\omega + 128.5)(j\omega + 188.5}{(j\omega + 0.3397 \pm j11.30)(j\omega + 82 \pm j119.8)} \quad (4\text{-}35)$$

Using the straight line approximations (Ref 6:255), the Eq 4-35 denominator presents positive slopes of 40 dB while the numerator gives slopes of negative 80 dB which results in a second order response. The denominator effects do not become prominent until 20 Hz. To explain the "second order response" measured at CGTIF (Ref 19) the Z

response (SSP Isolation), Figure 4.2 is analyzed. A -30 dB slope approximation is measured by FJSRL engineers (Ref 19) for the vertical direction. The two second order responses theoretically at 1.3 Hz and 4.0 Hz or measured at 1.2 Hz and 3.5 Hz (Ref 19) cause large magnitude overshoots which would distort any straight line approximation over such a narrow bandwidth.

Based on the frequency analysis, the active LQ controller synthesis first considers the second stage dynamics. The reduced order controller is compared to a truth model representing the SSP dynamics, neglecting pier dynamics. Also from a classical controls viewpoint, the active controller design is a difficult problem with the small phase and gain margins theoretically present for the full SSP isolation system.

V. Active Controller Design

Introduction

An active digital controller is designed using Linear Quadratic (LQ) synthesis techniques based on several alternate descriptions of the SSP dynamics. These alternatives arise by considering the SSP isolation in the passive response analysis along with the dominance of the upper level resonances. The use of the upper level actuators is expanded as a serious controls issue by including additional active control actuators between the lower level and the pier.

Each alternative is developed using standard state variable notation and partitioned submatrices from the differential equations written to describe the SSP dynamics in Chapter III. A simulation of isolator misalignments is included to evaluate translational and rotational cross coupling effects.

A linear quadratic cost function and control law is defined to design a digital controller to meet the required SSP performance specifications. A general procedure is outlined for controller design process along with design policy based on general SSP dynamics constraints. Each controller is then designed and analyzed with classical theory cited to reinforce the digital performance. Now, the SSP state representation is discussed for the continuous time domain.

SSP State Space Representation

The dynamics of the SSP describe a linear time invariant system using standard state variable notation (Ref 6:27, 12) as

$$\bar{X}(t) = A\,\bar{X}(t) + B\,\bar{U}(t) \qquad (5\text{-}1)$$

$$\overset{\circ}{\bar{X}}(t) = C\,\bar{X}(t) + D\,\bar{U}(t) \qquad (5\text{-}2)$$

where $\overset{\circ}{\bar{X}}(t)$, state vector derivative with respect to time, column vector

$\bar{X}(t)$, state vector column vector

A, square matrix, order equal to dynamics states of system (n)

B, input control matrix, n X r, where r is number of controls, n is order of system

C, output matrix, p X n, where p is number of desired outputs, n is order of system

D, feed thru matrix, p X r, represents controls appearing in output

All the time dependence notation is later dropped for convenience but is still implied. All derivatives are with respect to time, an inertial reference frame, with constant mass, nominal perturbed position and initial conditions as indicated. The SSP state vectors and the A system matrix are now defined in partitioned form using SSP generic state variables as

$$\bar{X} = \begin{bmatrix} \bar{X}_x \\ \bar{X}_y \\ \bar{X}_z \\ \bar{X}_\psi \\ \bar{X}_\phi \\ \bar{X}_\Theta \end{bmatrix} \quad \text{and} \quad \dot{\bar{X}} = \begin{bmatrix} \dot{\bar{X}}_x \\ \dot{\bar{X}}_y \\ \dot{\bar{X}}_z \\ \dot{\bar{X}}_\psi \\ \dot{\bar{X}}_\phi \\ \dot{\bar{X}}_\Theta \end{bmatrix} \tag{5-3}$$

where,

$\bar{X}_x$, $\bar{X}_y$, and $\bar{X}_z$ are generic state variables for translation motion

$\bar{X}_\psi$, $\bar{X}_\phi$, and $\bar{X}_\Theta$ are generic state variables for rotation motion

$$A = \begin{bmatrix} A_x & \bar{0} & \bar{0} & \bar{0} & \bar{0} & A_{x\Theta} \\ \bar{0} & A_y & \bar{0} & \bar{0} & \bar{0} & A_{y\Theta} \\ \bar{0} & \bar{0} & A_z & A_{z\psi} & A_{z\phi} & \bar{0} \\ \bar{0} & \bar{0} & A_{\psi z} & A_\psi & \bar{0} & \bar{0} \\ \bar{0} & \bar{0} & A_{\phi z} & \bar{0} & A_\phi & \bar{0} \\ A_{\Theta x} & A_{\Theta y} & \bar{0} & \bar{0} & \bar{0} & A_\Theta \end{bmatrix} \tag{5-4}$$

where A, system matrix

A_x , A_y , A_z , represent translation dynamics

A_ψ , A_ϕ , A_Θ , represent rotation dynamics

$A_{x\Theta}$, $A_{y\Theta}$, $A_{z\psi}$, $A_{z\phi}$, represent translation-rotation cross coupling dynamics

$A_{\psi z}$, $A_{\phi z}$, $A_{\Theta x}$, $A_{\Theta x}$, represent rotation-translation cross coupling dynamics

$\bar{0}$, represents zero matrices

For each candidate controller proposed, various A partitions and state vectors are rewritten into either reduced order controller models or partitions representing a specific controller loop (really a single degree of freedom). The state vectors and A matrix partitions are expanded in Appendix J. The A matrices based on coefficients specified in Appendix F and G, are rewritten in state form for Appendix J. To simulate the cross coupling terms, isolator misalignments are simulated under random isolator placement deviations of plus or minus a one-half inch over a uniform distribution. Cross coupling coefficients are also given in Appendix J along with the simulated isolator placement distances.

As each controller design is discussed, the B, C, and D continuous time matrices are derived for the LQ synthesis. Root locus and Nichols plots are made from TOTAL using classical techniques to predict controller performance and stability. In each case a basic controller structure is developed along with a truth model structure reflecting cross coupling effects.

Six basic controllers are developed, one for each of the six degrees of freedom - three translational (X, Y, Z) and three rotational (ψ, ϕ, θ). Six independent control loops are derived using second and first stage (SSP) isolation. Truth models are derived using particular controller loops and the appropriate simulated cross coupling terms. Reduced

order models are derived from the SSP isolation configurations by recognizing the dominance of the second stage isolation dynamics from the transmissibility and pole-zero analysis in Chapter IV. Next the LQ design philosophy is specified along with a description of the proposed control law structure.

Linear Quadratic (LQ) Synthesis

Of the numerous digital controller design methodologies available, linear quadratic synthesis offers an optimum controller derived on the basis of system state description and a direct interaction with a performance index. Classical theory (Ref 6:486) describes the performance index and cost weighting matrix applied to continuous time controllers. A LQ controller guarantees stability for any choice of weighting matrices, using classical pole placement techniques (Ref 12). A digital controller is proposed for the SSP because of the system flexibility, expandability and desirable control characteristics not found in analog controllers. In either, the continuous or digital controller, the difficult Riccati (Ref 6:495) equations are solved for the optimum feedback solution. The digital solution is usually easier to obtain than the continuous solution (Ref 12). Further theoretical development on the LQ synthesis for digital controllers is covered in reference 12. The LQ synthesis used in this study is a proportional integral (PI) controller which guarantees a type 1 property desired for disturbance

rejection (Ref 12, 6:176). Integration of the controller with the SSP physical system is shown in Figure 5.1. The LQ-PI digital controller structure is based on a control difference or "Pseudo-Rate" (Ref 12) whose characteristics have a cost weighting matrix assigned to the system state representation which is augmented to the control input rate. This LQ-PI design assures zero steady state tracking and a non-zero setpoint (Ref 12). The non-zero setpoint requires the control input to keep the SSP in the nominal position for which this study's dynamic model is valid. Secondly, the zero steady state tracking works to keep the accelerations and tilts for each axis within the performance required by the specifications. The LQ-PI controller structure with the SSP dynamics is shown in Figure 5.2A. The discrete controller representation is shown in Figure 5.2B.

The LQ-PI controller design is driven by a cost function described as

$$J = \int_{t_o}^{t_{n+1}} [\bar{Y}^T Y_c \bar{Y} + \bar{U}^T U_c \bar{U} + \mathring{\bar{U}}^T U_r \mathring{\bar{U}}] dt \qquad (5\text{-}5)$$

where J, quadratic cost function

$\bar{Y}$, system output desired

Y_c, output cost weighting matrix

$\bar{U}$, control input vector

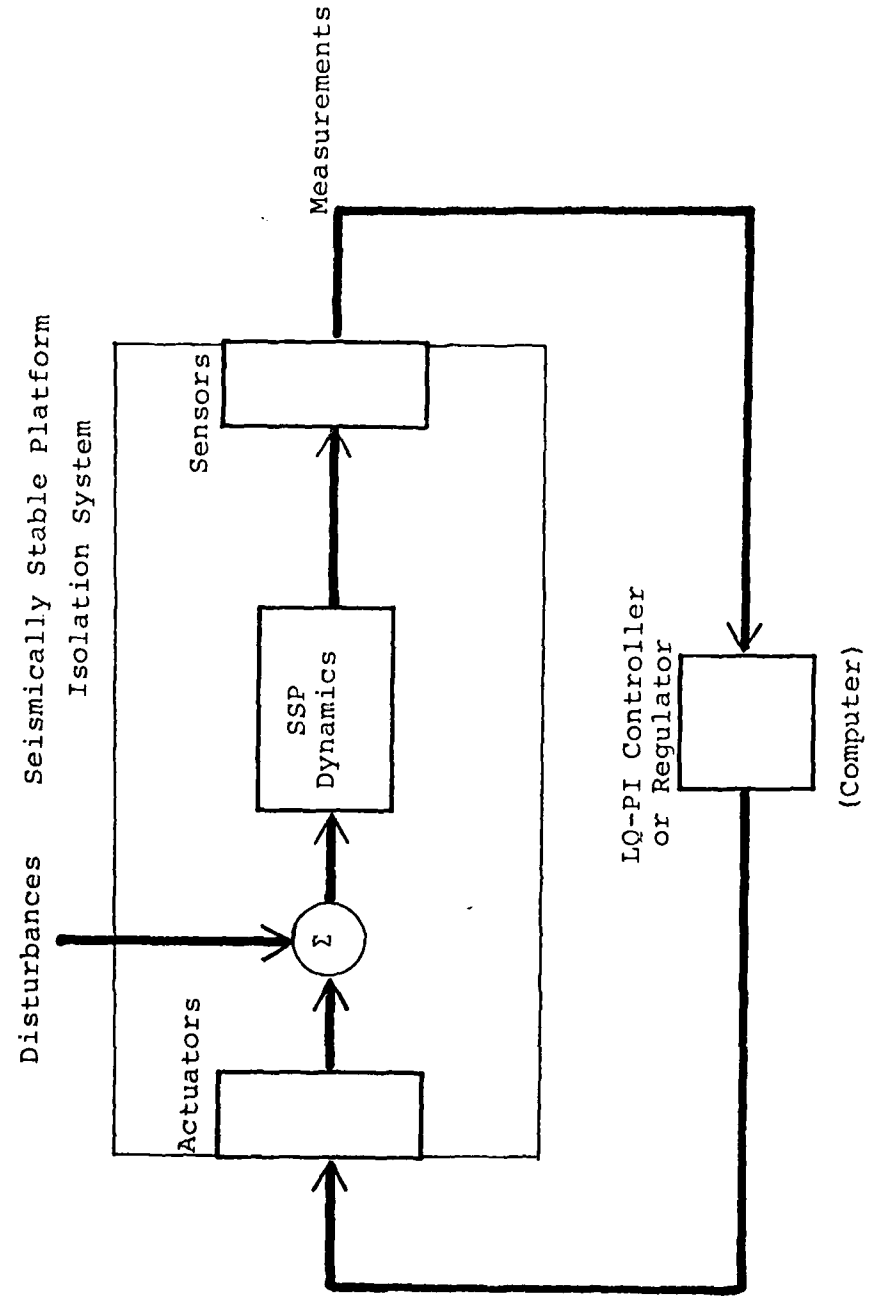

Figure 5.1 SSP Isolation and Controller

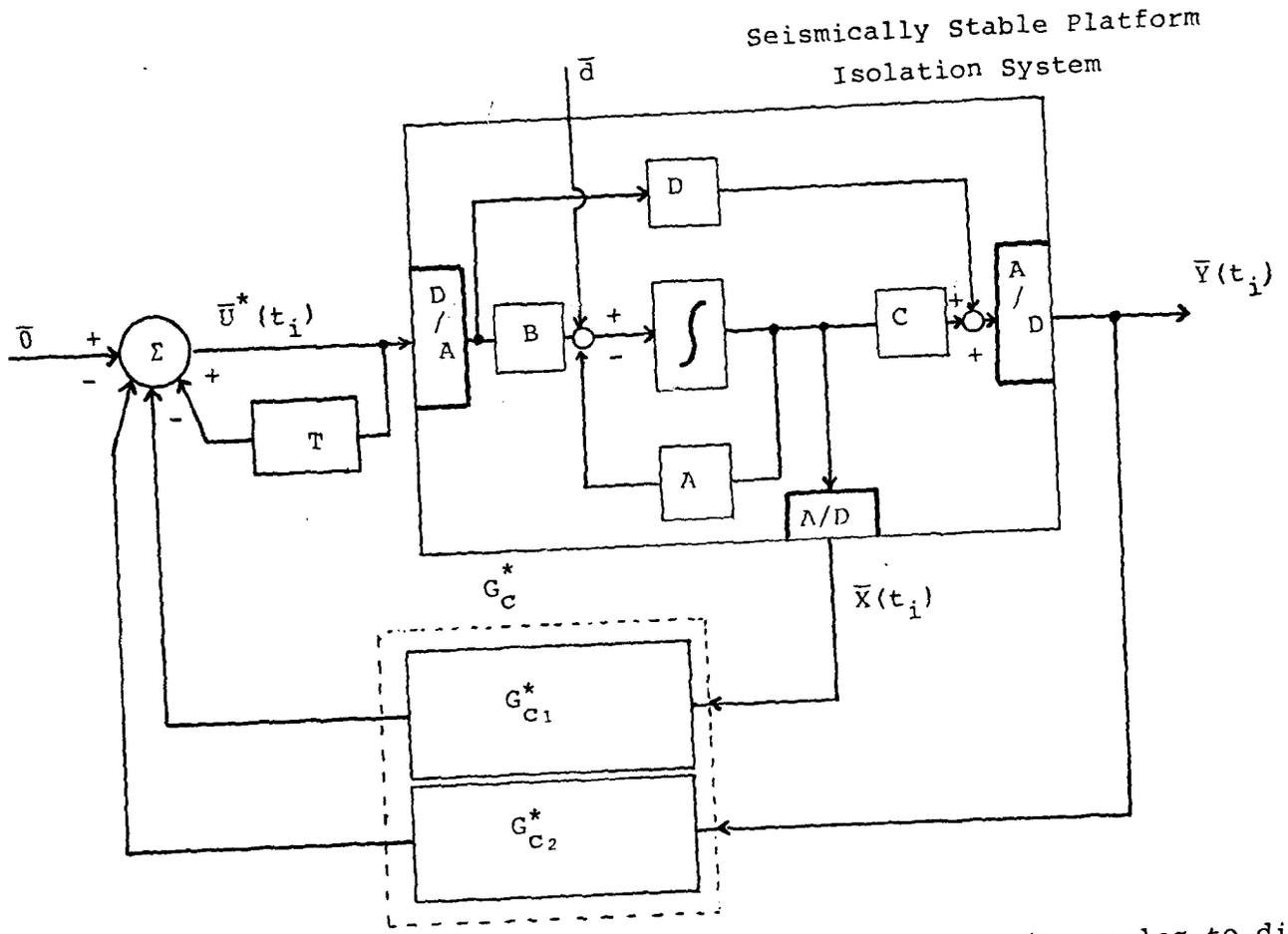

where, $\bar{d}$, disturbance vector $\bar{0}$, zero command input vector A/D, analog to digital D/A, digital to analog t_i, discrete time T, one sample delay

Figure 5.2A Continuous Time System Interface to Discrete Controller With Perfect State Knowledge

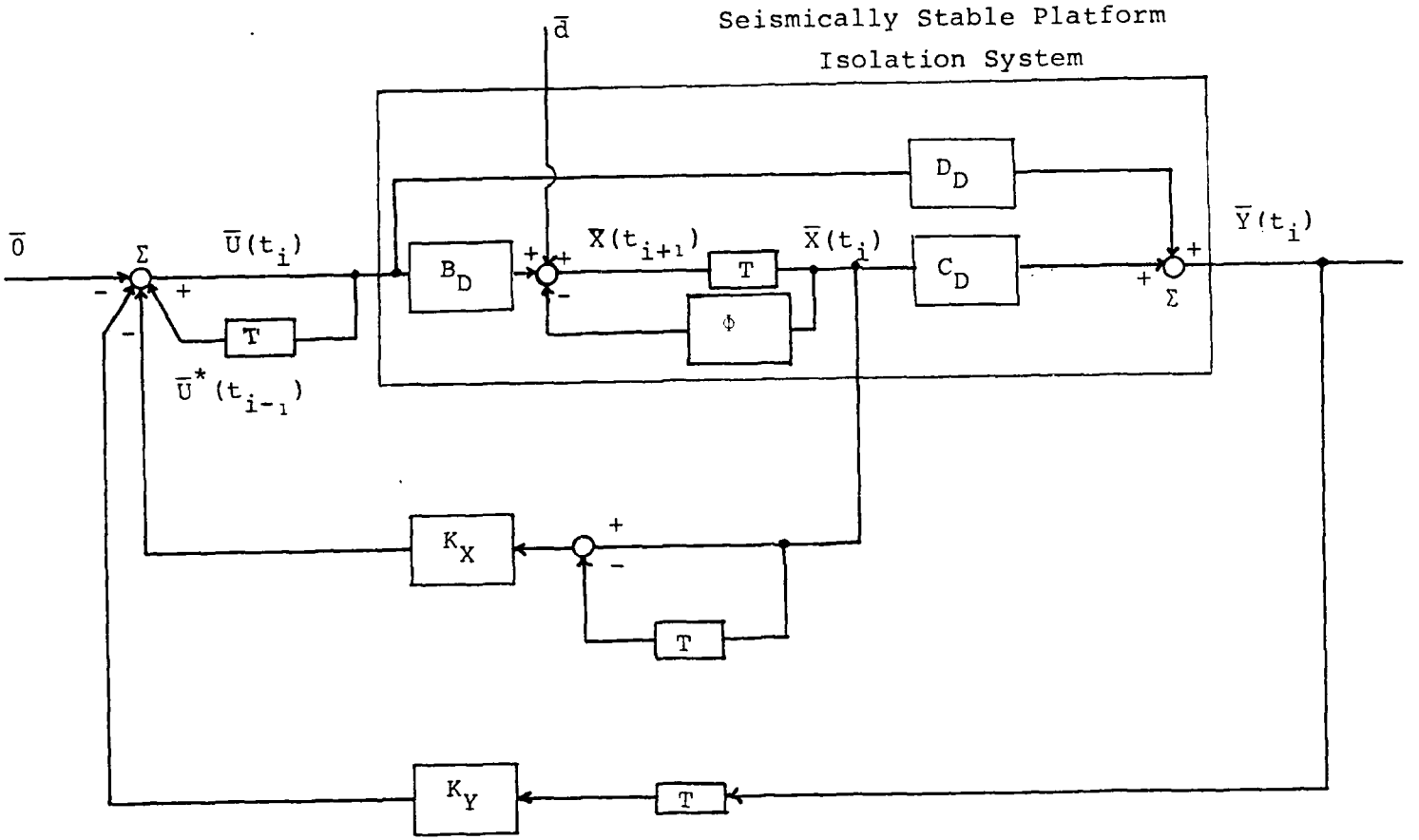

where $\bar{d}$, disturbance vector $\bar{0}$, command zero input vector T, one sample delay
D, subscript for discrete t_i, discrete sample time

Figure 5.2B Discrete SSP System Representation and Digital Controller/LQ-PI Structure

U_c, control cost weighting matrix

$\dot{\bar{U}}$, control input rate vector

U_r, control rate cost weighting matrix

(^{T} denotes transpose)

The quadratic cost function in Eq 5-5 provides the pseudo-rate constraint by the U_r cost parameter. Since constant gain matrices are desired for computation simplification, the integration is carried out ignoring a final transient in system performance and considers the time interval to approach infinity for the steady state system performance.

The digital Riccati (Ref 12) of Eq 5-5 specifies G_c^* the optimum feedback gain. This feedback gain is shown in Figure 2A separated into two separate partitions as

$$G_c^* = [G_{c_1}^* \mid G_{c_2}^*] \tag{5-6}$$

The actual controller gain K_X and K_Z of Figure 5.2B is related to G_c^* by

$$[G_c^*] = [G_{c_1} \mid G_{c_2}] \tag{5-7a}$$

$$= [K_X \quad K_Z] \begin{bmatrix} \Phi - I & B_D \\ C_D & D_D \end{bmatrix} \tag{5-7b}$$

$$= [K_X \quad K_Z] \quad [\Xi] \tag{5-7c}$$

where K_X , state feedback matrix

K_Z , output feedback matrix

Φ , state transistion matrix

I , identity matrix

B_D , discrete input matrix

C_D , discrete output matrix

D_D , discrete feedforward matrix

$\bar{U}$, $\bar{X}$, Φ, have discrete time argument t_i implied. These various forms are presented to simplify the discussion later in the controller design process.

The feedback gains in K_X and K_Z would be actually implemented in a real time SSP controller, while Π in Eq 5-7c represents the digital approximation of a continuous time system for a given sampling frequency. The T symbol in Figures 5.2A and 5.2B is the time delay between sample periods and in a digital controller implementation is a value held (delayed) in computer memory. Such diagrams can be confusing, because, for instance, a value for the difference of $\bar{X}(t_i)$ and the output of a delay is indicated for Figure 5.2B. This difference is equal to the value of $\bar{X}(t_i)$ at the time t_i minus the value of $\bar{X}(t_{i-1})$ - the output of the delay from the last sample time.

The digital controller structure in Figure 5.2B represents the following control input expression:

$$\bar{U}^*(t_i) = \bar{U}^*(t_{i-1}) - K_X[\bar{X}(t_i) - \bar{X}(t_{i-1})]$$

$$- K_Z[C_D \; D_D] \quad \bar{X}(t_{i-1})$$

$$\bar{U}(t_{i-1}) \qquad (5\text{-}8)$$

The closed loop eigenvalues of the system shown in Figure 5.2B are $(\Phi - B_D \; G_C^*)$ which is shown from the following discrete state difference equations.

$$\bar{X}(t_{i+1}) = \Phi(t_{i+1}, t_i) \; \bar{X}(t_i)$$

$$+ B_D(t_i)[G_C^*(t_i) \; \bar{X}(t_i)] \qquad (5\text{-}9a)$$

$$= [\Phi(t_{i+1}, t_i) - B_D(t_i) \; G_C^*(t_i)] \; \bar{X}(t_i) \qquad (5\text{-}9b)$$

If the system described by the state transition matrix Φ, is stable, then the closed loop eigenvalues of the LQ-PI structure are stable (Ref 12). Stability is addressed later by controllability and observability issues in a general design approach.

Digital Controller Design Assumptions

Several assumptions in the controller design are made in the SSP configuration, controller performance evaluation, and digital constraints. First the SSP configuration is discussed.

A full representation of the SSP would include upper and lower level, and seismic block (pier) structural resonances, as well as the first and second stage pneumatic isolator and foundation soil dynamics. By assumption, the structural resonant modes of the SSP are neglected in this study. Similarly, the pier dynamics by actual transmissibility measurements appear to be above the 20 Hz upper active controller bandwidth. Theoretical pier investigations in Chapter IV do place pier isolation effects at least on the upper edge of controller bandwidth (Ref 1). Certainly seismic disturbances would also need to be modeled if a full truth model was intended. A truth model is a mathematical representation which attempts to describe the known system characteristics of a dynamic system. This study is concerned with the goal of extending the -40 dB/decade (Ref 14:5) transmissibility to lower frequency bounds than presently possible with passive isolation. This study considers the SSP truth model as the dynamics of the first and second stage pneumatic isolator dynamics with cross coupling effects generated by possible simulated random isolator misalignments.

Neglecting pier dynamics poses two significant analytical dilemmas for the controller design. First, if the pier adds no dynamics, it becomes part of the Earth reference frame, or an inertial frame. The actuator must be connected to some structure, the pier in this case. Secondly, the actuators being connected to the upper level, allow, in addition, a direct feedthrough force appearing

directly as an acceleration (specific force) in the translational motion and as a torque in the rotational motion performance measurements. These points are brought out in each controller design and assuming no pier dynamics gives an optimistic controller environment. If pier dynamics are allowed, they would appear transformed directly on the upper level. A transformation would occur simply because the actuator force is now with respect to the pier coordinate frame, a non-inertial reference. All expressions derived in Chapter III, Appendix F and G are specifically derived for the equations of motion describing the six degrees of freedom of the upper, lower level and pier centers of mass with respect to the Earth as an inertial reference frame. For the digital controller design, the state representation of the SSP, considers the pier as an inertial reference for the actuators, and includes only the second and first stage isolation dynamics. Controller actuators are proposed between the upper level and pier (Ref 14). Lower level actuators are added for this study based on physical intuition that more actuators could better "steady" the lower level and the SSP.

To use the LQ synthesis technique, alternate representations of the SSP dynamics are developed for candidate digital controllers by describing each in the state notation of Eqs 5-1 and 5-2. Cost analysis is also proposed for each in the forms needed by Eq 5-5. Actual controller

design is done using a program CGTPIF (Ref 7) which has an option which accepts continuous time system matrices (A,B,C,D),cost criteria and yields a digital controller as shown in Figure 5.2B. Figure 5.2B is a discrete representation of the SSP dynamics and control law. No digital approximations are made for the dynamics of the analog to digital (A/D) converters. The sampling frequency is 200 Hz which is selected to be ten times 20 Hz, the highest frequency limit on the controller bandwidth.

The CGTPIF digital controller design software has options intended for time domain analysis and is adapted for LQ-PI controller feasibility. No frequency domain analysis with a Bode plot or PSD options is available. To evaluate the LQ-PI feasibility, passive isolation time responses are made using TOTAL for a unit step input and compared to CGTPIF time responses with initial conditions appropriate to the TOTAL analysis. Early efforts on the FJSRL Iso-Pad controller design (Ref 4) used unit step time responses over a four second settling time criteria to meet controller specifications. Approximations are made for the resulting exponentially damped sinewave unit step response. First, a unit step can be scaled, as was done in Chapter IV transmissibilities studies, as long as the system operation remains linear. The unit step could be considered as an one g input disturbance for translation control and as one arcsecond tilt disturbance for rotation control analysis.

These inputs can be scaled appropriately once true disturbance magnitudes are known without reaccomplishing the controller simulations. Secondly, the damped frequency is an approximation of the acceleration output frequency content for the translation controllers. The tilt specifications are given in time response constraints and are evaluated directly from the CGTPIF analysis for the rotation controllers. The controller design approach using CGTPIF is now discussed.

Controller Design Approach

The SSP digital controller is approached as six individual controllers - one for each degree of freedom. Actually, only four loops are needed because the X and Y, and ψ and ϕ loop pairs are identical.

Within each loop, two system A matrices are possible by considering the full SSP isolation dynamics or a reduced order model using only the upper level dynamics. In the SSP isolation controller structure, three further permutations are possible using combinations of the upper and lower level actuators. These permutations result in one multiple-input multiple-output (MIMO) system or two single-input single-output (SISO) systems - the upper or lower level actuators for control inputs. The translation (X, Y, Z) controller has a direct feedthrough of the actuator (specific force or acceleration) along with state combinations to the

output (upper level) acceleration, while the rotation controller (ψ, ϕ, θ) output tilt is a system state with no feedthrough contribution.

In summary, four configurations are analyzed for the two basic controllers in each direction designated as

1. SSP Isolation (MIMO) - Upper and Lower Level Actuators
2. SSP Isolation (SISO) - Upper Level Actuators
3. SSP Isolation (SISO) - Lower Level Actuators
4. Second Stage Isolation (SISO) - Upper Level Actuators

Controller costs are specified for Eq 5-5 in each controller design. The actuator cost weight U_c is derived using guidelines (Ref 11) for a control weighting equal to the reciprocal of the maximum actuator force squared. The maximum SSP force available is ten pounds (Ref 14:24) which yields a 0.01 weighting for U_c. The control rate U_r is assumed to be 0.1, as ten times the actuator cost weight. The output cost Y_c is varied from 1 to 100 with the results noted in each controller design section. The cost weighting matrices have zeros added for the MIMO and SISO configurations to account for input control configurations, no cross cost considerations, and a desired system output penality.

Controllability and observability analysis is theoretically commented on in each controller section using basic analysis of the B input matrix and C output matrix for controllability

and observability measures directly. The results in each case is verified using a software package "MIMO" (Ref 13) but is not listed in the study.

All configurations suffer from being weakly controllable which is a direct function of the coefficient value in the B input matrices being either scaled by large mass (translation) or moment of inertia (rotation). For example, B_X matrix for X controller is scaled by the upper and lower masses. The factor $1/m_U$ scales Eq F-5 by 0.0019 which is evident in the last row of A_X and B_X in the X - Controller (SSP Isolation). To avoid the controllability problem, the candidate controller design uses the B input coefficient resulting from the dynamics equations in Appendix F and G, but the CGTPIF simulation used values scaled to one. Physically, any input actuator force is attenuated by such a mass scaling factor and is describing the reality that a small force does little to induce an acceleration or tilt to a large mass.

Observability theoretically is the most serious control problem for the SSP. Only the second stage isolation controller types have outputs using upper level states. The translation controllers do not have their acceleration outputs as distinct system state while the tilt output of the rotation controllers is. The SSP isolation type controller has no outputs for the control law taken from the lower level.

Unfortunately, the lower level is physically inaccessible and instrument monitoring is unlikely, so the SSP isolation - MIMO system has observability problems as will be demonstrated.

A controller is now designed for each of the four basic configurations in each direction (degree of freedom). A root locus and Nichols plot is included to give insight into the controller performance based on classical concepts. The unit step responses from the TOTAL and CGTPIF simulation programs are included for performance evaluation. Digital controller designs for successful (with Riccati solutions) CGTPIF simulations are listed in Appendix K by direction loop name configuration type.

X - Controller (SSP Isolation)

The truth model for the X controller is rewritten from the partitions of Eqs J-8A and J-8F for the X state variable and cross coupling terms as

$$\begin{bmatrix} \dot{\bar{X}}_X \\ \bar{X}_\Theta \end{bmatrix} = \begin{bmatrix} A_X & A_X \\ A_{\Theta X} & A_\Theta \end{bmatrix} \begin{bmatrix} \bar{X}_X \\ \bar{X}_\Theta \end{bmatrix} + \begin{bmatrix} B_X & \bar{0} \\ \bar{0} & B_\Theta \end{bmatrix} \begin{bmatrix} \bar{U}_X \\ \bar{U}_\Theta \end{bmatrix} \tag{5-10}$$

$$Y_X = C_X \bar{X}_X + D_X \bar{U}_X \tag{5-11}$$

The X state space model using SSP dynamics for X loop, with no rotational cross coupling (no truth model), reduces Eq 5-10 to

$$\dot{\bar{X}}_X = A_X \bar{X}_X + B_X \bar{U}_X \tag{5-12}$$

Using the state notation from Eq J-2 and the A matrix values from Eq J-10, the X state representation is written completely as

$$\begin{bmatrix} \dot{X}_1 \\ \dot{X}_2 \\ \dot{X}_3 \\ \dot{X}_4 \end{bmatrix} = \begin{bmatrix} 0.0000 & 1.0000 & 0.0000 & 0.0000 \\ -2740.0000 & -6.7424 & 1140.6054 & 1.7230 \\ 0.0000 & 0.0000 & 0.0000 & 1.0000 \\ 631.6547 & 1.5080 & -631.6547 & -1.5080 \end{bmatrix} \begin{bmatrix} X_1 \\ X_2 \\ X_3 \\ X_4 \end{bmatrix} \tag{5-13}$$

The root locus of the X open loop is obtained by considering the X transmissibility for the SSP isolation as a unity feedback continuous time system. The root locus is shown in Figure 5.3. Four complex poles are located near the imaginary axis with two poles in the left half plane (LHP) (Ref 6). The lower frequency complex poles pair seek out the two system zeros while the higher frequency poles cross the imaginary axis into the right half plane (RHP) along a vertical asymptote parallel to the imaginary axis. The cross effect between the two pair of complex poles is a stability consideration because of the SSP isolation minimum phase and gain margins. All root locus for the SSP isolation (translation and rotation) dynamics have the same general shape and analysis comments. The poles and zeros are repeated from Eq 4-35:

$$\text{Poles: } p_{1,2} = -0.4079 \pm j1823$$
$$p_{3,4} = -3.717 \pm j55.00$$

$$\text{Zeros: } z_1 = -397.9$$
$$z_2 = -418.9$$

A Nichols plot for the open loop transfer function is in Figure 5.4 which shows how the 5.29 dB (6.5 Hz) gain margin and 5.39° (4.5 Hz) phase margin affect controller stability. A unit step continuous time response is shown in Figure 5.5 with a ±0.20 damped sine wave at 3.13 Hz (on a bias of one) approximatedat four seconds for comparison to the CGTPIF unit step responses. Other characteristics of Figure 5.5

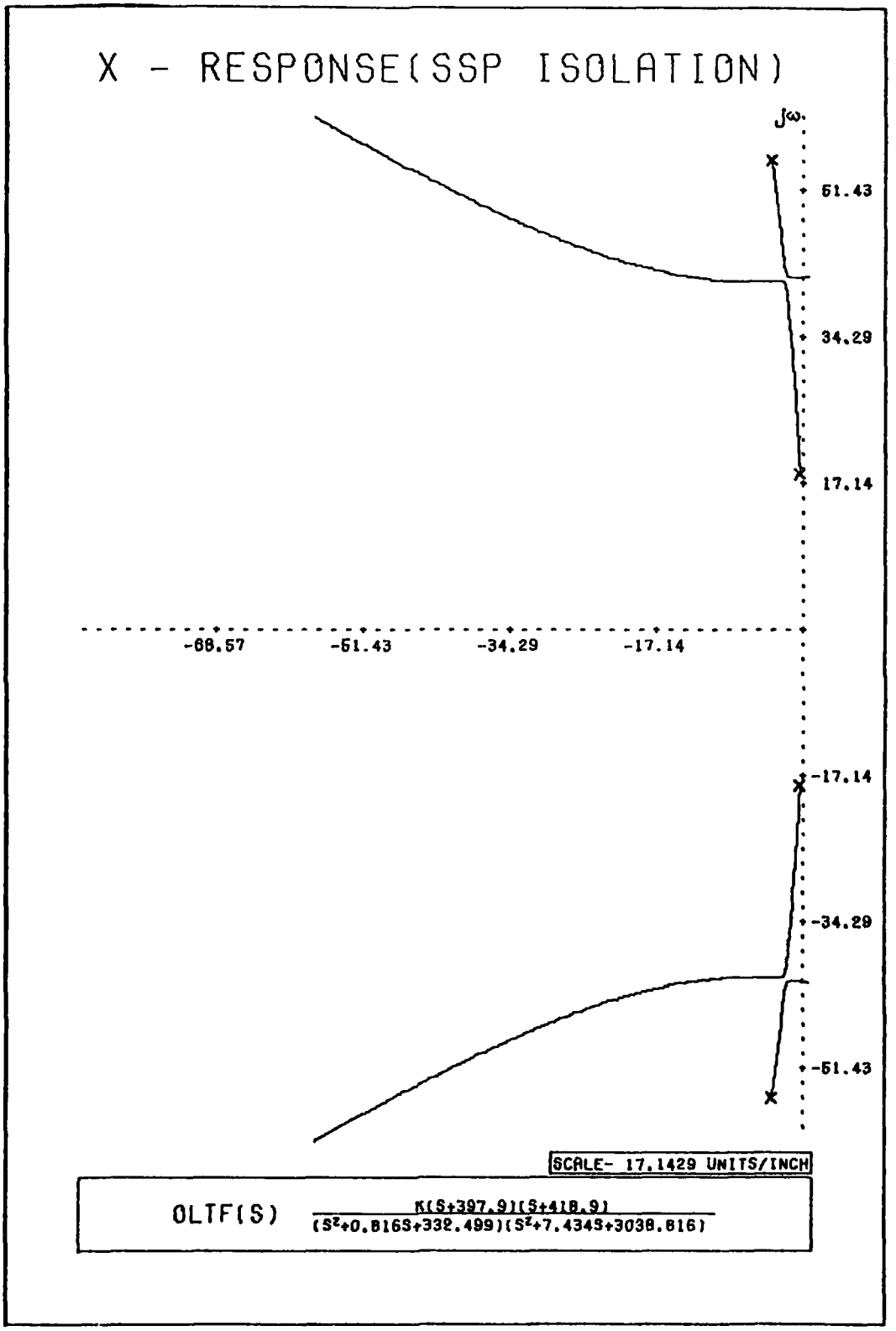

Figure 5.3 X - Response (SSP Isolation) - Root Locus

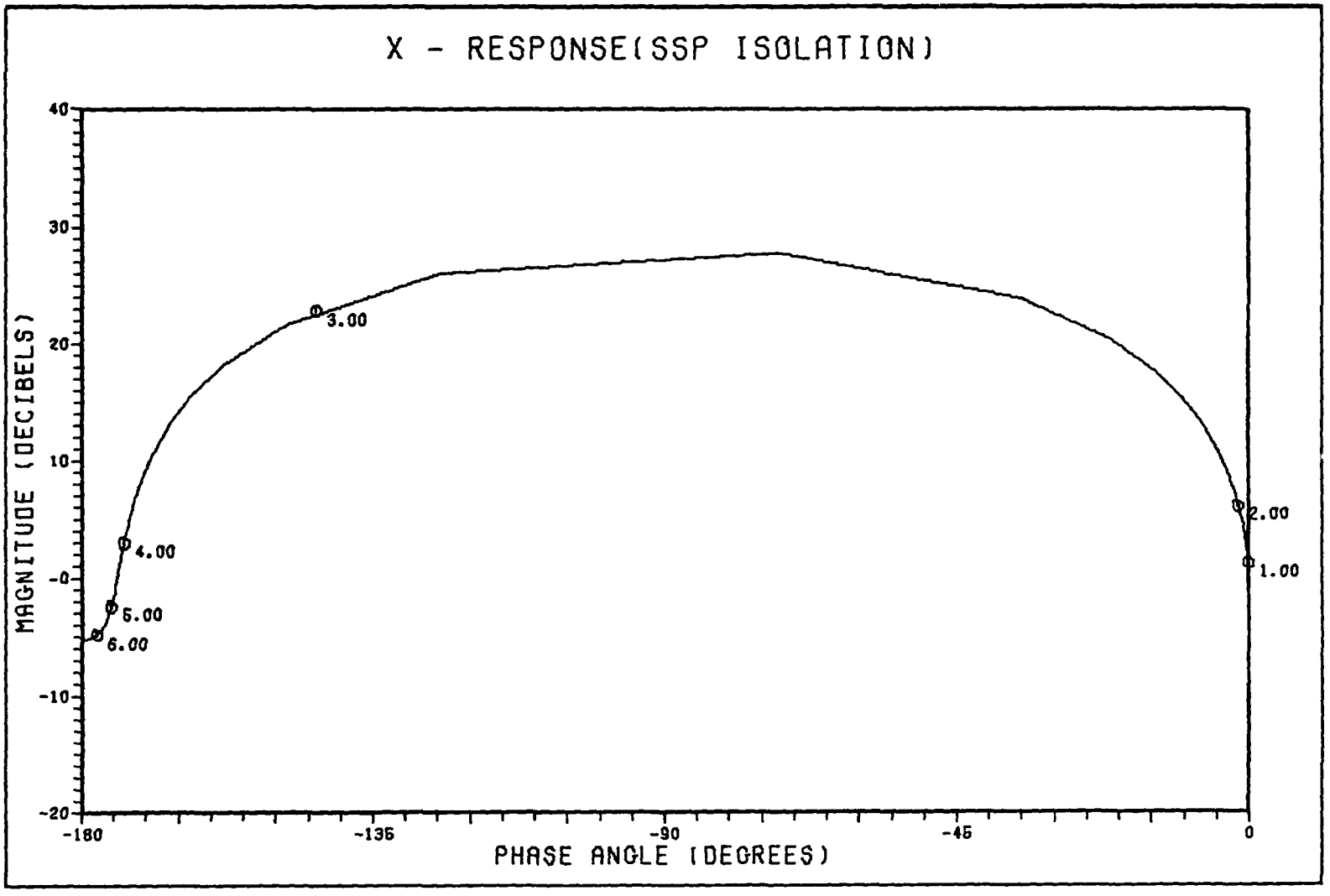

Figure 5.4 X - Response (SSP Isolation) - Nichols Plot

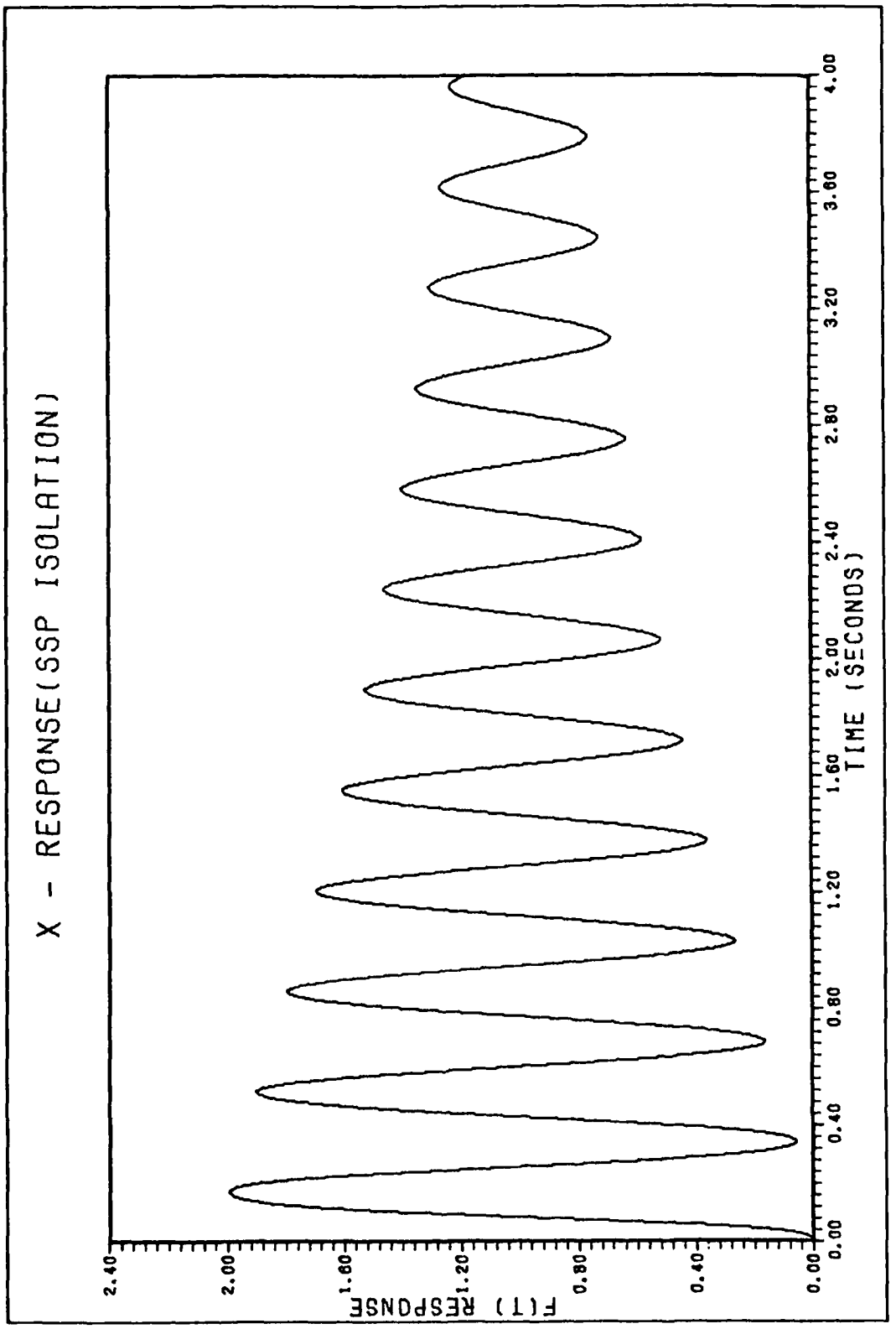

Figure 5.5 X - Response (SSP Isolation) - Time Response

are summarized in Table 4.4, under the $TX_{U/P}(t)$ response.

Various SISO type controllers are tried using the following actuator configurations as

Upper Level Actuator:

$$B_X F_X = \begin{bmatrix} 0.0000 \\ 0.0000 \\ 0.0000 \\ 0.0019 \end{bmatrix} \quad [F_X] \qquad D_X = \begin{bmatrix} 0.0000 \\ 0.0019 \end{bmatrix} \tag{5-14}$$

Lower Level Actuator:

$$B_X f_X = \begin{bmatrix} 0.0000 \\ 0.0034 \\ 0.0000 \\ 0.0000 \end{bmatrix} \quad [f_X] \qquad D_X = \begin{bmatrix} 0.0034 \\ 0.0000 \end{bmatrix} \tag{5-15}$$

The output is the same in both configurations:

$$Y_2 = [631.6547 \quad 1.5080 \quad -631.6547 \quad -1.5080] \begin{bmatrix} X_1 \\ X_2 \\ X_3 \\ X_4 \end{bmatrix} \tag{5-16}$$

F_X and f_X are the $\bar{U}_X$ terms in Eq 5-12 which represent the X upper and lower level actuator resultant forces. The lower actuators are indicated by f in Figure 3.4. Resultant forces from these actuators use a subscript for the summation orientation on the SSP. No solutions are possible from CGTPIF for these SISO configurations, even with B_X scaled to one to account for the weak controllability. These controllers are not fully observable and controllable. More design analysis is done with SISO configurations for the Z controller.

A MIMO configuration is tried using the upper and lower actuators with the only output being the upper level acceleration, which is a combination of system states and not fully observable. The B_X and C_X matrices are listed below:

$$B_X\bar{U}_X = \begin{bmatrix} 0.0000 & 0.0000 \\ 0.0034 & 0.0000 \\ 0.0000 & 0.0000 \\ 0.0000 & 0.0019 \end{bmatrix} \begin{bmatrix} f_X \\ F_X \end{bmatrix} \tag{5-17}$$

$$\begin{bmatrix} Y_1 \\ Y_2 \end{bmatrix} = \begin{bmatrix} 0.0000 & 0.0000 & 0.0000 & 0.0000 \\ 631.6547 & 1.5080 & -631.6547 & -1.5080 \end{bmatrix} \begin{bmatrix} X_1 \\ X_2 \\ X_3 \\ X_4 \end{bmatrix} + \begin{bmatrix} 0.0034 & 0.0000 \\ 0.0000 & 0.0019 \end{bmatrix} \begin{bmatrix} f_X \\ F_X \end{bmatrix} \tag{5-18}$$

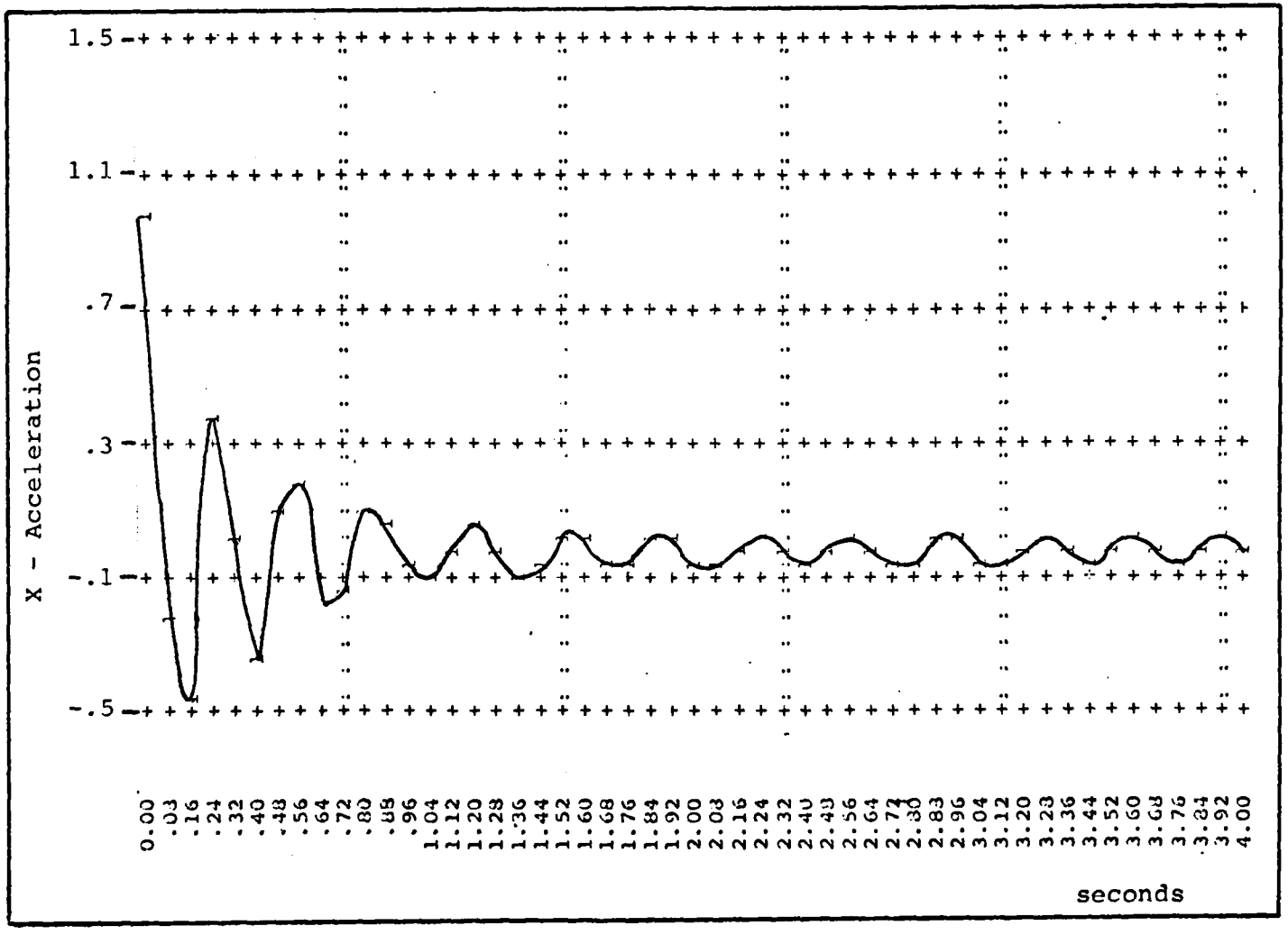

Figure 5.6 X - Controller (SSP Isolation)

CGTPIF provided a solution which is listed as Case 1, Design A in Appendix L. An approximate estimate of the system response can be made from Figure 5.6 as a peak-to-peak response (4 seconds) of ±0.02 damped sinewave at 3.12 Hz on a bias of one. The X acceleration unit step response is simulated by an initial condition of 0.0016 for state X_1. The Y_1 output is a zero row because the lower level is not readily accessible. The B_X input matrix is scaled to one to compensate for weak controllability. No increase is possible in the output cost Y_c without destabilizing the system output.

X - Controller (Second Stage Isolation) - SISO

The upper level and the second stage isolation dynamics partitioned from Eq 5-18 yield the reduced order model as

$$\begin{bmatrix} \dot{X}_3 \\ \dot{X}_4 \end{bmatrix} = \begin{bmatrix} 0.0000 & 1.0000 \\ -631.6547 & -1.5080 \end{bmatrix} + \begin{bmatrix} X_3 \\ X_4 \end{bmatrix} \begin{bmatrix} 0.0000 \\ 0.0019 \end{bmatrix} F_X \tag{5-19}$$

$$Y_2 = [-631.6547 \quad -1.5080] \begin{bmatrix} X_3 \\ X_4 \end{bmatrix} + [0.0019] F_X \tag{5-20}$$

The reduced order system root locus is shown in Figure 5.7. Two complex poles have their root locus return to LHP an implied zero in the far LHP, not shown due to plot

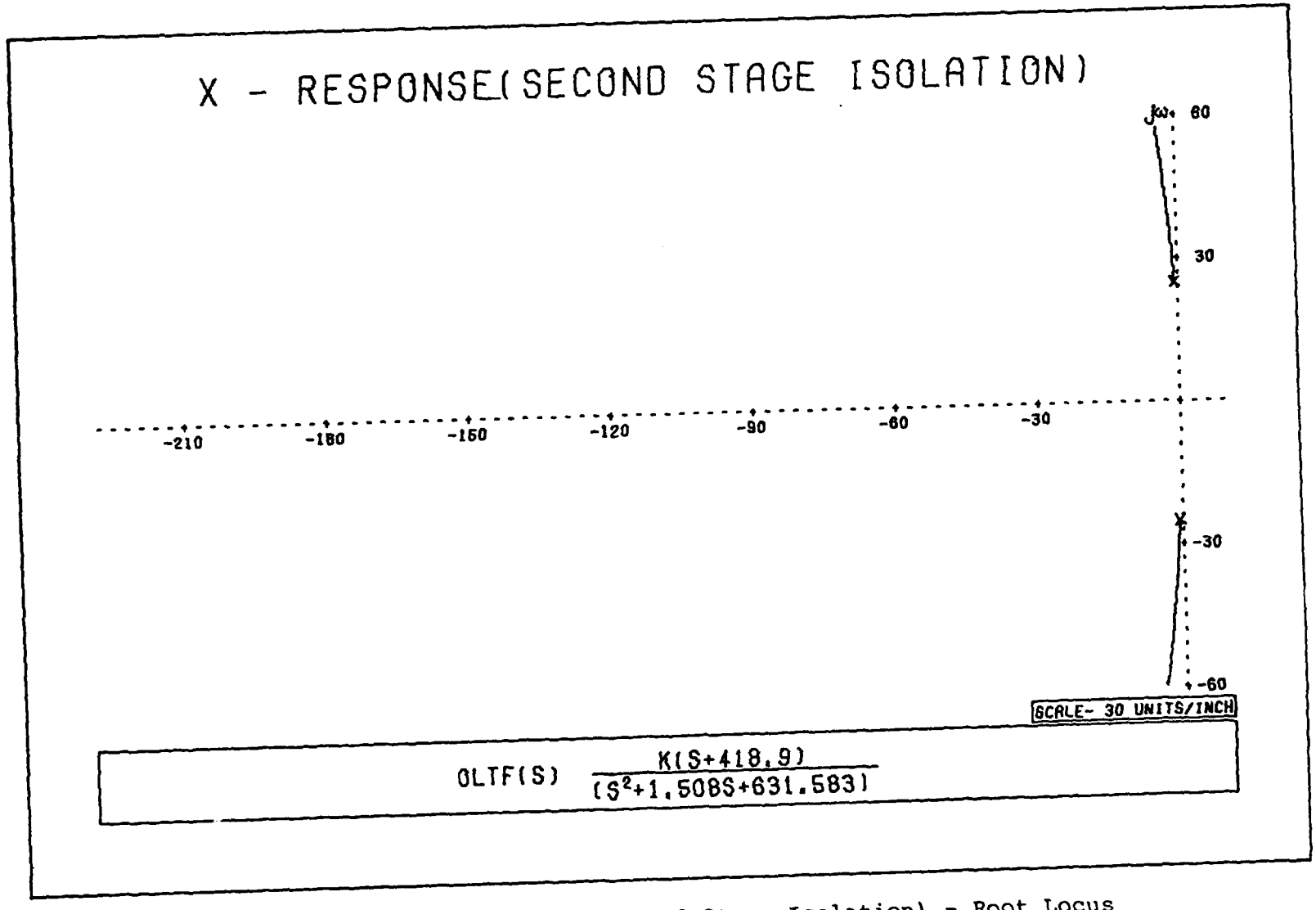

Figure 5.7 X - Response (Second Stage Isolation) - Root Locus

scale. This root locus plot is typical for the second stage reduced order models for all directions. Essentially, this reduced order controller does not go unstable due to higher gains, because the system eigenvalues are moved further into LHP. The second stage isolation poles and zeros for the open loop transfer function are:

Poles: $p_{1,2} = -0.7540 \pm j25.12$

Zeros: $z_1 = -418.9$

A 10 degree phase margin can be approximated from the Nichols plot in Figure 5.8. Gain margin is not a constraint either in the Nichols plot or the root locus plot.

A unit step time plot for the open loop continuous time response is shown in Figure 5.9 which shows ±0.075 damped sine wave at 4.17 Hz on a bias of one. A summary of Figure 5.9 is listed in Table 4.6 for $TX_{U/L}(t)$ response.

Case 2, Design A is the CGTPIF digital controller for the X second stage dynamics reduced order controller. The CGTPIF unit step response shows in Figure 5.10 (at 4 seconds) a ±0.08 damped sine wave at 4.17 Hz for an initial condition of X_3 equal to -0.0016. The LQ-PI controller removed the bias present before in Figure 5.9 produced by TOTAL. For CGTPIF, B_X is scaled to one as weak controllability compensation and the output cost is kept to one to prevent instability.

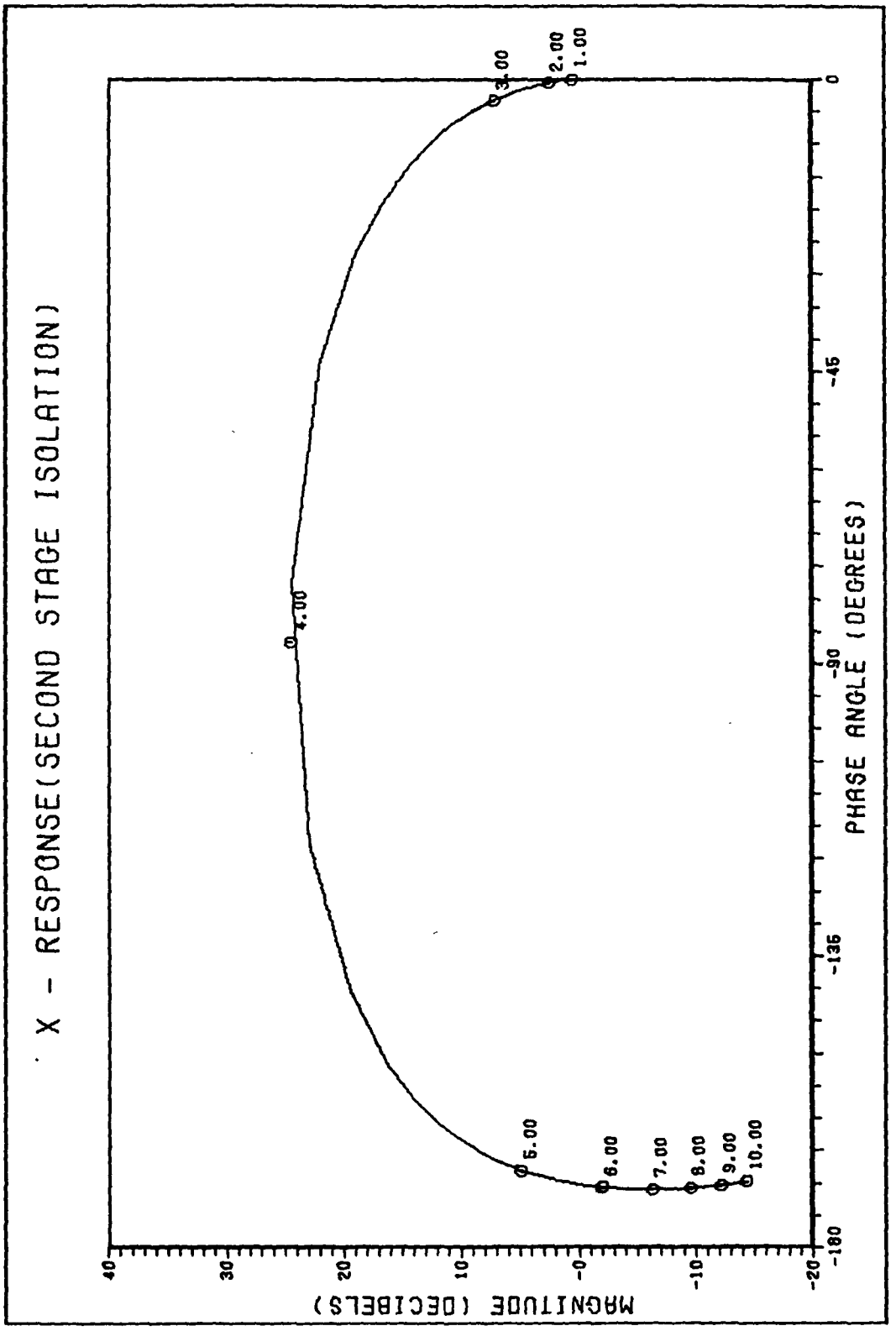

Figure 5.8 X- Response (Second Stage Isolation) - Nichols Plot

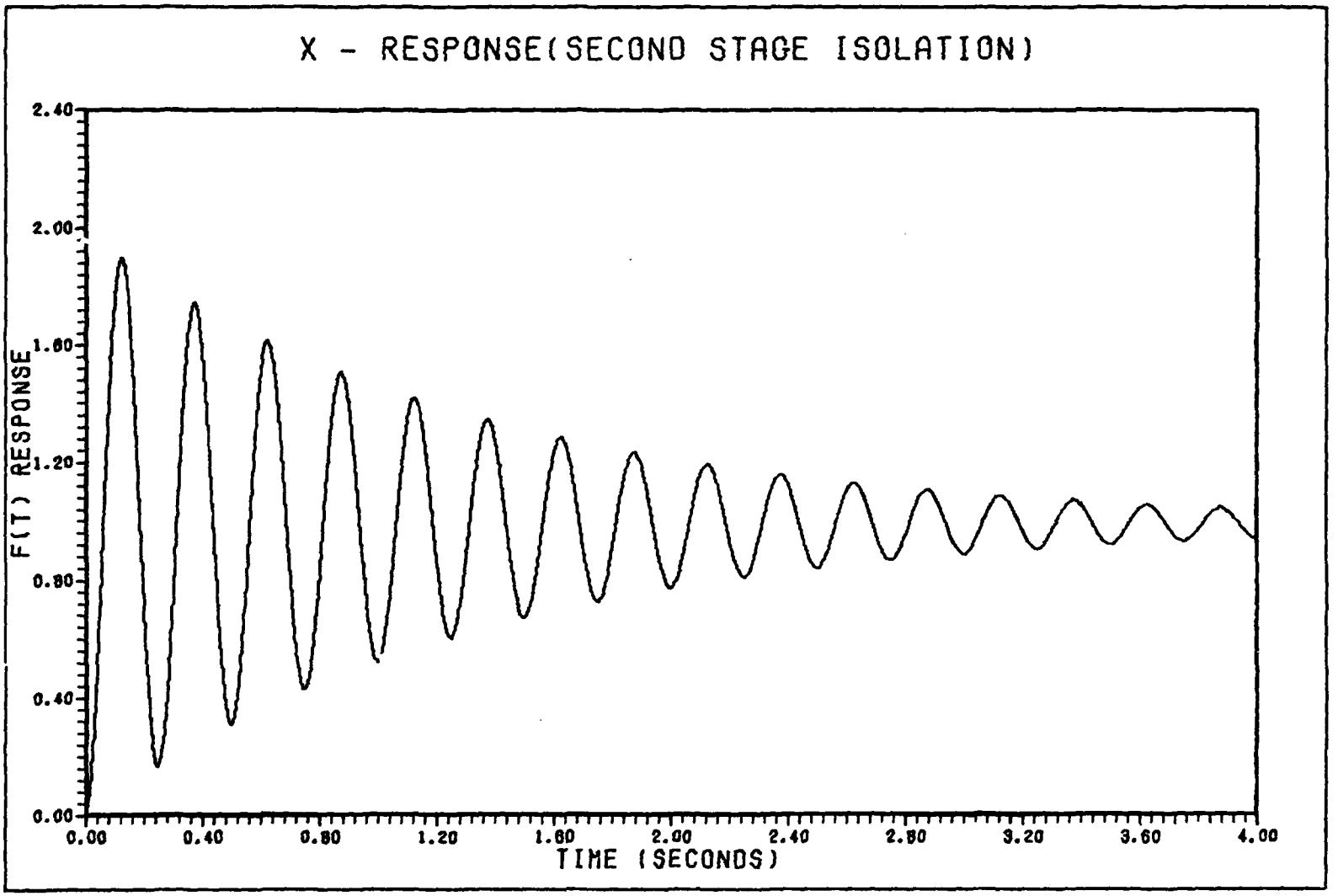

Figure 5.9 X - Response (Second Stage Isolation) - Time Response

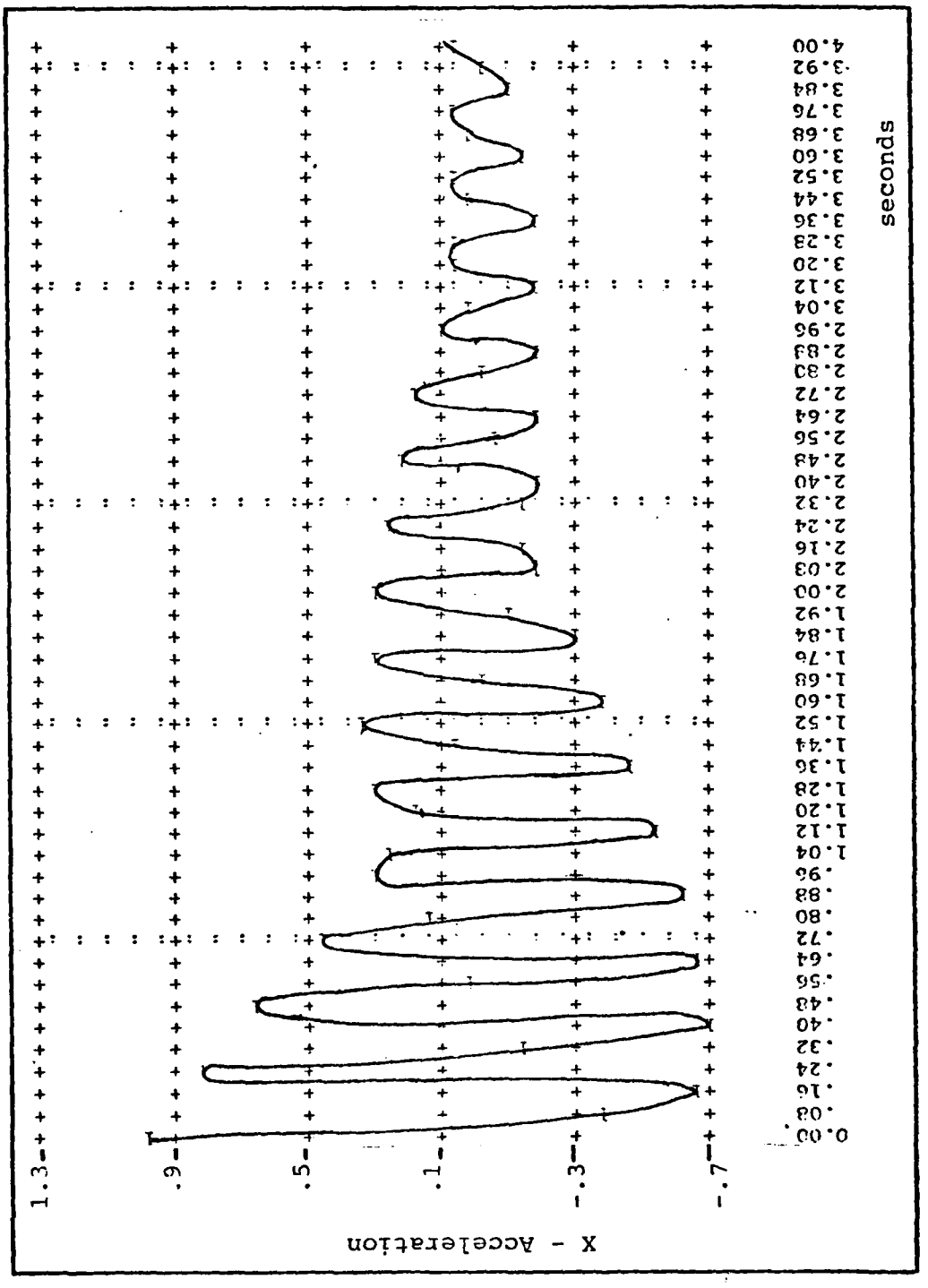

Figure 5.10 X - Controller (Second Stage Isolation)

Z - Controller (SSP Isolation)

The truth model for the Z controller is rewritten from the partitions of Eqs J-8c, J-8d and J-8e for the Z state variables and cross coupling terms as

$$\begin{bmatrix} \dot{\bar{X}}_z \\ \dot{\bar{X}}_\psi \\ \dot{\bar{X}}_\phi \end{bmatrix} = \begin{bmatrix} A_z & A_{z\psi} & A_{z\phi} \\ A_{\psi z} & A_\psi & \bar{0} \\ A_{\phi z} & \bar{0} & A_\phi \end{bmatrix} \begin{bmatrix} \bar{X}_z \\ \bar{X}_\psi \\ \bar{X}_\phi \end{bmatrix} + \begin{bmatrix} B_z & \bar{0} & \bar{0} \\ \bar{0} & B_\psi & \bar{0} \\ \bar{0} & \bar{0} & B_\phi \end{bmatrix} \begin{bmatrix} \bar{U}_z \\ \bar{U}_\psi \\ \bar{U}_\phi \end{bmatrix} \tag{5-21}$$

$$\bar{Y}_z = C_z \bar{X}_z + D_z \bar{U}_z \tag{5-22}$$

The Z state space model using SSP dynamics for Z loop reduces Eq 5-21 to

$$\dot{\bar{X}}_z = A_z \bar{X}_z + B_z \bar{U}_z \tag{5-23}$$

Using the state notation from Eq J-4 and A matrix values from Eq J-18, Eq 5-23 is written as

$$\begin{bmatrix} \dot{X}_9 \\ \dot{X}_{10} \\ \dot{X}_{11} \\ \dot{X}_{12} \end{bmatrix} = \begin{bmatrix} 0.0000 & 1.0000 & 0.0000 & 0.0000 \\ -589.8553 & -3.1292 & 230.9726 & 1.2254 \\ 0.0000 & 0.0000 & 0.0000 & 1.0000 \\ 127.9101 & 0.6786 & -127.9101 & -0.6786 \end{bmatrix} \begin{bmatrix} X_9 \\ X_{10} \\ X_{11} \\ X_{12} \end{bmatrix} \tag{5-24}$$

The Z root locus plotted in Figure 5.11 is analyzed and commented on similarly to the X - SSP Isolation open loop root locus.

Poles and zeros are repeated from Eq 4-33:

$$\text{Poles:} \quad p_{1,2} = -0.1883 \pm j8.422$$
$$p_{3,4} = -1.716 \pm j25.37$$
$$\text{Zeros:} \quad z_{1,2} = -188.5$$

A Nichols plot drawn in Figure 5.12 depicts the 5.25 dB (3.0 Hz) gain margin and 5.71° (2.0 Hz). A unit step continuous time response is shown in Figure 5.13 with a ±0.60 damped sine wave at 1.32 Hz (on a bias of one) approximated at the four second time criteria for comparison to CGTPIF. A further summary of Figure 5.13 is made in Table 4.4 under the $TZ_{U/P}(t)$ response.

Several SISO controllers are proposed using the following actuator configurations as.

Upper Level Actuators:

$$B_Z F_Z = \begin{bmatrix} 0.0000 \\ 0.0000 \\ 0.0000 \\ 0.0019 \end{bmatrix} \qquad D_Z = \begin{bmatrix} 0.0000 \\ 0.0019 \end{bmatrix} \tag{5-25}$$

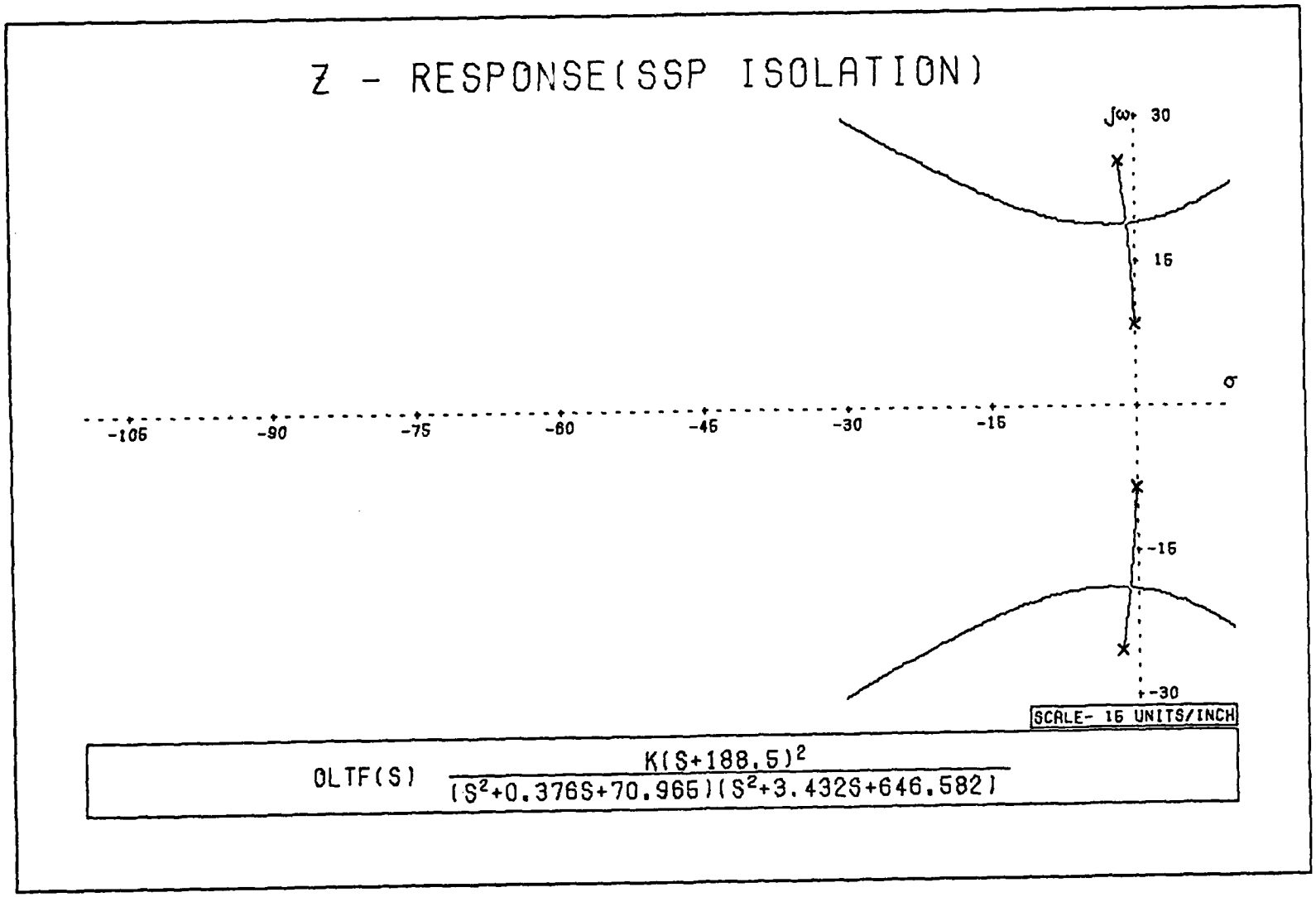

Figure 5.11 Z - Response (SSP Isolation) - Root Locus

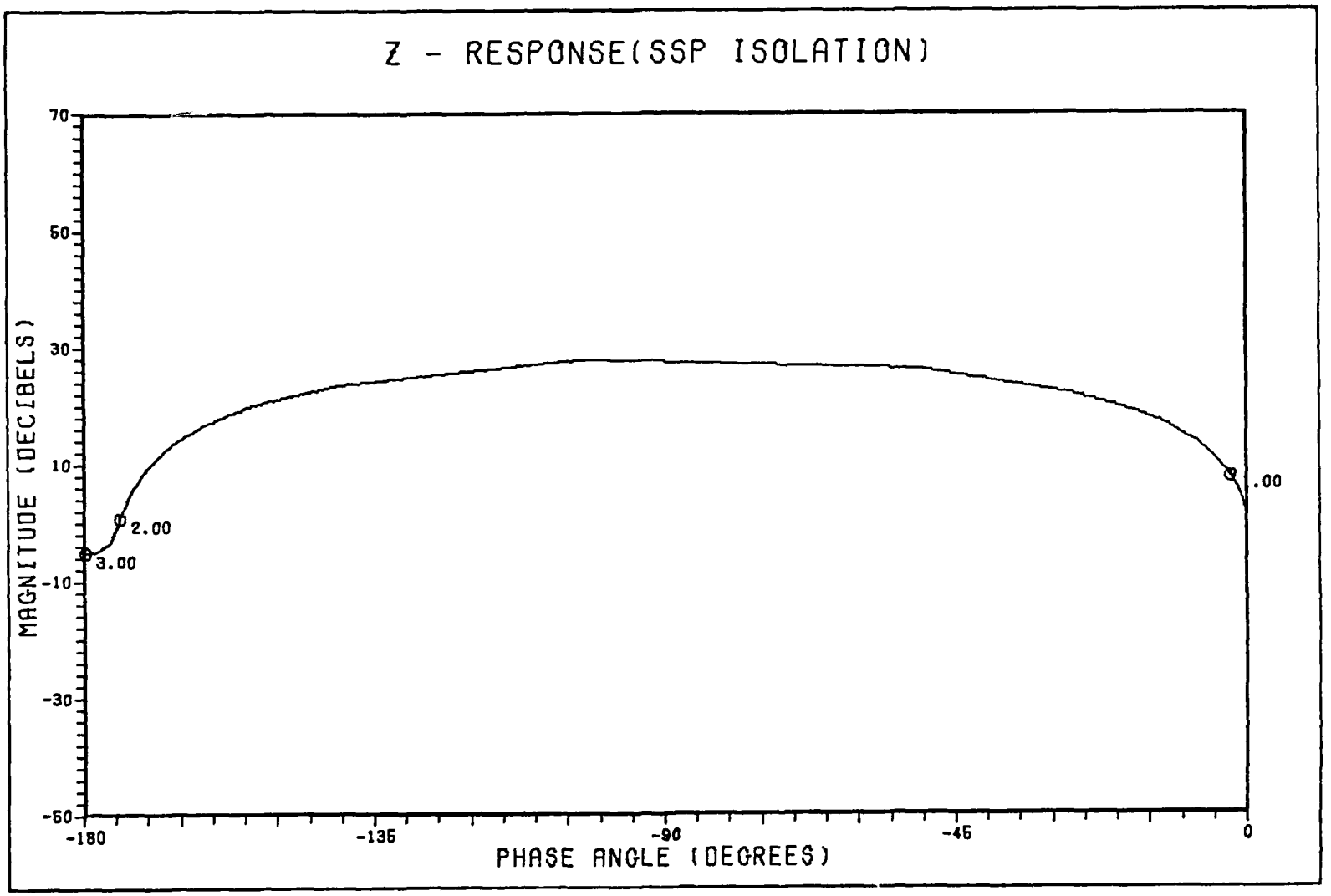

Figure 5.12 Z - Response (SSP Isolation) - Nichols Plot

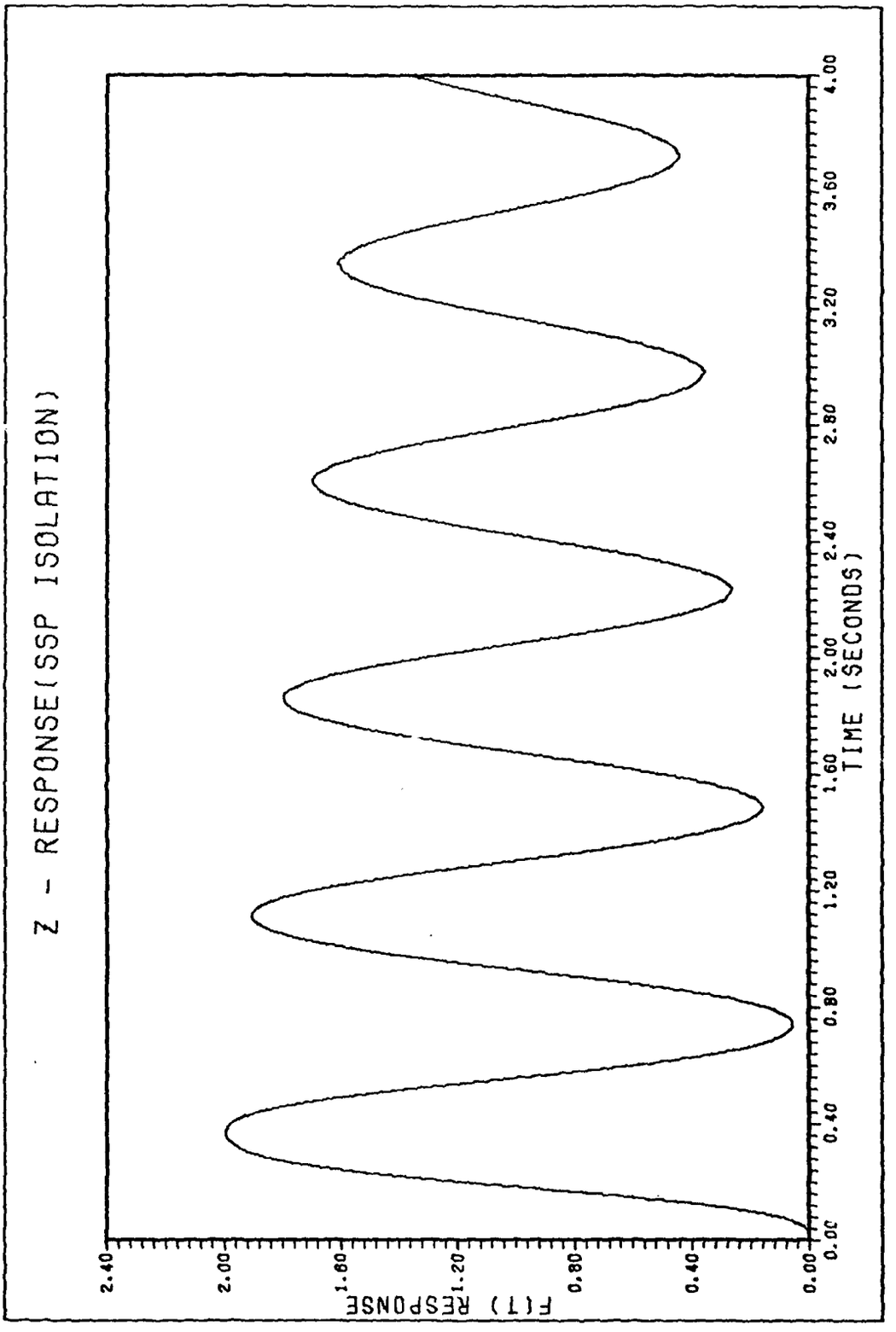

Figure 5.13 Z - Response (SSP Isolation) - Time Response

Lower Level Actuators:

$$B_Z f_Z = \begin{bmatrix} 0.0000 \\ 0.0034 \\ 0.0000 \\ 0.0000 \end{bmatrix} \qquad f_Z D_Z = \begin{bmatrix} 0.0034 \\ 0.0000 \end{bmatrix}$$

(5-26)

The output expression is the same in both designs:

$$[Y_6] = [127.9101 \quad 0.6786 \quad -127.9101 \quad -0.6786] \begin{bmatrix} X_9 \\ X_{10} \\ X_{11} \\ X_{12} \end{bmatrix}$$

(5-27)

Only the upper actuator configuration (SISO) provided a digital controller design from CGTPIF. The output cost Y_C is varied from 1000 to 10,000 with the following performance results:

Y_C	Z - Acceleration
1000 (Design A)	±0.1 damped sine wave (1.35 Hz, bias -0.5)
10,000 (Design B)	±0.6 damped sine wave (1.35 Hz)
100,000	no solution from CGTPIF

The input matrix B_Z is not scaled and the designs are listed in Case 3, Appendix L. Of all the SISO controllers for any SSP isolation, CGTPIF gave a solution for the Z direction. No step responses are available but their form is similar to Figure 5.14. The only explanation is the double zero in the root locus at -188.5 and is probably a theoretical dynamic structure not necessarily possible in the actual SSP dynamics.

A MIMO design is built using the following B_Z, Y_C expressions:

$$B_Z = \begin{bmatrix} 0.0000 & 0.0000 \\ 0.0034 & 0.0000 \\ 0.0000 & 0.0000 \\ 0.0000 & 0.0019 \end{bmatrix} \begin{bmatrix} f_Z \\ F_Z \end{bmatrix} \tag{5-28}$$

$$\begin{bmatrix} Y_5 \\ Y_6 \end{bmatrix} = \begin{bmatrix} 0.0000 & 0.0000 & 0.0000 & 0.0000 \\ 127.9101 & 0.6786 & -127.9101 & -0.6786 \end{bmatrix} \begin{bmatrix} X_9 \\ X_{10} \\ X_{11} \\ X_{12} \end{bmatrix}$$

$$+ \begin{bmatrix} 0.0000 & 0.0000 \\ 0.0000 & 0.0019 \end{bmatrix} \begin{bmatrix} f_Z \\ F_Z \end{bmatrix} \tag{5-29}$$

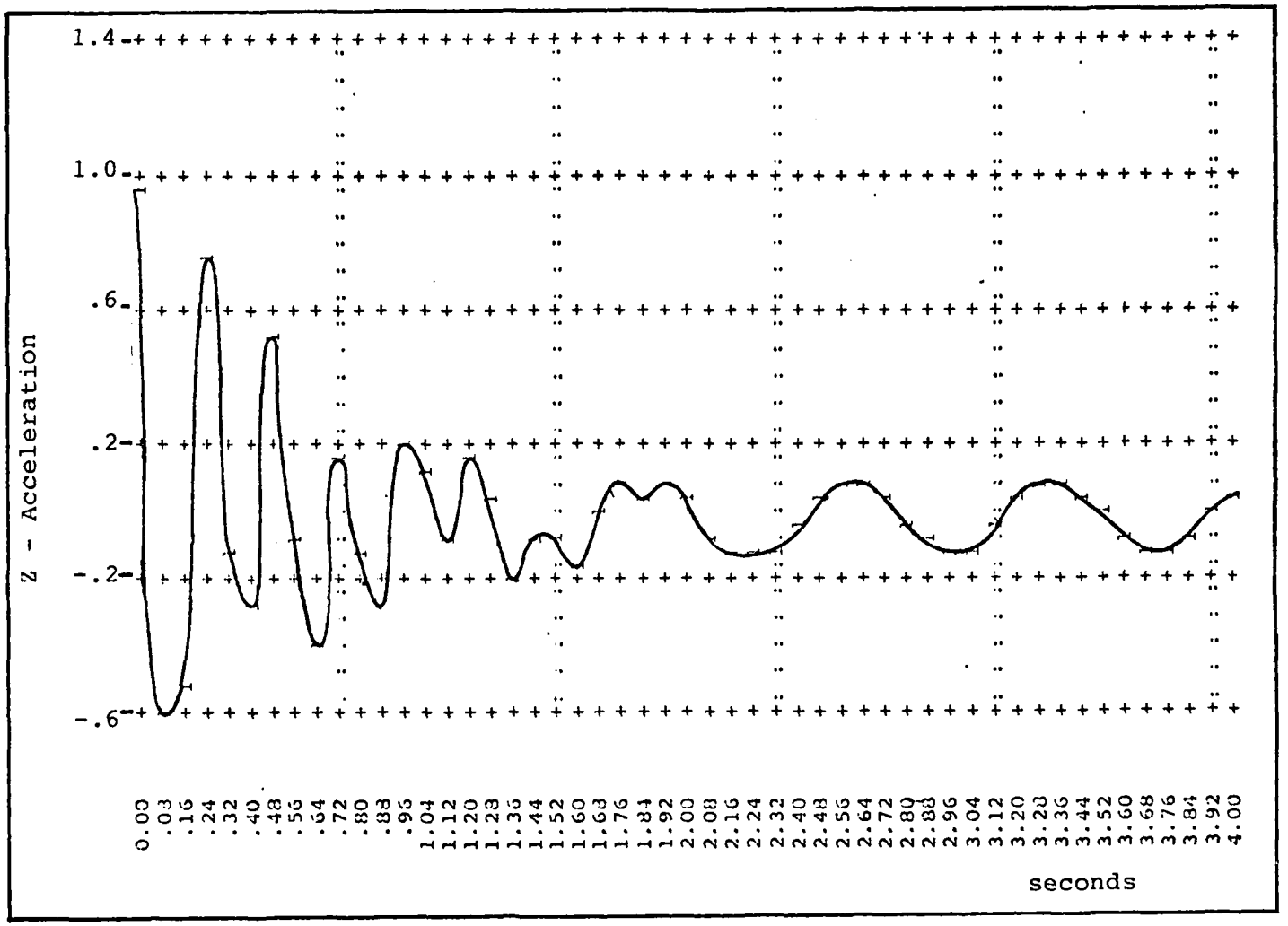

Figure 5.14 Z - Controller (SSP Isolation)

CGTPIF obtained a digital design listed in Appendix L, Case 3, Design C. The unit step acceleration for an initial condition on X_9 of 0.0078 is shown in Figure 5.14. The performance approximated at 4 seconds in Figure 5.14 is ±0.0729 damped sine wave at 1.32 Hz. The input matrix B_Z is scaled to one and Y_c could not be increased past one. The discrete B_D input matrix is listed in Case C.

Z - Controller (Second Stage Isolation) - SISO

The upper level and the second stage isolation dynamics partitioned from Eq 5-24 yield the reduced order model as

$$\begin{bmatrix} \dot{X}_{11} \\ \dot{X}_{12} \end{bmatrix} = \begin{bmatrix} 0.0000 & 1.0000 \\ -127.9101 & -0.6786 \end{bmatrix} \begin{bmatrix} X_{11} \\ X_{12} \end{bmatrix} + \begin{bmatrix} 0.0019 \end{bmatrix} F_Z \qquad (5\text{-}30)$$

$$Y_6 = \begin{bmatrix} -127.9101 & -0.6786 \end{bmatrix} \begin{bmatrix} X_{11} \\ X_{12} \end{bmatrix} + \begin{bmatrix} 0.0019 \end{bmatrix} F_Z \qquad (5\text{-}31)$$

A root locus for the upper level dynamics is shown in Figure 5.15 and is typical of the second stage root locus as discussed for the X controller. The second stage isolation poles and zeros for the open loop transfer function from Eq 4-50 are:

Poles: $p_{1,2} \approx -0.3393 \pm j11.30$

Zeros: $z_1 = -188.5$

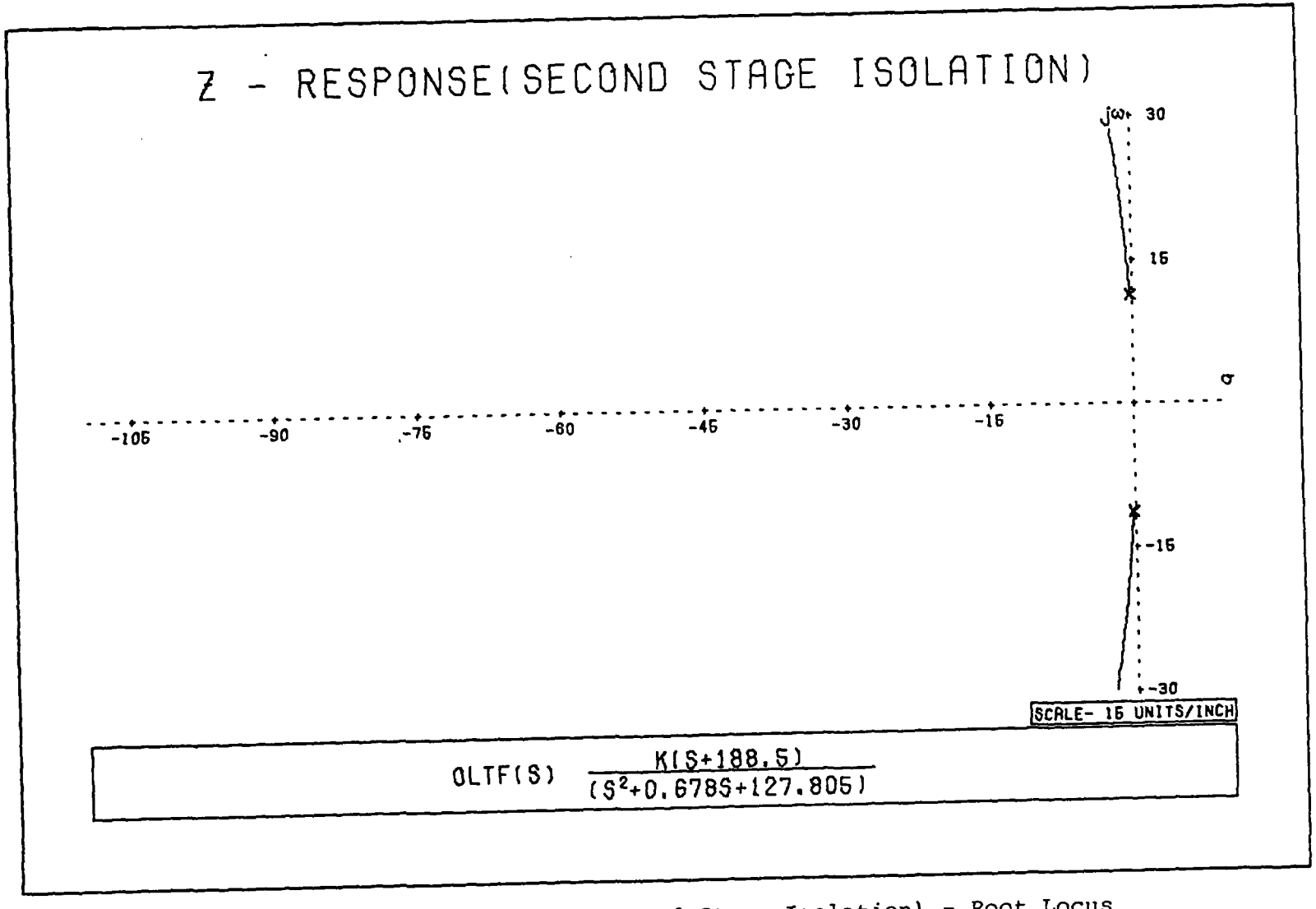

Figure 5.15 Z - Response (Second Stage Isolation) - Root Locus

A 10 degree phase margin can be interpreted from Figure 5.16. Gain margin is not a constraint either in the Nichols plot or root locus.

A unit step time response for the open loop continuous time system is shown in Figure 5.17 which shows at four seconds a ±0.3 damped sine wave at 1.79 Hz on a bias of one. A summary of Figure 5.17 is listed in Table 4.6 for $TZ_{U/L}(t)$ response.

Case 4, Design A is the CGTPIF digital controller designed for the Z second stage isolation. The CGTPIF unit step response shows at four seconds in Figure 5.18 a ±0.5021 damped sine wave at 1.92 Hz for an initial condition of X_{11} equal to -0.0078. The designed controller removed the bias present in the open loop response. The digital controller required B_Z scaled to one and Y_c equal to one for a solution.

PSI - Controller (SSP Isolation)

The truth model for the ψ controller is rewritten from the partitions of Eq J-8c and J-8d for the ψ state variables and cross coupling terms as

$$\begin{bmatrix} \dot{\bar{X}}_z \\ \dot{\bar{X}}_\psi \end{bmatrix} = \begin{bmatrix} A_z & A_{z\psi} \\ A_{\psi z} & A_\psi \end{bmatrix} \begin{bmatrix} \bar{X}_z \\ \bar{X}_\psi \end{bmatrix} + \begin{bmatrix} B_z & \bar{0} \\ \bar{0} & B_\psi \end{bmatrix} \begin{bmatrix} \bar{U}_z \\ \bar{U}_\psi \end{bmatrix} \tag{5-32}$$

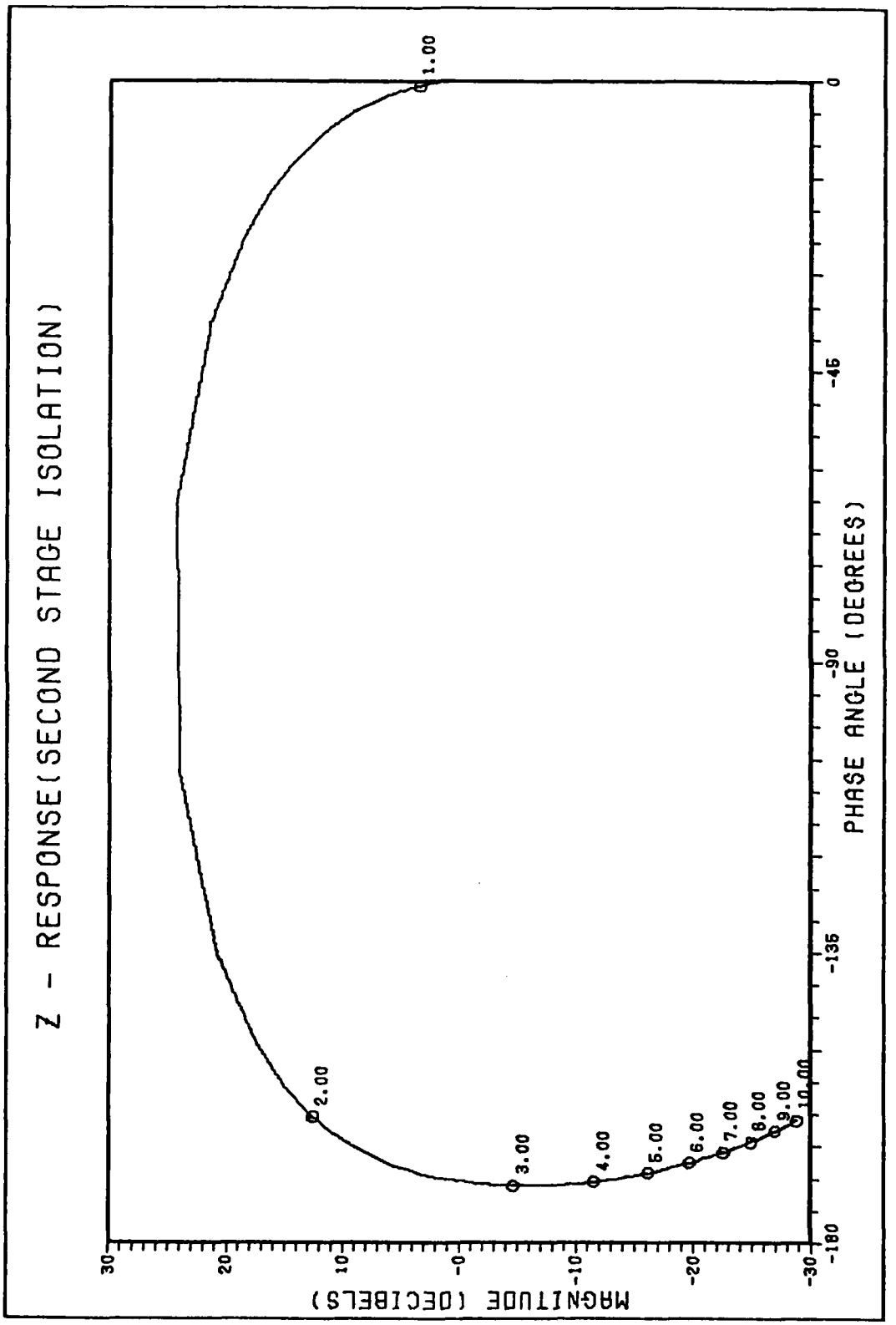

Figure 5.16 Z - Response (Second Stage Isolation) - Nichols Plot

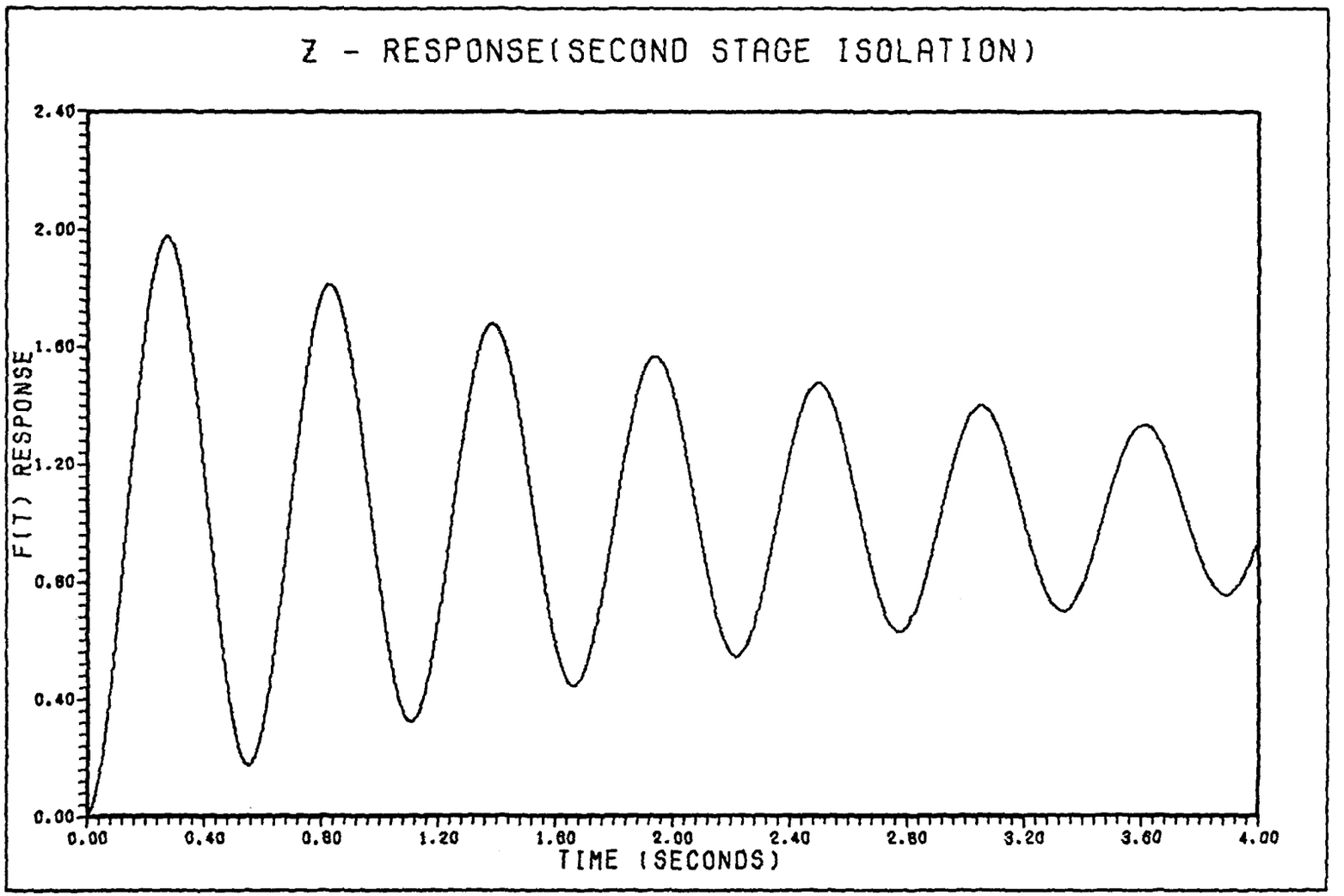

Figure 5.17 Z - *Response* (Second Stage Isolation) - Time Response

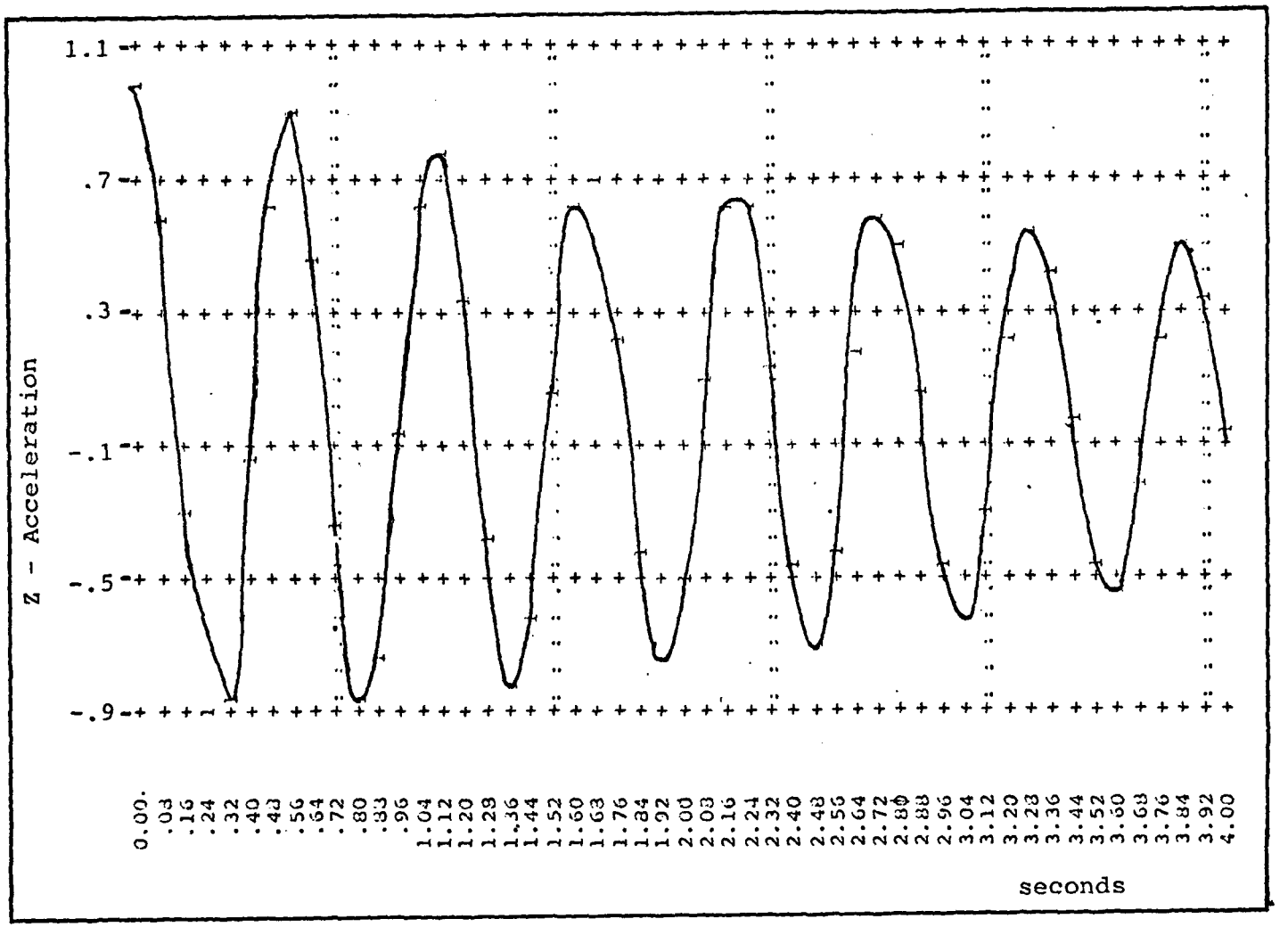

Figure 5.18 Z - Controller (Second Stage Isolation)

$$\bar{Y}_{\psi} = C_{\psi}\,\bar{X}_{\psi} + D_{\psi}\,\bar{U}_{\psi} \qquad (5\text{-}33)$$

The state space model using the SSP dynamics for ψ loop reduces Eq 5-32 to

$$\bar{X}_{\psi} = A_{\psi}\,\bar{X}_{\psi} + B_{\psi}\,\bar{U}_{\psi} \qquad (5\text{-}34)$$

Using the state notation from Eq J-5 and the A matrix values from Eq J-26, Eq 5-34 is written as

$$\begin{bmatrix} \dot{X}_{13} \\ \dot{X}_{14} \\ \dot{X}_{15} \\ \dot{X}_{16} \end{bmatrix} = \begin{bmatrix} 0.0000 & 1.0000 & 0.0000 & 0.0000 \\ -1425.4116 & -7.5620 & 563.1032 & 2.9870 \\ 0.0000 & 0.0000 & 0.0000 & 1.0000 \\ 281.5035 & 1.4934 & -284.0217 & -1.5068 \end{bmatrix} \begin{bmatrix} X_{13} \\ X_{14} \\ X_{15} \\ X_{16} \end{bmatrix} \qquad (5\text{-}35)$$

The root locus of the ψ open loop is derived from ψ transmissibility for the SSP isolation with a unit feedback continuous time system. The root locus is drawn in Figure 5.19 and is analyzed for the same general form for the X SSP isolation controller.

The poles and zeros are repeated from Eq 4-42:

Poles: $p_{1,2} = -0.4201 \pm j12.58$

$p_{3,4} = -4.160 \pm j39.38$

Zeros: $z_{1,2} = -188.5$

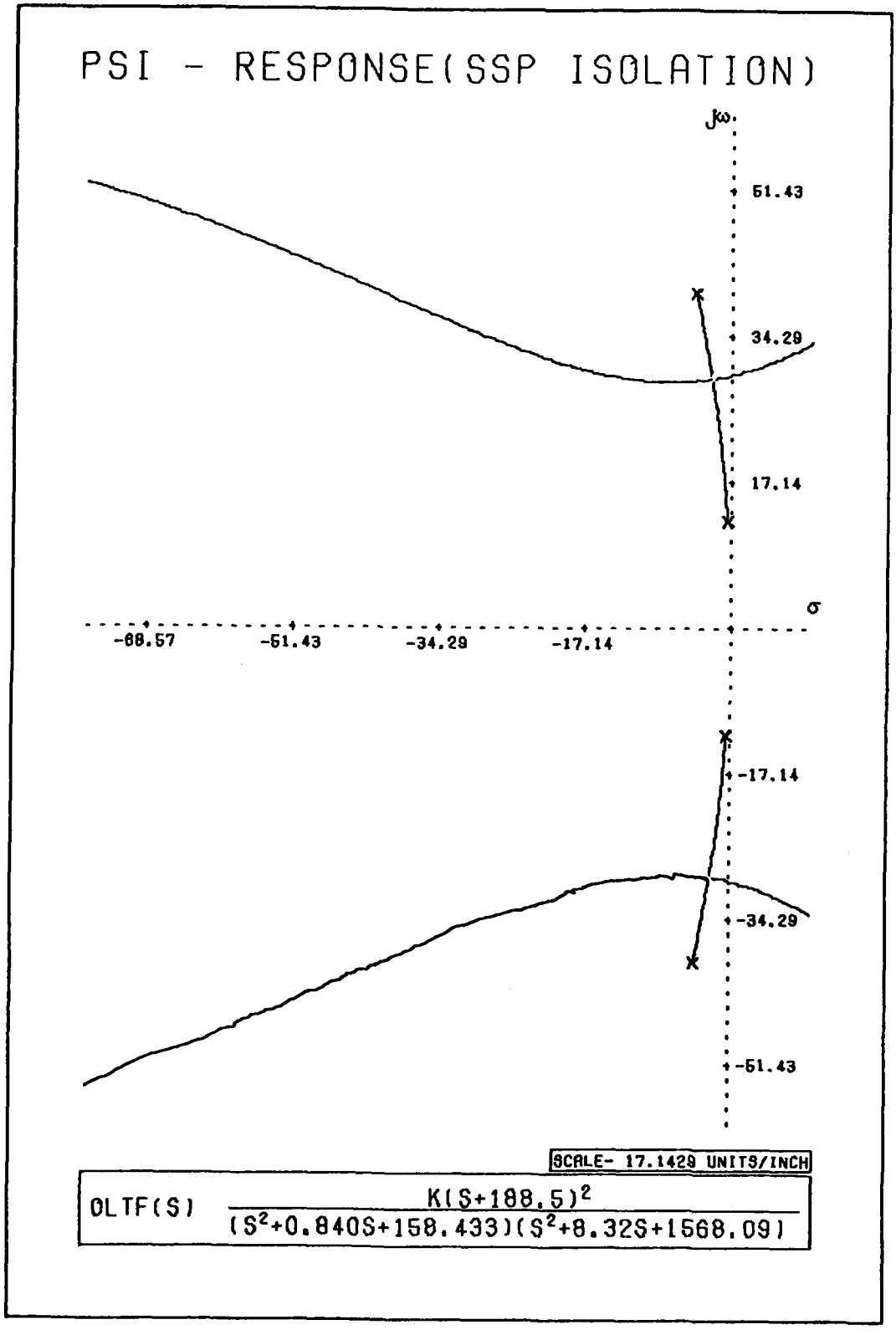

Figure 5.19 PSI - Response (SSP Isolation) - Root Locus

A Nichols plot is drawn in Figure 5.20 which shows the 6.33 dB (4.7 Hz) gain margin and 8.3° (3.1 Hz) phase margin for this controller design. The continuous time unit step response is plotted in Figure 5.21 which at four seconds is a ±0.3 damped sine wave at 2.08 Hz (on a bias of one) to be compared later to the CGTPIF discrete time response. A summary of Figure 5.21 is listed in Table 4.4 under $T\psi_{U/P}(t)$ response.

Two SISO controllers are planned using the following actuator configurations as

Upper Level Actuator:

$$B_\psi T_\psi = \begin{bmatrix} 0.0000 \\ 0.0000 \\ 0.0000 \\ 0.0004 \end{bmatrix} [T_\psi] \qquad (5\text{-}36)$$

Lower Level Actuator:

$$B_\psi t_\psi = \begin{bmatrix} 0.0000 \\ 0.0009 \\ 0.0000 \\ 0.0000 \end{bmatrix} [t_\psi] \qquad (5\text{-}37)$$

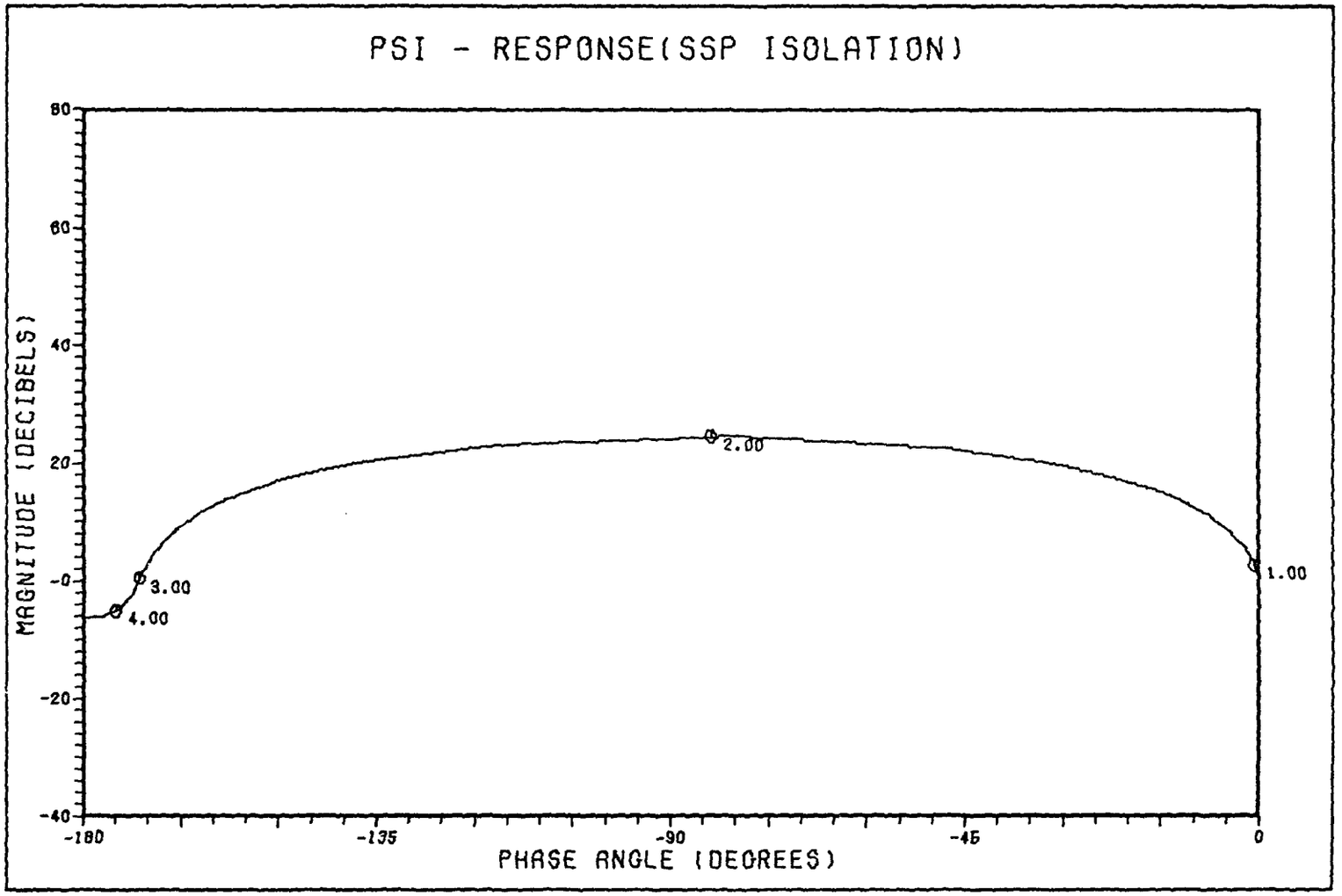

Figure 5.20 PSI - Response (SSP Isolation) - Nichols Plot

AD-A115 559 AIR FORCE INST OF TECH WRIGHT-PATTERSON AFB OH SCHOO--ETC F/G 17/7
ANALYSIS AND DESIGN OF A DIGITAL CONTROLLER FOR A SEISMICALLY S--ETC(U)
DEC 81 S W FRANCIS
UNCLASSIFIED AFIT/GE/EE/81D-22 NL

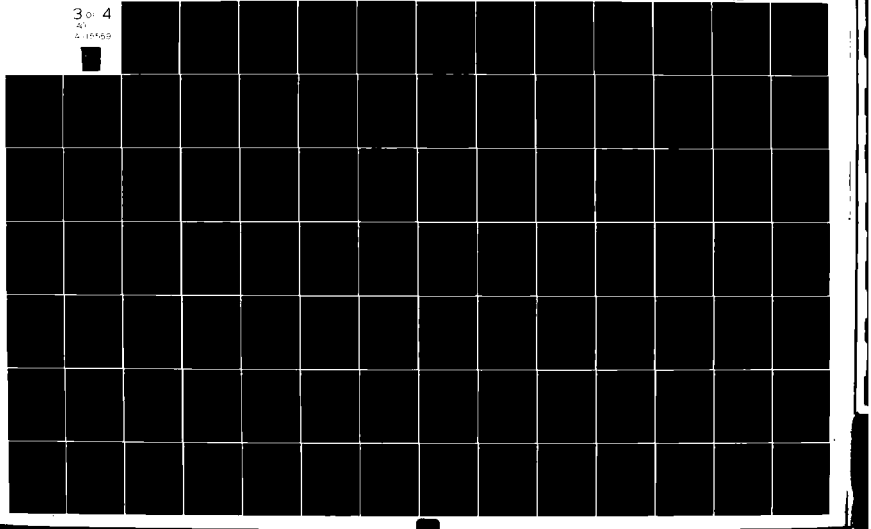

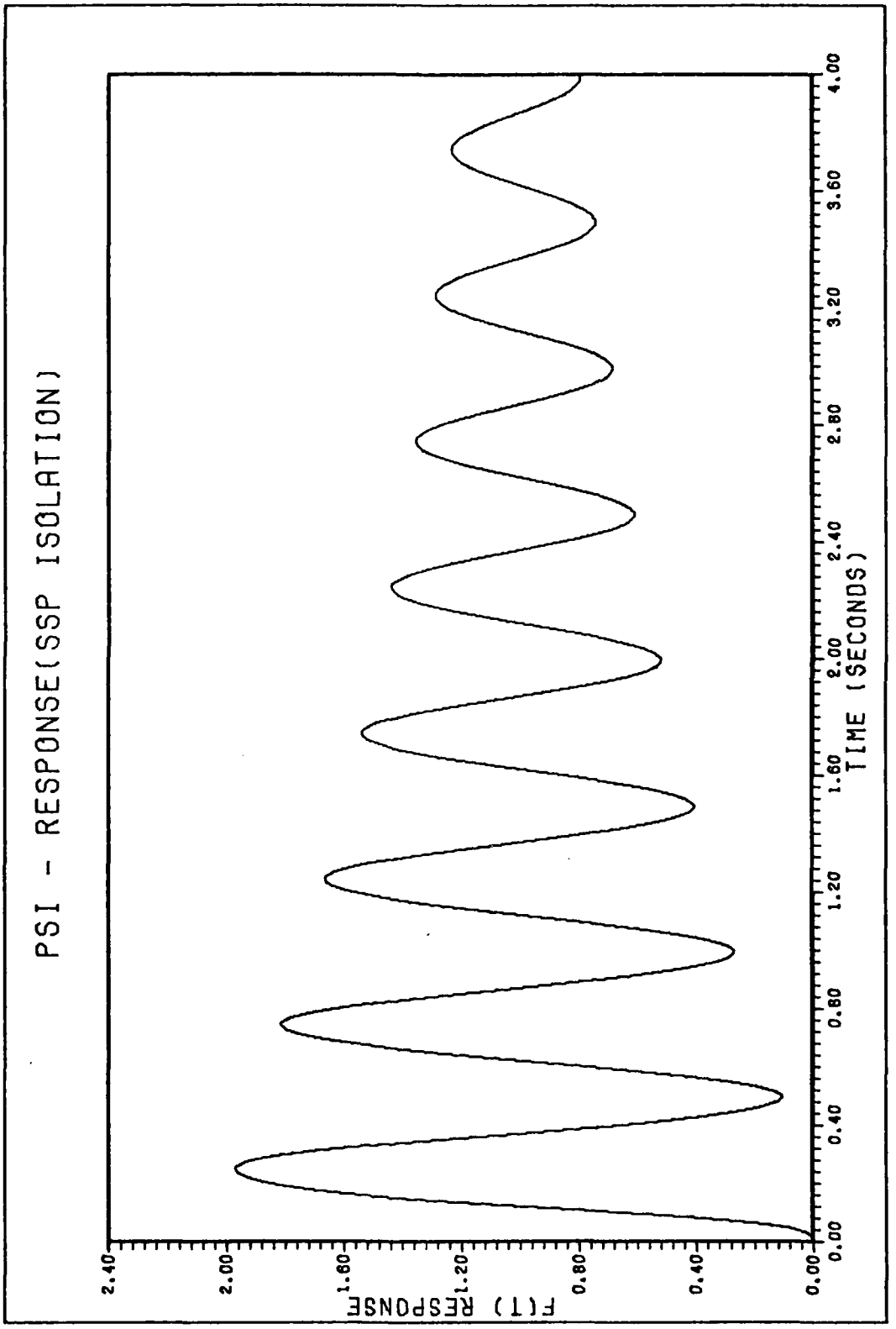

Figure 5.21 PSI - Response (SSP Isolation) - Time Response

The output is the same in both configurations:

$$Y_\theta = [0.0000 \quad 0.0000 \quad 10.0000] \begin{bmatrix} X_{13} \\ X_{14} \\ X_{15} \\ X_{16} \end{bmatrix} \tag{5-38}$$

Notice the Y_θ output is simply the ψ tilt and also $D_\psi = \overline{0}$. The B_ψ terms in Eq 5-36 and Eq 5-37 are scaled by the X moments of inertia for the upper and lower levels. Based on past experience, B_ψ will be scaled to one as was done for translational controllers due to CGTPIF not being able to reach a solution. The translation analogy to the large mass and small force or torque in this case parallels rotational dynamics from the translational physical realities. The U_ψ vector has upper level ψ torques (T_ψ) and lower level ψ torques (t_ψ). Appendix F, Eq F-14 and F-15 relate the actuators and torques.

CGTPIF gives no SISO solution for the ψ controller. Again, observability and controllability deficiencies plaqued the controller design process.

A MIMO controller is proposed using the following input matrix and output equation:

$$B_\psi U_\psi = \begin{bmatrix} 0.0000 & 0.0000 \\ 0.0009 & 0.0000 \\ 0.0000 & 0.0000 \\ 0.0000 & 0.0004 \end{bmatrix} \begin{bmatrix} t_\psi \\ T_\psi \end{bmatrix} \tag{5-39}$$

$$\begin{bmatrix} Y_7 \\ Y_8 \end{bmatrix} = \begin{bmatrix} 0.0000 & 0.0000 & 0.0000 & 0.0000 \\ 0.0000 & 0.0000 & 1.0000 & 0.0000 \end{bmatrix} \begin{bmatrix} X_{13} \\ X_{14} \\ X_{15} \\ X_{16} \end{bmatrix} \tag{5-40}$$

CGTPIF obtained the digital controller listed in Case 5, Design A in Appendix K. The unit tilt discrete response is plotted in Figure 5.22. An approximation is made of Figure 5.22 at 4 seconds estimating a ±0.1760 damped sine wave at 2.0 Hz response. This response resulted from an initial condition for X_{13} equal to one. The Y_7 output is a zero row assuming the lower level is not accessible. The B_ψ matrix is scaled to one for weak controllability compensation and Y_c is not set above one, since the tilt output is unstable for high costs.

PSI - Controller (Second Stage Isolation)

The upper level and the second stage isolation dynamics partitioned from Eq 5-40 yield the reduced order model as

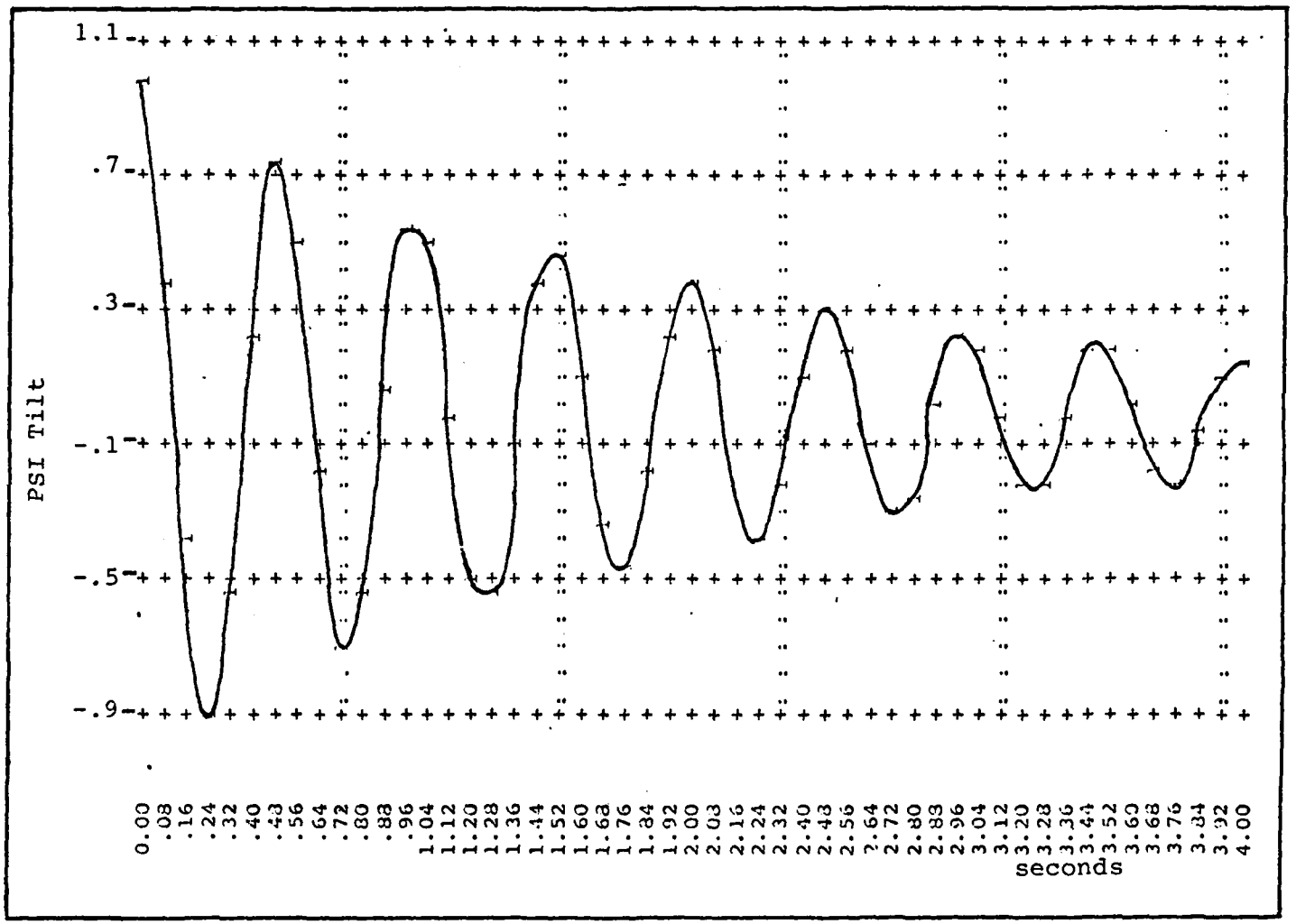

Figure 5.22 PSI - Controller (SSP Isolation)

$$\begin{bmatrix} \dot{X}_{15} \\ \dot{X}_{16} \end{bmatrix} = \begin{bmatrix} 0.0000 & 1.0000 \\ -284.0217 & -1.5080 \end{bmatrix} \begin{bmatrix} X_{15} \\ X_{16} \end{bmatrix} + [0.0004)\ T_{\psi} \quad (5\text{-}41)$$

$$Y_8 = [1.0000 \quad 0.0000] \begin{bmatrix} X_{15} \\ X_{16} \end{bmatrix} \quad (5\text{-}42)$$

The PSI second stage isolation open loop root locus is shown in Figure 5.23. This is a typical second stage root locus as described for the X direction. The open loop poles and zeros from Eq 4-56 are repeated as:

Poles: $p_{1,2} = -0.7499 \pm j16.80$

Zeros: $z_1 = -188.5$

The typical second stage 10 degree phase margin is read from Figure 5.24, PSI - Response (Second Stage Isolation) - Nichols Plot. Neither the root locus or Nichols plot indicate a gain margin problem.

An open loop unit step continuous time response is plotted in Figure 5.25 which shows at four seconds a ±0.075 damped sine wave at 2.5 Hz on a bias of one. A summary of Figure 5.25 is available in Table 4.6 for the $T\psi_{U/L}(t)$ response.

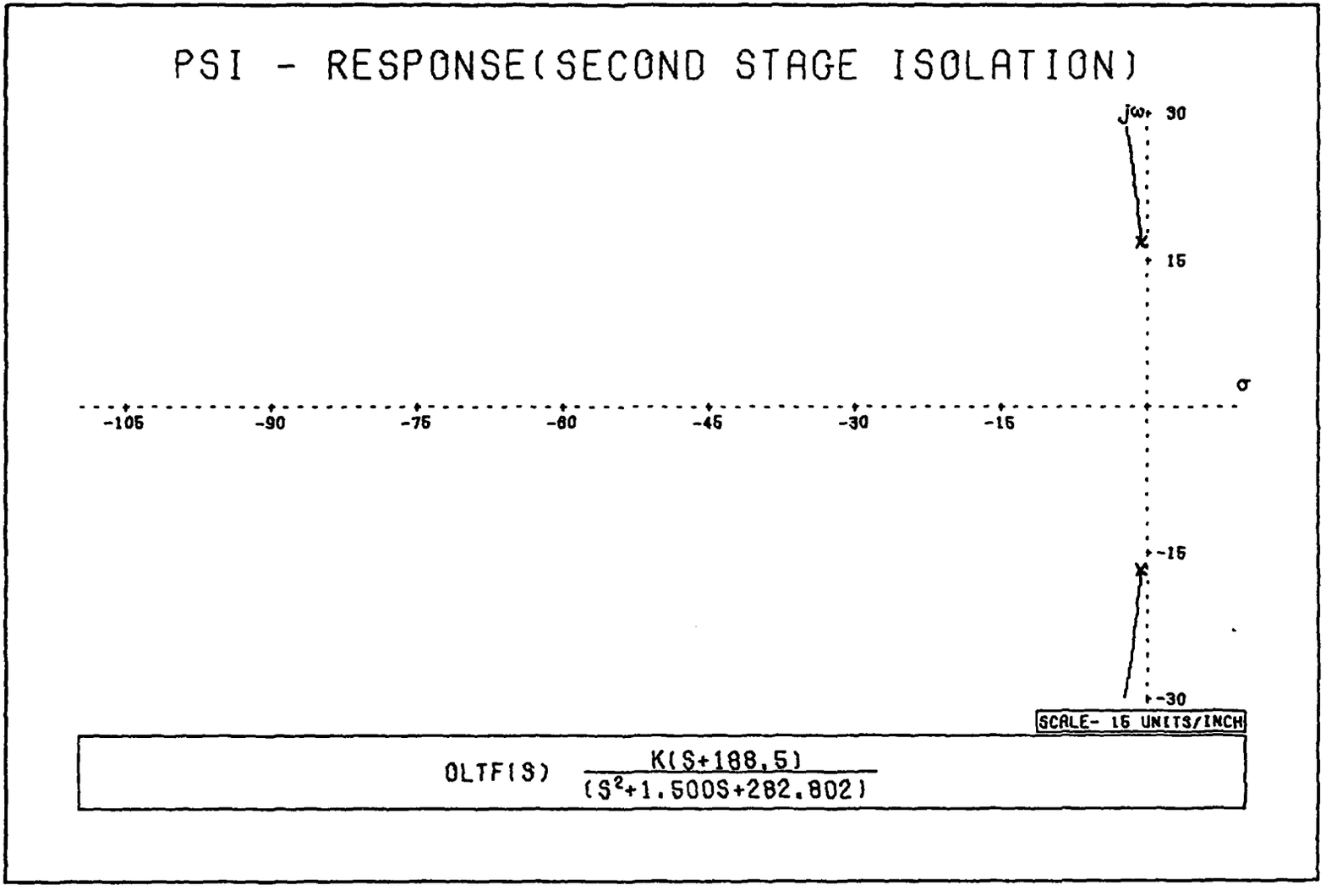

Figure 5.23 PSI - Response (Second Stage Isolation) - Root Locus

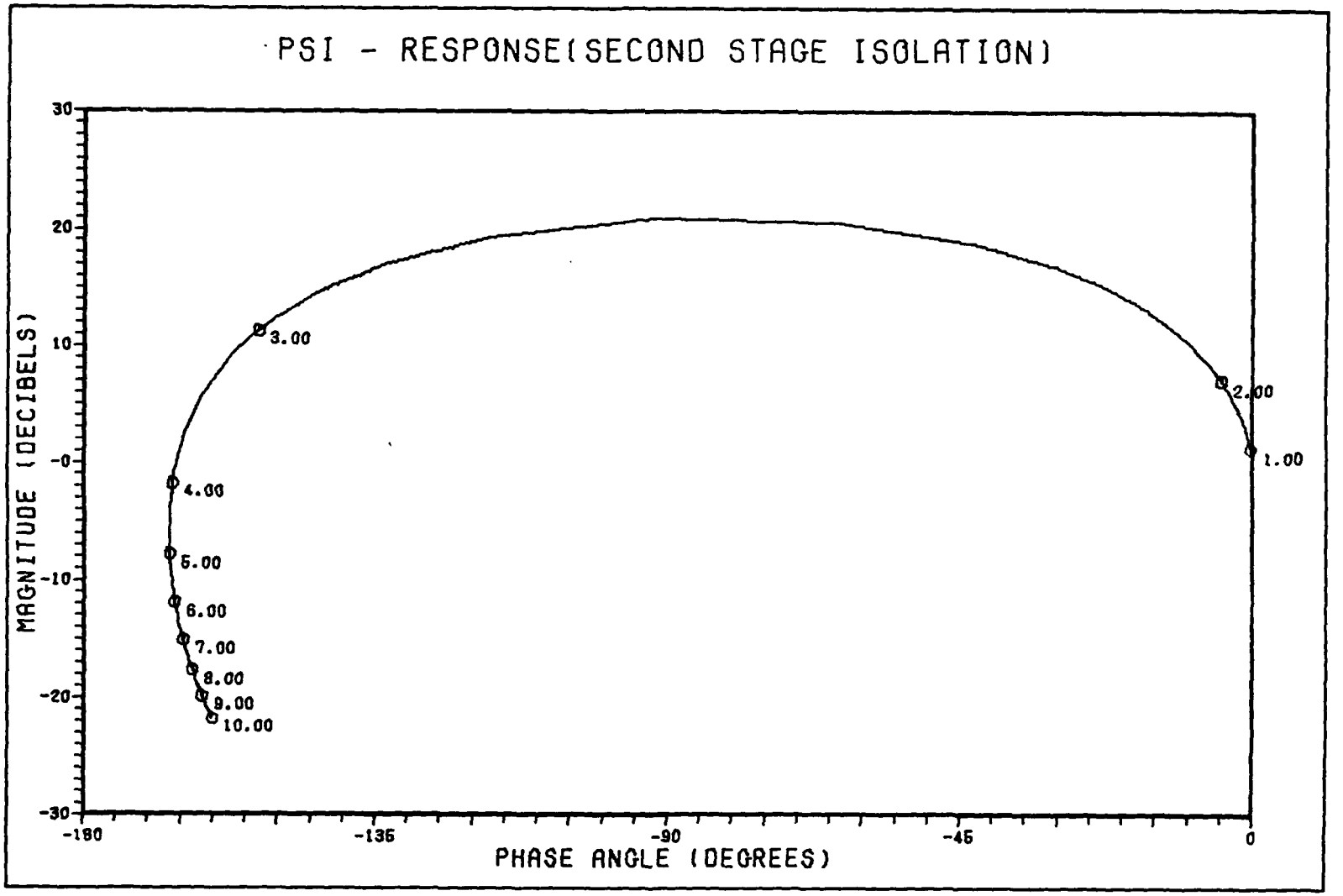

Figure 5.24 PSI - Response (Second Stage Isolation) - Nichols Plot

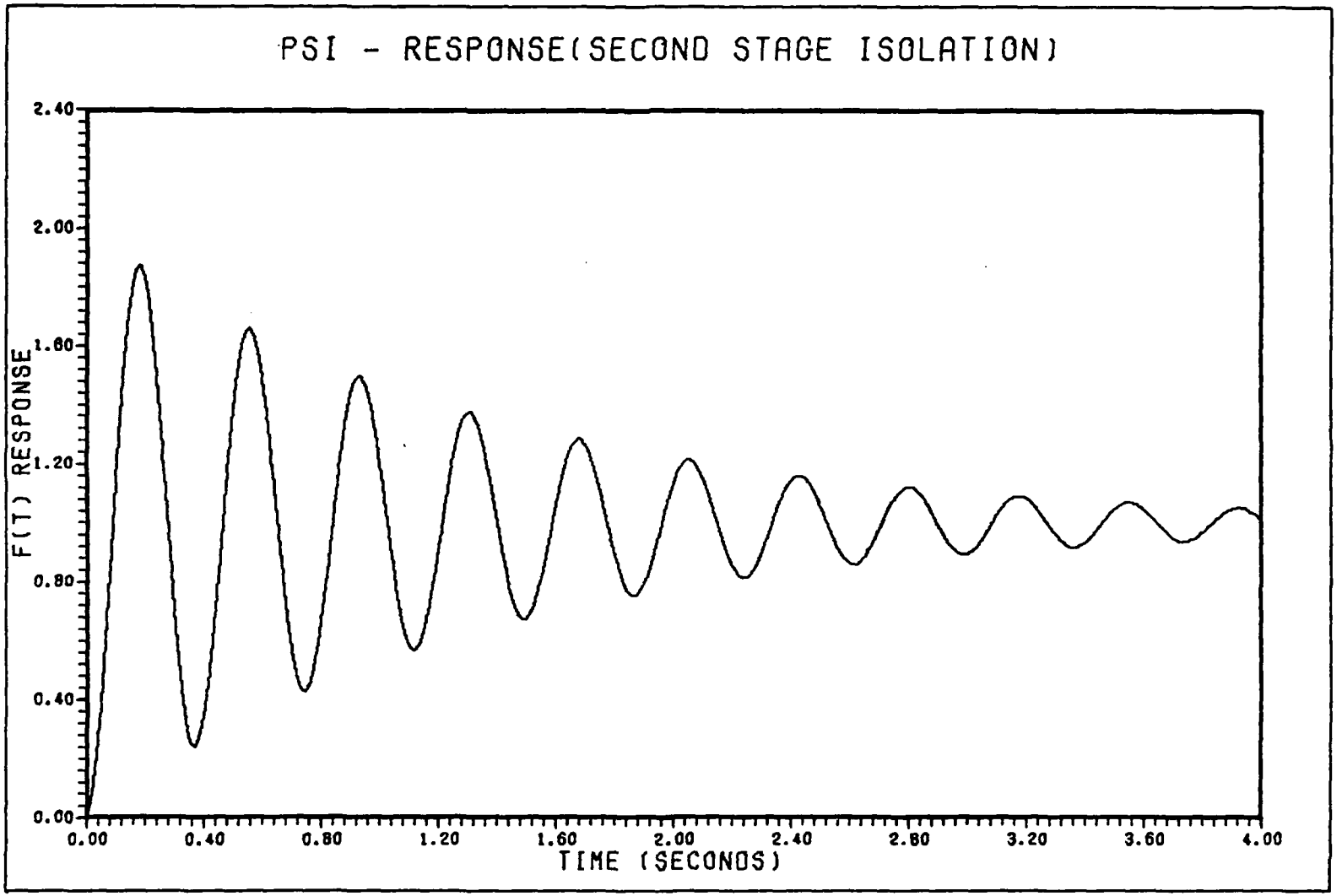

Figure 5.25 PSI - Response (Second Stage Isolation) - Time Response

Case 6, Design A is the resulting digital controller from CGTPIF. The input matrix B_ψ is scaled to one for weak controllability and the output cost Y_c is kept at one because increased costs destabilize the output tilt. The unit tilt response is shown in Figure 5.26 which at four seconds is a ±0.010ᵹ damped sine wave at 2.78 Hz for an X_{15} initial condition equal to one.

Theta - Controller (SSP Isolation)

The truth model for the ⊖ controller is rewritten from the partitions of Eqs J-8a, J-8b and J-8f for the Θ state variables and cross coupling terms as

$$\begin{bmatrix} \dot{\bar{X}}_x \\ \dot{\bar{X}}_y \\ \dot{\bar{X}}_\Theta \end{bmatrix} = \begin{bmatrix} A_x & \bar{0} & A_{x\Theta} \\ \bar{0} & A_y & A_{y\Theta} \\ A_{\Theta x} & A_{\Theta y} & A \end{bmatrix} \begin{bmatrix} \bar{X}_x \\ \bar{X}_y \\ \bar{X}_\Theta \end{bmatrix} + \begin{bmatrix} B_x & \bar{0} & \bar{0} \\ \bar{0} & B_y & \bar{0} \\ \bar{0} & \bar{0} & B_\Theta \end{bmatrix} \begin{bmatrix} \bar{U}_x \\ \bar{U}_y \\ \bar{U}_\Theta \end{bmatrix} \tag{5-43}$$

$$\bar{Y}_\Theta = C_\Theta \bar{X}_\Theta + D_\Theta \bar{U}_\Theta \tag{5-44}$$

The state space model using SSP dynamics for the loop reduces Eq 5-43 to

$$\dot{\bar{X}}_\Theta = A_\Theta \bar{X}_\Theta + B_\Theta \bar{U}_\Theta \tag{5-45}$$

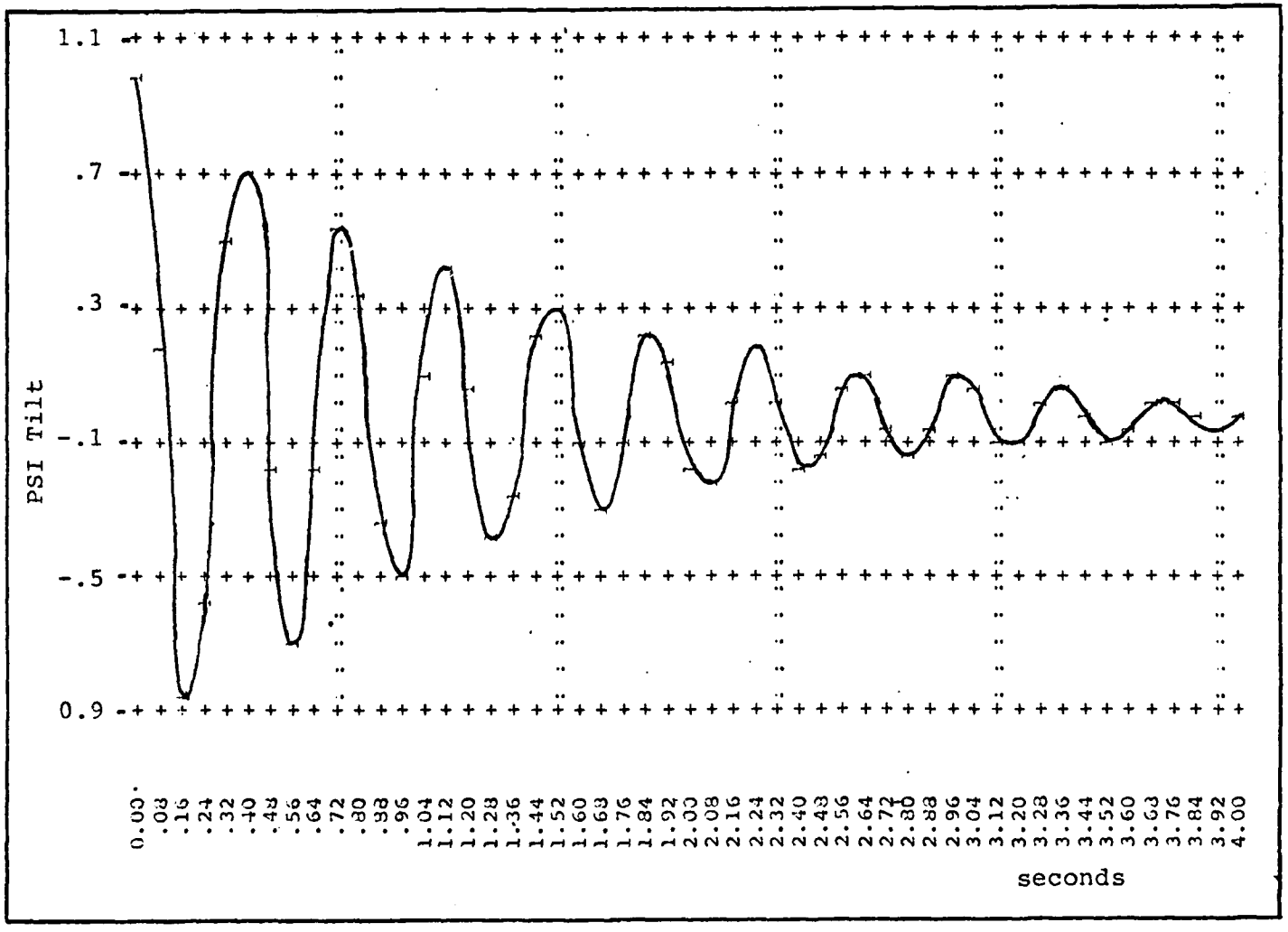

Figure 5.26 PSI - Controller (Second Stage Isolation)

Using the state notation from Eq J-7 and the A matrix values from Eq J-36, Eq 5-45 is written as

$$\begin{bmatrix} \dot{X}_{21} \\ \dot{X}_{22} \\ \dot{X}_{23} \\ \dot{X}_{24} \end{bmatrix} = \begin{bmatrix} 0.0000 & 1.0000 & 0.0000 & 0.0000 \\ -6104.7858 & -15.0218 & 2560.1284 & 6.1119 \\ 0.0000 & 0.0000 & 0.0000 & 1.0000 \\ 1279.9637 & 3.0557 & -1289.5446 & -3.0786 \end{bmatrix} \begin{bmatrix} X_{21} \\ X_{22} \\ X_{23} \\ X_{24} \end{bmatrix} \tag{5-46}$$

The root locus is drawn in Figure 5.27 with the usual SSP isolation form and general comments made for the X SSP isolation root locus. The poles and zeros are repeated from Eq 4-39:

$$\begin{aligned} \text{Poles:} \quad & p_{1,2} = -0.8363 \pm j26.10 \\ & p_{3,4} = -8.273 \pm j81.81 \\ \text{Zeros:} \quad & z_1 = -397.9 \\ & z_2 = -418.9 \end{aligned}$$

A Nichols plot is drawn in Figure 5.28 showing the 6.22 dB (9.8 Hz) gain margin and 7.1° (7.0 Hz) phase margin. A continuous time unit step response is shown in Figure 5.29 with a ±0.05 damped sine wave at 4.17 Hz (on a bias of one) approximated at the 4 second comparison time. More information on the time response is listed in Table 4.4 under the function $T\Theta_{U/P}(t)$.

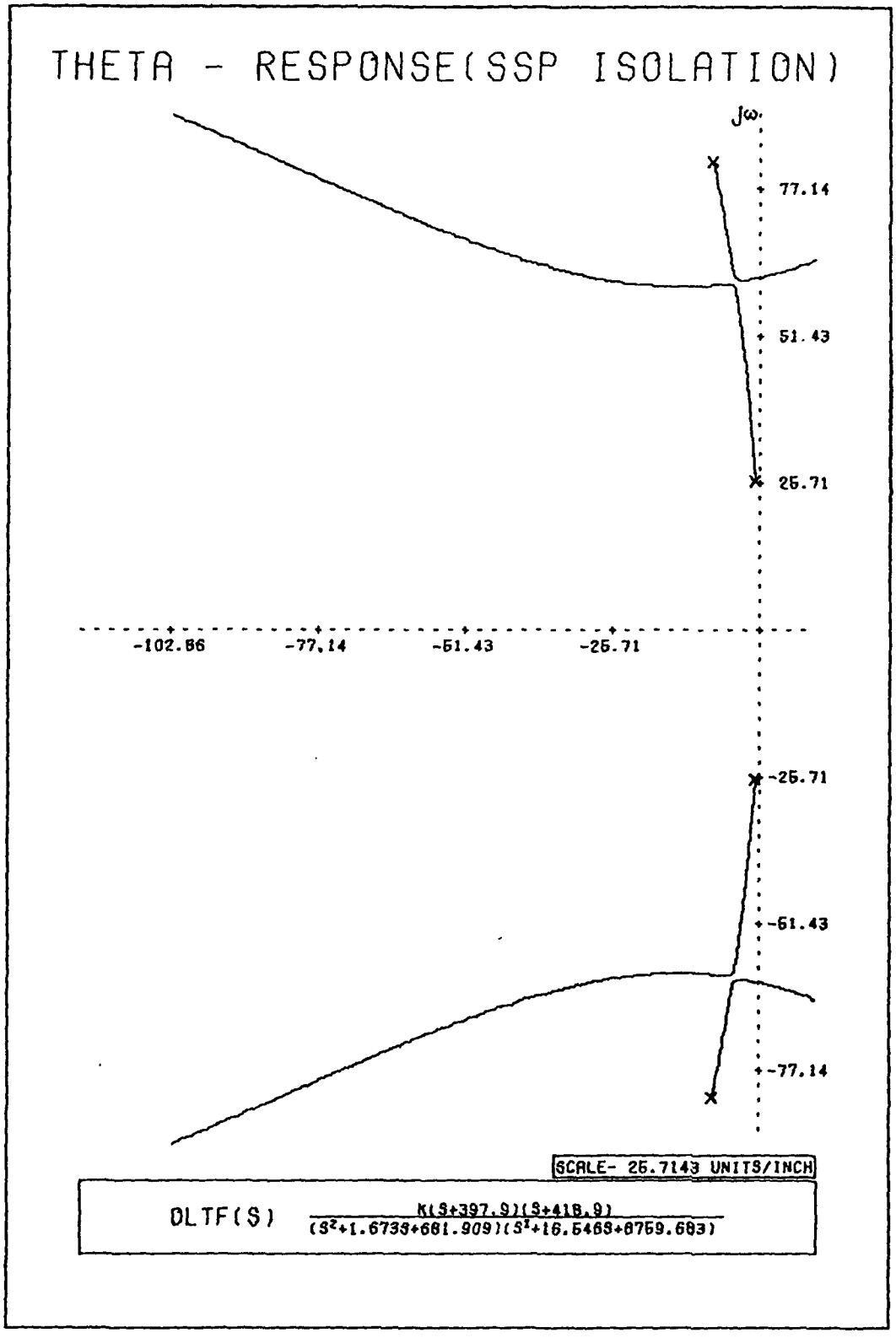

Figure 5.27 Theta - Response (SSP Isolation) - Root Locus

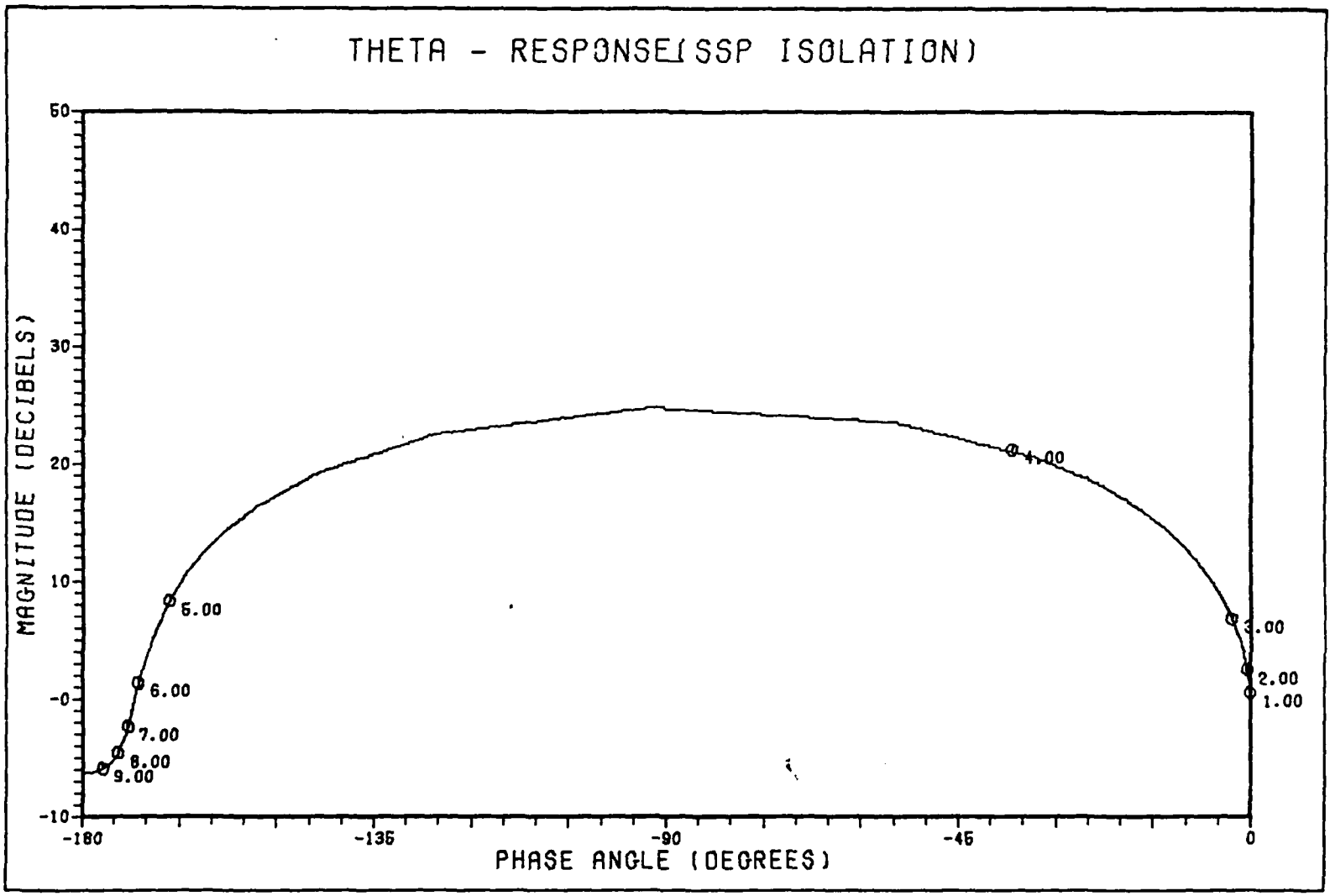

Figure 5.28 Theta - Response (SSP Isolation) - Nichols Plot

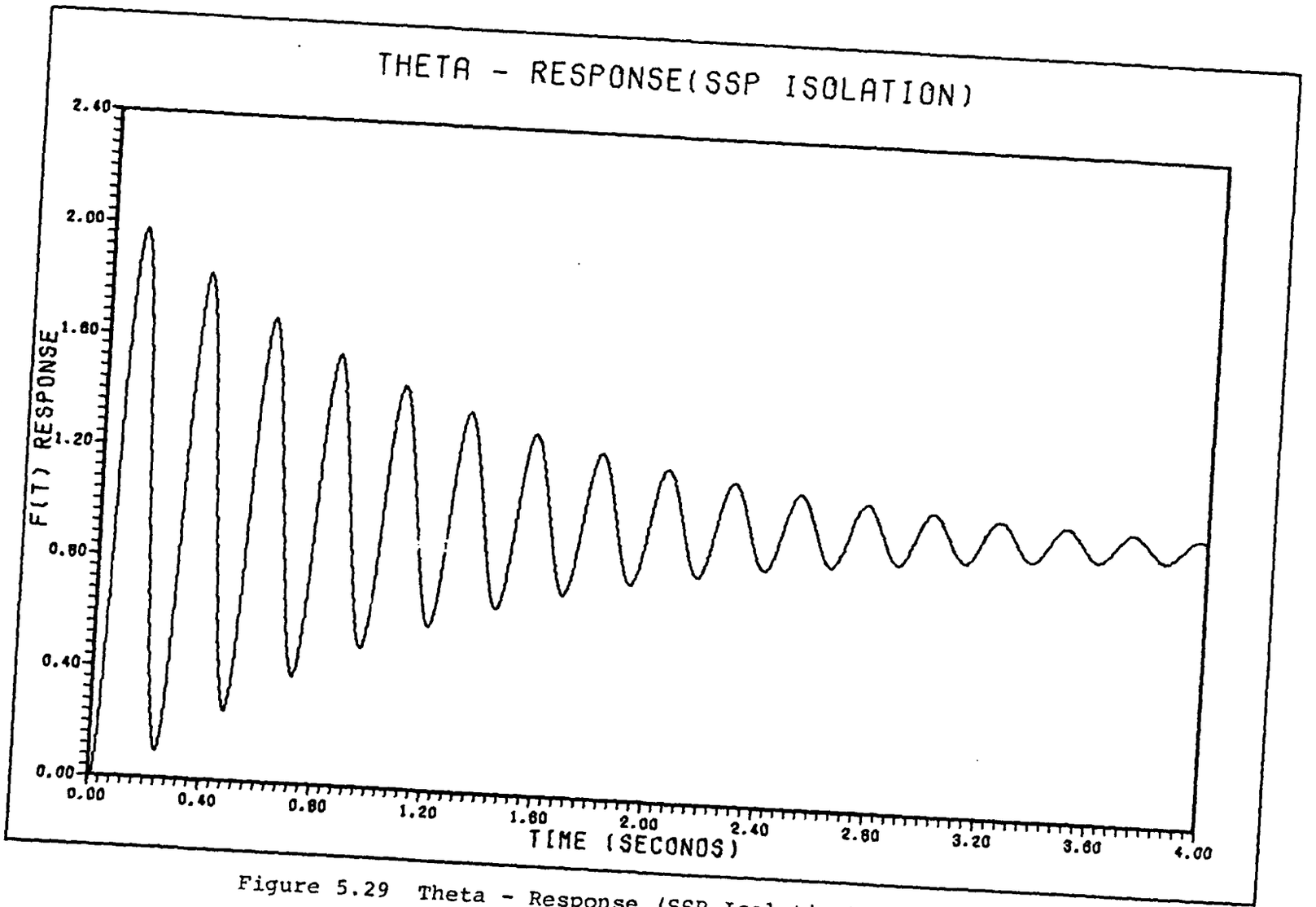

Figure 5.29 Theta - Response (SSP Isolation) - Time Response

Several SISO controllers are attempted using the following actuator configurations:

Upper Level Actuator:

$$B_\Theta T_\Theta = \begin{bmatrix} 0.0000 \\ 0.0000 \\ 0.0000 \\ 0.0001 \end{bmatrix} [T_\Theta] \qquad (5\text{-}47)$$

Lower Level Actuator:

$$B_\Theta t_\Theta = \begin{bmatrix} 0.0000 \\ 0.0004 \\ 0.0000 \\ 0.0000 \end{bmatrix} [t_\Theta] \qquad (5\text{-}48)$$

The output is the same in both configurations:

$$[Y_{12}] = [0.0000 \quad 0.0000 \quad 1.0000 \quad 0.0000] \begin{bmatrix} X_{21} \\ X_{22} \\ X_{23} \\ X_{24} \end{bmatrix} \qquad (5\text{-}49)$$

The Y_{12} output is the 0 tilt. No SISO solutions are possible from CGTPIF. The input matrix B_Θ is scaled to one, but observability and controllability problems prevented an optimum controller solution.

A MIMO controller is specified using the upper and lower actuators with the output as the Θ tilt for the following system expressions:

$$B_\Theta \bar{U}_\Theta = \begin{bmatrix} 0.0000 & 0.0000 \\ 0.0004 & 0.0000 \\ 0.0000 & 0.0000 \\ 0.0000 & 0.0001 \end{bmatrix} \begin{bmatrix} t_\Theta \\ T_\Theta \end{bmatrix} \tag{5-50}$$

$$\begin{bmatrix} Y_{11} \\ Y_{12} \end{bmatrix} = \begin{bmatrix} 0.0000 & 0.0000 & 0.0000 & 0.0000 \\ 0.0000 & 0.0000 & 1.0000 & 0.0000 \end{bmatrix} \begin{bmatrix} X_{21} \\ X_{22} \\ X_{23} \\ X_{24} \end{bmatrix} \tag{5-51}$$

The Y_{11} output is a zero row because the lower level is physically inaccessible.

CGTPIF provided the solution listed in Case 7, Design A, Appendix K. An estimate is made from the Θ unit tilt discrete time response in Figure 5.30 for the tilt at 4 seconds to be ±0.019 damped sine wave at 4.17 Hz for an initial condition for state X_{21} equal to one. The B_Θ input matrix is scaled to one for controllability compensation and Y_c the output cost remained at one for tilt output stability.

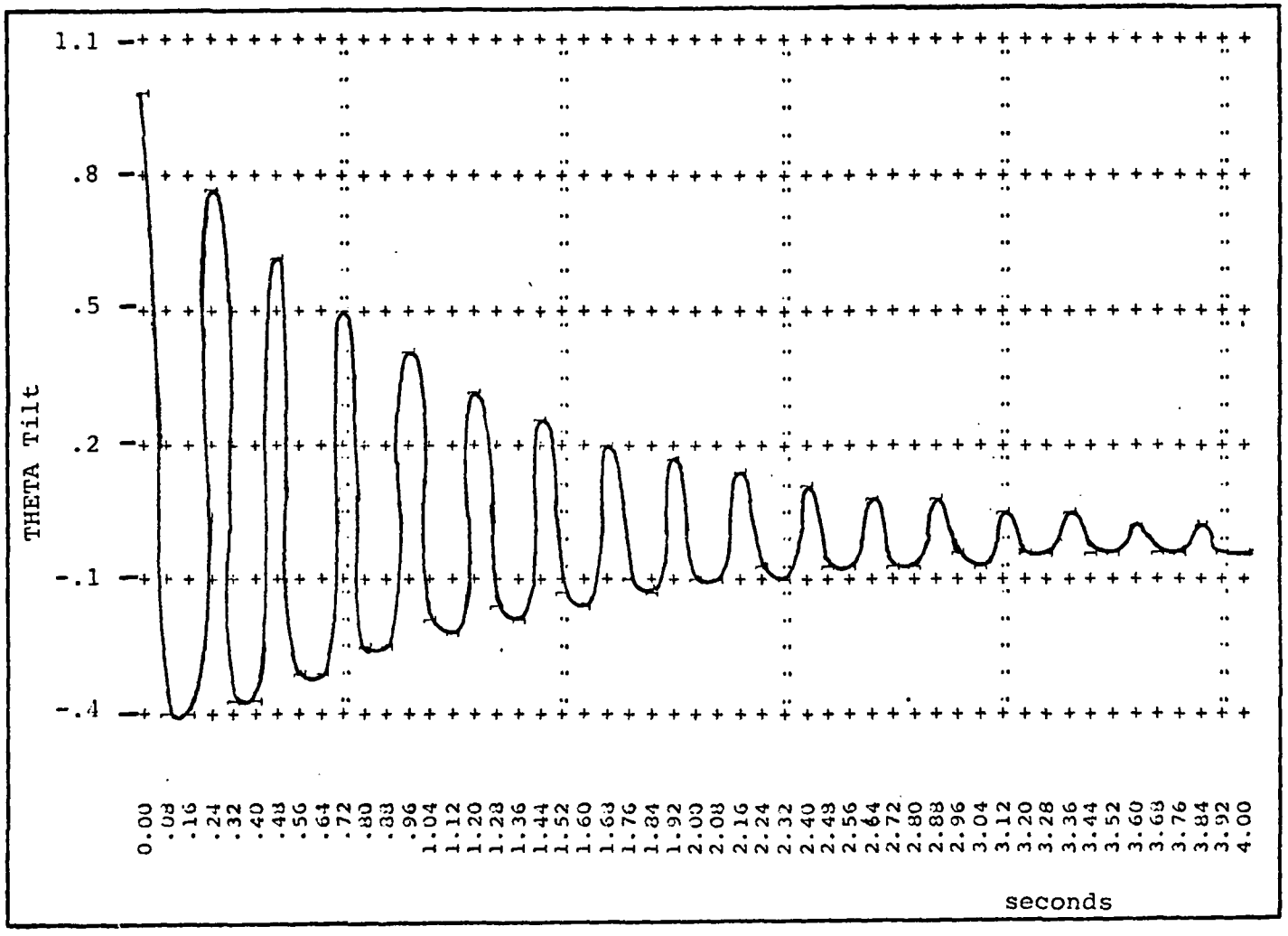

Figure 5.30 THETA - Controller (SSP Isolation)

Theta - Controller (Second Stage Isolation)

The upper level and the second stage isolation dynamics partitioned from Eq 5-46

$$\begin{bmatrix} X_{23} \\ X_{24} \end{bmatrix} = \begin{bmatrix} 0.0000 & 1.0000 \\ -1289.5446 & -3.0786 \end{bmatrix} \begin{bmatrix} X_{23} \\ X_{24} \end{bmatrix} + [0.0002]\ T\Theta \qquad (5\text{-}52)$$

$$Y_{12} = [1.0000 \quad 0.0000] \begin{bmatrix} X_{23} \\ X_{24} \end{bmatrix} \qquad (5\text{-}53)$$

The reduced order system open loop root locus is shown in Figure 5.31 and is typical of the second stage isolation dynamics. Poles and zeros are repeated from Eq 4-59 as:

Poles: $p_{1,2} = -1.530 \pm j35.77$

Zeros: $z_1 = -418.9$

About a 12° phase margin is indicated in the Nichols plot drawn in Figure 5.32. Gain margin is not a constraint in either the Nichols plot or root locus.

A continuous time response is plotted in Figure 5.33 with a flat step response at the four second criteria point. A summary of Figure 5.33 is given in Table 4.6 under the $T\Theta_{U/L}(t)$ response.

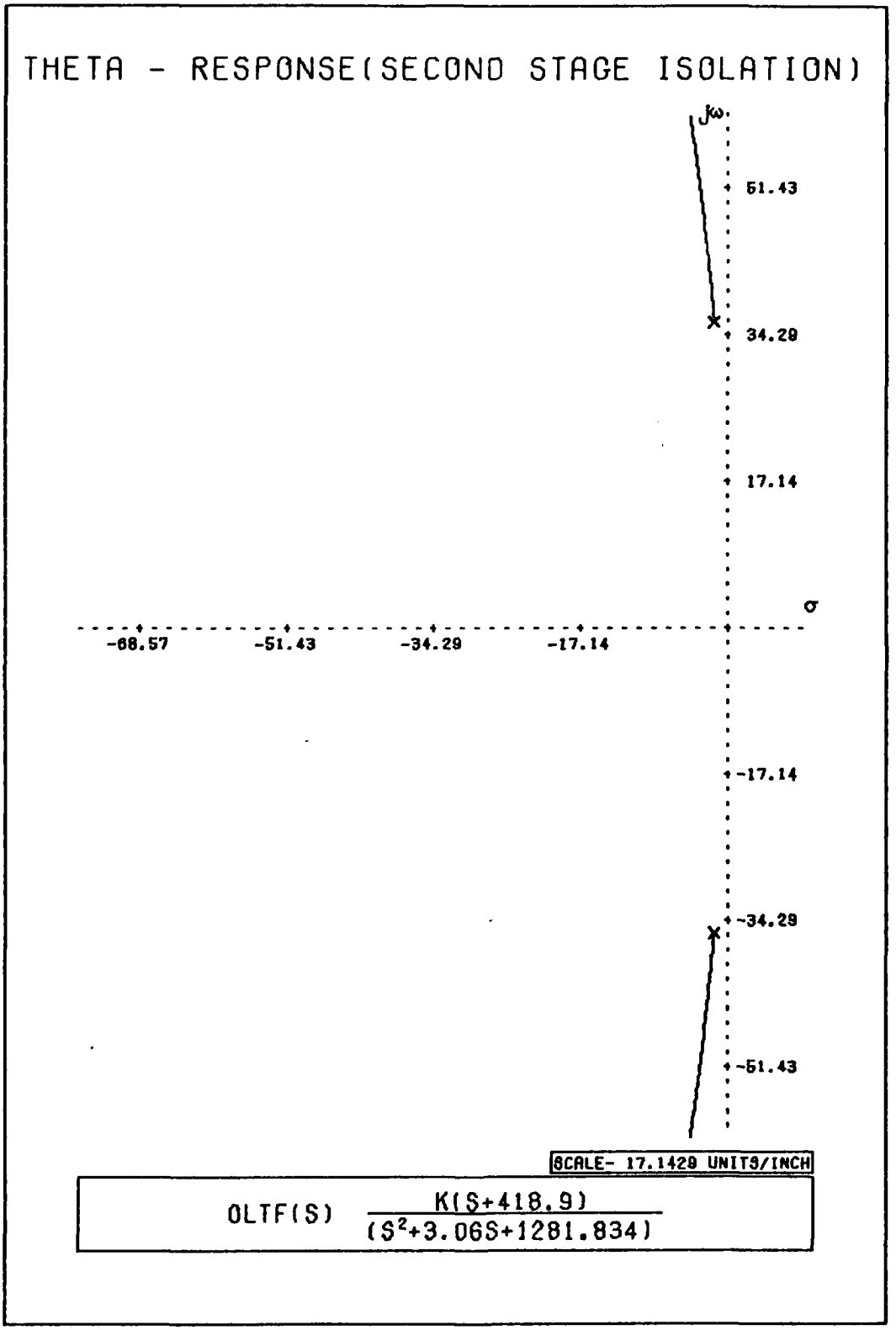

Figure 5.31 Theta - Response (Second Stage Isolation) - Root Locus

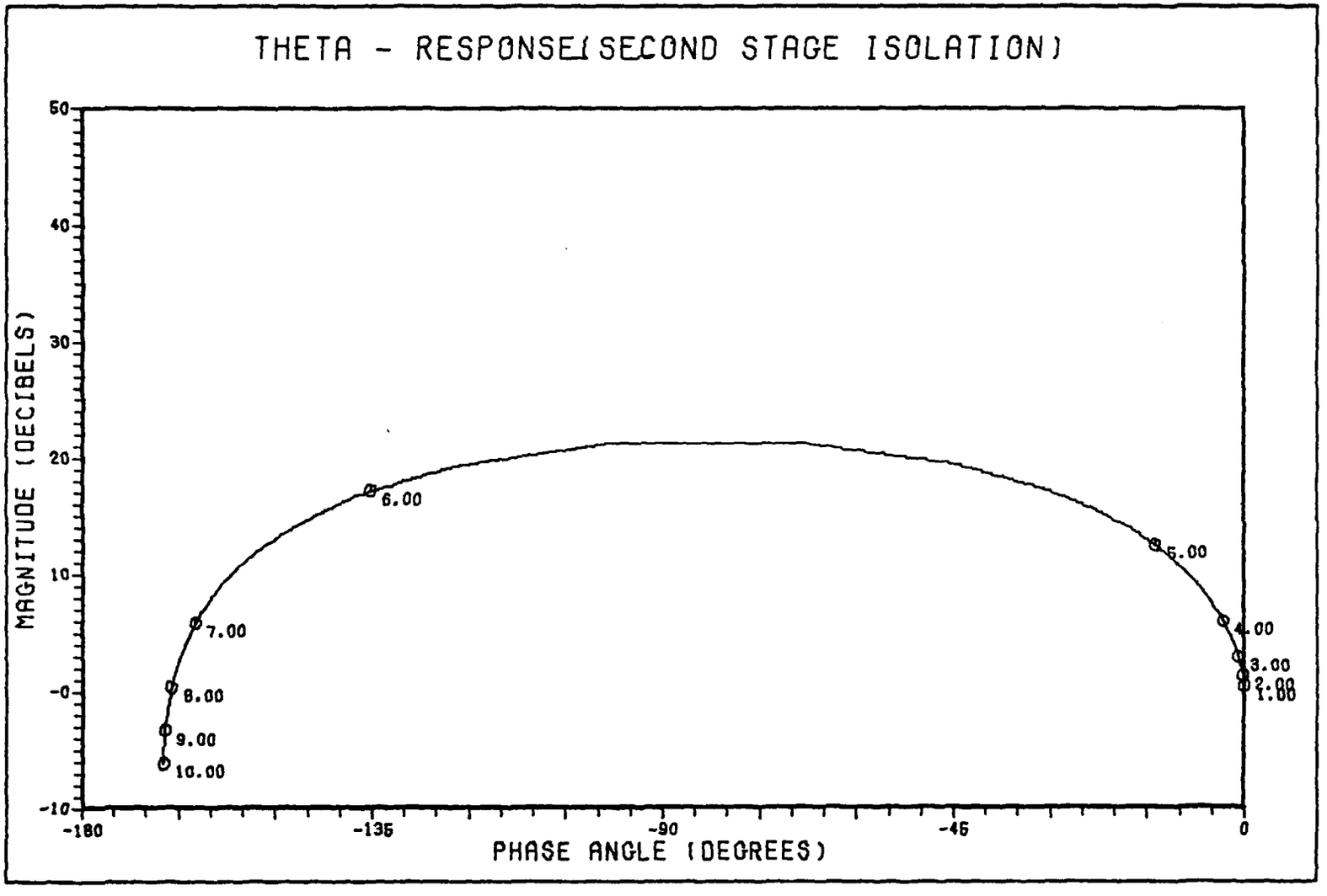

Figure 5.32 Theta - Response (Second Stage Isolation) - Nichols Plot

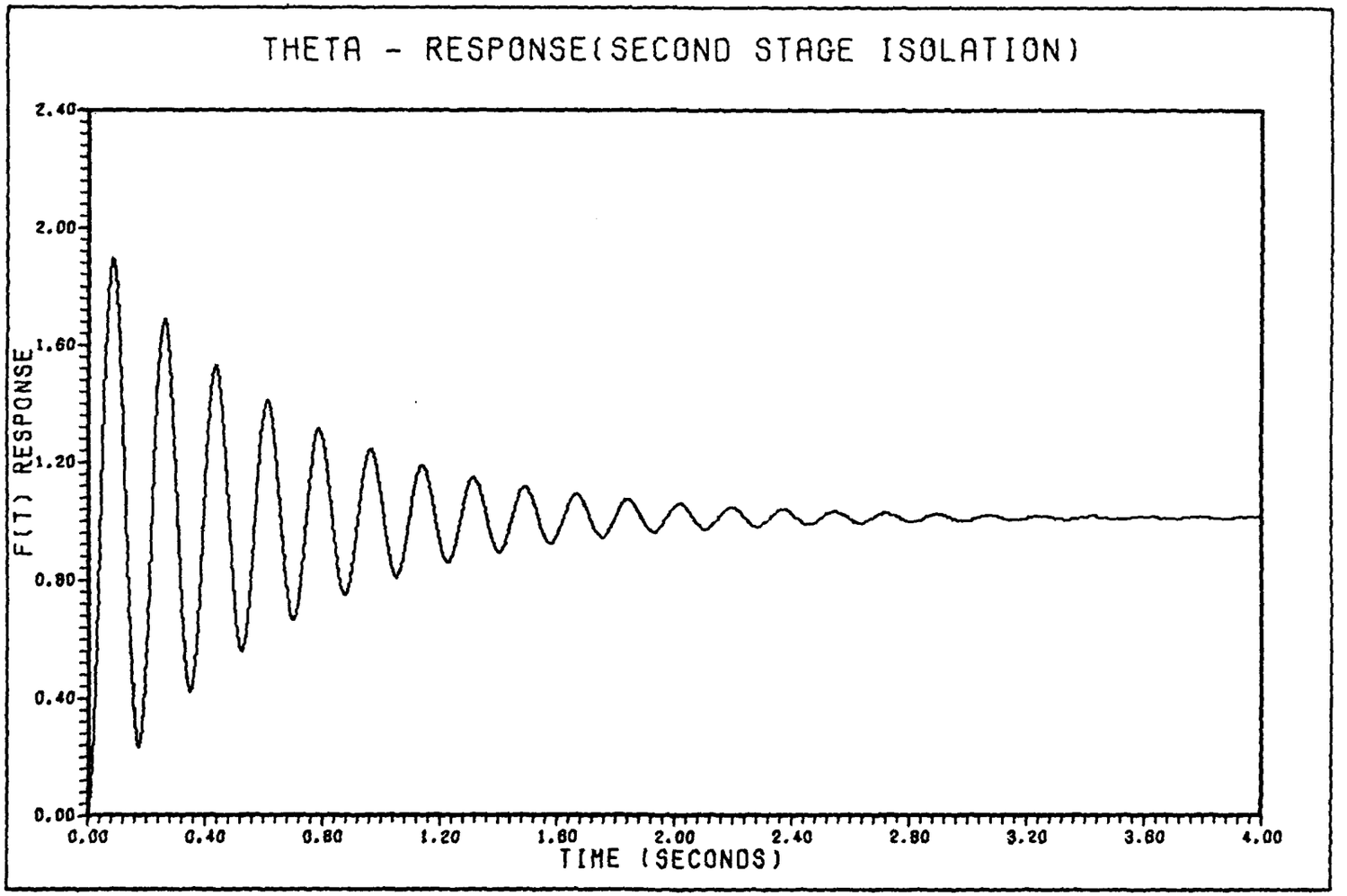

Figure 5.33 Theta -- Response (Second Stage Isolation) - Time Response

CGTPIF provided a digital controller design in Case 8, Appendix K. Design A is plotted for comparison in Figure 5.34 at four seconds is a ± 0.0011 damped sine wave operating at 6.25 Hz. B_θ is scaled to one and Y_c is limited to one for output stability. Design B, with B_θ unscaled gives a ±0.01 damped sine wave at 6.25 Hz on a -0.01 bias, with no plot available - the form would be similar to Figure 5.34. Design B offered no improvement with increasing Y_c.

Summary

Four control issues result from the controller design effort - observability, controllability and SISO/MIMO configurations. These areas are discussed by reviewing the control designs for the translation and rotation controller.

The translation controller performance is approximated by analyzing the continuous open loop unit acceleration steps from TOTAL and the discrete time step responses from CGTPIF, a certain point in time - four seconds elapsed response time. The unit step and output response can give a measure of transmissibility, namely, if unit input disturbance is applied to a linear system and the output is 0.01, the system offered -40 dB attenuation. In frequency domain analysis, sinusoid inputs would have to be assumed for a rough approximation. Since this is a feasibility study, such a rough estimate can be made. Also this approximation gives some idea of the frequency content of the system output - but only for the damped sine wave frequency. The Z - Controller

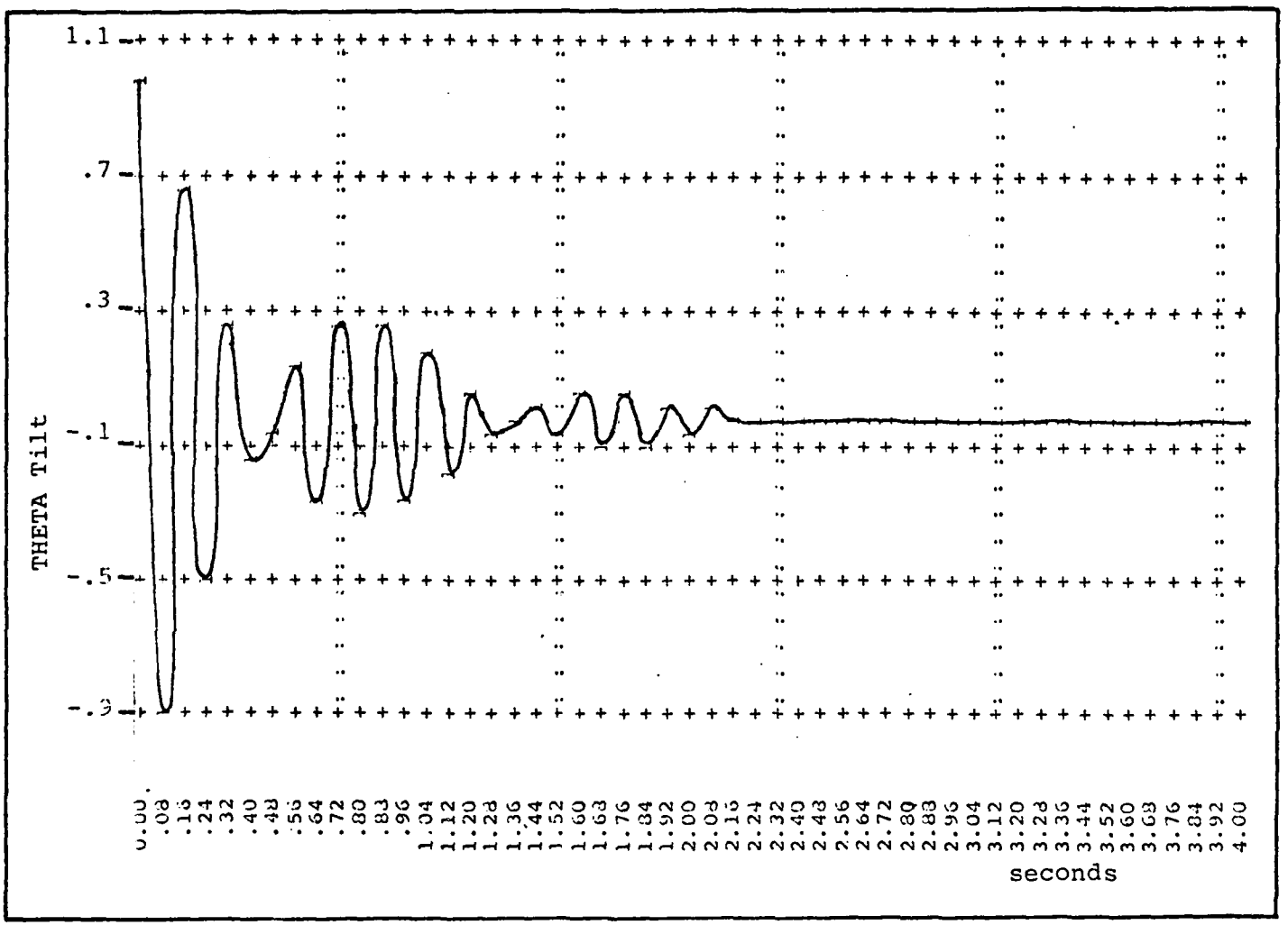

Figure 5.34 THETA - Controller (Second Stage Isolation)

VI. Conclusions and Recommendations

Conclusions

Analytically, the pneumatic isolators in a dual isolator stage configuration have severe phase and gain margin limitations which can be seen in any one of the six degrees of freedom - in either the appropriate Bode plots, root locus plots or Nichols plots. A single level of pneumatic isolation avoids the minimum phase and gain margin characteristics but sacrifices the much needed passive transmissibility attenuation to acceleration and tilt disturbances. The lightly damped response of the pneumatic isolator yields high resonant magnitude peaks well within the SSP operation of bandwidth and produces corresponding slow time responses.

The actuator energy requirements are very substantial because of the large SSP mass and moment of inertia scaling factors present in all controller designs evidenced by weak controllability.

Observability is a major control issue. The translation control loop output is an acceleration which is a combination of system states making observability difficult. Rotational controllers have a tilt output that is a distinct system state, but the rotation and the translation controllers both cannot observe the lower level states at all. No lower level outputs are taken for the LQ-PI control law because in the actual controller implementation no instrumentation is provided for state estimation.

The rotational performance could be reviewed, since the specification is a displacement constraint not a power spectral density. The SISO controllers did provide design solutions within the ±0.02 tilt specification, but not realistic in light of the truth model. Also all the SISO controller B inputs had to be scaled indicating weak controllability. The Theta - SSP Isolation Controller - MIMO met the tilt specification with the B matrix unscaled, again the truth model simulation deteriorated the performance. Observability is a problem for the lower level states. The tilt output is a system state which improved stability as opposed to the translation acceleration output which are system state combinations.

One important CGTPIF application note did result. In cases where B is scaled to one, almost no tolerance is given to increasing the output cost which causes outputs to go unstable and grow with time. Since this is a basic feasibility study, no further efforts are made to delineate the CGTPIF solution instabilities due to SSP dynamics (observability and controllability) or CGTPIF numerical difficulties, or combinations of both. A quick review of Appendix K shows a wide dynamic numerical range.

As a precaution, the digital controlled sample frequency is increased to 2 KHz with no performance improvement noted in the discrete time step responses or controller stabilities. No tabulation or plots of this simulation are made.

The SSP theoretical models should be taken seriously since they accurately predict vertical acceleration resonant frequencies and account for the observed "second order responses" resulting from a combination of high resonant magnitudes and second order attenuations discussed in Chapter IV.

Recommendations

1. Further SSP active controller efforts should either verify this study's dynamics or develop new dynamic models that can be verified by site measurement. Only when such a dynamics model exists should a careful digital controller be designed, simulated and verified.

2. Further SSP measurements could verify or disprove the rotational dynamics. Cross correlation between rotational and translational measurements would identify the magnitude of cross coupling modes.

3. More elaborate active controllers could be studied as discussed in Reference 16, using this study's dynamics model as a starting point.

4. Engineers could accept the passive response and estimate and predict axis accelerations and tilts, compensating the test inertial instrument evaluation profiles based on proven parameter estimation schemes (Ref 12).

5. CIGTF could reconsider the passive response offered by the underground test facilities in abandoned mines. Such

a natural isolation system would not have the lightly damped, high resonant peaks that pneumatic isolators do exhibit. Soil dynamics have higher damping ratios and could be augmented with a second stage fluid isolation system, similar to those techniques used in mechanical gyroscopes.

6. Future seismic isolation systems could consider single level pneumatic and/or fluid isolation. Single level pneumatic isolation would avoid phase and gain margin constraints and instabilities of dual pneumatic isolation. Fluid isolation would exhibit a better time response by avoiding lightly damped dynamics.

Bibliography

1. Alexander, Dick. Develop a Formulation for a Control Loop for Seismically Stable Platform. Thesis Topic. Holloman AFB, New Mexico: Central Inertial Guidance Test Facility (CIGTF), 6585th Test Group (GDLC).

2. Barry Controls. Serva-Levl Isolation System Operation and Maintenance Manual for "AL" or "X-15" Isolator. Report #DSW 247. Burbank, California, March 1978.

3. Broderson, Emil. Stabilization of a Seismic Isolation Block Inertial Instrument Test. MS Thesis. Colorado Springs, Colorado: Frank J. Seiler Research Lab, US Air Force Academy, 1974. (AD-786057)

4. Brunson, Richard L. An Optimal State Estimator for the FJSRL Instrument Test Platform. MS Thesis. Wright-Patterson AFB, Ohio: Air Force Institute of Technology, March 1976. (A023173)

5. Burkhart, Martin J. A Digital Controller for Horizontal Angular Motion of the FJSRL Seismic Isolation Platform. MS Thesis. Wright-Patterson AFB, Ohio: Air Force Institute of Technology, June 1976. (A027433)

6. D'Azzo, John J. and Constantine H. Houpis. Linear Control System Analysis Conventional and Modern. New York: McGraw-Hill Book Company, 1975.

7. Floyd, Richard. Design of Advanced Digital Flight Control Systems via Command Generator Tracker (CGT) Synthesis Methods. MS Thesis. Wright-Patterson AFB, Ohio: Air Force Institute of Technology, December 1981.

8. Holcomb, L. Gary. "The Lower Limits of Seismic Background Noise Levels," Proceedings of AIAA Guidance and Control Conference. Albuquerque, New Mexico: American Institute of Aeronautics and Astronautics, 20 August 1981.

9. Larimer, Stanley J. TOTAL User's Manual. Wright-Patterson AFB, Ohio: Air Force Institute of Technology, March 1978.

10. Likins, Peter W. Elements of Engineering Mechanics. New York, McGraw-Hill Book Company, 1973.

11. Lowrie, L.M. and T.H. Pearce. Seismic Measurements at Holloman Track. Holloman AFB Report. Washington DC: US Department of Commerce, Coast and Geodetic Survey, June 1963.

12. Maybeck, Peter S. Stochastic Models, Estimation, and Control, Volume 2 (tentative title), unpublished text. Air Force Institute of Technology, Wright-Patterson Air Force Base, Ohio.

13. McClendon, James R. MIMO-Multiple Input Multiple Output User's Manual. Wright-Patterson Air Force Base, Ohio: Air Force Institute of Technology, School of Engineering, August 1979.

14. Measurement Analysis Corporation. Design and Analysis of a Seismically Stable Platform. Report # TR7015.003. Prepared for US Air Force Systems Command, 6585th Test Group, Holloman AFB, New Mexico. Torrance, California June 25, 1980.

15. Paola, R.D., C. R. Kochakian and K. Tsulsume. Geokinetic Considerations for Advanced Testing of Gyros and Accelerometers - Part A. Hardware and Instrumentation. Report # 75-1066. AIAA Guidance and Control Conference, Boston, Massachusetts: August 20-22, 1975.

16. Porter, B. Distributed Multivariable Digital Control. Report USAME/DC 1101/81. Lancashire, England: University of Salford, 1981.

17. Ruzicka and Derby. SVM-7 Influence of Damping in Vibration Isolation. Washington, DC: Shock and Vibration Information Center, Monograph Series, Naval Research Lab.

18. Schelonka, L.P. Central Inertial Guidance Test Facility, 6585th Test Group (telephone conversation). Holloman Air Force Base, New Mexico, 11 September 1981.

19. Simmons, B.J., Research Associate, FJSRL, USAF Academy (personal correspondence) Subject: SSP Tests on 24-25 August 1981. Colorado Springs, Colorado, September 9, 1981.

20. Simmons, B.J., R.M. Hanes and F.S. Heming. "Dynamic Analysis of Test Platform," Proceedings of AIAA Guidance and Control Conference. Report # AIAA-81-1816. Albuquerque, New Mexico: American Institute of Aeronautics and Astronautics, August 20, 1981.

21. Simmons, B.J. Seismic Motion Stability, Measurement and Precision Control - Final Report. Report # SRL-TR-79-0015. Colorado Springs, Colorado: US Air Force Academy, December 1979.

22. SRL-TR-76-0014. Multi-Sensor Measurement of the Motion Stability of an Active Control Isolation Test Pad. Washington, DC: Air Force Systems Command, July 1976.

23. Toler, Phillip J. Analysis and Implementation of Optimal Estimation and Control for the FJSRL Seismic Isolation Platform. MS Thesis. Wright-Patterson AFB, Ohio: Air Force Institute of Technology, School of Engineering, December 1978. (A064179)

24. Whitesell, W.J. and T.R. Hooten. "Progress and Plans for the Development of a Precision Guidance Test Facility," CIGTF Symposium, Holloman AFB, New Mexico: October 1979.

Appendix A SSP Physical Dimensions

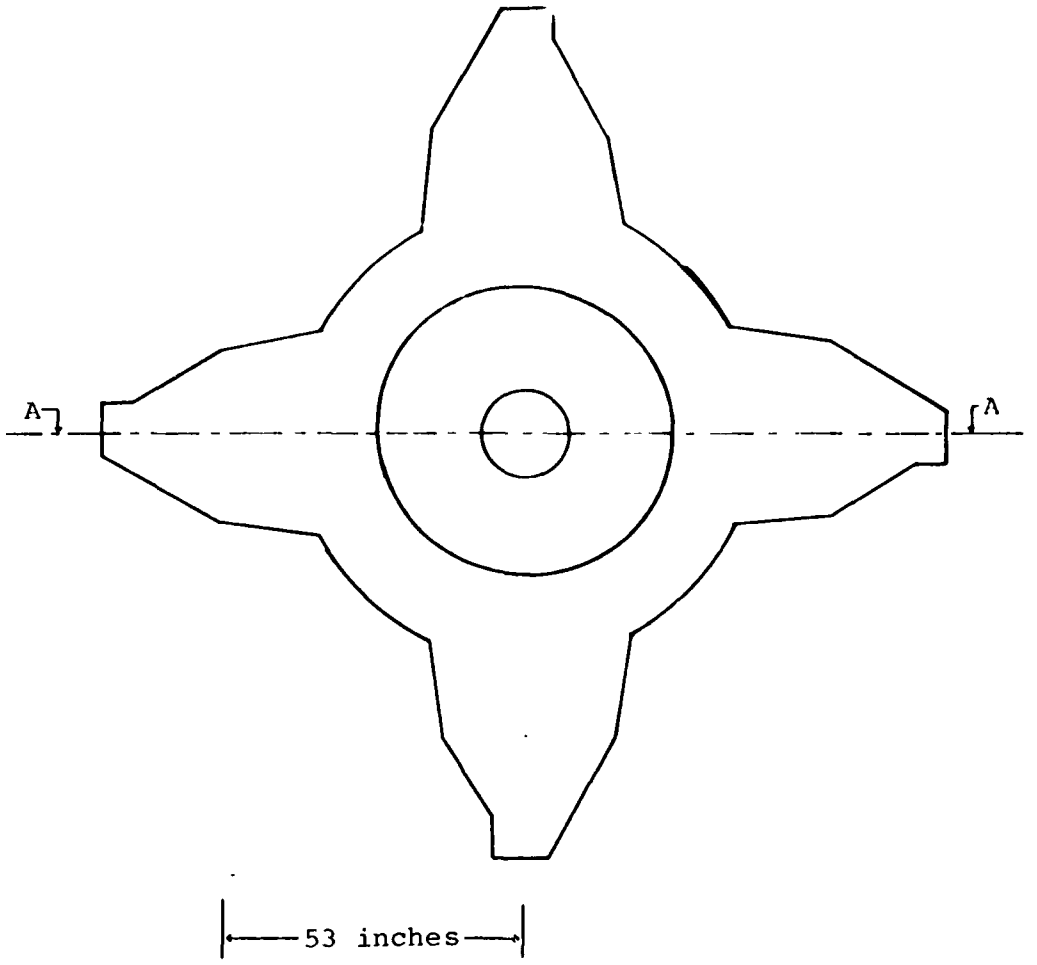

Section A-A

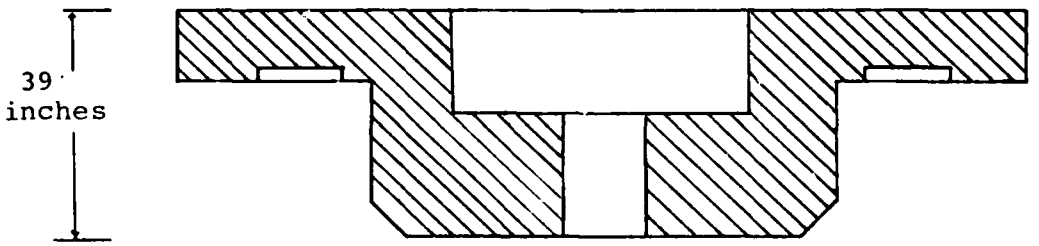

Drawn to 30th scale.

Figure A.1 Upper Level

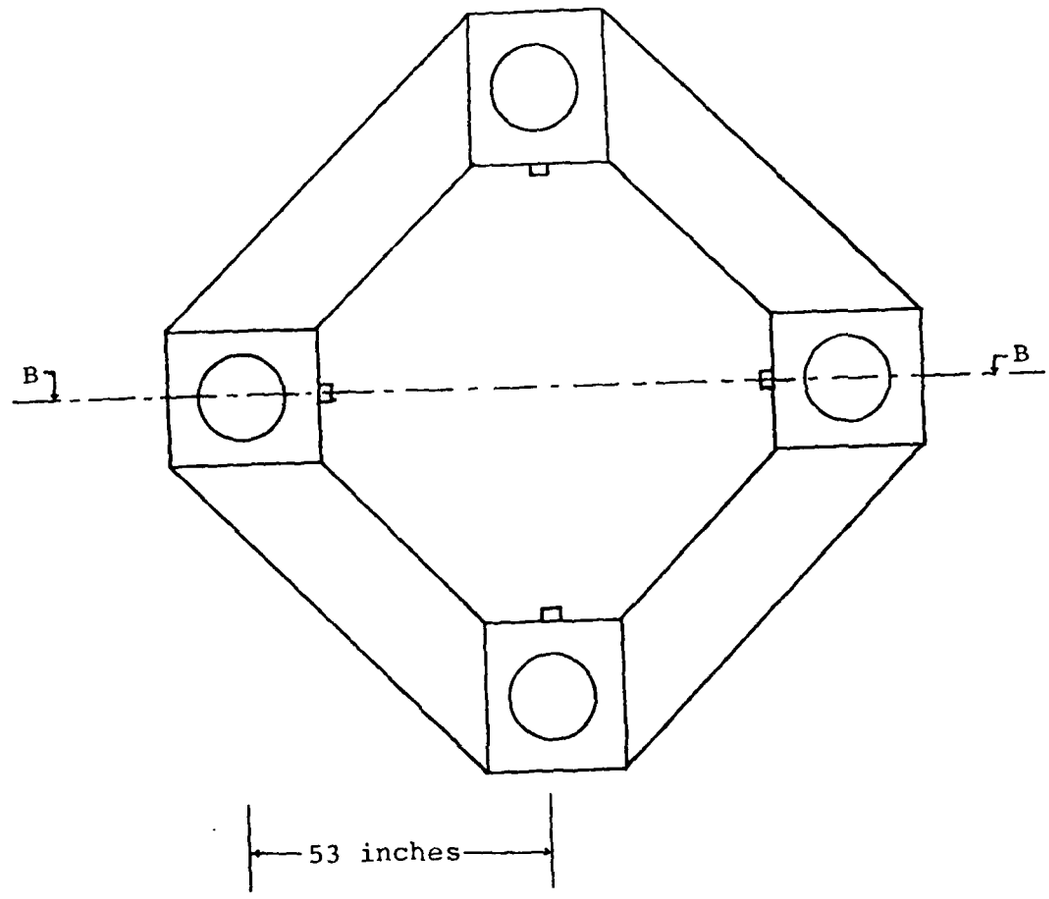

Section B-B

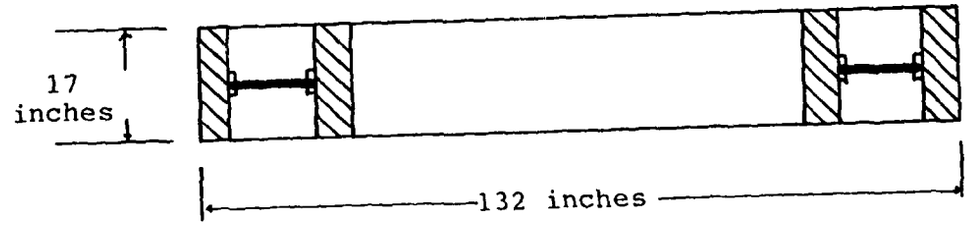

Drawn to 30th scale.

Figure A.2 Lower Level

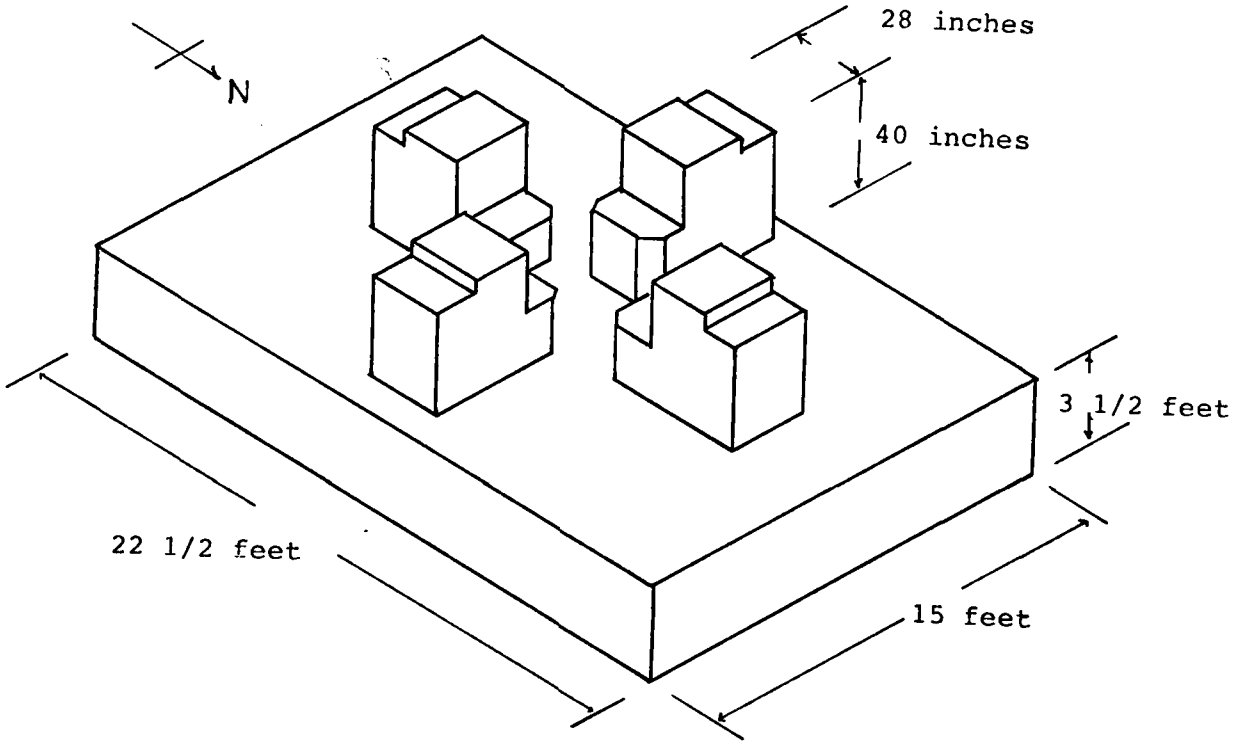

Dimensions as shown.

Figure A.3 Pier and Seismic Block

Appendix B CSDL Specification Calculations and Conversions

Item 1, CSDL specification, conversion from meru's to arcseconds/second.

$$10^{-5}\text{meru} = \frac{10^{-5}\text{meru}\ (0.015\ \text{arcsecond/second}}{\text{meru}}$$

$$= 1.5 \times 10^{-7}\ \text{arcseconds/second}$$

Item 2, an error of one arcsecond on the Earth's surface is approximately 100 feet. For an hour, the one arcsecond error corresponds to the following average velocities and acceleration (expressed in g's).

$V_{av} = 100$ feet/hour — V_{av}, average velocity

$$A_{av} = \frac{V_{av}}{\text{hour}} = \frac{100\ \text{feet}}{(\text{hour})^2}$$ — 1 hour = 3600 seconds

$$= \frac{100\ \text{feet}}{(3600\ \text{seconds})^2}$$ — g, gravity units, 32.2 feet/second^2

$$= \frac{100\ \text{feet}}{(3600)^2\ \text{seconds}^2\ \frac{32.2\ \text{feet}}{\text{second}^2}}$$

$\approx 10^{-7}$g's

The SSP must meet 10^{-8}g's, to be ten times better than the measurement environment. TGG instruments are

expected to be ten times more accurate than present instruments, thus 10^{-9}g's.

Item 3, measurement bandwidth is derived as follows:

$$f = \frac{1}{T} \qquad \text{where T, period (seconds)}$$

f, frequency (Hz)

$$f = \frac{1}{100 \text{ sec}} = 10^{-2}\text{Hz}$$

for a one hundred twenty day period:

$$f = \frac{1}{(120 \text{ days})(24 \text{ hours/day})(60\text{min/day})(60\text{sec/min})}$$

$$= 9.64 \times 10^{-8}\text{Hz}$$

$$\approx 10^{-8}\text{Hz}$$

Appendix C. Direction Cosine Matrix Transformation

Angular rotation for the SSP are taken in the order ψ_U , ϕ_U and Θ_U for the upper level about the $\hat{e}_1$, $\hat{e}_2$, and $\hat{e}_3$ axis respectively. Θ_U corresponds to an azimuth angle and ϕ_U and ψ_U are tilt angles available possibly from tiltmeters.

$$\begin{bmatrix} \hat{a}_1 \\ \hat{a}_2 \\ \hat{a}_3 \end{bmatrix} = \begin{bmatrix} \cos\Theta_U & \sin\Theta_U & 0 \\ -\sin\Theta_U & \cos\Theta_U & 0 \\ 0 & 0 & 1 \end{bmatrix} \begin{bmatrix} \hat{e}_1 \\ \hat{e}_2 \\ \hat{e}_3 \end{bmatrix} \qquad \text{(C-1)}$$

$$\underline{a} = C^{ae}(\Theta_U)\underline{e} \qquad \text{(C-2)}$$

$$\bar{\omega}^{ae} = \dot{\Theta}_U \hat{a}_3 = \dot{\Theta}_U \hat{e}_3 \qquad \text{(C-3)}$$

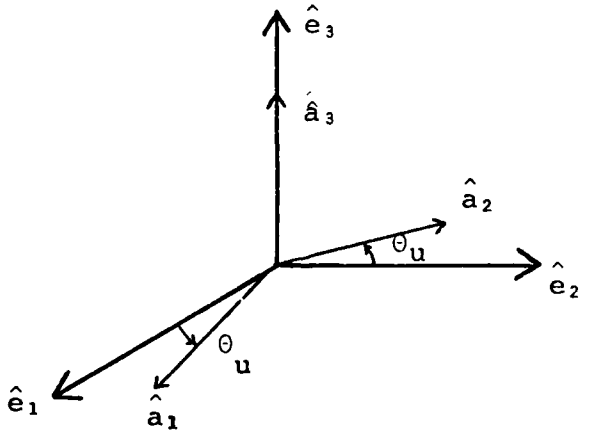

Θ Rotation about $\hat{e}_3$

$$\begin{bmatrix} \hat{b}_1 \\ \hat{b}_2 \\ \hat{b}_3 \end{bmatrix} = \begin{bmatrix} \cos\phi_U & 0 & -\sin\phi_U \\ 0 & 1 & 0 \\ \sin\phi_U & 0 & \cos\phi_U \end{bmatrix} \begin{bmatrix} \hat{a}_1 \\ \hat{a}_2 \\ \hat{a}_3 \end{bmatrix} \qquad \text{(C-4)}$$

$$\underline{b} = C^{ba}(\phi_U)\underline{a} \qquad \text{(C-5)}$$

$$\underline{\omega}^{ba} = \dot{\phi}_U \hat{a}_2 = \dot{\phi}_U \hat{b}_2 \qquad \text{(C-6)}$$

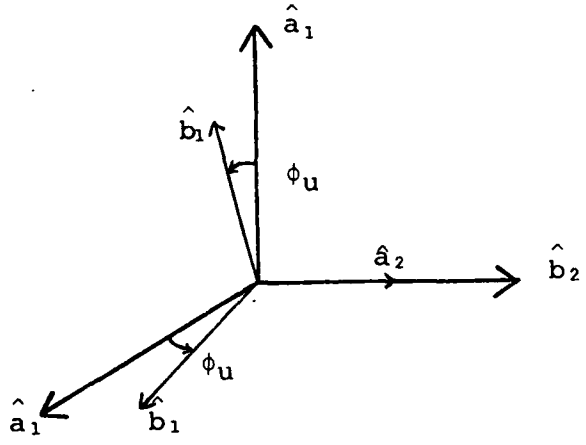

ϕ Rotation about $\hat{a}_2$

$$\begin{bmatrix} \hat{u}_1 \\ \hat{u}_2 \\ \hat{u}_3 \end{bmatrix} = \begin{bmatrix} 1 & 0 & 0 \\ 0 & \cos\psi_U & \sin\psi_U \\ 0 & -\sin\psi_U & \cos\psi_U \end{bmatrix} \begin{bmatrix} \hat{b}_1 \\ \hat{b}_2 \\ \hat{b}_3 \end{bmatrix} \qquad \text{(C-7)}$$

$$\bar{\omega}^{ub} = \dot{\psi}_U \hat{b}_1 = \dot{\psi}_U \hat{u}_1 \qquad \text{(C-8)}$$

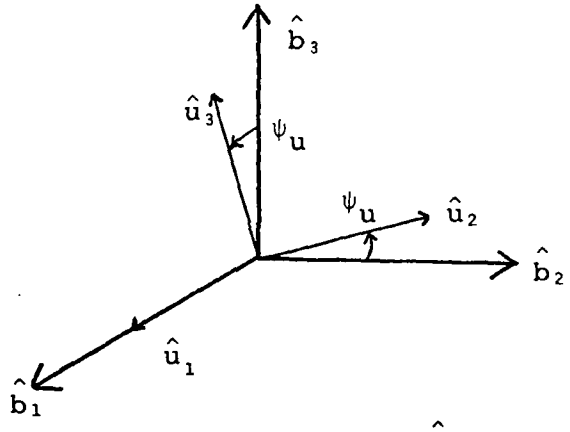

ψ Rotation about $\hat{b}_1$

Using the individual direction cosine matrices, a transformation from $\underline{e}$ to $\underline{u}$ is obtained using intintesimal rotations where

$$\sin\Theta \approx \Theta$$

$$\cos\Theta \approx 1$$

and any angular products (for example $(\psi_U \Theta_U)$) equal to zero. Since the SSP motion is considered for perturbed small angular

excursions about a nominal position and first order approximations; these approximations are justified.

$$\underline{u} = C^{ub}(\psi_U)\ C^{ba}(\phi_U)\ C^{ae}(\Theta_U)\underline{e} \tag{C-9}$$

$$\underline{u} = \begin{bmatrix} 1 & 1 & 0 \\ 0 & 1 & \psi_U \\ 0 & -\psi_U & 1 \end{bmatrix} \begin{bmatrix} 1 & 0 & -\phi_U \\ 0 & 1 & 0 \\ \phi_U & 0 & 1 \end{bmatrix} \begin{bmatrix} 1 & \Theta_U & 0 \\ -\Theta_U & 1 & 0 \\ 0 & 0 & 1 \end{bmatrix} \underline{e} \tag{C-10}$$

$$\underline{u} = \begin{bmatrix} 1 & \Theta_U & -\phi_U \\ -\Theta_U & 1 & \psi_U \\ \phi_U & -\psi_U & 1 \end{bmatrix} \underline{e} \tag{C-11}$$

Transformation matrices for the lower level (L) and pier (P) are derived similarly, and are

$$\underline{l} = \begin{bmatrix} 1 & \Theta_L & -\phi_L \\ -\Theta_L & 1 & \psi_L \\ \phi_L & -\psi_L & 1 \end{bmatrix} \underline{e} \tag{C-12}$$

$$\underline{p} = \begin{bmatrix} 1 & \Theta_P & -\phi_P \\ -\Theta_P & 1 & \psi_P \\ \phi_P & -\psi_P & 1 \end{bmatrix} \quad \underline{e} \qquad \text{(C-13)}$$

$$\bar{\omega}^{ue} = \bar{\omega}^{ub} + \bar{\omega}^{ba} + \bar{\omega}^{ae}$$

$$= \dot{\psi}_U \hat{u}_1 + \dot{\phi}_U \hat{b}_2 + \dot{\Theta}_U \hat{a}_3 \qquad \text{(C-14)}$$

Using appropriate direction cosine matrix $\bar{\omega}^{ue}$ in the upper level unit vectors ($\underline{u}$) are,

$$\bar{\omega}^{ue} = \dot{\psi}_U \hat{u}_1 + \dot{\phi}_U(\cos\psi_U \hat{u}_2 - \sin\psi_U \hat{u}_3)$$
$$+ \dot{\Theta}_U(-\sin\phi_U \hat{u}_1 + \cos\phi_U(\sin\psi_U \hat{u}_2 + \cos\psi_U \hat{u}_3)) \qquad \text{(C-15)}$$

With small angle approximations and first order terms retained,

$$\bar{\omega}^{ue} = \dot{\psi}_U \hat{u}_1 + \dot{\phi}_U \hat{u}_2 + \dot{\Theta}_U \hat{u}_3 \qquad \text{(C-16)}$$

Physically this means angular accelerations will not couple into each other under perturbed assumptions about a nominal position.

Expressions for the lower level and pier angular accelerations follow the same derivation and approximations.

$$\bar{\omega}^{le} = \dot{\psi}_L \hat{l}_1 + \dot{\phi}_L \hat{l}_2 + \dot{\theta}_L \hat{l}_3 \qquad \text{(C-17)}$$

$$\bar{\omega}^{pe} = \dot{\psi}_P \hat{p}_1 + \dot{\phi}_P \hat{p}_2 + \dot{\theta}_P \hat{p}_3 \qquad \text{(C-18)}$$

Appendix D. Perturbation of a Body Center

To understand translational and rotational motions of the SSP, an upper level corner (or suspension point) in the u_1 or easterly (E) orientation is analyzed. A nominal position is defined as when the $\underline{u}$ and $\underline{e}$ unit vectors coincide with $\overline{UE}_o$ and $\overline{U}_o$ the nominal corner and center of mass locations respectively. A translational and rotational perturbation moves the $\underline{U}$ frame to the orientation shown below.

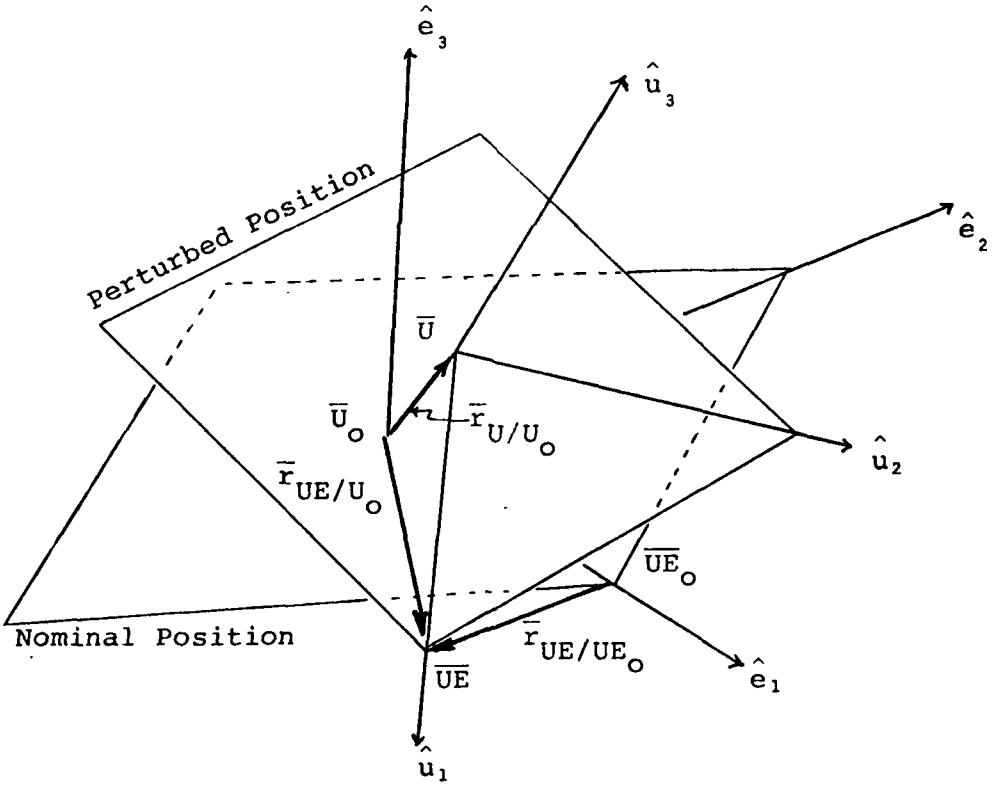

Figure D.1, Perturbation of a Corner

The following vectors and points are defined for the Figure D.1.

Points -

$\bar{U}_o = x_{U_o}\hat{e}_1 + y_{U_o}\hat{e}_2 + z_{U_o}\hat{e}_3$ - nominal center of mass position for upper level

$\bar{U} = x_U\hat{e}_1 + y_U\hat{e}_2 + z_U\hat{e}_3$ - perturbed center of mass position for upper level

$\overline{UE}_o = x_{UE_o}\hat{e}_1 + y_{UE_o}\hat{e}_2 + z_{UE_o}\hat{e}_3$ - nominal upper level corner position (easterly)

$\overline{UE} = x_{UE}\hat{e}_1 + y_{UE}\hat{e}_2 + z_{UE}\hat{e}_3$ - perturbed upper level corner position (easterly)

Vectors -

$\bar{r}_{U/U_o}$ - position vector for new position of center of mass with respect to nominal center of mass position.

$\bar{r}_{UE/U_o}$ - position vector new corner displacement with respect to nominal center of mass.

$\bar{r}_{UE/UE_o}$ - position vector describing new corner position with respect to nominal center position.

$\bar{r}_{UE/U}$, $\bar{r}_{UE/U_o}$ - position vector locating corner from center of mass in either the perturbed or nominal orientation, respectively. Both are equal and constant for an assumed solid body structure.

l_{UE} - distance an upper level (U), easterly (E) corner is from center of mass. Corner is assumed in same vertical plane as center of mass. $l_{UE}\hat{e}_1$, or $l_{UE}\hat{u}_1$

Since the new corner describes the needed motion expressions, two vector equivalences of $\bar{r}_{UE/U_o}$ are written below.

$$\bar{r}_{UE/U_o} = \bar{r}_{UE_o/U_o} + \bar{r}_{UE/UE_o} \quad \text{(D-1)}$$

$$= l_{UE}\hat{e}_1 + x_{UE}\hat{e}_1 + y_{UE}\hat{e}_2 + z_{UE}\hat{e}_3 \quad \text{(D-2)}$$

$$\bar{r}_{UE/U_o} = \bar{r}_{U/U_o} + \bar{r}_{UE/U} \quad \text{(D-3)}$$

$$= x_U\hat{e}_1 + y_U\hat{e}_2 + z_U\hat{e}_3 + l_{UE}\hat{u}_1 \quad \text{(D-4)}$$

Using Eq (C-11), Appendix C,

$$\underline{u} = \begin{bmatrix} 1 & \Theta_U & -\phi_U \\ -\Theta_U & 1 & \psi_U \\ \phi_U & -\psi_U & 1 \end{bmatrix} \quad e \quad \text{(C-11)}$$

Eq (D-4) becomes

$$\bar{r}_{UE/U_O} = x_U\hat{e}_1 + y_U\hat{e}_2 + z_U\hat{e}_3 + l_{UE}(\hat{e}_1 + \theta_U\hat{e}_2 - \phi_U\hat{e}_3) \quad (D-5)$$

$$= (x_U + l_{UE})\hat{e}_1 + (y_U + l_{UE}\theta_U)\hat{e}_2 + (z_U - l_{UE}\phi_U)\hat{e}_3 \quad (D-6)$$

Eq (D-2) is the measurements an inertial instrument might make where Eq (D-6) relates the translational and rotational states. Equating the two equations by component relates measurements and states.

$$x_{UE} = x_U \quad (D-7)$$

$$y_{UE} = y_U + l_{UE}\theta_U \quad (D-8)$$

$$z_{UE} = z_U - l_{UE}\phi_U \quad (D-9)$$

For notation reduction $\overline{UE}$ replaces $\bar{r}_{UE/UO}$. The vector $\overline{UE}$ is now differentiated with respect to time in the Earth frame.

$$\overline{UE} = (x_U + l_{UE})\hat{e}_1 + (y_U + l_{UE}\theta_U)\hat{e}_2 + (z_U - l_{UE}\phi_U)\hat{e}_3 \quad (D-6)$$

$$\dot{\overline{UE}} = \dot{x}_U\hat{e}_1 + (\dot{y}_U + l_{UE}\dot{\theta}_U)\hat{e}_2 + (\dot{z}_U - l_{UE}\dot{\phi}_U)\hat{e}_3 \quad (D-10)$$

Defining corner perturbation vectors $\overline{UN}$, $\overline{UW}$ and $\overline{US}$ for the north, west and south upper level corners respectively, position and velocity vectors are derived and differentiated as was done for $\overline{UE}$ and $\overset{\circ}{\overline{UE}}$.

$$\overline{UN} = (x_U - l_{UN}\theta_U)\hat{e}_1 + (y_U + l_{UN})\hat{e}_2 + (z_U + l_{UN}\psi_U)\hat{e}_3 \quad \text{(D-11)}$$

$$\overset{\circ}{\overline{UN}} = (\overset{\circ}{x}_U - l_{UN}\overset{\circ}{\theta}_U)\hat{e}_1 + \overset{\circ}{y}_U\hat{e}_2 + (\overset{\circ}{z}_U + l_{UN}\overset{\circ}{\phi}_U)\hat{e}_3 \quad \text{(D-12)}$$

$$\overline{UW} = (x_U - l_{UW})\hat{e}_1 + (y_U - l_{UW}\theta_U)\hat{e}_2 + (z_U + l_{UW}\phi_U)\hat{e}_3 \quad \text{(D-13)}$$

$$\overset{\circ}{\overline{UW}} = \overset{\circ}{x}_U\hat{e}_1 + (\overset{\circ}{y}_U - l_{UW}\overset{\circ}{\theta}_U)\hat{e}_2 + (\overset{\circ}{z}_U + l_{UW}\overset{\circ}{\phi}_U)\hat{e}_3 \quad \text{(D-14)}$$

$$\overline{US} = (x_U + l_{US}\theta_U)\hat{e}_1 + (y_U - l_{US})\hat{e}_2 + (z_U - l_{US}\psi_U)\hat{e}_3 \quad \text{(D-15)}$$

$$\overset{\circ}{\overline{US}} = (\overset{\circ}{x}_U + l_{US}\overset{\circ}{\theta}_U)\hat{e}_1 + \overset{\circ}{y}_U\hat{e}_2 + (\overset{\circ}{z}_U - l_{US}\overset{\circ}{\psi}_U)\hat{e}_3 \quad \text{(D-16)}$$

These corner vector and their derivatives are used in deriving the equations of motion for the SSP upper level. The lower level and pier subsystems are described by similar equations with the U subscript replaced by L and P respectively. The coupling of translation and rotation motions is apparent from the $\overline{UE}$, $\overline{UN}$, $\overline{UW}$ and $\overline{US}$ expressions.

Appendix E. SSP Lumped Spring and Damper Constants

The second order approximations developed in Eqs 3-7 and 3-10 are used to derive the spring and damper coefficients for the Z and X (also Y) directions. References are cited indicating information source in MAC SSP report (Ref 14).

Second Stage Isolation

f_{VN} = 1.8 Hz, vertical natural frequency (Ref 14:C-53)

m_U = 530.22 lb-sec^2-Ft, upper mass (Ref 14:E-33)

k_{SZ} = 16955.12 lb/ft

c_{SZ} = 89.95 lb-sec/ft

f_{HN} = 4.0 Hz, horizontal natural frequency (Ref 14:C-53)

$k_{SX} = k_{SY}$ = 83728.99 lb/ft

$c_{SX} = c_{SY}$ = 199.89 lb-sec/ft

Load for each isolator is considered as one-fourth the upper level. Damping coefficient was 0.03 for vertical and horizontal directions (Ref14:C-10).

First Stage Isolation

f_{VN} = 1.8 Hz, vertical natural frequency (Ref 14:C-53)

Load = $m_U + m_L$ = 823.85 lb-sec^2-ft (Ref 14:E-106)

k_{FZ} = 26344.68 lb/ft

which exceeds vertical stiffness specification of 16920 lb/ft (1410 lb/in)

c_{FZ} = 139.76 lb-sec/ft

f_{HN} = 3.8 Hz, horizontal natural frequency

$k_{FX} = k_{FY}$ = 117,412.70 lb/ft

which exceeds horizontal specification of 75,360 lb/ft (6280 lb/in) (Ref 14:K-27)

$c_{FX} = c_{FY}$ = 295.05 lb-sec/ft

Load for each isolator is considered as one-fourth the combined mass of upper and lower levels. Damping coefficient was 0.03 for vertical and horizontal directions (Ref 14:C-10).

SSP Moments of Inertia

The moments of inertia are listed below, (Ref 14:D-19)

for m_U

$$I_{UZ} = 5095.8 \text{ ft-lb-sec}^2$$

$$I_{UX} = I_{UY} = 2340 \text{ ft-lb/sec}^2$$

for m_L

$$I_{LZ} = 2547.7 \text{ ft-lb-sec}^2$$

$$I_{LX} = I_{LY} = 1169.8 \text{ ft-lb/sec}^2$$

Pier Lumped Parameters

All parameters are simply taken from MAC study, (Ref 14:F-26), using damping coefficients resulting from soil analysis (Reichert Model).

$$k_{GZ} = 1.2 \times 10^8 \text{ lb/ft}$$

$$c_{GZ} = 9.34 \times 10^5 \text{ lb-sec/ft}$$

$$k_{GX} = k_{GY} = 1.08 \times 10^8 \text{ lb/ft}$$

$$c_{GX} = c_{GY} = 5.41 \times 10^5 \text{ lb-sec/ft}$$

These parameters represent the combined spring, damper dynamics in a given direction for the total load of seismic pier and the SSP. In terms of SSP Lumped Parameters model the K and C values must be divided by four or

$$k_{GZ} = k_Z/4 = 3.00 \times 10^7 \text{ lb/ft}$$

$$c_{GZ} = c_Z/4 = 2.34 \times 10^5 \text{ lb-sec/ft}$$

$$k_{GX} = k_{GY} = k_X/4 = 2.70 \times 10^7 \text{ lb/ft}$$

$$c_{GX} = c_{GY} = c_Y/4 = 1.35 \times 10^5 \text{ lb/ft}$$

Pier Moments of Inertia

The pier moments of inertia are calculated considering the seismic mass as a homogeneous rectangular concrete block of mass 5403.73 lb-sec^2-ft (Ref 14:F-26), standard moment of inertia formulas (Ref 10:525). Dimensions of seismic block are taken from Appendix B.

$$I_{PY} = 107{,}925.50 \text{ lb-ft-sec}^2$$

$$I_{PX} = 234{,}575.42 \text{ lb-ft-sec}^2$$

$$I_{PY} = 329{,}289.80 \text{ lb-ft-sec}^2$$

I_{PX} is used in all transmissibility calculations since a higher value of moment of inertia represents a lower natural frequency and greater concern to controller development. I_{PY} would concern frequencies outside the active controller bandwidth, approximately a horizontal natural frequency of 30 Hz.

Appendix F. SSP Three Degree of Freedom - Translation

Eqs 3-21, 3-22, and 3-23 result from Newton's Second Law, $\bar{F} = m\bar{a}$. This appendix reduces their vector differential equations using Eqs D-6, D-10, D-11 thru D-16 for the upper level, lower level and pier displacements and velocities in the force equations for the e frame.

First, the vector terms and common coefficients are made in Eqs 3-9, 3-10, and 3-11.

$$m_U \ddot{\bar{U}} = -[C_S] \begin{bmatrix} \dot{\overline{UE}} \\ \dot{\overline{UN}} \\ \dot{\overline{UW}} \\ \dot{\overline{US}} \end{bmatrix} - [K_S] \begin{bmatrix} \overline{UE} \\ \overline{UN} \\ \overline{UW} \\ \overline{US} \end{bmatrix}$$

$$+[C_S] \begin{bmatrix} \dot{\overline{LE}} \\ \dot{\overline{LN}} \\ \dot{\overline{LW}} \\ \dot{\overline{LS}} \end{bmatrix} + [K_S] \begin{bmatrix} \overline{LE} \\ \overline{LN} \\ \overline{LW} \\ \overline{LS} \end{bmatrix}$$

$$+ \bar{F}_{UE} + \bar{F}_{UN} + \bar{F}_{UW} + \bar{F}_{US} \qquad \text{(F-1)}$$

$$
m_L \ddot{\overline{L}} = -[C_P + C_S] \begin{bmatrix} \dot{\overline{LE}} \\ \dot{\overline{LN}} \\ \dot{\overline{LW}} \\ \dot{\overline{LS}} \end{bmatrix} - [K_P + K_S] \begin{bmatrix} \overline{LE} \\ \overline{LN} \\ \overline{LW} \\ \overline{LS} \end{bmatrix}
$$

$$
+ [C_F] \begin{bmatrix} \dot{\overline{PE}} \\ \dot{\overline{PN}} \\ \dot{\overline{PW}} \\ \dot{\overline{PS}} \end{bmatrix} + [K_F] \begin{bmatrix} \overline{PE} \\ \overline{PN} \\ \overline{PW} \\ \overline{PS} \end{bmatrix}
$$

$$
+ [C_S] \begin{bmatrix} \dot{\overline{UE}} \\ \dot{\overline{UN}} \\ \dot{\overline{UW}} \\ \dot{\overline{US}} \end{bmatrix} + [K_S] \begin{bmatrix} \overline{UE} \\ \overline{UN} \\ \overline{UW} \\ \overline{US} \end{bmatrix}
$$

(F-2)

$$
m_P \ddot{\overline{P}} = -[C_G + C_F] \begin{bmatrix} \dot{\overline{PE}} \\ \dot{\overline{PN}} \\ \dot{\overline{PW}} \\ \dot{\overline{PS}} \end{bmatrix} - [K_G + K_F] \begin{bmatrix} \overline{PE} \\ \overline{PN} \\ \overline{PW} \\ \overline{PS} \end{bmatrix}
$$

$$
+ [C_G] \begin{bmatrix} \dot{\overline{GE}} \\ \dot{\overline{GN}} \\ \dot{\overline{GW}} \\ \dot{\overline{GS}} \end{bmatrix} + [K_G] \begin{bmatrix} \overline{GE} \\ \overline{GN} \\ \overline{GW} \\ \overline{GS} \end{bmatrix}
$$

$$+ \quad [C_F] \begin{bmatrix} \dot{\overline{LE}} \\ \dot{\overline{LN}} \\ \dot{\overline{LW}} \\ \dot{\overline{LS}} \end{bmatrix} - [K_F] \begin{bmatrix} \overline{LE} \\ \overline{LN} \\ \overline{LW} \\ \overline{LS} \end{bmatrix}$$

$$- \overline{F}_{PE} - \overline{F}_{PN} - \overline{F}_{PW} - \overline{F}_{PS} \qquad \text{(F-3)}$$

Eq F-1 expanded using transformation from Appendix E.

$$m_U \begin{bmatrix} \ddot{x}_U \\ \ddot{y}_U \\ \ddot{z}_U \end{bmatrix} = - \begin{bmatrix} \dot{x}_U & (\dot{y}_U + l_{UE}\dot{\theta}_U) & (\dot{z}_U - l_{UE}\dot{\phi}_U) \\ (\dot{x}_U - l_{UN}\dot{\theta}_U) & \dot{y}_U & (\dot{z}_U + l_{UN}\dot{\psi}_U) \\ \dot{x}_U & (\dot{y}_U - l_{UW}\dot{\theta}_U) & (\dot{z}_U + l_{UW}\dot{\phi}_U) \\ (\dot{x}_U + l_{US}\dot{\theta}_U) & \dot{y}_U & (\dot{z}_U - l_{US}\dot{\psi}_U) \end{bmatrix} \begin{bmatrix} c_{SX} \\ c_{SY} \\ c_{SZ} \end{bmatrix}$$

$$- \begin{bmatrix} (x_U + l_{UE}) & (y_U + l_{UE}\theta_U) & (z_U - l_{UE}\phi_U) \\ (x_U - l_{UN}\theta_U) & (y_U + l_{UN}) & (z_U + l_{UN}\psi_U) \\ (x_U - l_{UW}) & (y_U - l_{UW}\theta_U) & (z_U + l_{UW}\phi_U) \\ (x_U + l_{US}\theta_U) & (y_U - l_{US}) & (z_U - l_{US}\psi_U) \end{bmatrix} \begin{bmatrix} k_{SX} \\ k_{SY} \\ k_{SZ} \end{bmatrix}$$

$$
+\begin{bmatrix}
\dot{x}_L & (\dot{y}_L + l_{UE}\dot{\theta}_L) & (\dot{z}_L - l_{UE}\dot{\phi}_L) \\
(\dot{x}_L - l_{LN}\dot{\theta}_L) & \dot{y}_L & (\dot{z}_L + l_{UN}\dot{\phi}_L) \\
\dot{x}_L & (\dot{y}_L - l_{LW}\dot{\theta}_L) & (\dot{z}_L + l_{LW}\dot{\phi}_L) \\
(\dot{x}_L + l_{LS}\dot{\theta}_L) & \dot{y}_L & (\dot{z}_L - l_{LS}\dot{\phi}_L)
\end{bmatrix}
\begin{bmatrix} c_{SX} \\ c_{SY} \\ c_{SZ} \end{bmatrix}
$$

$$
+\begin{bmatrix}
(x_L - l_{LE}) & (y_L + l_{LE}\theta_L) & (z_L - l_{LE}\phi_L) \\
(x_L - l_{LN}\theta_L) & (y_L + l_{LN}) & (z_L + l_{LN}\psi_L) \\
(x_L - l_{LW}) & (y_L - l_{LW}\theta_L) & (z_L + l_{LW}\phi_L) \\
(x_L - l_{LS}\theta_L) & (y_L - l_{LS}) & (z_L - l_{LS}\psi_L)
\end{bmatrix}
\begin{bmatrix} k_{SX} \\ k_{SY} \\ k_{SZ} \end{bmatrix}
$$

$$
+\begin{bmatrix} 0 \\ -F_{HE} \\ F_{VE} \end{bmatrix} + \begin{bmatrix} -F_{HN} \\ 0 \\ F_{VN} \end{bmatrix} + \begin{bmatrix} 0 \\ -F_{HW} \\ F_{VW} \end{bmatrix} + \begin{bmatrix} -F_{HS} \\ 0 \\ F_{VS} \end{bmatrix}
$$

(F-4)

Similar expansions for the lower level and pier can be made using transforms from Appendix D. These expansions are included in the following expressions for all three bodies in the $\hat{e}_1$, $\hat{e}_2$, and $\hat{e}_3$ degrees of translational freedom.

For the $\hat{e}_1$ direction the pure translation components and rotation cross coupling terms have also been segregated,

$$m_U \ddot{X}_U = - 4c_{SX}\dot{x}_U - 4k_{SX}x_U - k_{SX}(r_{UE} - r_{UW})$$
$$+ 4c_{SX}\dot{x}_L + 4k_{SX}x_L - k_{SX}(l_{UE} - l_{UW})$$
$$- c_{SX}(l_{US} - l_{UN})\dot{\theta}_U - k_{SX}(l_{US} - l_{UN})\theta_U$$
$$+ c_{SX}(l_{LS} - l_{LN})\dot{\theta}_L + k_{SX}(l_{LS} - l_{LN})\theta_L$$
$$- F_{HN} - F_{HS} \qquad \text{(F-5)}$$

$$m_L \ddot{X}_L = -4(c_{FX} + c_{SX})\dot{x}_L - 4(k_{FX} + k_{SX})x_L - (k_{FX} + k_{SX})(l_{LE} - l_{LW})$$
$$+ 4c_{FX}\dot{x}_P + 4k_{FX}x_P + k_{FX}(l_{PE} - l_{PW})$$
$$+ 4c_{SX}\dot{x}_U + 4k_{SX}x_U + k_{SX}(l_{UE} - l_{UW})$$
$$-(c_{FX} + c_{SX})(l_{LS} - l_{LN})\dot{\theta}_L - (k_{FX} + k_{SX})(l_{LS} - l_{LN})\theta_L$$
$$+ c_{FX}(l_{PS} - l_{PN})\dot{\theta}_P + k_{FX}(l_{PS} - l_{PN})\theta_P$$
$$+ c_{SX}(l_{US} - l_{UN})\dot{\theta}_U + k_{SX}(l_{US} - l_{UN})\theta_U$$
(F-6)

$$m_P \ddot{X}_P = -4(c_{GX} + c_{FX})\dot{x}_P - 4(k_{GX} + k_{FX})x_P - (k_{GX} + k_{FX})(l_{PE} - l_{PW})$$
$$+ 4c_{GX}\dot{x}_G + 4k_{GX}x_G + k_{GX}(l_{GE} - l_{GW})$$
$$4c_{FX}\dot{x}_L + 4k_{FX}x_L + k_{FX}(l_{LE} - l_{LW})$$
$$-(c_{GX} + c_{FX})(l_{PS} - l_{PN})\dot{\theta}_P - (k_{GX} + k_{FX})(l_{PS} - l_{PN})\theta_P$$
$$+ c_{GX}(l_{GS} - l_{GN})\dot{\theta}_G + k_{GX}(l_{GS} - l_{GN})\theta_G$$
$$c_{FX}(l_{LS} - l_{LN})\dot{\theta}_L + k_{FX}(l_{LS} - l_{LN})\theta_L$$
(F-7)

Similarly for the $\hat{e}_2$ direction, the complete translation equations are as follows,

$$
\begin{aligned}
m_U \ddot{Y}_U = & -4c_{SY}\dot{Y}_U && - 4k_{SY}Y_U && -k_{SY}(l_{UN} - l_{US}) \\
& -4c_{SY}\dot{Y}_L && + 4k_{SY}Y_L && +k_{SY}(l_{LN} - l_{LS}) \\
& -c_{SY}(l_{UE} - l_{UW})\dot{\theta}_U && - k_{SY}(l_{UE} - l_{UW})\theta_U \\
& +c_{SY}(l_{LE} - l_{LW})\dot{\theta}_L && + k_{SY}(l_{LE} - l_{LW})\theta_L \\
& -F_{HW} - F_{HE}
\end{aligned}
\qquad \text{(F-8)}
$$

$$
\begin{aligned}
m_L \ddot{Y}_L = & -4(c_{FY} + c_{SY})\dot{Y}_L - 4(k_{FY} + k_{SY})Y_L - (k_{FY} + k_{SY})(l_{LN} - l_{LS}) \\
& +4c_{FY}\dot{Y}_P && +4k_{FY}Y_P && + k_{FY}(l_{PN} - l_{PS}) \\
& 4c_{SY}\dot{Y}_U && 4k_{SY}Y_U && k_{SY}(l_{UN} - l_{US}) \\
& -(c_{FY} + c_{SY})(l_{LE} - l_{LW})\dot{\theta}_L - (k_{FY} + k_{SY})(l_{LE} - l_{LW})\theta_L \\
& + c_{FY}(l_{PE} - l_{PW})\dot{\theta}_P && + k_{FY}(l_{PE} - l_{PW})\theta_P \\
& + c_{SY}(l_{UE} - l_{UW})\dot{\theta}_U && + k_{SY}(l_{UE} - l_{UW})\theta_U
\end{aligned}
\qquad \text{(F-9)}
$$

$$
\begin{aligned}
m_P \overset{\circ\circ}{y}_P = \; & -4(c_{GY} + c_{FY})\overset{\circ}{y}_P - 4(k_{GY} + k_{FY})y_P - (k_{GY} + k_{FY})(l_{PN} - l_{PS}) \\
& +4c_{GY}\,\overset{\circ}{y}_G \qquad +4k_{GY}y_G \qquad + k_{GY}\,(l_{GN} - l_{GS}) \\
& +4c_{FY}\,\overset{\circ}{y}_L \qquad +4k_{FY}y_L \qquad + k_{FY}\,(l_{LN} - l_{LS}) \\
& -(c_{GY} + c_{FY})(l_{PE} - l_{PW})\overset{\circ}{\theta}_P - (k_{GY} + k_{FY})(l_{PE} - l_{PW})\theta_P \\
& + c_{GY}\,(l_{GE} - l_{GW})\overset{\circ}{\theta}_G \qquad + k_{GY}\,(l_{GE} - l_{GW})\theta_G \\
& + c_{FY}\,(l_{LE} - l_{UW})\overset{\circ}{\theta}_L \qquad + k_{FY}\,(l_{LE} - l_{LW})\theta_L
\end{aligned}
\tag{F-10}
$$

Equations for the $\hat{e}_3$ direction follow the same scheme used in the $\hat{e}_1$ and $\hat{e}_2$ directions. The complete translation equations are listed below.

$$
\begin{aligned}
m_U \overset{\circ\circ}{z}_U = \; & -4c_{SZ}\overset{\circ}{z}_U - 4k_Z z_U \\
& +4c_{SZ}\overset{\circ}{z}_L + 4k_{SZ}z_L \\
& - c_{SZ}(l_{UN} - l_{US})\overset{\circ}{\psi}_U - k_{SZ}(l_{UN} - l_{US})\psi_U \\
& - c_{SZ}(l_{UW} - l_{UE})\overset{\circ}{\phi}_U - k_{SZ}(l_{UW} - l_{UE})\phi_U \\
& + c_{SZ}(l_{LN} - l_{LS})\overset{\circ}{\psi}_L + k_{SZ}(l_{LN} - l_{LS})\psi_L \\
& + c_{SZ}(l_{LW} - l_{LE})\overset{\circ}{\phi}_L + k_{SZ}(l_{LW} - l_{LE})\phi_L \\
& + F_{VE} + F_{VN} + F_{VW} + F_{VS}
\end{aligned}
\tag{F-11}
$$

$$
\begin{aligned}
m_L \ddot{z}_L = \; & -4(c_{FZ} + c_{SZ})\dot{z}_L - 4(k_{FZ} + k_{SZ}) z_L \\
& +4c_{FZ}\,\dot{z}_P \qquad\qquad +4k_{FZ}\, z_P \\
& +4c_{SZ}\,\dot{z}_U \qquad\qquad +4k_{SZ}\, z_U \\
& - (c_{FZ} + c_{SZ})(l_{LN} - l_{LS})\dot{\psi}_L - (k_{FZ} + k_{SZ})(l_{LN} - l_{LS})\psi_L \\
& - (c_{FZ} + c_{SZ})(l_{LW} - l_{LE})\dot{\phi}_L - (k_{FZ} + k_{SZ})(l_{LW} - l_{LE})\phi_L \\
& + c_{FZ}\,(l_{PN} - l_{PS})\dot{\psi}_P \qquad + k_{FZ}\,(l_{PN} - l_{PS})\psi_P \\
& + c_{FZ}\,(l_{PW} - l_{PE})\dot{\phi}_P \qquad + k_{FZ}\,(l_{PW} - l_{PE})\phi_P \\
& + c_{SZ}\,(l_{UN} - l_{US})\dot{\psi}_U \qquad + k_{SZ}\,(l_{UN} - l_{US})\psi_U \\
& + c_{SZ}\,(l_{UW} - l_{UE})\dot{\phi}_U \qquad + k_{SZ}\,(l_{UW} - l_{UE})\phi_U
\end{aligned}
\tag{F-12}
$$

$$
\begin{aligned}
m_P \ddot{z}_P = \; & -4(c_{GZ} + c_{FZ})\dot{z}_P - 4(k_{GZ} + k_{FZ})z_P \\
& +4c_{GZ}\,\dot{z}_G \qquad\qquad +4k_{GZ}\,z_G \\
& +4c_{FZ}\,\dot{z}_L \qquad\qquad +4k_{FZ}\,z_L \\
& - (c_{GZ} + c_{FZ})(l_{PN} - l_{PS})\dot{\psi}_P - (k_{GZ} + k_{FZ})(l_{PN} - l_{PS})\psi_P \\
& - (c_{GZ} + c_{FZ})(l_{PW} - l_{PE})\dot{\phi}_P - (k_{GZ} + k_{FZ})(l_{PW} - l_{PE})\phi_P \\
& + c_{GZ}\,(l_{GN} - l_{GS})\dot{\psi}_G \qquad + k_{GZ}\,(l_{GN} - l_{GS})\psi_G \\
& + c_{GZ}\,(l_{GW} - l_{GE})\dot{\phi}_G \qquad + k_{GZ}\,(l_{GW} - l_{GE})\phi_G \\
& + c_{FZ}\,(l_{LN} - l_{LS})\dot{\psi}_L \qquad + k_{FZ}\,(l_{LN} - l_{LS})\psi_L \\
& + c_{FZ}\,(l_{LW} - l_{LE})\dot{\phi}_L \qquad + k_{FZ}\,(l_{LW} - l_{LE})\phi_L \\
& - F_{VE} - F_{VN} - F_{VW} - F_{VS}
\end{aligned}
\qquad \text{(F-13)}
$$

NOTE: Equations for $\hat{e}_3$ direction do not have $(l_{US} - l_{UN})k_{SY}$ and similar terms because the isolator suspension points, the corners of each level, are in the horizontal plane containing body center of mass. The SSP was designed so weight could be added or subtracted to adjusted center of mass for various gyro test tables and test items.

The following matrices could be used to relate upper level actuators (or lower) shown in Figure 3.4 to resultant forces for six degrees of freedom. An assumption is made that one half the actuator force is available for translation or rotation controller command.

The vertical actuators are utilized as:

$$\begin{bmatrix} F_{VN} \\ F_{VS} \\ F_{VW} \\ F_{VE} \end{bmatrix} = \begin{bmatrix} \frac{1}{L} & \frac{1}{4} & 0 \\ -\frac{1}{L} & \frac{1}{4} & 0 \\ 0 & \frac{1}{4} & \frac{1}{L} \\ 0 & \frac{1}{4} & -\frac{1}{L} \end{bmatrix} \begin{bmatrix} T_X \\ F_Z \\ T_Y \end{bmatrix} \qquad \text{(F-14)}$$

Similarly the horizontal actuators are controlled as:

$$\begin{bmatrix} F_{HN} \\ F_{HS} \\ F_{HW} \\ F_{HE} \end{bmatrix} = \begin{bmatrix} 0 & \frac{1}{L} & \frac{1}{2} \\ 0 & -\frac{1}{L} & \frac{1}{2} \\ \frac{1}{2} & \frac{1}{L} & 0 \\ \frac{1}{2} & -\frac{1}{L} & 0 \end{bmatrix} \begin{bmatrix} F_X \\ T_Z \\ F_Y \end{bmatrix} \qquad \text{(F-15)}$$

where, F, indicates upper actuators (f could easily be substituted for lower level)

L, actuator corner location from center of mass.

Appendix G SSP Three Degrees of Freedom - Rotation

The mechanics of the rotation equation derivation are shown for the upper level isolator moments in vector notation. Essentially the method is

$$\bar{I}\,\bar{\alpha} = I_{UX}\overset{\circ\circ}{\psi}_U\hat{e}_1 + I_{UY}\overset{\circ\circ}{\phi}_U\hat{e}_2 + I_{UZ}\overset{\circ\circ}{\theta}_U\hat{e}_3$$

$$= \sum_{i=UE}^{US} \bar{r} \times \bar{F}_i \qquad \text{(G-1)}$$

where

I_{UX} , I_{UY} , I_{UZ} are moments of inertia about $\hat{e}_1$, $\hat{e}_2$ and $\hat{e}_3$ axes

$\bar{r}_i$ isolator moment arms (UE, UN, UW, US)

F_i isolator forces for each corner

$\sum_{i=UE}^{US}$ sum all force moment arms from UE, UW, UN to US

The process proceeds using linear approximations for moment arms, namely

$$\overline{UE} = l_{UE}\hat{e}_1$$

$$\overline{UN} = l_{UN}\hat{e}_2$$
$$\overline{UW} = l_{UW}\hat{e}_1$$
$$\overline{US} = l_{US}\hat{e}_2 \qquad \text{(G-2)}$$

No e components arise because isolator suspension points are assumed to be in a horizontal plane containing body center of gravity. This assumption is reasonable for the SSP (upper level, lower level) due to construction specifications and adjustable center of mass capability with lead shot compensation for gyro table loading. The pier clearly violates this assumption, but will be dealt with later.

The process continues with basically a cross product of all force terms (right hand side) of Eq F-1.

$$[I_{UX}\ddot{\psi}_U + I_{UY}\ddot{\phi}_U + I_{UZ}\ddot{\Theta}_U]\underline{e} =$$
$$-(l_{UE}\hat{e}_1) \times (-[C_S]\dot{\overline{UE}} - [K_S]\overline{UE})$$
$$+(l_{UN}\hat{e}_2) \times (-[C_S]\dot{\overline{UN}} - [K_S]\overline{UN})$$
$$+(-l_{UW}\hat{e}_1) \times (-[C_S]\dot{\overline{UW}} - [K_S]\overline{UW})$$
$$+(-l_{US}\hat{e}_2) \times (-[C_S]\dot{\overline{US}} - [K_S]\overline{US})$$

$$+(l_{LE}\hat{e}_1) \times ([C_S]\dot{\overline{LE}} + [K_S]\overline{LE})$$

$$+(l_{UN}\hat{e}_2) \times ([C_S]\dot{\overline{LN}} + [K_S]\overline{LN})$$

$$+(-l_{UW}\hat{e}_1) \times ([C_S]\dot{\overline{LW}} + [K_S]\overline{LW})$$

$$+(-l_{US}\hat{e}_2) \times ([C_S]\dot{\overline{LS}} + [K_S]\overline{LS})$$

$$+ \overline{T} \qquad \text{(G-3)}$$

The vector $\overline{T}$ is a torque produced by the active controller actuators and is specified

$$\begin{aligned}\overline{T} = {} & [l_{UE}F_{VE} + l_{UN}F_{VN} + l_{UW}F_{VW} + l_{US}F_{VS})]\hat{e}_1 \\ & + [(l_{UE})(-F_{HE}) + (-l_{UW})(-F_{HW})]\hat{e}_2 \\ & + [(l_{UN})(-F_{UN}) + (-l_{US})(-F_{US})]\hat{e}_3\end{aligned} \qquad \text{(G-4)}$$

Minus signs are retained because they emphasize the actuator orientation. Note also, the sign on the actuators forces and their parallel to force column vectors in Eq F-4.

The cross product operation shown in (G-3) is continued for the lower level.

$$(I_{LX}\ddot{\psi}_L + I_{LY}\ddot{\phi}_L + I_{LZ}\ddot{\theta}_L)\underline{e} =$$

$$+(l_{LE}\hat{e}_1) \times (-[C_P + C_S]\dot{\overline{LE}} - [K_P + K_S]\overline{LE})$$

$$+(l_{LN}\hat{e}_2) \times (-[C_P + C_S]\dot{\overline{LN}} - [K_P + K_S]\overline{LN})$$

$$+(-l_{LW}\hat{e}_1) \times (-[C_P + C_S]\dot{\overline{LW}} - [K_P + K_S]\overline{LW})$$

$$+(-l_{LS}\hat{e}_2) \times (-[C_P + C_S]\dot{\overline{LS}} - [K_P + K_S]\overline{LS})$$

$$+(l_{PE}\hat{e}_1) \times ([C_F]\dot{\overline{PE}} + [K_P]\overline{PE})$$

$$+(l_{PN}\hat{e}_2) \times ([C_F]\dot{\overline{PN}} + [K_P]\overline{PN})$$

$$+(-l_{PW}\hat{e}_1) \times ([C_F]\dot{\overline{PW}} + [K_P]\overline{PW})$$

$$+(-l_{PS}\hat{e}_2) \times ([C_F]\dot{\overline{PS}} + [K_P]\overline{PS})$$

$$+(l_{UE}\hat{e}_1) \times ([C_S]\dot{\overline{UE}} + [K_S]\overline{UE})$$

$$+(l_{UN}\hat{e}_2) \times ([C_S]\dot{\overline{UN}} + [K_S]\overline{UN})$$

$$+(-l_{UW}\hat{e}_1) \times ([C_S]\dot{\overline{UW}} + [K_S]\overline{UW})$$

$$+(-l_{US}\hat{e}_2) \times ([C_S]\dot{\overline{US}} + [K_S]\overline{US}) \qquad \text{(G-5)}$$

The moment arms used for pier forces, namely $l_{UE}\hat{e}_1$, etc., are certainly bad assumptions since isolator suspension points do not lie in the center of mass plane. For this study the approximation is justified in the passive response considerations.

Continuing the cross product for the pier, the equations are

$$[I_{PX}\ddot{\psi}_P + I_{PY}\ddot{\phi}_P + I_{PZ}\ddot{\theta}_P]\underline{e} =$$

$$+(l_{PE}\hat{e}_1) \times (-[C_G + C_F]\dot{\overline{PE}} - [K_G + K_F]\overline{PE})$$

$$+(l_{PN}\hat{e}_2) \times (-[C_G + C_F]\dot{\overline{PN}} - [K_G + K_F]\overline{PN})$$

$$+(-l_{PW}\hat{e}_1) \times (-[C_G + C_F]\dot{\overline{PW}} - [K_G + K_F]\overline{PW})$$

$$+(-l_{PS}\hat{e}_2) \times (-[C_G + C_F]\dot{\overline{PS}} - [K_G + K_F]\overline{PS})$$

$$+(l_{GE}\hat{e}_1) \times ([C_G]\dot{\overline{GE}} + [K_G]\overline{GE})$$

$$+(l_{GN}\hat{e}_2) \times ([C_G]\dot{\overline{GN}} + [K_G]\overline{GN})$$

$$+(-l_{GW}\hat{e}_1) \times ([C_G]\dot{\overline{GW}} + [K_G]\overline{GW})$$

$$+(-l_{GS}\hat{e}_2) \times ([C_G]\dot{\overline{GS}} + [K_G]\overline{GS})$$

$$+(l_{LE}\hat{e}_1) \times ([C_F]\dot{\overline{LE}} + [K_F]\overline{LE})$$

$$+(l_{LN}\hat{e}_2) \times ([C_F]\dot{\overline{LN}} + [K_F]\overline{LN})$$

$$+(-l_{LW}\hat{e}_1) \times ([C_F]\dot{\overline{LW}} + [K_F]\overline{LW})$$

$$+(-l_{LS}\hat{e}_2) \times ([C_F]\dot{\overline{LS}} + [K_F]\overline{LS})$$

$$- \overline{T} \qquad \text{(G-6)}$$

Eq G-4 defined $\overline{T}$. The operations indicated in Eqs G-3, G-5 and G-6 are carried out with the components tabulated into $\hat{e}_1$, $\hat{e}_2$ and $\hat{e}_3$ components containing the pure rotation and translation cross coupling terms.

The results for the $\hat{e}_1$ direction are

$$
\begin{aligned}
I_{UX}\overset{\circ\circ}{\psi}_U = & -c_{SZ}(l_{UN}l_{UN} + l_{US}l_{US})\overset{\circ}{\psi}_U - k_{SZ}(l_{UN}l_{UN} + l_{US}l_{US})\psi_U \\
& +c_{SZ}(l_{UN}l_{LN} + l_{US}l_{LS})\overset{\circ}{\psi}_L + k_{SZ}(l_{UN}l_{LN} + l_{US}l_{LS})\psi_L \\
& -c_{SZ}(l_{UN} - l_{US})\overset{\circ}{z}_U - k_{SZ}(l_{UN} - l_{US})z_U \\
& +c_{SZ}(l_{UN} - l_{US})\overset{\circ}{z}_L + k_{SZ}(l_{UN} - l_{US})z_L \\
& +l_{UN}F_{VN} - l_{US}F_{VS}
\end{aligned}
$$

$$
\begin{aligned}
I_{LX}\overset{\circ\circ}{\psi}_L = & -(c_{FZ} + c_{SZ})(l_{LN}l_{LN} + l_{LS}l_{LS})\overset{\circ}{\psi}_L - (k_{FZ} + k_{SZ})(l_{LN}l_{LN} + l_{LS}l_{LS})\overset{\circ}{\psi}_L \\
& +c_{FZ}(l_{LN}l_{PN} + l_{LS}l_{PS})\overset{\circ}{\psi}_P + k_{FZ}(l_{LN}l_{PN} + l_{LS}l_{PS})\psi_P \\
& +c_{SZ}(l_{LN}l_{UN} + l_{LS}l_{US})\overset{\circ}{\psi}_U + k_{SZ}(l_{LN}l_{UN} + l_{LS}l_{US})\psi_U \\
& -(c_{FZ} + c_{SZ})(l_{LN} - l_{LS})\overset{\circ}{z}_L - (k_{FZ} + k_{SZ})(l_{LN} - l_{LS})z_L \\
& +c_{FZ}(l_{LN} - l_{LS})\overset{\circ}{z}_P + k_{FZ}(l_{LN} - l_{LS})z_P \\
& +c_{SZ}(l_{LN} - l_{LS})\overset{\circ}{z}_U + k_{SZ}(l_{LN} - l_{LS})z_U
\end{aligned}
$$

$$I_{PX}\overset{\circ\circ}{\psi}_P = -(c_{GZ} + c_{FZ})(l_{PN}l_{PN} + l_{PS}l_{PS})\overset{\circ}{\psi}_P - (k_{GZ} + k_{FZ})(l_{PN}l_{PN} + l_{PS}l_{PS})\psi_P$$

$$+c_{GZ}(l_{PN}l_{GN} + l_{PS}l_{GS})\overset{\circ}{\psi}_G + k_{GZ}(l_{PN}l_{GN} + l_{PS}l_{GS})\psi_G$$

$$+c_{FZ}(l_{PN}l_{LN} + l_{PS}l_{LS})\overset{\circ}{\psi}_L + k_{FZ}(l_{PN}l_{LN} + l_{PS}l_{LS})\psi_L$$

$$-(c_{GZ} + c_{FZ})(l_{PN} - l_{PS})\overset{\circ}{z}_P - (k_{GZ} + k_{FZ})(l_{PN} - l_{PS})z_P$$

$$+ c_{GZ}(l_{PN} - l_{PS})\overset{\circ}{z}_G + k_{GZ}(l_{PN} - l_{PS})z_G$$

$$+ c_{FZ}(l_{PN} - l_{PS})\overset{\circ}{z}_L + k_{FZ}(l_{PN} - l_{PS})z_L$$

$$- l_{UN}F_{VN} + l_{US}F_{VS} \qquad \text{(G-7)}$$

The $\hat{e}_2$ rotation equations are as follows

$$I_{UY}\overset{\circ\circ}{\phi}_U = -c_{SZ}(l_{UE}l_{UE} + l_{UW}l_{UW})\overset{\circ}{\phi}_U - k_{SZ}(l_{UE}l_{UE} + l_{UW}l_{UW})\phi_U$$

$$+c_{SZ}(l_{UE\ LE} + l_{UW\ LW})\overset{\circ}{\phi}_L + k_{SZ}(l_{UE\ LE} + l_{UW\ LW})\phi_L$$

$$-c_{SZ}(l_{UW} - l_{UE})\overset{\circ}{z}_U - k_{SZ}(l_{UW} - l_{UE})z_U$$

$$+c_{SZ}(l_{UW} - l_{UE})\overset{\circ}{z}_L + k_{SZ}(l_{UW} - l_{UE})z_L$$

$$-l_{UE}F_{VE} + l_{UW}F_{VW}$$

$$I_{LY}\ddot{\phi}_L = -(c_{FZ} + c_{SZ})(l_{LE}l_{LE} + l_{LW}l_{LW})\dot{\psi}_L - (k_{FZ} + k_{SZ})(l_{LE}l_{LE} + l_{LW}l_{LW})\psi_L$$

$$+c_{FZ}(l_{LE}l_{PE} + l_{LW}l_{PW})\dot{\psi}_P + k_{FZ}(l_{LE}l_{PE} + l_{LW}l_{PW})\psi_P$$

$$+c_{SZ}(l_{LE}l_{UE} + l_{LW}l_{PW})\dot{\psi}_U + k_{SZ}(l_{LE}l_{UE} + l_{LW}l_{PW})\psi_U$$

$$-(c_{FZ} + c_{SZ})(l_{LW} - l_{LE})\dot{z}_L - (k_{FZ} + k_{SZ})(l_{LW} - l_{LE})z_L$$

$$+c_{FZ}(l_{LW} - l_{LE})\dot{z}_P + k_{FZ}(l_{LW} - l_{LE})z_P$$

$$+c_{SZ}(l_{LW} - l_{LE})\dot{z}_U + k_{SZ}(l_{LW} - l_{LE})z_U$$

$$I_{PY}\ddot{\phi}_P = -(c_{GZ} + c_{FZ})(l_{PE}l_{PE} + l_{PW}l_{PW})\dot{\phi}_P - (k_{GZ} + k_{FZ})(l_{PE}l_{PE} + l_{PW}l_{PW})\phi_P$$

$$+c_{GZ}(l_{PE}l_{GE} + l_{PW}l_{GW})\dot{\phi}_G + k_{GZ}(l_{PE}l_{GE} + l_{PW}l_{GW})\phi_G$$

$$+c_{FZ}(l_{PE}l_{LE} + l_{PW}l_{LW})\dot{\phi}_L + k_{FZ}(l_{PE}l_{LE} + l_{PW}l_{LW})\phi_L$$

$$-(c_{GZ} + c_{FZ})(l_{PW} - l_{PE})\dot{z}_P - (k_{GZ} + k_{FZ})(l_{PW} - l_{PE})z_P$$

$$+c_{GZ}(l_{PW} - l_{PE})\dot{z}_G + k_{GZ}(l_{PW} - l_{PE})z_G$$

$$+c_{FZ}(l_{PW} - l_{PE})\dot{z}_L + k_{FZ}(l_{PW} - l_{PE})z_L$$

$$+l_{UE}F_{VE} - l_{UW}F_{VW} \qquad \text{(G-8)}$$

Similarly, the $\hat{e}_3$ rotation equations are as follows

$$
\begin{aligned}
I_{UZ}\ddot{\theta}_U = &- \left[\begin{array}{c} c_{SX}(l_{UN}l_{UN} + l_{US}l_{US}) \\ + \\ c_{SY}(l_{UE}l_{UE} + l_{UW}l_{UW}) \end{array} \right] \dot{\theta}_U - \left[\begin{array}{c} k_{SX}(l_{UN}l_{UN} + l_{US}l_{US}) \\ + \\ k_{SY}(l_{UE}l_{UE} + l_{UW}l_{UW}) \end{array} \right] \theta_U \\
&+ \left[\begin{array}{c} c_{SX}(l_{UN}l_{LN} + l_{US}l_{LS}) \\ + \\ c_{SY}(l_{UE}l_{LE} + l_{UW}l_{LW}) \end{array} \right] \dot{\theta}_L + \left[\begin{array}{c} k_{SX}(l_{UN\ LN} + l_{US\ LS}) \\ + \\ k_{SY}(l_{UE}l_{LE} + l_{UW}l_{LW}) \end{array} \right] \theta_L \\
&- c_{SX}(l_{US} - l_{UN})\dot{x}_U - k_{SX}(l_{US} - l_{UN})x_U \\
&+ c_{SX}(l_{US} - l_{UN})\dot{x}_L + k_{SX}(l_{US} - l_{UN})x_L \\
&- c_{SY}(l_{UE} - l_{UW})\dot{y}_U - k_{SY}(l_{UE} - l_{UW})y_U \\
&+ c_{SY}(l_{UE} - l_{UW})\dot{y}_L + k_{SY}(l_{UE} - l_{UW})y_L \\
&- l_{UE}F_{HE} + l_{UN}F_{HN} + l_{UW}F_{HW} - l_{US}F_{HS}
\end{aligned}
$$

$$I_{LZ}\ddot{\Theta}_L = -\begin{bmatrix}(c_{FX}+c_{SX})(l_{LN}l_{LN}+l_{LS}l_{LS})\\+\\(c_{FY}+c_{SY})(l_{LE}l_{LE}+l_{LW}l_{LW})\end{bmatrix}\dot{\Theta}_L - \begin{bmatrix}(k_{FX}+k_{SX})(l_{LN}l_{LN}+l_{LS}l_{LS})\\+\\(k_{FY}+k_{SY})(l_{LE}l_{LE}+l_{LW}l_{LW})\end{bmatrix}\Theta_L$$

$$+\begin{bmatrix}c_{FX}(l_{LN}l_{PN}+l_{LS}l_{PS})\\+\\c_{FY}(l_{LE}l_{PE}+l_{LW}l_{PW})\end{bmatrix}\dot{\Theta}_P + \begin{bmatrix}k_{FX}(l_{LN}l_{PN}+l_{LS}l_{PS})\\+\\k_{FY}(l_{LE}l_{PE}+l_{LW}l_{PW})\end{bmatrix}\Theta_P$$

$$+\begin{bmatrix}c_{SX}(l_{LN}l_{UN}+l_{LS}l_{US})\\+\\c_{SY}(l_{LE}l_{UE}+l_{LW}l_{UW})\end{bmatrix}\dot{\Theta}_U + \begin{bmatrix}k_{SX}(l_{LN}l_{UN}+l_{LS}l_{US})\\+\\k_{SY}(l_{LE}l_{UE}+l_{LW}l_{UW})\end{bmatrix}\Theta_U$$

$$-(c_{FX}+c_{SX})(l_{LS}-l_{LN})\dot{x}_L - (k_{FX}+k_{SX})(l_{LS}-l_{LN})x_L$$

$$+\ c_{FX}(l_{LS}-l_{LN})\dot{x}_P + k_{FX}(l_{LS}-l_{LN})x_P$$

$$+\ c_{SX}(l_{LS}-l_{LN})\dot{x}_U + k_{SX}(l_{LS}-l_{LN})x_U$$

$$-(c_{FY}+c_{SY})(l_{LE}-l_{LW})\dot{y}_L - (k_{FY}+k_{SY})(l_{LE}-l_{LW})y_L$$

$$+\ c_{FY}(l_{LE}-l_{LW})\dot{y}_P + k_{FY}(l_{LE}-l_{LW})y_P$$

$$+\ c_{SY}(l_{LE}-l_{LW})\dot{y}_U + k_{SY}(l_{LE}-l_{LW})y_U$$

$$
\begin{aligned}
I_{PZ}\ddot{\theta}_P = & -\begin{bmatrix}(c_{GZ} + c_{FX})(l_{PN}l_{PN} + l_{PS}l_{PS}) \\ + \\ (c_{GY} + c_{FY})(l_{PE}l_{PE} + l_{PW}l_{PW})\end{bmatrix}\dot{\theta}_P - \begin{bmatrix}(k_{GX} + k_{FX})(l_{PN}l_{PN} + l_{PS}l_{PS}) \\ + \\ (k_{GY} + k_{FY})(l_{PE}l_{PE} + l_{PW}l_{PW})\end{bmatrix}\theta_P \\
& + \begin{bmatrix}c_{GX}(l_{PN}l_{GN} + l_{PS}l_{GS}) \\ + \\ c_{GY}(l_{PE}l_{GE} + l_{PW}l_{GW})\end{bmatrix}\dot{\theta}_G + \begin{bmatrix}k_{GX}(l_{PN}l_{GN} + l_{PS}l_{GS}) \\ + \\ k_{GY}(l_{PE}l_{GE} + l_{PW}l_{GW})\end{bmatrix}\theta_G \\
& + \begin{bmatrix}c_{FX}(l_{PN}l_{LN} + l_{PS}l_{LS}) \\ + \\ c_{FY}(l_{PE}l_{LE} + l_{PW}l_{LW})\end{bmatrix}\dot{\theta}_L + \begin{bmatrix}k_{FX}(l_{PN}l_{LN} + l_{PS}l_{LS}) \\ + \\ k_{FY}(l_{PE}l_{LE} + l_{PW}l_{LW})\end{bmatrix}\theta_L \\
& - (c_{GX} + c_{FX})(l_{PS} - l_{PN})\dot{x}_P - (k_{GX} + k_{FX})(l_{PS} - l_{PN})x_P \\
& + c_{GX}(l_{PS} - l_{PN})\dot{x}_G + k_{GX}(l_{PS} - l_{PN})x_G \\
& + c_{FX}(l_{PS} - l_{PN})\dot{x}_L + k_{FX}(l_{PS} - l_{PN})x_L \\
& - (c_{GY} - c_{FY})(l_{PE} - l_{PW})\dot{y}_P - (k_{GY} + k_{FY})(l_{PE} - l_{PW})y_P \\
& + c_{GY}(l_{PE} - l_{PW})\dot{y}_G + k_{GY}(l_{PE} - l_{PW})y_G \\
& + c_{FY}(l_{PE} - l_{PW})\dot{y}_L + k_{FY}(l_{PE} - l_{PW})y_L \\
& + l_{UE}F_{HE} - l_{UN}F_{HN} - l_{UW}F_{HW} + l_{US}F_{HS}
\end{aligned}
\qquad \text{(G-9)}
$$

Appendix H. Simple Three Mass System Transfer Function Polynomial Coefficients

$$\frac{Z_U(s)}{Z_G(s)} = \frac{As^3 + Bs^2 + Cs + D}{Es^6 + Fs^5 + Gs^4 + Hs^3 + Is^2 + Js + K}$$

where numerator terms are

$$A = c_S c_F c_G$$

$$B = c_S c_G k_F + c_F c_G k_S + c_S c_F k_G$$

$$C = c_F k_G k_S + c_G k_F k_S + c_S k_F k_G$$

$$D = k_S k_F k_G$$

and denominator terms are

$$E = m_U m_L m_P$$

$$F = m_U m_P (c_F + c_S) + m_U m_L (c_F + c_G) + m_L m_P c_S$$

$$G = m_P m_U (k_S + k_F) + m_P c_S c_F + m_P m_L k_S + m_U c_G (c_F + c_S) + m_L c_S (c_G + c_F) + m_U m_L (k_G + k_F)$$

$$H = m_P(c_S k_F + c_F k_S) + m_U c_G(k_F + k_S)$$

$$+m_U(c_F k_S + c_S k_F) + c_S c_G c_F + m_L k_S(c_G + c_F)$$

$$+m_U k_G(c_F + c_S) + m_L c_S(k_G + k_F)$$

$$I = m_L k_S(k_F + k_G) + m_P k_S k_F + m_U k_F(k_G + k_S)$$

$$+m_U k_G k_S + c_S(c_F k_G + k_F c_G) + c_F c_G k_S$$

$$J = C$$

$$K = D$$

All terms in the coefficients A thru J are dimensionally consistant using basic units of L, T, M or length, time and mass, respectively.

Appendix I. Transmissibility Polynomial Coefficients

The following coefficients were calculated from lumped parameter spring and damper values given in Appendix E using algorithums developed for the full, dual and single isolation transmissibilities.

Full Isolation

The full isolation transfer function numerator and denominator polynomial are expressed in the notation of Appendix H

$TZ_{U/G}(j\omega)$ polynomial coefficients are

A = 223.3061

B = 112,875.4751

C = 18,750,416.3104

D = 1,019,400,524.282

E = 1.0000

F = 176.7548

G = 23,603.6706

H = 209,405.7952

I = 16,105,109.6289

J = C

K = D

$TX_{U/G}(j\omega)$ or $TY_{U/G}(j\omega)$ polynomial coefficients are

A = 606.8114

B = 616,791.8850

C = 200,095,712.8612

D = 20,192,239,747.25

E = 1.0000

F = 108.5847

G = 24,277.2135

H = 508,769.0142

I = 69,169,079.5072

J = C

K = D

$T\Theta_{U/G}(j\omega)$ polynomial coefficients are

A = 886.4462

B = 901.025.9320

C = 292,305,120.3192

D = 29,497,358,961.09

E = 1.0000

F = 50.3383

G = 14,480.0687

H = 379,095.3026

I = 53,235,281.9575

J = C

K = D

$T\psi_{U/G}(j\omega)$ or $T\phi_{U/G}(j\omega)$ polynomial coefficients are

A = 590.0608

B = 298,260.4301

C = 49,545,813.4351

D = 2,693,648,362.547

E = 1.0000

F = 93.6203

G = 13,351.4852

H = 248,416.7087

I = 19,281,576.4410

J = C

K = D

Dual Isolation

The dual isolation transmissibilities polynomial coefficients are listed using the notation of Eq 4-29.

$TZ_{U/P}(j\omega)$ polynomial coefficients are

a = 1.2919

b = 487.0599

c = 45,904.7099

d = 1.0000

e = 3.8078

f = 719.0572

g = b

h = c

$TZ_{L/P}(j\omega)$ polynomial coefficients are

a = 117.2864

b = 37,177.3628

c = 2,840,484.2000

d = 1.0000

e = 173.6255

f = 22,471.5806

g = b

h = c

$TZ_{U/G}(j\omega)$ polynomial coefficients are

a = 111.2444

b = 35,261.6579

c = 2,694,091.4752

d = 1.0000

e = 164.6773

f = 21,313.4451

g = b

h = c

$TX_{U/P}(j\omega)$ polynomial coefficients are

a = 6.0610

b = 4950.7948

c = 1,010,309.3674

d = 1.0000

e = 8.2503

f = 3377.7858

g = d

h = c

$TX_{L/P}(j\omega)$ polynomial coefficients are

a = 143.4204

b = 85,704.0493

c = 11,393,496.8012

d = 1.0000

e = 101.7669

f = 20,786.5958

g = b

h = c

$TX_{U/G}(j\omega)$ polynomial coefficients are

a = 143.1919

b = 88,565.0200

c = 11,973,740.2255

d = 1.0000

e = 96.6045

f = 19,789.7791

g = b

h = c

$T\Theta_{U/P}(j\omega)$ polynomial coefficients are

a = 27.6590

b = 22,592.4016

c = 4,610,434.4703

d = 1.0000

e = 18.2194

f = 7470.1610

g = b

h = c

$T\Theta_{L/P}(j\omega)$ polynomial coefficients are

a = 96.5325

b = 57,685.1711

c = 7,668,666.9828

d = 1.0000

e = 35.1309

f = 7720.9232

g = b

h = c

$T\Theta_{U/G}(j\omega)$ polynomial coefficients are

a = 97.3424

b = 60,206.8298

c = 8,139,793.1175

d = 1.0000

e = 34.9107

f = 7,747.9586

g = b

h = c

$T\Psi_{U/P}(j\omega)$ polynomial coefficients are

a = 6.9904

b = 2635.3787

c = 248,380.7404

d = 1.0000

e = 9.1608

f = 1,733.7900

g = b

h = c

$T\psi_{L/P}(j\omega)$ polynomial coefficients are

a = 131.1338

b = 41,566.6994

c = 3,175,845.3040

d = 1.0000

e = 86.0130

f = 11,278.3372

g = b

h = c

$T\psi_{U/G}(j\omega)$ polynomial coefficients are

a = 125.2327

b = 39,695.5854

c = 3,032,856.2097

d = 1.0000

e = 85.0357

f = 11,142.5359

g = b

h = c

Single Isolation

The single isolation transmissibilities are listed in standard polynomial transfer function form.

$$TZ_{U/L}(j\omega) = \frac{0.6785j\omega + 127.9100}{(j\omega)^2 + 0.6785(j\omega) + 127.9100}$$

$$TZ_{L/P}(j\omega) = \frac{0.6785j\omega + 127.900}{(j\omega)^2 + 0.6785(j\omega) + 127.9100}$$

$$TZ_{P/G}(j\omega) = \frac{149.9780j\omega + 19,269.1221}{(j\omega)^2 + 149.9780(j\omega) + 19,269.1221}$$

$$TX_{U/L}(j\omega) = \frac{1.5079j\omega + 631.6547}{(j\omega)^2 + 1.5079(j\omega) + 631.6547}$$

$$TX_{L/P}(j\omega) = \frac{1.4325j\omega + 570.0683}{(j\omega)^2 + 1.4325(j\omega) + 570.0683}$$

$$TX_{P/G}(j\omega) = \frac{86.8716j\omega + 17,342.2099}{(j\omega)^2 + 86.8716(j\omega) + 17,342.2099}$$

$$T\Theta_{U/L}(j\omega) = \frac{3.0607j\omega + 1,282.0922}{(j\omega)^2 + 3.0607(j\omega) + 1,282.0922}$$

$$T\Theta_{L/P}(j\omega) = \frac{3.0120j\omega + 1,198.6119}{(j\omega)^2 + 3.0120j\omega + 1,198.6119}$$

$$T\Theta_{P/G}(j\omega) = \frac{31.3219j\omega + 6,252.8156}{(j\omega)^2 + 31.3219(j\omega) + 6,252.8156}$$

$$T\psi_{U/L}(j\omega) = \frac{1.4997j\omega + 282.6902}{(j\omega)^2 + 1.4997(j\omega) + 282.6902}$$

$$T\psi_{L/P}(j\omega) = \frac{1.5535j\omega + 292.8440}{(j\omega)^2 + 1.5535(j\omega) + 292.8440}$$

$$T\psi_{P/G}(j\omega) = \frac{81.7504j\omega + 10,503.2636}{(j\omega)^2 + 81.7504(j\omega) + 10,503.2636}$$

Appendix J. SSP State Representation - Upper and Lower Level Dynamics

The state vector $\bar{X}$ is written in terms of SSP variable and then in true state vector notation.

$$\bar{X} = \begin{bmatrix} \bar{X}_x \\ \bar{X}_y \\ \bar{X}_z \\ \bar{X}_\psi \\ \bar{X}_\phi \\ \bar{X}_\theta \end{bmatrix} \tag{J-1}$$

where for translation

$$\bar{X}_x = \begin{bmatrix} X_L \\ \dot{X}_L \\ X_U \\ \dot{X}_U \end{bmatrix} = \begin{bmatrix} X_1 \\ X_2 \\ X_3 \\ X_4 \end{bmatrix} \tag{J-2}$$

$$\bar{X}_y = \begin{bmatrix} Y_L \\ \dot{Y}_L \\ Y_U \\ \dot{Y}_U \end{bmatrix} = \begin{bmatrix} X_5 \\ X_6 \\ X_7 \\ X_8 \end{bmatrix} \tag{J-3}$$

$$\bar{X}_z = \begin{bmatrix} Z_L \\ \dot{Z}_L \\ Z_U \\ \dot{Z}_U \end{bmatrix} = \begin{bmatrix} X_9 \\ X_{10} \\ X_{11} \\ X_{12} \end{bmatrix} \tag{J-4}$$

where for rotations

$$\bar{X}_\psi = \begin{bmatrix} \psi_L \\ \dot{\psi}_L \\ \psi_U \\ \dot{\psi}_U \end{bmatrix} = \begin{bmatrix} X_{13} \\ X_{14} \\ X_{15} \\ X_{16} \end{bmatrix} \tag{J-5}$$

$$\bar{X}_\phi = \begin{bmatrix} \phi_L \\ \dot{\phi}_L \\ \phi_U \\ \dot{\phi}_U \end{bmatrix} = \begin{bmatrix} X_{17} \\ X_{18} \\ X_{19} \\ X_{20} \end{bmatrix} \tag{J-6}$$

$$\bar{X}_{\Theta} = \begin{bmatrix} \Theta_L \\ \dot{\Theta}_L \\ \Theta_U \\ \dot{\Theta}_U \end{bmatrix} \qquad \begin{bmatrix} X_{21} \\ X_{22} \\ X_{23} \\ X_{24} \end{bmatrix} \tag{J-7}$$

The A matrix is written in terms of partition notation and then in terms of SSP isolator placement lengths from each body center of mass, spring and damper variable.

$$A = \left[\begin{array}{c|c|c|c|c|c} A_x & & & & & A_{x\Theta} \\ \hline & A_y & & & & A_{y\Theta} \\ \hline & & A_z & A_{z\psi} & A_{z\phi} & \\ \hline & & A_{\psi z} & A_{\psi} & & \\ \hline & & A_{\phi z} & & A_{\phi} & \\ \hline A_{\Theta x} & A_{\Theta y} & & & & A_{\Theta} \end{array}\right] \begin{array}{l} \text{(J-8a)} \\ \text{(J-8b)} \\ \text{(J-8c)} \\ \text{(J-8d)} \\ \text{(J-8e)} \\ \text{(J-8f)} \end{array}$$

Zero matrixes are omitted, but understood from Eq 5-4. Each partition is represented from Appendix F and G differential equations as shown on the following pages.

$$A_x = \begin{bmatrix} 0 & 1 & 0 & 0 \\ \frac{-4(k_{FX} + k_{SX})}{m_L} & \frac{-4(c_{FX} + c_{SX})}{m_L} & \frac{4k_{SX}}{m_L} & \frac{4c_{SX}}{m_L} \\ 0 & 0 & 0 & 1 \\ \frac{4k_{SX}}{m_U} & \frac{4c_{SX}}{m_U} & \frac{-4k_{SX}}{m_U} & \frac{-4c_{SX}}{m_U} \end{bmatrix} \qquad (J-9)$$

$$= \begin{bmatrix} 0.0000 & 1.0000 & 0.0000 & 0.0000 \\ -2740.0700 & -6.7424 & 1140.6054 & 1.7230 \\ 0.0000 & 0.0000 & 0.0000 & 1.0000 \\ 631.6547 & 1.5080 & -631.6547 & -1.5080 \end{bmatrix} \qquad (J-10)$$

$$A_{x\Theta} = \begin{bmatrix} 0 & 0 & 0 & 0 \\ \dfrac{-(k_{FX}+k_{SX})(l_{LS}-l_{LN})}{m_L} & \dfrac{-(c_{FX}+c_{SX})(l_{LS}-l_{LN})}{m_L} & \dfrac{k_{SX}(l_{US}-l_{UN})}{m_L} & \dfrac{c_{SX}(l_{US}-l_{UN})}{m_L} \\ 0 & 0 & 0 & 0 \\ \dfrac{+k_{SX}(l_{LS}-l_{LN})}{m_U} & \dfrac{+c_{SX}(l_{LS}-l_{LN})}{m_U} & \dfrac{-k_{SX}(l_{US}-l_{UN})}{m_U} & \dfrac{-c_{SX}(l_{US}-l_{UN})}{m_U} \end{bmatrix} \qquad (J\text{-}11)$$

$$= \begin{bmatrix} 0.0000 & 0.0000 & 0.0000 & 0.0000 \\ -17.0906 & -0.0421 & -15.5144 & -0.0370 \\ 0.0000 & 0.0000 & 0.0000 & 0.0000 \\ 3.9398 & 0.0094 & 8.5917 & 0.0205 \end{bmatrix} \qquad (J\text{-}12)$$

$$A_y = \begin{bmatrix} 0 & 1 & 0 & 0 \\ \frac{-4(k_{FY} + k_{SY})}{m_L} & \frac{-4(c_{FY} + c_{SY})}{m_L} & \frac{4k_{SY}}{m_L} & \frac{4c_{SY}}{m_L} \\ 0 & 0 & 0 & 1 \\ \frac{4k_{SY}}{m_U} & \frac{4c_{SY}}{m_U} & \frac{-4k_{SY}}{m_U} & \frac{-4c_{SY}}{m_U} \end{bmatrix} \quad \text{(J-13)}$$

$$= \begin{bmatrix} 0.0000 & 1.0000 & 0.0000 & 0.0000 \\ -2740.0700 & -6.7424 & 1140.6054 & 2.7230 \\ 0.0000 & 0.0000 & 0.0000 & 1.0000 \\ 631.6547 & 1.5080 & -631.6547 & -1.5080 \end{bmatrix} \quad \text{(J-14)}$$

$$A_{y\Theta} = \begin{bmatrix} 0 & 0 & 0 & 0 \\ \dfrac{-(k_{FY}+k_{SY})(l_{LE}-l_{LW})}{m_L} & \dfrac{-(c_{FY}+c_{SY})(l_{LE}-l_{LW})}{m_L} & \dfrac{+k_{SY}(l_{UE}-l_{UW})}{m_L} & \dfrac{c_{SY}(l_{UE}-l_{UW})}{m_L} \\ 0 & 0 & 0 & 0 \\ \dfrac{k_{SY}(l_{LE}-l_{LW})}{m_U} & \dfrac{c_{SY}(l_{LE}-l_{LW})}{m_U} & \dfrac{-k_{SY}(l_{UE}-l_{UW})}{m_U} & \dfrac{-c_{SY}(l_{UE}-l_{UW})}{m_U} \end{bmatrix} \quad \text{(J-15)}$$

$$= \begin{bmatrix} 0.0000 & 0.0000 & 0.0000 & 0.0000 \\ -10.1590 & -0.0250 & -4.9012 & -0.0117 \\ 0.0000 & 0.0000 & 0.0000 & 0.0000 \\ 2.3419 & 0.0056 & 2.7142 & 0.0065 \end{bmatrix} \quad \text{(J-16)}$$

$$A_z = \begin{bmatrix} 0 & 1 & 0 & 0 \\ \frac{-4(k_{FZ} + k_{SZ})}{m_L} & \frac{-4(c_{FZ} + c_{SZ})}{m_L} & \frac{4k_{SZ}}{m_L} & \frac{4c_{SZ}}{m_L} \\ 0 & 0 & 0 & 1 \\ \frac{4k_{SZ}}{m_U} & \frac{4c_{SZ}}{m_U} & \frac{-4k_{SZ}}{m_U} & \frac{-4c_{SZ}}{m_U} \end{bmatrix} \qquad \text{(J-17)}$$

$$= \begin{bmatrix} 0.0000 & 1.0000 & 0.0000 & 0.0000 \\ -589.8553 & -3.1292 & 230.9726 & 1.2254 \\ 0.0000 & 0.0000 & 0.0000 & 1.0000 \\ 127.9101 & 0.6786 & -127.9101 & -0.6786 \end{bmatrix} \qquad \text{(J-18)}$$

$$A_{z\psi} = \begin{bmatrix} 0 & 0 & 0 & 0 \\ \dfrac{-(k_{FZ}+k_{SZ})(l_{LN}-l_{LS})}{m_L} & \dfrac{-(c_{FZ}+c_{SZ})(l_{LN}-l_{LS})}{m_L} & \dfrac{+k_{SZ}(l_{UN}-l_{US})}{m_L} & \dfrac{c_{SZ}(l_{UN}-l_{US})}{m_L} \\ 0 & 0 & 0 & 0 \\ \dfrac{k_{SZ}(l_{LN}-l_{LS})}{m_U} & \dfrac{c_{SZ}(l_{LN}-l_{LS})}{m_U} & \dfrac{-k_{SZ}(l_{UN}-l_{US})}{m_U} & \dfrac{-c_{SZ}(l_{UN}-l_{US})}{m_U} \end{bmatrix} \quad \text{(J-19)}$$

$$= \begin{bmatrix} 0.0000 & 0.0000 & 0.0000 & 0.0000 \\ 3.6791 & 0.0195 & 3.1417 & 0.0167 \\ 0.0000 & 0.0000 & 0.0000 & 0.0000 \\ -0.7978 & -0.0042 & -1.7398 & -0.0092 \end{bmatrix} \quad \text{(J-20)}$$

$$A_{z\phi} = \begin{bmatrix} 0 & 0 & 0 & 0 \\ \dfrac{-(k_{FZ}+k_{SZ})(l_{LW}-l_{LE})}{m_L} & \dfrac{-(c_{FZ}+c_{SZ})(l_{LW}-l_{LE})}{m_L} & \dfrac{k_{SZ}(l_{UW}-l_{UE})}{m_L} & \dfrac{c_{SZ}(l_{UW}-l_{UE})}{m_L} \\ 0 & 0 & 0 & 0 \\ \dfrac{k_{SZ}(l_{LW}-l_{LE})}{m_U} & \dfrac{c_{SZ}(l_{LW}-l_{LE})}{m_U} & \dfrac{-k_{SZ}(l_{UW}-l_{UE})}{m_U} & \dfrac{-c_{SZ}(l_{UW}-l_{UE})}{m_U} \end{bmatrix} \quad \text{(J-21)}$$

$$= \begin{bmatrix} 0.0000 & 0.0000 & 0.0000 & 0.0000 \\ 2.1869 & 0.0116 & 0.9925 & 0.0053 \\ 0.0000 & 0.0000 & 0.0000 & 0.0000 \\ -0.4742 & -0.0025 & -0.5496 & -0.0029 \end{bmatrix} \quad \text{(J-22)}$$

AD-A115 559 AIR FORCE INST OF TECH WRIGHT-PATTERSON AFB OH SCHOO--ETC F/G 17/7
ANALYSIS AND DESIGN OF A DIGITAL CONTROLLER FOR A SEISMICALLY S--ETC(U)
DEC 81 S W FRANCIS
UNCLASSIFIED AFIT/GE/EE/81D-22 NL

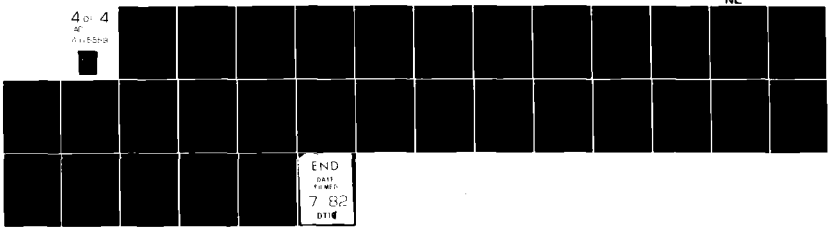

$$A_{\psi z} = \begin{bmatrix} 0 & 0 & 0 & 0 \\ \dfrac{-(k_{FZ}+k_{SZ})(l_{LN}-l_{LS})}{I_{LX}} & \dfrac{-(c_{FZ}+c_{SZ})(l_{LN}-l_{LS})}{I_{LX}} & \dfrac{k_{SZ}(l_{LN}-l_{LS})}{I_{LX}} & \dfrac{c_{SZ}(l_{LN}-l_{LS})}{I_{LX}} \\ 0 & 0 & 0 & 0 \\ \dfrac{k_{SZ}(l_{UN}-l_{US})}{I_{UX}} & \dfrac{c_{SZ}(l_{UN}-l_{US})}{I_{UX}} & \dfrac{-k_{SZ}(l_{UN}-l_{US})}{I_{UX}} & \dfrac{-c_{SZ}(l_{UN}-l_{US})}{I_{UX}} \end{bmatrix} \qquad \text{(J-23)}$$

$$= \begin{bmatrix} 0.0000 & 0.0000 & 0.0000 & 0.0000 \\ 0.9235 & 0.0049 & -0.3616 & -0.0019 \\ 0.0000 & 0.0000 & 0.0000 & 0.0000 \\ 0.3942 & 0.0021 & -0.3942 & -0.0021 \end{bmatrix} \qquad \text{(J-24)}$$

$$A_{\psi} = \begin{bmatrix} 0 & 1 & 0 & 0 \\ \dfrac{-(k_{FZ}+k_{SZ})(l_{LN}l_{LN}+l_{LS}l_{LS})}{I_{LX}} & \dfrac{-(c_{FZ}+c_{SZ})(l_{LN}l_{LN}+l_{LS}l_{LS})}{I_{LX}} & \dfrac{k_{SZ}(l_{LN}l_{UN}+l_{LS}l_{US})}{I_{LX}} & \dfrac{c_{SZ}(l_{LN}l_{UN}+l_{LS}l_{US})}{I_{LX}} \\ 0 & 0 & 0 & 1 \\ \dfrac{k_{SZ}(l_{UN}l_{LN}+l_{US}l_{LS})}{I_{UX}} & \dfrac{c_{SZ}(l_{UN}l_{LN}+l_{US}l_{LS})}{I_{UX}} & \dfrac{-k_{SZ}(l_{UN}l_{UN}+l_{US}l_{US})}{I_{UX}} & \dfrac{-c_{SZ}(l_{UN}l_{UN}+l_{US}l_{US})}{I_{UX}} \end{bmatrix} \quad \text{(J-25)}$$

$$= \begin{bmatrix} 0.0000 & 1.0000 & 0.0000 & 0.0000 \\ -1425.4116 & -7.5620 & 563.1032 & 1.9874 \\ 0.0000 & 0.0000 & 0.0000 & 1.0000 \\ 281.5035 & 1.4934 & -284.0217 & -1.5068 \end{bmatrix} \quad \text{(J-26)}$$

$$A_{\phi z} = \begin{bmatrix} 0 & 0 & 0 & 0 \\ \dfrac{-(k_{FZ}+k_{SZ})(l_{LW}-l_{LE})}{I_{LY}} & \dfrac{-(c_{FZ}+c_{SZ})(l_{LW}-l_{LE})}{I_{LY}} & \dfrac{k_{SZ}(l_{LW}-l_{LE})}{I_{LY}} & \dfrac{c_{SZ}(l_{LW}-l_{LE})}{I_{LY}} \\ 0 & 0 & 0 & 0 \\ \dfrac{k_{SZ}(l_{UW}-l_{UE})}{I_{UY}} & \dfrac{c_{SZ}(l_{UW}-l_{UE})}{I_{UY}} & \dfrac{-k_{SZ}(l_{UW}-l_{UE})}{I_{UY}} & \dfrac{-c_{SZ}(l_{UW}-l_{UE})}{I_{UY}} \end{bmatrix} \quad \text{(J-27)}$$

$$= \begin{bmatrix} 0.0000 & 0.0000 & 0.0000 & 0.0000 \\ 0.5489 & 0.0029 & -0.2150 & -0.0011 \\ 0.0000 & 0.0000 & 0.0000 & 0.0000 \\ 0.1245 & 0.0007 & -0.1245 & -0.0007 \end{bmatrix} \quad \text{(J-28)}$$

$$A_\phi = \begin{bmatrix} 0 & 1 & 0 & 0 \\ \dfrac{-(k_{FZ}+k_{SZ})(l_{LE}l_{LE}+l_{LW}l_{LW})}{I_{LY}} & \dfrac{-(c_{FZ}+c_{SZ})(l_{LE}l_{LE}+l_{LW}l_{LW})}{I_{LY}} & \dfrac{k_{SZ}(l_{LE}l_{UE}+l_{LW}l_{UW})}{I_{LY}} & \dfrac{c_{SZ}(l_{LE}l_{UE}+l_{LW}l_{UW})}{I_{LY}} \\ 0 & 0 & 0 & 1 \\ \dfrac{k_{SZ}(l_{UE}l_{LE}+l_{UW}l_{LW})}{I_{UY}} & \dfrac{c_{SZ}(l_{UE}l_{LE}+l_{UW}l_{LW})}{I_{UY}} & \dfrac{-k_{SZ}(l_{UE}l_{UE}+l_{UW}l_{UW})}{I_{UY}} & \dfrac{-c_{SZ}(l_{UE}l_{UE}+l_{UW}l_{UW})}{I_{UY}} \end{bmatrix} \quad \text{(J-29)}$$

$$= \begin{bmatrix} 0.0000 & 1.0000 & 0.0000 & 0.0000 \\ -1436.7290 & -7.6220 & 565.9735 & 3.0026 \\ 0.0000 & 0.0000 & 0.0000 & 1.0000 \\ 282.9384 & 1.5010 & -284.6451 & -1.5101 \end{bmatrix} \quad \text{(J-30)}$$

$$A_{\theta x} = \begin{bmatrix} 0 & 0 & 0 & 0 \\ \dfrac{-(k_{FX}+k_{SX})(l_{LS}-l_{LN})}{I_{LZ}} & \dfrac{-(c_{FX}+c_{SX})(l_{LS}-l_{LN})}{I_{LZ}} & \dfrac{k_{SX}(l_{LS}-l_{LN})}{I_{LZ}} & \dfrac{c_{SX}(l_{LS}-l_{LN})}{I_{LZ}} \\ 0 & 0 & 0 & 0 \\ \dfrac{k_{SX}(l_{US}-l_{UN})}{I_{UZ}} & \dfrac{c_{SX}(l_{US}-l_{UN})}{I_{UZ}} & \dfrac{-k_{SX}(l_{US}-l_{UN})}{I_{UZ}} & \dfrac{-c_{SX}(l_{US}-l_{UN})}{I_{UZ}} \end{bmatrix} \quad \text{(J-31)}$$

$$= \begin{bmatrix} 0.0000 & 0.0000 & 0.0000 & 0.0000 \\ -1.9697 & -0.0048 & 0.8199 & 0.0020 \\ 0.0000 & 0.0000 & 0.0000 & 0.0000 \\ -0.8940 & -0.0021 & 0.8940 & 0.0021 \end{bmatrix} \quad \text{(J-32)}$$

$$A_{\theta y} = \begin{bmatrix} 0 & 0 & 0 & 0 \\ \dfrac{-(k_{FY}+k_{SY})(l_{LE}-l_{LW})}{I_{LZ}} & \dfrac{-(c_{FY}+c_{SY})(l_{LE}-l_{LW})}{I_{LZ}} & \dfrac{k_{SY}(l_{LE}-l_{LW})}{I_{LZ}} & \dfrac{c_{SY}(l_{LE}-l_{LW})}{I_{LZ}} \\ 0 & 0 & 0 & 0 \\ \dfrac{k_{SY}(l_{UE}-l_{UW})}{I_{UZ}} & \dfrac{c_{SY}(l_{UE}-l_{UW})}{I_{UZ}} & \dfrac{-k_{SY}(l_{UE}-l_{UW})}{I_{UZ}} & \dfrac{-c_{SY}(l_{UE}-l_{UW})}{I_{UZ}} \end{bmatrix} \quad \text{(J-33)}$$

$$= \begin{bmatrix} 0.0000 & 0.0000 & 0.0000 & 0.0000 \\ -1.1709 & -0.0029 & 0.4874 & 0.0012 \\ 0.0000 & 0.0000 & 0.0000 & 0.0000 \\ -0.2824 & -0.0007 & 0.2824 & 0.0007 \end{bmatrix} \quad \text{(J-34)}$$

$$A_\Theta = \begin{bmatrix} 0 & 1 & 0 & 0 \\ \dfrac{\left[(k_{FX}+k_{SX})\,(l_{LN}l_{LN}+l_{LS}l_{LS})+(k_{FY}+k_{SY})\,(l_{LE}l_{LE}+l_{LW}l_{LW})\right]}{I_{LZ}} & \dfrac{\left[(c_{FX}+c_{SX})\,(l_{LN}l_{LN}+l_{LS}l_{LS})+(c_{FY}+c_{SY})\,(l_{LE}l_{LE}+l_{LW}l_{LW})\right]}{I_{LZ}} & \dfrac{\left[k_{SX}(l_{LN}l_{UN}+l_{LS}l_{US})+k_{SY}(l_{LE}l_{UE}+l_{LW}l_{UW})\right]}{I_{LZ}} & \dfrac{\left[c_{SX}(l_{LN}l_{UN}+l_{LS}l_{US})+c_{SY}(l_{LE}l_{UE}+l_{LW}l_{UW})\right]}{I_{LZ}} \\ 0 & 0 & 0 & 1 \\ \dfrac{\left[k_{SX}(l_{UN}l_{LN}+l_{US}l_{LS})+k_{SY}(l_{UE}l_{LE}+l_{UW}l_{LW})\right]}{I_{UZ}} & \dfrac{\left[c_{SX}(l_{UN}l_{LN}+l_{US}l_{LS})+c_{SY}(l_{UE}l_{LE}+l_{UW}l_{LW})\right]}{I_{UZ}} & \dfrac{\left[k_{SX}(l_{UN}l_{UN}+l_{US}l_{US})+k_{SY}(l_{UE}l_{UE}+l_{UW}l_{UW})\right]}{I_{UZ}} & \dfrac{\left[c_{SX}(l_{UN}l_{UN}+l_{US}l_{US})+c_{SY}(l_{UE}l_{UE}+l_{UW}l_{UW})\right]}{I_{UZ}} \end{bmatrix} \quad \text{(J - 35)}$$

$$= \begin{bmatrix} 0.0000 & 1.0000 & 0.0000 & 0.0000 \\ -6104.7858 & -15.0218 & 2560.1284 & 6.1119 \\ 0.0000 & 0.0000 & 0.0000 & 1.0000 \\ 1279.9637 & 3.0557 & -1289.5446 & -3.0786 \end{bmatrix} \quad \text{(J-36)}$$

Random Isolator Placement

The preceding A partitions were calculated using random isolator placement. The isolator misalignments were assumed to be a uniform distribution having a mean of 53 inches and over a uniform distribution of plus or minus one-half inch. Granted, these misalignments do represent a "worse case" from MAC's specification (Ref 10:15) of plus or minus a one-quarter inch isolator placement.

The placements were generated by a CDC 6600 FORTRAN function RANF which returns random numbers between 0 and 1. The isolator locations were calculated according to the following equations.

$$l = \text{RANF} + 52.5$$

Placement values produced for the SSP isolators are given as

$$l_{UE} = 53.0796 \qquad l_{UN} = 53.4504$$
$$l_{UW} = 53.2860 \qquad l_{US} = 52.7976$$

$$l_{LE} = 52.9536 \qquad l_{LN} = 52.5060$$
$$l_{LW} = 52.7748 \qquad l_{LS} = 52.8048$$

$$l_{PE} = 53.1888 \qquad l_{PN} = 52.8816$$
$$l_{PW} = 52.6320 \qquad l_{PS} = 53.3316$$

Appendix K - CGTPIF Digital Controller Designs

Appendix K contains the results of designing possible digital LQ-PI controllers with CGTPIF. Only controllers proposed in Chapter V with solutions are listed on the following pages. Controller variables follow Eqs 5-6 and 5-7 for Figures 5.2A and 5.2B in Chapter V. Each controller type design is referred to by a case number from discussions in Chapter V for different actuator configurations and cost criteria designs indicated by a letter.

Case 1 X - Controller (SSP Isolation)

State Transistion Matrices

$$\Phi = \begin{bmatrix} 0.9664 & 4.8609E-03 & 1.2978E-02 & 4.4514E-05 \\ -13.29 & 0.9337 & 5.516 & 2.2286E-02 \\ 7.7361E-03 & 3.1432E-05 & 0.9922 & 4.9682E-03 \\ 3.052 & 1.5016E-02 & -3.102 & 0.9848 \end{bmatrix}$$

Sample period = 5 msec

Discrete Eigenvalues

$p_{1,2} = 0.9950 \pm j0.0910$

$p_{3,4} = 0.9586 \pm j0.2662$

$$B_D = \begin{bmatrix} 1.2290E-02 & 6.4835E-08 \\ 4.8609E-03 & 4.4514E-05 \\ 4.7276E-08 & 1.2452E-05 \\ 3.1432E-05 & 4.9682E-03 \end{bmatrix}$$

$$\Pi = \begin{bmatrix} -0.6949 & -0.1242 & -0.4318 & -0.4198 & 6.2523E-04 & 9.6769E-04 \\ 115.9 & -0.6321 & 83.17 & 52.31 & -5.9849E-16 & -0.2609 \\ -0.6171 & -0.1260 & -0.5125 & -0.1687 & 6.2523E-04 & -1.8617E-03 \\ 83.28 & 0.1300 & 117.0 & -52.85 & -1.5505E-15 & 0.2611 \\ 1.0711E-17 & 1.6697E-20 & -1.0677E-17 & -6.7544E-18 & 1.000 & 3.3689E-20 \\ 2.4581E-03 & 4.8181E-04 & 1.8773E-03 & 9.3165E-04 & -2.4016E-06 & 3.9567E-06 \end{bmatrix}$$

Case 1, Design A X - Controller (SSP Isolation) - MIMO

Cost Weighting Matrices

$$Y_c = \begin{bmatrix} 0 & 0 \\ 0 & 1 \end{bmatrix} \qquad U_c = \begin{bmatrix} 0.01 & 0.00 \\ 0.00 & 0.01 \end{bmatrix} \qquad U_r = \begin{bmatrix} 0.1 & 0.0 \\ 0.0 & 0.1 \end{bmatrix}$$

Regulator/Proportional Gain Matrix

$$G_c^* = \begin{bmatrix} -0.1253 & 1.6676E\text{-}02 & -0.3814 & -1.8625E\text{-}02 & 4.9209E\text{-}02 & -2.2915E\text{-}04 \\ 0.1069 & -1.2492E\text{-}02 & 0.4190 & 2.5229E\text{-}02 & -2.0502E\text{-}04 & 4.9296E\text{-}02 \end{bmatrix}$$

$$K_X = \begin{bmatrix} 0.7040 & 5.0632E\text{-}02 & 0.5422 & 1.974 \\ 0.3205 & -5.4862E\text{-}02 & 1.651 & -2.101 \end{bmatrix}$$

$$K_Z = \begin{bmatrix} 4.8892E\text{-}02 & -8.6256E\text{-}03 \\ 1.2373E\text{-}04 & 9.1706E\text{-}03 \end{bmatrix}$$

PI Regulator Poles

$p_{1,2}$ = -35.760 ± j74.5876

$p_{3,4}$ = -13.2019 ± j30.3775

p_5 = -86.2629

p_6 = -63.7806

Performance

X acceleration output for unit step response at 4 seconds is ±0.0247 magnitude damped sine wave at 3.12 Hz.

Case 2 X - Controller (Second Stage Isolation)

State Transition Matrix

$$\Phi = \begin{bmatrix} 0.9921 & 4.9681E\text{-}03 \\ -3.138 & 0.9845 \end{bmatrix}$$

Sample period = 5 msec

$$B_D = \begin{bmatrix} 1.2452E\text{-}05 \\ 4.9681E\text{-}03 \end{bmatrix}$$

$$\Pi = \begin{bmatrix} -0.1373 & 0.2165 & -2.6570E\text{-}03 \\ 57.50 & -90.68 & 0.4498 \\ 2.1732E\text{-}04 & -3.4274E\text{-}04 & 4.2064E\text{-}06 \end{bmatrix}$$

Case 2, Design A X - Controller (Second Stage Isolation) - SISO

Cost Weighting Matrices

Y_c = [1] U_c = [0.01] U_r = [0.1]

Regulator/Proportional Gain Matrix

G_c^* = [0.9736 4.2267E-02 4.9507E-02]

K_X = [2.297 -3.622]

K_Z = [1.6425E-02]

PI Regulator Poles

$p_{1,2}$ = -37.4681 ± j58.8408

p_3 = -83.2047

Performance

X acceleration output for unit step response at 4 seconds is ±0.0849 magnitude damped sine wave at 4.17 Hz.

Case 3 Z - Controller (SSP Isolation)

State Transistion Matrix

$$\Phi = \begin{bmatrix} 0.9927 & 4.9489E\text{-}03 & 2.8646E\text{-}03 & 1.9983E\text{-}05 \\ -2.917 & 0.9772 & 1.141 & 8.9155E\text{-}03 \\ 1.5864E\text{-}03 & 1.1066E\text{-}05 & 0.9984 & 4.9889E\text{-}03 \\ 0.6316 & 4.9372E\text{-}03 & -0.6356 & 0.0050 \end{bmatrix}$$

Discrete Eigenvalues

$P_{1,2} = 0.9982 \pm j0.0382$

$P_{3,4} = 0.9835 \pm j0.1213$ Sample period = 5 msec

$$B_D = \begin{bmatrix} 6.2754E\text{-}11 \\ 3.9966E\text{-}08 \\ 2.4965E\text{-}08 \\ 9.9778E\text{-}06 \end{bmatrix}$$ (SISO)

$$\Pi = \begin{bmatrix} -1.695 & -0.5575 & 0.1342 & -0.5868 & -2.0946E\text{-}03 \\ 182.8 & -0.5774 & 17.07 & 53.08 & -0.2650 \\ -0.8155 & -0.5609 & -0.7467 & -2.3296E\text{-}02 & -1.2713E\text{-}02 \\ 16.92 & 7.5734E\text{-}02 & 183.1 & -53.14 & 0.2528 \\ 3.8019E\text{-}05 & 2.0025E\text{-}05 & 1.7839E\text{-}05 & 6.5037E\text{-}06 & 3.4779E\text{-}07 \end{bmatrix}$$

Case 3, Design A Z - Controller (SSP Isolation) - SISO

Cost Weighting Matrices

Y_c = [1000] U_c = [0.01] U_r = [0.1]

Regulator/Proportional Gain Matrix

G_c^* = [0.9758 3.8630E-02 0.2589 0.4306 4.8950E-02]

K_X = [12.48 -0.6789 79.44 -21.41]

K_Z = [9.7595E-02]

PI Regulator Poles

$P_{1,2}$ = -1.8788 ± j25.3397

$P_{3,4}$ = -2.2631 ± j8.8878

P_5 = -63.7904

Performance

Acceleration output for unit step response at 4 seconds is ±0.1 magnitude damped sine wave at 1.35 Hz on -0.05 bias.

Case 3, Design B Z - Controller (SSP Isolation) - SISO

Cost Weighting Matrices

Y_c = [10,000] U_c = [0.01] U_r = [0.1]

Regulator/Proportional Gain Matrix

G_c^* = [4.395 -0.2408 5.290 1.408 4.8989E-02]

K_X = [-31.95 -5.172 250.4 -90.31]

K_Z = [0.03574]

Regulator PI Matrix Poles

$P_{1,2}$ = -3.0214 ± j25.0049

$P_{3,4}$ = -5.4695 ± j11.4728

Performance

Z acceleration output for unit step response at 4 seconds is ±0.06 magnitude damped sine wave at 1.35 Hz.

Case 3, Design C Z - Controller (SSP Isolation) - MIMO

Cost Weighting Matrices

$$Y_C = \begin{bmatrix} 0 & 0 \\ 0 & 1 \end{bmatrix} \qquad U_C = \begin{bmatrix} 0.01 & 0.00 \\ 0.01 & 0.01 \end{bmatrix} \qquad U_r = \begin{bmatrix} 0.1 & 0.0 \\ 0.0 & 0.1 \end{bmatrix}$$

Regulator/Proportional Gain Matrix

$$G_C^* = \begin{bmatrix} 5.3386E\text{-}02 & 6.9535E\text{-}03 & -0.1119 & -6.1461E\text{-}03 & 4.9056E\text{-}02 & -9.3112E\text{-}05 \\ -4.3295E\text{-}02 & -5.0419E\text{-}03 & 0.1172 & 8.8539E\text{-}03 & -8.8527E\text{-}05 & 4.9083E\text{-}02 \end{bmatrix}$$

$$K_X = \begin{bmatrix} 1.168 & 2.8536E\text{-}02 & -0.9160 & 0.6670 \\ -0.7928 & -3.7493E\text{-}02 & 1.442 & -0.7153 \end{bmatrix}$$

$$K_Z = \begin{bmatrix} 4.8893E\text{-}02 & -2.1472E\text{-}03 \\ 1.1476E\text{-}04 & 2.2734E\text{-}03 \end{bmatrix}$$

$$B_D = \begin{bmatrix} 1.2420E\text{-}05 & 3.1377E\text{-}08 \\ 4.9489E\text{-}03 & 1.9983E\text{-}05 \\ 1.7376E\text{-}08 & 1.2483E\text{-}05 \\ 1.1066E\text{-}05 & 4.9889E\text{-}03 \end{bmatrix}$$

PI Regulator Poles

$p_{1,2}$ = -22.1881 ± j35.6346

$p_{3,4}$ = - 6.2874 ± j14.4356

p_5 = -67.3529

p_6 = 63.7806

Performance

Z acceleration output for unit step response at 4 seconds is ±0.0729 magnitude damped sine wave at 1.32 Hz.

Case 4 Z - Controller (Second Stage Isolation)

State Transistion Matrix

$$\Phi = \begin{bmatrix} 0.9984 & 4.9889E\text{-}03 \\ -0.6381 & 0.9950 \end{bmatrix}$$

Sample Period = 5 msec

Discrete Eigenvalues

$$p_{1,2} = 0.9967 \pm j0.0564$$

$$B_D = \begin{bmatrix} 1.2483E\text{-}05 \\ 4.9889E\text{-}03 \end{bmatrix}$$

$$\Pi = \begin{bmatrix} -0.9632 & 0.3077 & -9.3406E\text{-}03 \\ 181.6 & -58.01 & 0.2871 \\ 7.5306E\text{-}03 & -2.4057E\text{-}03 & 7.3025E\text{-}05 \end{bmatrix}$$

Case 4, Design A Z - Controller (Second Stage Isolation) - SISO

Cost Weighting Matrices

Y_c = [1] U_c = [0.01] U_r = [0.1]

Regulator/Proportional Gain Matrix

G_c^* = [0.2099 1.2745E-02 4.9160E-02]

K_X = [2.294 -0.7329]

K_Z = [1.9901E-03]

PI Regulator Poles

$p_{1,2}$ = -21.9557 ± j27.5464

p_3 = -66.0739

Performance

Z acceleration output for unit step response at 4 seconds is ± 0.5021 magnitude damped sine wave at 1.92 Hz.

Case 5 PSI - Controller (SSP Isolation)

State Transistion Matrix

$$\Phi = \begin{bmatrix} 0.9825 & 4.8777E\text{-}03 & 6.9088E\text{-}03 & 4.8223E\text{-}05 \\ -6.939 & 0.9457 & 2.733 & 2.1406E\text{-}02 \\ 3.4538E\text{-}03 & 2.4109E\text{-}05 & 0.9965 & 4.9755E\text{-}03 \\ 1.366 & 1.0702E\text{-}02 & -1.400 & 0.9891 \end{bmatrix}$$

Sample period = 5 msec

Discrete Eigenvalues

$p_{1,2} = 0.9962 \pm j0.07018$

$p_3 = 0.9607 \pm j0.1699$

$$B_D = \begin{bmatrix} 1.2308E\text{-}03 & 7.5928E\text{-}08 \\ 4.8777E\text{-}03 & 4.8223E\text{-}05 \\ 3.7961E\text{-}08 & 1.2461E\text{-}05 \\ 2.4109E\text{-}05 & 4.9755E\text{-}03 \end{bmatrix}$$

$$\Pi = \begin{bmatrix} -1.561 & -0.1346 & 0.6526 & 2.6495E\text{-}02 & 0.0000 & 0.4181 \\ 199.4 & -0.5032 & 0.2348 & 1.2455E\text{-}03 & 0.0000 & 6.1646E\text{-}14 \\ 2.1820E\text{-}18 & 1.1102E\text{-}15 & 3.5527E\text{-}15 & 2.6645E\text{-}15 & 0.0000 & 1.0000 \\ 0.1174 & 6.2272E\text{-}04 & 199.9 & -0.5006 & 0.0000 & 1.0829E\text{-}12 \\ 1.5810E\text{-}03 & 7.508 & 51.28 & 38.00 & 0.0000 & 32.85 \\ 2.4602E\text{-}03 & 38.02 & 259.7 & 192.4 & 0.0000 & 166.3 \end{bmatrix}$$

Case 5, Design A PSI - Controller (SSP Isolation) - MIMO

Cost Weighting Matrices

$$Y_c = \begin{bmatrix} 0 & 0 \\ 0 & 1 \end{bmatrix} \qquad U_c = \begin{bmatrix} 0.01 & 0.00 \\ 0.00 & 0.01 \end{bmatrix} \qquad U_r = \begin{bmatrix} 0.1 & 0.0 \\ 0.0 & 0.1 \end{bmatrix}$$

Regulator/Proportional Gain Matrix

$$G_c^* = \begin{bmatrix} -5.8532E\text{-}06 & 2.3025E\text{-}06 & -2.6075E\text{-}05 & 1.0242E\text{-}05 & 4.8931E\text{-}02 & 2.3293E\text{-}07 \\ -2.1659E\text{-}05 & 1.0334E\text{-}05 & -1.0728E\text{-}04 & 4.6430E\text{-}05 & 2.3334E\text{-}07 & 4.8932E\text{-}02 \end{bmatrix}$$

$$K_X = \begin{bmatrix} 5.4683E\text{-}04 & 0.3674 & 2.511 & 1.859 \\ 2.2203E\text{-}03 & 1.860 & 12.71 & 9.416 \end{bmatrix}$$

$$K_Z = \begin{bmatrix} 0.0000 & 1.607 \\ 0.0000 & 8.139 \end{bmatrix}$$

PI Regulator Poles

$p_{1,2} = -4.1120 \pm j39.1618$

$p_{3,4} = -0.5558 \pm j12.6028$

$p_5 = -63.7808$

$p_6 = -63.7806$

Performance

PSI tilt output for unit step response at 4 seconds is ±0.1760 magnitude damped sine wave at 2.0 Hz.

Case 6 PSI - Controller (Second Stage Isolation)

State Transistion Matrix

$$\Phi = \begin{bmatrix} 0.9965 & 4.9753E\text{-}03 \\ -1.413 & 0.9890 \end{bmatrix}$$

Sample period = 5 msec

Discrete Eigenvalues

$$p_{1,2} = 0.9928 \pm j0.0837$$

$$B_D = \begin{bmatrix} 1.2461E\text{-}05 \\ 4.9753E\text{-}03 \end{bmatrix}$$

$$\Pi = \begin{bmatrix} 1.7764E\text{-}15 & -1.7764E\text{-}15 & 1.000 \\ 199.9 & -0.5005 & 1.3642E\text{-}12 \\ 443.4 & 199.9 & 284.0 \end{bmatrix}$$

Case 6, Design A PSI - Controller (Second Stage Isolation) - SISO

Cost Weighting Matrices

$Y_c = [1]$ $U_c = [0.01]$ $U_r = [0.1]$

Regulator/Proportional Gain Matrix

$G_c^* = [-8.1617E-05 \quad 1.8835E-05 \quad 4.8931E-02]$

$K_X = [21.70 \quad 9.780]$

$K_Z = [13.90]$

PI Regulator Poles

$p_{1,2} = -0.0806 \pm j16.8388$

$p_3 = -63.7808$

Performance

PSI tilt output for a unit step response at 4 seconds is ±0.0108 magnitude damped sine wave at 2.78 Hz.

Case 7 Theta - Controller (SSP Isolation)

State Trans tion Matrix

$$\Phi = \begin{vmatrix} 0.9267 & 4.6961E-03 & 3.0582E-02 & 1.2468E-04 \\ -28.51 & 0.8566 & 11.86 & 5.8900E-02 \\ 1.5301E-02 & 6.2334E-05 & 0.9842 & 4.9360E-03 \\ 5.937 & 2.9448E-02 & -6.206 & 0.9694 \end{vmatrix}$$

Sample period = 5 msec

$$B_D = \begin{bmatrix} 1.2040E-05 & 1.8842E-07 \\ 4.6961E-03 & 1.2468E-04 \\ 9.4203E-08 & 1.2404E-05 \\ 6.2334E-05 & 4.9360E-03 \end{bmatrix}$$

$$\Pi = \begin{bmatrix} -0.9915 & -3.0964E-02 & 0.4341 & 6.3941E-03 & 0.0000 & 0.4441 \\ 197.4 & -0.5063 & 1.070 & 2.5625E-03 & 0.0000 & 2.2307E-14 \\ 4.9960E-16 & 1.1102E-15 & 3.5527E-15 & 5.3291E-15 & 0.0000 & 1.0000 \\ 0.5349 & 1.2812E-03 & 199.5 & -0.5013 & 0.0000 & 1.3444E-12 \\ 3.769 & 8.422 & 147.8 & 40.10 & 0.0000 & 151.2 \\ 17.98 & 40.17 & 704.8 & 191.2 & 0.0000 & 721.1 \end{bmatrix}$$

Case 7, Design A Theta - Controller (SSP Isolation) - MIMO

Cost Weighting Matrices

$$Y_c = \begin{bmatrix} 0 & 0 \\ 0 & 1 \end{bmatrix} \qquad U_c = \begin{bmatrix} 0.01 & 0.00 \\ 0.00 & 0.01 \end{bmatrix} \qquad U_r = \begin{bmatrix} 0.1 & 0.0 \\ 0.0 & 0.1 \end{bmatrix}$$

Regulator/Proportional Gain Matrix

$$G_c^* = \begin{bmatrix} -3.7894E\text{-}06 & 2.8439E\text{-}07 & -1.6194E\text{-}05 & 1.1956E\text{-}06 & 4.8931E\text{-}02 & 2.8566E\text{-}08 \\ -1.4806E\text{-}05 & 1.2143E\text{-}06 & -6.6566E\text{-}05 & 5.1236E\text{-}06 & 2.8649E\text{-}08 & 4.8931E\text{-}02 \end{bmatrix}$$

$$K_X = \begin{bmatrix} 0.1845 & 0.4121 & 7.231 & 1.962 \\ 0.8799 & 1.965 & 34.49 & 9.359 \end{bmatrix}$$

$$K_Z = \begin{bmatrix} 0.0000 & 7.398 \\ 0.0000 & 35.28 \end{bmatrix}$$

PI Regulator Poles

$p_{1,2} = -8.2101 \pm j81.4983$

$p_{3,4} = -0.8557 \pm j26.1585$

$p_5 = -63.7807$

$p_6 = -63.7806$

Performance

Theta tilt output for unit step response at 4 seconds is ±0.0191 magnitude damped sine wave at 4.17 Hz.

Case 8 Theta - Controller (Second Stage Isolation)

State Transistion Matrix

$$\Phi = \begin{bmatrix} 0.9840 & 4.9351E\text{-}03 \\ -6.364 & 0.9688 \end{bmatrix}$$

Sample period = 5 msec

Discrete Eigenvalues

$$p_{1,2} = 0.9764 \pm j0.1771$$

$$B_D = \begin{bmatrix} 1.2403E\text{-}05 \\ 4.9351E\text{-}03 \end{bmatrix}$$

$$\Pi = \begin{bmatrix} 8.8818E\text{-}15 & 0.0000 & 1.0000 \\ 199.5 & -0.5013 & 3.1832E\text{-}12 \\ 1260. & 199.5 & 1290. \end{bmatrix}$$

Case 8, Design A Theta - Controller (Second Stage Isolation) - SISO

Cost Weighting Matrices

Y_c = [1] U_c = [0.01] U_r = [0.1]

Regulator/Proportional Gain Matrix

G_c^* = [-3.9347E-05 1.5538E-05 4.8931E-02]

K_X = [61.68 9.760]

K_Z = [63.10]

PI Regulator Poles

$p_{1,2}$ = -1.5440 ± j35.8775

p_3 = -63.7807

Performance

Theta tilt output for unit step response at 4 seconds is ±0.0011 magnitude damped sine wave at 6.25 Hz.

Case 8, Design B Theta - Controller (Second Stage Isolation) - SISO

Cost Weighting Matrices

Y_c = [1] U_c = [0.01] U_r = [0.1]

Regulator/Proportional Gain Matrix

G_C^* = [-7.8832E-09 3.1120E-10 4.8931E-02]

K_X = [3.0838E+05 4.8799E+04]

K_Z = [3.1549E+05]

PI Regulator Poles

$p_{1,2}$ = -1.5392 ± j35.8772

p_3 = -63.7806

Performance

Theta tilt output for a unit step response at 4 seconds is ±0.01 magnitude damped sine wave at 6.25 Hz at -.01 bias.

Vita

Captain Stanley W. Francis was born December 2, 1947, in Rochester, New Hampshire. In 1965 he graduated from Farmington High School, Farmington, New Hampshire. He enlisted in the United States Air Force in September 1969, and continued his education at Florida Technological University, where he obtained a Bachelor of Science - Electrical Engineering Degree in 1977. In June 1977, he was commissioned a Second Lieutenant in the United States Air Force. During his Air Force career, Capt Francis has been assigned to Air Force Technical Applications Center, Patrick AFB and the Defense Communications Engineering Center, Defense Communications Agency, Reston, Virginia. His current assignment is to the Air Force Institute of Technology as a student pursuing a Master of Science Degree in Electrical Engineering. Capt Francis is a member of IEEE, Eta Kappa Nu and AIAA.

UNCLASSIFIED

SECURITY CLASSIFICATION OF THIS PAGE *(When Data Entered)*

REPORT DOCUMENTATION PAGE	READ INSTRUCTIONS BEFORE COMPLETING FORM
1. REPORT NUMBER: AFIT/GE/EE/81*D-22	2. GOVT ACCESSION NO.: AD-A115 559
3. RECIPIENT'S CATALOG NUMBER	
4. TITLE *(and Subtitle)*: ANALYSIS AND DESIGN OF A DIGITAL CONTROLLER FOR A SEISMICALLY STABLE PLATFORM	5. TYPE OF REPORT & PERIOD COVERED: MS Thesis
	6. PERFORMING ORG. REPORT NUMBER
7. AUTHOR(s): Stanley W. Francis, Capt USAF	8. CONTRACT OR GRANT NUMBER(s)
9. PERFORMING ORGANIZATION NAME AND ADDRESS: Air Force Institute of Technology, Wright-Patterson AFB, Ohio 45433	10. PROGRAM ELEMENT, PROJECT, TASK AREA & WORK UNIT NUMBERS
11. CONTROLLING OFFICE NAME AND ADDRESS	12. REPORT DATE: 4 December 1981
	13. NUMBER OF PAGES: 316
14. MONITORING AGENCY NAME & ADDRESS *(if different from Controlling Office)*	15. SECURITY CLASS. *(of this report)*
	15a. DECLASSIFICATION/DOWNGRADING SCHEDULE

16. DISTRIBUTION STATEMENT *(of this Report)*

Approved for public release; distribution unlimited.

17. DISTRIBUTION STATEMENT *(of the abstract entered in Block 20, if different from Report)*

15 APR 1982

Dean for Research and Professional Development
Air Force Institute of Technology (ATC)
Wright-Patterson AFB, OH 45433

18. SUPPLEMENTARY NOTES

Approved for public release; IAW AFR 190-17

Frederick C. Lynch, Major, USAF
Director of Public Affairs

19. KEY WORDS *(Continue on reverse side if necessary and identify by block number)*

Pneumatic isolator, seismic platform, dual reactionary mass, digital controller, linear quadratic cost, proportional plus integral, performance index, transmissibility, vibration isolation, inertial instruments, Third Generation of Gyros

20. ABSTRACT *(Continue on reverse side if necessary and identify by block number)*

The Seismically Stable Platform (SSP) at the Central Inertial Guidance Facility, Holloman AFB, is a dual reactionary mass isolation platform designed to remove 10^{-8} g RMS/Hz accelerations and ±0.02 arcseconds angular position or tilt disturbances in all axes from a test environment intended for evaluating "Third Generation Gyro" inertial instruments.

DD FORM 1 JAN 73 1473 EDITION OF 1 NOV 65 IS OBSOLETE

UNCLASSIFIED

SECURITY CLASSIFICATION OF THIS PAGE *(When Data Entered)*

Disturbances are removed by two stages of pneumatic isolators comprising a passive isolation system and augmented by an active control system to cover the operational bandwidth from 10^{-4} Hz to 100 Hz.

A dynamic model of the SSP confirmed the passive vibration transmissibilities and identified severe limitations in gain and phase margin to the active controller design. The proposed digital controllers identified the SSP to be weakly controllable. The discrete state representation of the SSP and control law exhibited numerical difficulties detrimental to system stability.

This study recommends single stage pneumatic isolation of fluid isolators monitored by disturbance parameter estimation schemes.

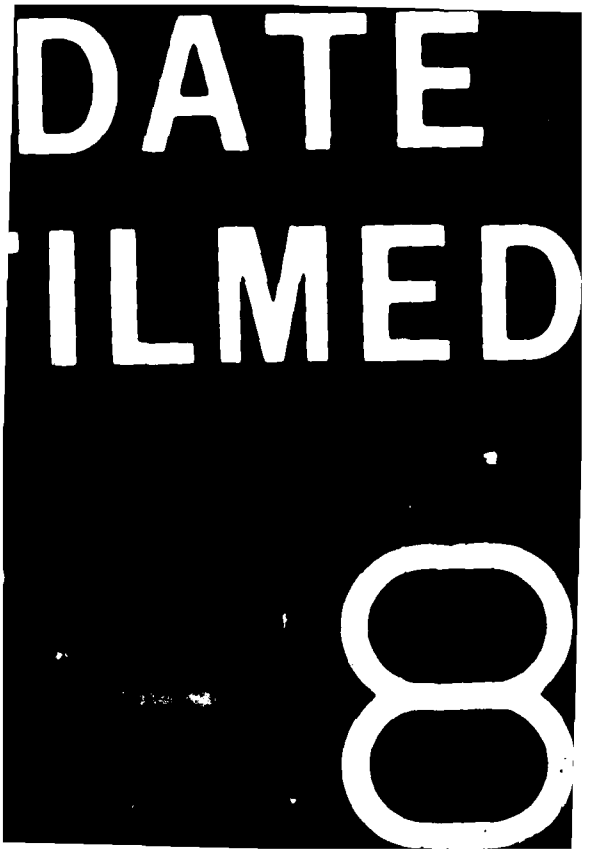
DATE
ILMED
8